

30642



National Library of Canada

Bibliothèque nationale du Canada

CANADIAN THESES ON MICROFICHE

THÈSES CANADIENNES SUR MICROFICHE

NAME OF AUTHOR/NOM DE L'AUTEUR BYONG KWON CHO

TITLE OF THESIS/TITRE DE LA THÈSE Studies of Catalytic Processing for Modified Claus Process

UNIVERSITY/UNIVERSITÉ Univ. of Alberta

DEGREE FOR WHICH THESIS WAS PRESENTED / GRADE POUR LEQUEL CETTE THÈSE FUT PRÉSENTÉE Master of Science

YEAR THIS DEGREE CONFERRED/ANNÉE D'OBTENTION DE CE GRADE 1975

NAME OF SUPERVISOR/NOM DU DIRECTEUR DE THÈSE I. G. Dalla Lana

Permission is hereby granted to the NATIONAL LIBRARY OF CANADA to microfilm this thesis and to lend or sell copies of the film.

L'autorisation est, par la présente, accordée à la BIBLIOTHÈQUE NATIONALE DU CANADA de microfilmer cette thèse et de prêter ou de vendre des exemplaires du film.

The author reserves other publication rights, and neither the thesis nor extensive extracts from it may be printed or otherwise reproduced without the author's written permission.

L'auteur se réserve les autres droits de publication; ni la thèse ni de longs extraits de celle-ci ne doivent être imprimés ou autrement reproduits sans l'autorisation écrite de l'auteur.

DATED/DATE Aug 28, 1975 SIGNED/SIGNÉ Byong Kwon Cho

PERMANENT ADDRESS/RÉSIDENCE FIXE Dept of Chemical Engineering
U of A
Edmonton, Alberta

INFORMATION TO USERS

**THIS DISSERTATION HAS BEEN
MICROFILMED EXACTLY AS RECEIVED**

This copy was produced from a microfiche copy of the original document. The quality of the copy is heavily dependent upon the quality of the original thesis submitted for microfilming. Every effort has been made to ensure the highest quality of reproduction possible.

PLEASE NOTE: Some pages may have indistinct print. Filmed as received.

Canadian Theses Division
Cataloguing Branch
National Library of Canada
Ottawa, Canada K1A 0N4

AVIS AUX USAGERS

**LA THESE A ETE MICROFILMEE
TELLE QUE NOUS L'AVONS RECUE**

Cette copie a été faite à partir d'une microfiche du document original. La qualité de la copie dépend grandement de la qualité de la thèse soumise pour le microfilmage. Nous avons tout fait pour assurer une qualité supérieure de reproduction.

NOTA BENE: La qualité d'impression de certaines pages peut laisser à désirer. Microfilmée telle que nous l'avons reçue.

Division des thèses canadiennes
Direction du catalogage
Bibliothèque nationale du Canada
Ottawa, Canada K1A 0N4

THE UNIVERSITY OF ALBERTA

STUDIES OF CATALYTIC PROCESSING
FOR MODIFIED CLAUS PLANTS

by

© BYONG KWON CHO

A THESIS

SUBMITTED TO THE FACULTY OF GRADUATE STUDIES AND RESEARCH
IN PARTIAL FULFILMENT OF THE REQUIREMENTS FOR THE DEGREE
OF MASTER OF SCIENCE

IN

CHEMICAL ENGINEERING

DEPARTMENT OF CHEMICAL ENGINEERING

EDMONTON, ALBERTA

FALL, 1975

THE UNIVERSITY OF ALBERTA
FACULTY OF GRADUATE STUDIES AND RESEARCH

The undersigned certify that they have read, and recommend to the Faculty of Graduate Studies and Research, for acceptance, a thesis entitled STUDIES OF CATALYTIC PROCESSING FOR MODIFIED CLAUS PLANTS submitted by BYONG KWON CHO in partial fulfilment of the requirements for the degree of Master of Science.

J. D. ...
.....
Supervisor

Richard ...
.....

2 M George
.....

H B ...
.....

Date *August 13, 1975*

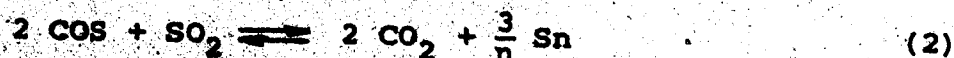
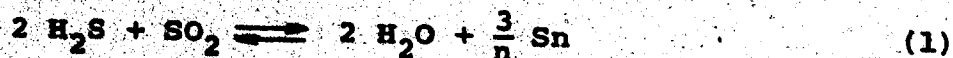
ABSTRACT

The purposes of this work were:

- 1) to develop and compare equilibrium calculations and a reactor modeling procedure for predicting the performance of a Claus process catalytic converter;
- 2) to evaluate under laboratory conditions a newly developed catalyst for the Claus process; and
- 3) to test for the maximum obtainable conversion level in a laboratory fixed-bed catalytic converter.

Before undertaking experimental measurement of reaction conversions, preliminary investigations were made to improve the accuracy of the gas chromatographic analysis and to ensure that no additional reaction other than that in the catalyst bed occurred.

To evaluate the bifunctional activity of a newly developed catalyst for two major reactions in a Claus unit:



an experimental study of four different types of catalysts was conducted. These catalysts included: pure γ -alumina (Kaiser S-201), 5.4% Cu-on-alumina, 12.08% Cu-on-alumina and 16.07% Cu-on-alumina. Kinetic studies using a 1 inch diameter integral fixed-bed reactor of 316 stainless steel were conducted at space velocities ranging from 25,000 to

150,000 hr⁻¹. A total of 83 kinetic runs were completed at 556 ± 2.8 °K, 932 ± 9 psia, and nearly constant feed composition, 2.9 ± 0.12 mole percent of H₂S (or COS) and 1.5 ± 0.12 mole percent of SO₂, with the balance N₂. The Cu-on-alumina catalyst proved to be a good bifunctional catalyst for Claus operational conditions. Its catalytic activity was dependent upon the copper content: for reaction (1), a copper content of about 5% by weight maximized the catalytic activity; while for reaction (2), the catalytic activity decreased as the copper content increased. The exact reason for this effect of copper content on the bifunctional catalytic activities is not clear at this point. It is postulated that the catalytic activity change may be attributed to sulfided copper for reaction (1) combined with elimination of Lewis-acid as well as basic sites on the γ-alumina surface by copper.

A total of 10 kinetic runs were carried out at very low space velocities, 4 and 100 hr⁻¹, to obtain the maximum obtainable conversion level of the Claus reaction in a fixed-bed integral reactor. The resulting experimental conversions were found to be greater than the predicted thermodynamic equilibrium conversions under the same reaction temperature. Some possible explanations for this discrepancy are examined.

Adiabatic reaction paths were calculated for the front-end burner section of a Claus unit. Their intersection with the equilibrium conversion curves was used

to predict the conversion attained. Then the catalytic converter performance was computed using a reaction rate expression developed by Liu (55) for a pure γ -alumina (Alon) and a one-dimensional two-phase catalytic reactor model under adiabatic conditions. In the Claus catalytic converter, it was predicted that external mass transfer resistances were insignificant at space velocities above 1000 hr^{-1} . The predicted temperature and reaction profiles along the reactor bed revealed that the feed temperature and the space velocity should be above 500°K and below 2000 hr^{-1} , respectively, to ensure significant reaction rates at the start of the reactor bed.

ACKNOWLEDGEMENTS

The author expresses sincere appreciation to many individuals who guided and assisted him in his research. In particular, he wishes to thank his thesis advisor, Professor I.G. Dalla Lana, for his encouragement, advice, and criticism during the course of this work.

The author is grateful to Mr. Jerry Moser for his advice in testing the gas chromatographic system and for his preparation of the new catalyst. The author wishes to thank Mr. Don Sutherland of the machine shop for calibration of thermocouples and for assistance in repair to the gas chromatographic system. The author is indebted also to the staff of the machine shop in the Department of Chemical Engineering. Special acknowledgement is given to Mr. Thomas Turner whose assistance was invaluable throughout this work, and to Mrs. E. Sherwin for her careful typing.

The author is sincerely grateful for financial support provided by the Department of Chemical Engineering and the Canadian Natural Gas Processing Association Research Fund.

Finally, the author is deeply indebted to his wife, E.C., for her patience, understanding, and support during his research.

TABLE OF CONTENTS

	<u>Page</u>
CHAPTER I INTRODUCTION	
1.1 Problems Related to the Claus Process	1
1.2 Previous Works	5
1.3 Topics to be Investigated in This Study	8
1.3.1 Evaluation of Bifunctional Catalysts	8
1.3.2 Prediction of Claus Process Performance	10
CHAPTER II LITERATURE SURVEY	
2.1 Claus Process	15
2.2 Sulfur Recovery Processes Related to Claus Units	16
2.3 Simultaneous Reactions in Claus Units	19
2.3.1 H ₂ S - Air Reaction	19
2.3.2 H ₂ S - SO ₂ Reaction	23
2.3.3 COS - SO ₂ Reaction	28
2.3.4 COS - H ₂ O Reaction	32
2.3.5 Sulfur Species Association-Dissociation Reaction	34
2.4 Catalysis by Some Transition Elements	40
2.5 Performance of a Claus Unit	41
2.5.1 Importance of Combustion Chamber or Burner Design	41
2.5.2 Performance of a Catalytic Converter	43
2.5.3 Claus Reactor Design	45

TABLE OF CONTENTS (continued)

	<u>Page</u>
CHAPTER III PREDICTION OF CLAUS UNIT PERFORMANCE	
3.1 Performance of the Front-end Burner	63
3.2 Performance of the Claus Catalytic Converter	83
3.3 Results of Reactor Modeling	92
CHAPTER IV DESCRIPTION OF EXPERIMENTAL SYSTEM	
4.1 Reactant Feeding System	103
4.2 Feed-Product Analysis System	106
4.2.1 Separation of the Component in GC Column	106
4.2.2 Selection-Sampling Valve Mode	111
4.2.3 Attenuator Setting	111
4.3 Reaction System	113
4.3.1 Feed Pre-heater	113
4.3.2 Reactor	115
4.3.3 Sulfur Condenser and Water Condenser	116
4.3.4 Sulfur Trap	118
4.4 Process Measuring and Control System	120
CHAPTER V EXPERIMENTAL PROCEDURE AND RESULTS	
5.1 General Procedure	122
5.1.1 Startup of the System	122
5.1.2 Catalyst Pretreatment and Kinetic Run	123
5.1.3 Shutdown Procedure	127
5.1.4 Materials	127

TABLE OF CONTENTS (continued)

	<u>Page</u>
5.2 Data Reduction Procedure	130
5.3 Experimental Results and Discussions	132
5.3.1 Preliminary Investigations	132
5.3.2 Comparison of Catalyst Activities	144
5.3.3 Performance Test on the Bifunctional Activity	160
5.3.4 Maximum Obtainable Conversion Level	162
CHAPTER VI CONCLUSION AND RECOMMENDATIONS	
6.1 Performance of Equipment	170
6.2 Prediction of a Claus Unit Performance	171
6.3 Evaluation of a Bifunctional Catalyst	174
6.4 Maximum Obtainable Conversion in the Claus Reaction	176
6.5 Reversible Reaction in the Claus Reaction	176
NOMENCLATURE	178
BIBLIOGRAPHY	183
APPENDIX A CALIBRATION OF GAS CHROMATOGRAPHIC SYSTEM	189
B CALIBRATION OF PROCESS MEASURING SYSTEM	214
C DERIVATION OF EQUATIONS FOR ADIABATIC REACTION PATHS IN THE FRONT-END BURNER	231
D ESTIMATION OF EFFECTIVE DIFFUSIVITY	243
E SIMPLIFICATION OF MODELING EQUATIONS	247

TABLE OF CONTENTS (continued)

	<u>Page</u>
F ASYMPTOTIC SOLUTION FOR EFFECTIVENESS FACTOR	260
G DERIVATION OF COLLOCATION EQUATION FOR EFFECTIVENESS FACTOR	266
H NUMERICAL SOLUTION FOR EFFECTIVENESS FACTOR	274
I SAMPLE CALCULATION OF DATA REDUCTION	287
J EXPERIMENTAL DATA FILE	317

LIST OF TABLES

<u>Table</u>		<u>Page</u>
1	Heat of Dissociation of Sulfur Species	35
2	Equilibrium Constants for Reactions (1.1) and (1.2)	64
3	dx/dT in the Front-end Burner	78
4	Comparison between Different Column Arrangements	109
5	Purities of Gases	128
6	Standard Catalyst Properties	129
7	Comparison of Reproducibility	141
A.1	Calibration of Chromatograph Attenuator	195
A.2	Calibration of Attenuator #1	196
A.3	Calibration of Attenuator #2	197
A.4	Calibration for SO_2-N_2 Mixture	200
A.5	GC Calibration Using Attenuation Scheme II	204
A.6	GC Calibration Using Attenuation Scheme III	207
B.1	DP-Cell Calibration (Feed Pressure at 30 psia)	216
B.2	DP-Cell Calibration (Feed Pressure at 25 psia)	217
B.3	DP-Cell Calibration (Feed Pressure at 20 psia)	218
B.4	Feed Absolute Pressure Transducer Calibration	220
B.5	Reactor Gauge Pressure Transducer Calibration #1 (at 480 Degree K)	222

LIST OF TABLES (continued)

		<u>Page</u>
B.6	Reactor Gauge Pressure Transducer Calibration #1 (at 500 Degree K)	222
B.7	Reactor Gauge Pressure Transducer Calibration #1 (at 560 Degree K)	223
B.8	Reactor Gauge Pressure Transducer Calibration #2 (at 560 Degree K)	224
B.9	Reactor Gauge Pressure Transducer Calibration #3 (at 560 Degree K)	225
B.10	Thermocouple Calibration for Reactor Inlet Temperature	227
B.11	Thermocouple Calibration for Reactor Outlet Temperature	228
B.12	Calibration of Water Feed Pump	229
B.13	Density Correction of Feed Water	230
J.1	Raw Data	320
J.2	Processed Data	321

LIST OF FIGURES

<u>Figure</u>		<u>Page</u>
1	Chemical Equilibrium between Sulfur Species at One Atmosphere	39
2	Fraction of the Equivalent Moles of S_2 Associated to S_6 or S_8	66
3	Effect of the Inert Content on Equilibrium Conversion of the Claus Reaction	72
4	Equilibrium Conversion and Adiabatic Reaction Path in the Front-end Burner	73
5	Illustration of a Reaction Path in the Waste-heat Boiler and the Catalytic Converter	75
6	Equilibrium Conversion of CO_2 in the Front-end Burner	79
7	Front-end Reaction Path	80
8	Effectiveness Factor as a Function of Thiele Modulus for Claus Reaction on Alon Catalyst	89
9	Temperature and Conversion Profiles along the Bed Depth	93
10	Effect of External Transport Resistance	95
11	Check on the Existence of Multiple Solutions due to the External Transport Resistances	96
12	Effect of the Feed Temperature on X-T Plot	98
13	Effect of the Feed Temperature on Temperature Profiles	99
14	Effect of the Feed Temperature on Conversion Profiles	100
15	Effect of the Space Velocity on Conversion Profiles	101
16	Schematic Diagram of the Reactant Feeding System	104

LIST OF FIGURES (continued)

<u>Figure</u>		<u>Page</u>
17	Schematic Diagram of the Analysis System	107
18	Typical Chromatogram for Separation of N_2 , CO_2 , H_2S , COS , SO_2 , and H_2O	110
19	Schematic Diagram of Reaction System	114
20	Sulfur Trap Performance Test	134
21	First Calibration of Gas Chromatograph	139
22	Performance Comparison between Different Integrating Systems	140
23	Second Calibration of Gas Chromatograph	142
24	Simultaneous Conversions Using Different Catalysts	146
25	Effect of Copper Content on the Conversion Level	148
26	Comparison of Individual Reaction Rate on 5.4% Cu-on-alumina Catalyst	156
27	Effect of Water Content in the Feed on Hydrolysis of COS on γ -alumina	159
28	Test of Bifunctional Characteristics of Cu-on-alumina Catalyst	161
29	Conversion Level as a Function of Space Time	164
30	Comparison between Predicted and Experimental Conversions as a Function of Reactor Outlet Temperature	165
A.1	GC Calibration Apparatus	191
A.2	Attenuation Scheme I	194
A.3	Attenuation Scheme II	194
A.4	Attenuation Scheme III	194
A.5	Homogeneous Reactor Effects in the Mixing Chamber During the Calibration Period	199

CHAPTER I

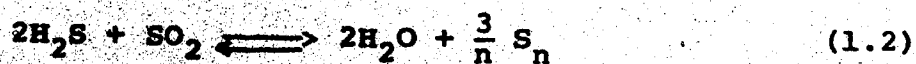
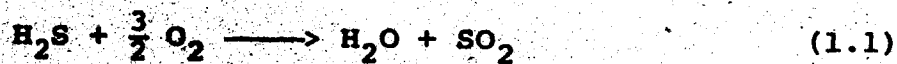
INTRODUCTION

1.1 Problems Related to the Claus Process:

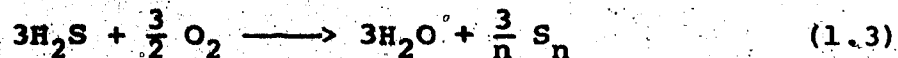
During past decades, extensive studies were conducted to effectively recover the sulfur from natural gas using a variety of chemical processes. Recently these sulfur recovery processes have become more and more important due not only to the economic value of the product sulfur but also to more strict air pollution control policies.

A major source of sulfur in Canada has been from hydrogen sulfide in natural gas, particularly in Alberta, and in acid-gas streams in petroleum refineries. Among many different kinds of sulfur recovery processes, the modified Claus process has been almost exclusively applied to the natural gas plant to convert hydrogen sulfide in the sour gas stream to high grade pure sulfur.

The major reactions involved in the Claus plant are:



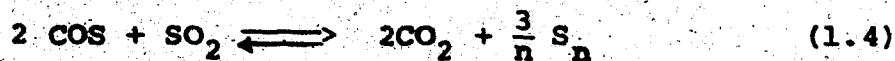
which make the overall reaction of



Reaction (1.1) shows free flame combustion of hydrogen sulfide by air in the front-end burner to provide sulfur dioxide which acts as a reactant for reaction (1.2) in the catalytic converter. Because of high temperatures in the burner, reaction (1.2) also proceeds to the extent of roughly 50 - 70% conversion of H_2S via homogeneous kinetics.

Though the major Claus reaction is reaction (1.2) other side reactions usually take place together with the major one.

The most significant and important side reaction from the kinetic point of view is



Reaction (1.4) may occur due to the carbonyl sulfide impurity which is introduced by the reaction between hydrogen sulfide and carbon dioxide in the burner, or from COS present in the acid gas (33).

The Claus reaction is much more complicated than it seems to be in its simplistic reaction formula. This reaction was found to be catalyzed by various substances such as the glass surface, iron, water vapor, and even liquid sulfur, and so on (97,72,53).

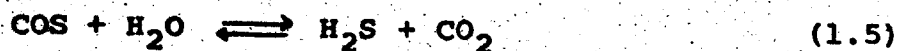
To understand the true reaction kinetics of this reaction on the γ -alumina surface has been an extremely difficult subject to study due to the difficulties of eliminating the various catalytic effects caused by substances other than alumina. Among these side-catalysing effects, the additional catalytic effect due to the product sulfur in its liquid form was the most difficult problem to eliminate or solve. To eliminate side catalysing effect due to the condensed liquid sulfur others have tried using sulfur condenser (72,53), electric precipitator (81), or ice bath (37, 39). But the elimination efficiencies have never been critically checked.

Another problem related to the Claus process is the uncertainty on the equilibrium distribution of sulfur molecular species during the reaction period, since above 1000°K all the sulfur species may exist in the form of S_2 , while at room temperature as S_8 (75).

Therefore, the Claus process may become exothermic or endothermic according to the operating temperature level of the reactor (24). The problems related to the equilibrium distribution between sulfur species with different molecular formula were attacked by many chemists but with controversial results.

One of the most important problems which

remains to be solved in the Claus plant is the effect of minor reactions on the overall process performances. In earlier studies the reaction (1.4) was found to affect the catalytic activity of γ -alumina due to the poisoning effect of the product CO_2 (65). Subsequently, the poisoning effect was observed only under dry gaseous conditions, i.e. in the presence of H_2O , reaction (1.4) is by-passed in favor of the more rapid reaction



Here the need for some type of improved bifunctional catalysts arises to improve the overall Claus process performance since COS impurity is almost inevitably present in practical operational conditions (33). Actually, the loss of sulfur due to unconverted COS is almost 30 percent of the total sulfur loss (15). Until recently this problem was not solved satisfactorily because of the lack of the experimental data for both of the reactions on some bifunctional catalysts.

From a practical point of view, it is surprising that few data are available to apply to the Claus plant design for a catalytic fixed-bed reactor. The most important data for application to the plant design is the intrinsic rate expression on the specified

catalyst surface, physical parameters of the reaction systems and catalysts, and most of all, the effectiveness factor of catalyst pellets.

Recently the intrinsic rate data have become available owing to the painstaking works by some researchers (65,66,72) for some type of catalysts. However, the availability of other information is limited to the extent of primitive estimates of the physical parameters or of the effectiveness of the catalyst pellets for the developed intrinsic rate expression. No published data may be easily applied to the practical situation. These kinds of studies are really in need for improving, developing and predicting more efficient sulfur recovery in natural gas processing plants.

1.2 Previous Works:

After the Claus process to recover sulfur from the H_2S containing gaseous stream had been invented in 1883 by the British chemist, C.F. Claus, this process has been widely adopted in the natural gas plants as a major scheme to recover the elemental sulfur since the first commercial application by H. Bahr in 1936.

In 1953, Gannon and Elkins (35) carried out pioneering kinetic measurements of this Claus reaction

using Porocel catalyst in an integral fixed-bed reactor over the temperature range of 230 to 300°C at low space velocity ranging from 240 to 1920 hr⁻¹.

In the late 1960's, an extensive research program was initiated at the University of Alberta to investigate intensively the Claus process as this process has become more and more widely applied in almost all natural gas plants in Alberta. The first investigation was carried out by Cormode (21) using Porocel catalyst to obtain kinetic data in a recycle differential flow reactor. McGregor (72) carried out a series of 80 experimental runs in a similar but improved differential recycle reactor, performed at four different temperature levels between 481 and 560°K and at varying partial pressure of H₂S, SO₂ and H₂O to obtain the intrinsic rate expression with activation energy for the forward reaction of the reversible Claus reaction.

McGregor (72) found that water vapor has a retarding effect on the forward rate of the Claus reaction at higher concentration and an accelerating effect at lower concentration, presumably by the hydrogen-bonding due to the water vapor on γ -alumina OH-site. The rate expression obtained by Dalla Lana et al. (25) using McGregor's experimental data (72)

was

$$-r_{SO_2} = 1.56 \times 10^{-4} \left[\frac{P_{H_2S} P_{SO_2}^{1/2}}{1 + 0.00423 P_{H_2O}} \right] \exp \left[\frac{-7440}{R_g T} \right] \dots \dots (1.6)$$

Liu (65) investigated the effect of NaOH-doping on the activity of γ -alumina for the Claus reaction, and found that a 2% doped γ -alumina showed highest activity for this reaction. Liu (65) also observed and explained (19) the CO_2 poisoning effect in the reaction (1.4).

Karren (53) carried out some 50 experimental runs using the same recycle differential bed reactor as used in McGregor's work, but with the sulfur condenser capacity increased. During his study Karren (53) found that the liquid sulfur acted as an active catalyst for the Claus reaction and the elimination of condensed liquid sulfur in the product stream was critically important to get accurate reaction rate expression on the catalyst surface.

Most recently Liu (66) investigated the Claus reaction using an infrared spectroscopic reactor cell to get an intrinsic rate expression without external and internal transport resistances and obtained

$$-r_{SO_2} = 1.28 \times 10^{-4} \left[\frac{P_{H_2S} P_{SO_2}^{1/2}}{(1 + 0.006 P_{H_2O})^2} \right] \exp \left[\frac{-7350}{R_g T} \right]$$

..... (1.7)

for the Claus reaction over Alon catalyst. The form of the rate expression obtained by Liu (66) was almost the same as that obtained by McGregor (72) except the retarding effect of water vapor was increased compared to McGregor's result. It is worth noting that the remarkable similarity held even though a pure γ -alumina catalyst was used by Liu and a commercial bauxite by McGregor.

1.3 Topics to be Investigated in This Study:

1.3.1 Evaluation of Bifunctional Catalysts:

Some work has been reported (22,23,35,36,37,65) to develop and/or improve active catalysts for the reaction between H_2S and SO_2 . In parallel with the reaction between H_2S and SO_2 , more attention has been paid recently to the reaction between COS and SO_2 (36,37,65,90). However, each of these studies was confined to one particular chemical reaction process with the view of investigating catalytic activities or a reaction rate expression for each separate reaction.

In practice, one approach adopted by industry has been to use a different catalyst more active for the COS-SO₂ reaction, but requiring a higher operating temperature than alumina, in plants where COS problems are more severe. More exotic catalysts such as Co-Mo supported on alumina have been used for this purpose.

This problem could be solved more simply by developing a bifunctional catalyst which actively catalyses both the H₂S-SO₂ and the COS-SO₂ (or COS-H₂O) reactions simultaneously. For this purpose one such bifunctional catalyst has been developed at the University of Alberta in 1973 to improve the Claus plant operational condition (23).

The present study has been designed to investigate the performance of this newly developed bifunctional catalyst for reaction (1.2) and (1.4) in Claus plants. In this study it is intended to compare its catalytic activity with that of standard alumina catalyst under the same range of reaction conditions encountered in industrial reactors but over a short-term reaction period. By this investigation a basis for understanding the bifunctional activity of the proposed catalyst may be provided. The catalysts tested included a standard γ -alumina (Kaiser S-201), 5.4% Cu-alumina, 12.08% Cu-alumina, and 16.07% Cu-alumina.

1.3.2 Prediction of Claus Process Performance

1.3.2.1 Prediction of Thermodynamic Equilibrium

In a conventional modified Claus process, elemental sulfur is formed through a two-step reaction procedure as was described in reaction equations (1.1) and (1.2). Many investigators (9,35,72,74,84) tried to compute and predict equilibrium conversion for reaction (1.2) but paid little attention to the significant endothermic effect at temperatures above 850°K and to the effect of the inert gas content on the conversion level. These facts occur due to the different distribution among the sulfur species between S_2 , S_6 and S_8 at different system temperatures. Regarding the sulfur species distribution over the various temperature range, much work has been done during past decades to try to get definite conclusion still leaving the work in a controversial subject (75,88,89).

In this work the sulfur species in equilibrium were assumed to exist in the forms of S_2 , S_6 and S_8 . That is



Furthermore each of the above three species was assumed to be in equilibrium with the others at the given temperature and pressure in state of the minimum total free energy. Equilibrium conversion calculation was performed using the free energy minimization method originally programmed by McGregor (72).

Finally, the computed equilibrium conversion level was compared to the maximum obtainable conversion which could be obtained experimentally, i.e. at the lowest possible space velocity.

1.3.2.2 Prediction of Reaction Path in the Front-End Burner

The prediction of adiabatic reaction path in the front-end burner by the consecutive reactions (1.1) and (1.2) should be very useful to evaluate and compare actual process performance in individual stages with the corresponding idealized performance limits (24). To provide such a useful and convenient way of predicting the reaction path along the front-end burner before a catalytic converter, a graphical approach was developed in this study in attempt to present calculated values for "once-through" processes. This graphical approach may be readily extended to a number of problems occurring in closed systems:

(1) the prediction of equilibrium conversions of H_2S to SO_2 and S_x as a function of temperature for acid-gas compositions ranging from 100% H_2S content, providing the diluting gas (N_2 or CO_2) remains chemically inert;

(2) the estimation of non-equilibrium reaction paths in the front-end burner, from a specified inlet temperature and gas composition to a final flame temperature at which chemical equilibrium is assumed to be reached;

(3) the use of these reaction paths to facilitate comparison of actual burner performance with the equilibrium prediction; and,

(4) the estimation of sequential cooler and catalytic converter paths after the waste-heat boiler.

This predicted reaction path diagram may be compared to the actual process operating conditions when the latter are plotted on the equilibrium conversion-temperature diagram. Comparison of actual reaction paths and conversion per stage with predicted values should provide a useful criterion for determining detrimental or improved process conditions.

1.3.2.3 Prediction of Reaction Path in the Catalytic Converter

In a "once-through" sulfur recovery process, additional sulfur is formed by alternately cooling the gas stream and then passing it through a bed of catalysts. Elemental sulfur produced may be removed by cooling between stages. The graphical procedure to predict the overall process performance then requires calculating adiabatic conversion - temperature paths for the catalytic stages as well as for the front-end burner section. The heat release in the beds of catalysts is usually substantial, necessitating cooling between catalytic stages. The large diameter of 15 to 20 feet and comparatively shallow depth of 3 to 4 feet of catalyst beds for the Claus process ensure that the assumption of adiabatic operation is realistic.

In this study the catalyst bed was modeled in the two-phase mode originally proposed by Liu and Amundson (62,63) to check the effect of external transport limitations using pre-estimated internal transport effects. The internal transport limitations were checked by the Paterson's asymptotic method (82) and by Van Den Bosch's interior collocation method (99), and finally a standard computation was performed by applying the method of Weisz and Hicks (106) in computing the effectiveness factor in the Claus reaction

system. The computations were all performed on the basis of the rate equation (1.7) obtained by Liu (66) on the Alon catalyst.

Using the computed results the converter design or catalyst performance may be easily obtained since the effectiveness factor is readily accessible on the Thiele modulus - effectiveness factor diagram for this specific catalyst and reaction condition.

CHAPTER II

LITERATURE SURVEY

2.1 Claus Process:

Sulfur recovery units of the Claus type with a thermal and one or more catalytic stages have been applied for more than twenty years in oil refineries and natural gas treating plants in those instances where large quantities of hydrogen sulfide are produced.

In the modern modified form of the Claus process a number of stages, usually three or four today, of catalytic reaction are used to increase yield of the elemental sulfur since the high exit temperature in a single-stage converter could limit sulfur yields to the equilibrium values. The sulfur recovery efficiency has been closely approached to the theoretically possible yield ranging 94 to 96 percent recovery (26). The remaining 4 to 6 percent of the sulfur present in the Claus unit off-gas, is converted into sulfur dioxide in a catalytic reactor or a thermal incinerator, and then discharged into the atmosphere.

The overall Claus process consists of two stages, in which one-third of hydrogen sulfide is burned completely to form sulfur dioxide in the first stage

according to the reaction (1.1). The product gas from this step is then blended with the remaining two-thirds of hydrogen sulfide and passed to a catalytic converter wherein hydrogen sulfide and sulfur dioxide formed elemental sulfur and water as presented in reaction (1.2).

Hydrocarbons present as impurities fed to the furnace with hydrogen sulfide are converted to carbon dioxide or else pass through as hydrocarbons in the Claus reaction process. Carbon dioxide and some hydrogen sulfide react in the furnace to form carbonyl sulfide according to reaction (1.4). Some carbonyl sulfide appears to pass through the catalytic reactors and is therefore lost. So desulfurization of Claus off-gases has recently received special attention (6,50,78) since stricter emission control regulations require increased efficiencies of the sulfur removal processes. However, most of Claus tail-gas treating processes have proven to be rather costly (6) and the best approach may therefore be to improve the performance of the Claus process itself in the hope of eliminating the need for subsequent tail-gas processing.

2.2 Sulfur Recovery Processes Related to Claus Units:

Numerous processes have been studied and proposed for recovery of sulfur from hydrogen sulfide-

containing waste gas streams (95). Most of these processes can be divided into three major categories which are related to the Claus process.

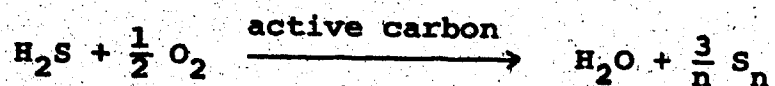
- (1) Direct catalytic conversion to sulfur.
- (2) Absorption and catalytic conversion to sulfur.
- (3) Adsorption and catalytic conversion to sulfur.

Direct catalytic conversion scheme is applied for high concentration of hydrogen sulfide and is the most widely used process in present sulfur recovery plants from natural gas, and will be discussed in more detail in the following section.

The absorption or adsorption scheme before conversion to sulfur is usually applied for gas streams with low concentration of hydrogen sulfide to provide high concentration of hydrogen sulfide in the absorption medium or in the adsorbed state which is enough to initiate the catalytic reaction. In the absorption process, various organic and inorganic liquid solutions are employed as an absorbent such as potassium carbonate, sodium hydroxide, and monoethanolamine or diethanolamine (95). One typical example of such a process is the SCOT process (78) which was developed to increase the efficiency of Claus conversion by absorbing H_2S from the Claus off-gas in which it is present in very low concentration.

The adsorption process usually involves zeolite, activated carbon, or alumina as an adsorbent. The main objectives are to use the adsorbing properties to increase the dilute hydrogen sulfide concentration and then, the ability to act as a catalyst for the reaction of hydrogen sulfide and sulfur dioxide.

In the presence of free oxygen, hydrogen sulfide is catalysed to elemental sulfur by activated carbon as indicated by the following reaction (69).



Another different approach to hydrogen sulfide control is the Sulfreen process developed by Lurgi Apparate-Technik and S.N.P.A. (58). This process utilizes the catalytic ability of activated carbon for a high efficiency of Claus redox reaction to yield elemental sulfur.



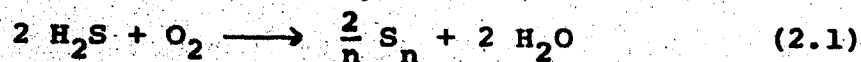
Overall removal efficiency of a Claus-plus-Sulfreen plant has been reported to reach 99.0% or more with sulfur removal efficiency of Sulfreen process of up to 85% (58,69). The Ram River plant in Alberta, started up in 1972, has a Claus unit followed by the Sulfreen process.

2.3 Simultaneous reactions in Claus Units:

Major reaction in the Claus unit in a sulfur recovery plant is the catalytic reaction between H_2S and SO_2 . However, appreciable amount of COS or CS_2 is produced in the furnace and waste-heat boilers by reaction between hydrocarbons and CO_2 in air (33). According to Cameron and Beavon (15) one-third of sulfur loss in the Claus unit is due to the presence of COS which may not easily be converted to elemental sulfur. Therefore, the conversion of COS to elemental sulfur is a very important factor to improve the overall Claus unit performance.

2.3.1 H_2S - Air Reaction

Oxidation reaction between H_2S and air occurs in the furnace and waste-heat boilers of a Claus unit.



$$\Delta H = -123,924 \text{ cal/gmole of } H_2S$$

This reaction provides sensible heat by its large amount of heat of reaction to raise the feed stream temperature of Claus reactants to the catalytic converter. This fact necessitates a better understanding of this oxidation process than currently available

and one aspect of this is the accurate determination of thermodynamic equilibria between H_2S and air under Claus furnace conditions. Then, the adiabatic oxidation reaction path may be predicted based upon the equilibrium data.

After Gamson and Elkins (35) made the first study on the reaction equilibria between hydrogen sulfide and air using Kelley's data (54) for the equilibrium constants between the various sulfur polymers, many investigators paid attention to the equilibrium calculation using various kinds of techniques.

Recently McGregor (72) used White's free energy minimization technique (108) to compute the reaction equilibrium in Claus process units using the free energy data compiled by McBride et al. (71) to get results of a slightly higher equilibrium conversion level than Gamson and Elkins'.

Bennett and Meisen (9) computed the reaction equilibrium for the reaction between H_2S and air over the temperature range of up to $2000^\circ K$. In their calculation they included significantly increased number of chemical species thought to be present at equilibrium under the condition of oxygen to hydrogen sulfide feed ratio of 0.2 to 1.8. The computed results have shown that considerable amounts of SO , SH , S_2O , H_2S_2

and H_2 are present at equilibrium condition at higher temperature range of above $1500^\circ K$. They also included in their calculation S_7 , S_1 , S_3 , S_4 and S_5 in addition to S_2 , S_6 and S_8 which was employed by McGregor's computation (72). For all the species included the results by Bennett and Meisen (9) were almost the same as McGregor's with their computed results falling in the range between Gamson and Elkins' and McGregor's. Bennett and Meisen (9) demonstrated that stoichiometric feed ratio of H_2S and air is the best strategy for sulfur yield without an additional preheater before the furnace.

Neumann (80) investigated the effect of CO_2 and H_2O content on the equilibrium conversion of H_2S by the reaction of H_2S with air in the front-end burner of a Claus unit over the temperature range between 800 and $2500^\circ K$. In his material balance calculation S_2 was considered to be the only sulfur species existing in the product stream. According to his data, the conversion of H_2S was adversely affected by the presence of H_2O but favorably by CO_2 in the feed stream. His computed results also indicated that no significant amount of CS_2 , SO_3 , O_2 , CH_4 , NH_3 , NO and NO_2 were produced in the front-end burner over the above temperature range.

On the other hand catalytic oxidation of H_2S with oxygen has been an interesting subject in the pollution and odor control point of view. Ross and Jeanes (92) studied the oxidation of hydrogen sulfide over cobalt molybdate on α -alumina and related catalysts using an integral reactor to reduce the hydrogen sulfide concentration below the odor threshold level, 0.007 ppm.

Steijns and Mars (96) studied the catalytic oxidation of hydrogen sulfide into elemental sulfur with molecular oxygen over the temperature range of 130 to 200°C employing active carbon, molecular sieve 13X and liquid sulfur as catalysts. The results showed that liquid sulfur acts as a catalyst for H_2S oxidation. The kinetics and the activation energy of the reaction were found to be essentially equal on various catalysts of different chemical composition. They also found that the small pores less than 12 Å in pore diameter were filled with sulfur and the catalyst surface area was lost as the reaction proceeds. The catalyst, however, was found to be almost equally active as the sulfur-free catalyst, which could be explained by the catalytic ability of liquid sulfur trapped in the pores.

2.3.2 H₂S - SO₂ Reaction

After Claus (20) discovered the catalytic reaction process between H₂S and SO₂ over the iron oxide catalyst, the Claus process has become the common sulfur recovery scheme from H₂S produced in the coke oven until the late 18th century. Starting from the significant contribution by Gamson and Elkins (35), who studied this reaction in an integral bed reactor packed with 4/8 mesh Porocel catalysts, many researchers (22,35,36,65,72) devoted themselves to improving this famous process. Many of the research activities have been focused on the development of improved catalysts.

The catalysts usually employed for this reaction were sulfides or oxides of aluminum and other transition elements. Among these iron oxide, bauxite, manganese oxide, alumina, glass alumino silicate, cobalt sulfide, molybdenum sulfide and cobalt molybdenum-alumina have been most frequently studied. Recently active carbon and liquid sulfur have also been the subject of many research projects (58,96).

Claus originally used iron oxide for his invention of this process. But today, bauxite has become one of the most popular catalysts used in Claus sulfur plants. One of the problems related to the bauxite catalyst is the mechanical strength of the catalyst pellets.

In an early stage of this process, Gamsqn and Elkins (35) studied the kinetics of the reaction between H_2S and SO_2 in an integral bed reactor using alumina as a catalyst in their pioneering work for this Claus reaction kinetics. The data were obtained at very low space velocity of 240 to 1920 hr^{-1} over the temperature range of 230 to 300°C. The resulting conversions of H_2S to elemental sulfur were 92.9 to 97.9% which were inconsistent with their thermodynamic analysis of this reaction because their measured conversions were higher than thermodynamic equilibrium conversions for the given reaction temperature and pressure.

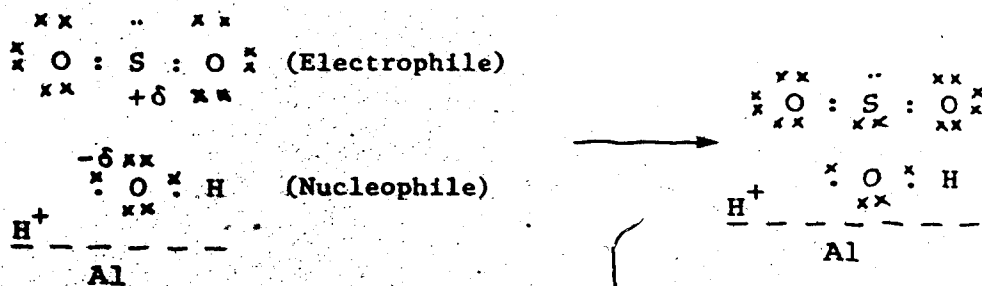
Pyrex glass surface was found to be an active catalyst for this Claus reaction by Taylor and Wesley (97). The proposed reaction rate on the glass surface was proportional to the external surface area of glass with the reaction order being a first order with respect to SO_2 partial pressure and 3/2 order with respect to H_2S partial pressure.

Hammer (45) studied the kinetics and mechanism of major reaction of the sulfur plant using cobalt-molybdenum-alumina catalyst mixtures in the glass differential reactor. From his experimental data Hammer (45) concluded that Claus reaction takes place predominantly on the external surface of the catalyst.

A dual site mechanism for H_2S and SO_2 on the catalyst surface was proposed by Hammer (45). According to this mechanism adsorbed H_2S dissociates into H^+ and SH^- and then reacts with adsorbed SO_2 .

Deo et al. (28) studied the adsorption and surface reaction of H_2S and SO_2 on γ -alumina using an infrared spectrometric technique to conclude that a strong hydrogen bonding exists between both H_2S or SO_2 and surface hydroxyl groups and a chemisorbed form of SO_2 exists on γ -alumina which reacts with H_2S according to the Claus reaction.

Most of the adsorption of H_2S and SO_2 on γ -alumina were found to be physical adsorption on Lewis-acid sites (67). But chemisorption has been generally regarded as a precursor to catalytic reactions. Liu and Dalla Lana (67) found that the chemisorption of H_2S and SO_2 on basic sites of γ -alumina was very small but vitally involved in the reaction mechanism. On the other hand Khalafalla and Haas (57) proposed a mechanism for the chemisorption of SO_2 on an OH^- nucleophilic site as



George (37) used a commercial cobalt-molybdate on γ -alumina (Girdler G-35) as a catalyst to study the Claus reaction in the integral bed reactor. The initial rate was obtained by fitting the experimental data to the expression proposed by Mezaki and Kittrell (76)

$$X = A_1 \tanh \left[A_2 \left(\frac{W}{F} \right) \right] \quad (2.2)$$

and extrapolating to zero conversion. The resulting rate expression for H_2S-SO_2 reaction was

$$-r_{H_2S} = \frac{k P_{H_2S}}{(1 + 0.1 P_{H_2O})} \quad (2.3)$$

George also noted sulfidation of catalyst particles during the reaction by observing the change of color of the catalyst from original deep blue to black.

On the effect of mass transfer resistance in the Claus reaction system Landau et al. (59) studied H_2S-SO_2 reaction over a bauxite catalyst and concluded that the reaction was controlled by mass transfer resistance. Unfortunately, however, these authors did not investigate whether it was film or pore diffusion effect which was controlling the reaction rate.

McGregor (72) also investigated the diffusion effect on the reaction rate, under the practical plant

operational condition, concluding that external mass transfer resistance had negligible effect while internal pore diffusion effect was the rate controlling factor through his diagnostic calculation. In McGregor's kinetic study for the reaction of $\text{H}_2\text{S}-\text{SO}_2$ with Porocel catalyst of 28/35 mesh size it was concluded that only the external surface area of the catalyst was actively catalysing the reaction. In spite of the diagnostic calculation results showing the significant effect of pore diffusion, McGregor failed to observe any significant effect of internal mass transfer resistance in the data obtained and concluded that produced sulfur, which would primarily be S_8 at 260°C , would be very slow in diffusing out of the catalyst pore and might be forming a monolayer or more on the internal surface. When a monolayer or more of sulfur forms on the capillary walls, the effective diameter is so reduced that reactants cannot diffuse in and more likely, S_8 which may have been formed within the pore, cannot diffuse out. Sulfur thus presumably remains permanently inside the catalyst pore.

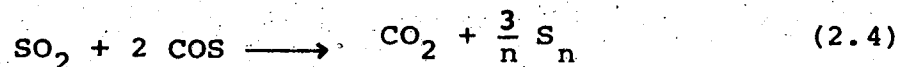
George (37) also investigated the diffusion effect on the reactions $\text{H}_2\text{S}-\text{SO}_2$, $\text{COS}-\text{SO}_2$, and found that there existed significant pore diffusion effect with $\text{H}_2\text{S}-\text{SO}_2$ reaction and negligible with $\text{COS}-\text{SO}_2$ and

COS-H₂O reactions. These results are to some extent foreseeable from the fact that H₂S-SO₂ reaction rate was observed to be much faster than the other two reaction rates.

According to Pearson (83) commercial cobalt-molybdenum catalyst was as active (84% conversion) as the active alumina (S-201) (83% conversion) for H₂S-SO₂ reaction at the reaction temperature of 275°C and the gas space velocity of 50,000 hr⁻¹ in a micro reactor.

2.3.3 COS - SO₂ Reaction

The reduction of SO₂ by COS proceeds according to the reaction



with heat of reaction (60)

$$\Delta H = 6760 - 2.75 T + 0.0028 T^2$$

Lepsoe (60) investigated the kinetics and efficiency of various catalysts for this reaction using a quartz tube reactor filled with catalysts. According to Lepsoe's observation this reaction proceeds slowly even in the absence of a catalyst at 800°C and almost any kind of hot surface is capable of catalysing the reaction at this temperature. Lepsoe (60) also

observed that pyrrhotite was an efficient catalyst for this reaction at 700°C, and at lower temperatures alumina in slightly hydrated and acid-soluble forms (boehmite) was a remarkably efficient catalyst, and that lightly calcined Guiana bauxite and activated alumina were both satisfactory. No detailed investigations regarding the reaction mechanism have been made in his report except the probability of formation of surface compounds between sulfur dioxide and the catalyst. Adsorption of sulfur dioxide was manifested by the fact that the catalyst tenaciously retained sulfur dioxide once it had been exposed to concentrated sulfur dioxide-gas mixtures. The activity of the alumina catalyst was found to be reduced after it was exposed to high temperatures for long periods. In the temperature range of 300 to 600°C, the reduction of SO₂ by COS appeared to be first order with respect to SO₂.

Gamson and Elkins (35) also studied this reaction over bauxite catalysts in an integral bed reactor and found that with a gas stream mole fraction of 5.5% COS, 2.75% SO₂, and 91.75% N₂ yields of 90% or better were obtainable over the temperature range between 250 and 350°C at a space velocity of 200 hr⁻¹, which was far below the practical sulfur plant operational condition.

Liu (19,65) conducted kinetics and mechanistic studies of this reaction using a recycle differential reactor over γ -alumina in the temperature range of 552 to 557°K. It was found that the reaction only proceeds over a short period of time due to catalyst poisoning by carbon dioxide which is one of the products formed by this reaction. Their investigation by means of infrared spectrophotometry showed that carbon dioxide was irreversibly chemisorbed on the surface of γ -alumina and thus presumably occupied the sites important for the reaction, which in turn poisoned the catalyst.

Liu (65) suggested through his IR study on this reaction mechanism that COS was not adsorbed on any of the surface hydroxyl groups of γ -alumina but only physically adsorbed on γ -alumina through sulfur atom at Lewis-acid sites (the surface aluminum ions). Liu (65) also suggested that SO_2 formed hydrogen bonding with the surface hydroxyl group. He attributed the poisoning phenomena in COS- SO_2 reaction on γ -alumina to the chemisorbed CO_2 on the surface Lewis-acid site as a result of the surface reaction between adsorbed COS and SO_2 , eventually making no surface Lewis-acid site available for physical adsorption of COS. Subsequent studies revealed that CO_2 poisoning did not

occur when H_2O was present because of the occurrence of the very rapid hydrolysis of COS to H_2S .

Querido (90) used Cu-on-alumina, CuO-on-alumina, and MoO_3 -on-alumina catalysts to investigate a catalytic reaction between COS and SO_2 at the temperature range of 986 to 506°F with contact times ranging from 0.07 to 0.35 sec. in a tubular reactor. In Querido's experiments, CuO-on-alumina performed well only at temperatures above 1000°F while MoO_3 -on-alumina was poisoned very quickly by sulfur. His results showed that Cu-on-alumina catalyst was most active for COS- SO_2 reaction.

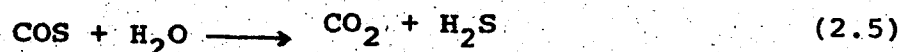
George (37) also studied on kinetics of this reaction using cobalt-molybdate on γ -alumina catalyst in a integral bed reactor. The resulting rate expression was reported to be first order with respect to COS and zero order with respect to SO_2 with an activation energy of 18.0 kcal/gmole. In his study any poisoning effect by CO_2 product in this reaction was not observed on cobalt-molybdate on γ -alumina catalyst which was in contrast to the strong poisoning effect by CO_2 on pure γ -alumina catalysts as reported by Chuang et al. (19).

George (36) also revealed that catalyst basicity had no significant influence on the reaction rate of COS- SO_2 reaction on the cobalt-molybdate on γ -alumina

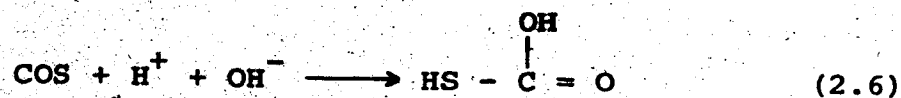
catalyst, and that CO_2 adsorption on this catalyst was reversible, which is in contrast to the observations on the pure γ -alumina catalyst by Chuang et al. (19).

For $\text{COS-SO}_2\text{-H}_2\text{O}$ reaction Pearson (83) obtained a conversion level of 29% with commercial cobalt-molybdenum catalyst and 12% with the active alumina catalyst at the reaction temperature of 275°C and the gas space velocity of $50,000 \text{ hr}^{-1}$ in a micro reactor. For the low space velocity of around 400 hr^{-1} , however, the difference in catalyst activity could not be detected since the conversion level was 100% for both catalysts with $\text{COS-SO}_2\text{-H}_2\text{O}$ reaction.

2.3.4 COS - H_2O Reaction



Buchböck (14) studied the reaction of COS in aqueous water to find that this reaction was catalysed by hydroxyl ion. The proposed mechanism of OH^- catalysed reaction was



Buchböck also found that the reaction closely followed the unimolecular reaction mechanism at $15 \sim 40^\circ\text{C}$ with the reaction rate constant of $\ln k = -11737/T + 45.66$,

which corresponded to an activation energy of 23240 cal/gmole.

Thompson et al. (98) extensively investigated the reaction kinetics between COS and H₂O in the aqueous solution, in alcohol, and in the gas phase. Their reaction rate constant was given by

$$k = 1.06 \times 10^{12} \exp(-22179/R_g T)$$

for the reaction in aqueous solution. For the gas phase reaction the activation energy was found to be 25720 cal/gmole.

Namba and Shiba (79) studied the kinetics of hydrolysis of COS and CS₂ on the alumina catalyst at the temperature range of 220° to 330°C. The rates of hydrolysis in both reactions were found to be of first order with respect to COS or CS₂ with activation energy of 2.9 kcal/gmole and 9.6 kcal/gmole respectively.

A reaction rate proposed by George (37) for COS-H₂O reaction over cobalt-molybdate on γ -alumina catalyst was first order with respect to COS and zero order with respect to H₂O, and activation energy was 12.0 kcal/gmole. According to George's data this hydrolysis reaction rate is five times faster than the rate of COS-SO₂ reaction but fifteen times slower than the rate of H₂S-SO₂ reaction on the same cobalt-molybdate on γ -alumina catalyst.

George (36) also found that catalyst basicity significantly increased the rate for COS hydrolysis reaction. His data showed that the hydrolysis rate over the cobalt-molybdate on γ -alumina catalyst containing 3.9% NaOH was 25 times faster than the rate over the same catalyst without NaOH loading at 230°C. This increased rate was explained in terms of the presence of abstractable protons in the reactants.

Pearson (83) found that the active alumina (S-201) was almost two times as active (85% conversion) as commercial cobalt-molybdenum catalyst (43% conversion) for the hydrolysis reaction of COS at the temperature of 275°C and the gas space velocity of 50,000 hr^{-1} .

2.3.5 Sulfur Species Association-Dissociation Reaction

Experimental investigations on the degree of association between sulfur atoms existing in sulfur vapor can be traced back well over a century. After careful scrutiny of his experimental data, Preuner (88) concluded that four species (S_8 , S_6 , S_4 and S_2) were adequate to explain his experimental isotherm at 448°C. However, Preuner and Schupp (89) corrected Preuner's previous conclusion when they obtained experimental data covering the temperature range of 300° to 800°C and pressures of 7.5 to 1182 mm Hg, which could be

fitted with the assumption of three species (S_8 , S_6 , and S_2). Again, there was another correction of the Preuner and Schupp's data by Braune et al. (12) after they measured sulfur vapor density. These latter authors argued that S_8 , S_6 and S_2 were insufficient to explain their experimental results, and they revived S_4 thus returning to Preuner's initial conclusion.

The heat of dissociation given by Preuner and Schupp, and Braune et al., is tabulated in Table 1.

TABLE 1. HEAT OF DISSOCIATION OF SULFUR SPECIES

<u>Reaction</u>	<u>ΔH in cal/gmole</u>	
	<u>Preuner & Schupp</u>	<u>Braune et al.</u>
$S_8 \rightleftharpoons 4 S_2$	99600	92180
$S_6 \rightleftharpoons 3 S_2$	67100	63710
$S_4 \rightleftharpoons 2 S_2$	-	28400
$3 S_8 \rightleftharpoons 4 S_6$	30500	21700

Berkowitz and Marquhart (11) confirmed the presence of S_2 , S_3 , S_5 , S_6 , S_7 and S_8 with negligible amount of S_9 and S_{10} at a temperature of about $400^\circ K$ using a mass spectrometric technique.

Bartlett et al. (7) studied the general kinetics of the conversion of S_6 to S_8 and found that commercial

alumina had a powerful catalytic effect on the conversion of S_6 to S_8 . Their resulted mechanism was based on the polymerization of the S_6 , followed by depolymerization of S_8 which could occur by thermal initiation such as the spontaneous ring-opening of S_6 . Berkowitz and Chupka (10) suggested a mechanism by which the catalytic effect takes place, involves the opening of the S_8 rings of rhombic sulfur with the formation of chains of unknown length. From the data of Preuner and Schupp (89), Kelley (54) developed equations for calculation of equilibrium constants at any temperature for the following reactions.



The equilibrium of the Claus reaction was theoretically investigated by Gamson and Elkins (35) for the first time considering the equilibrium distribution between the sulfur molecules S_2 , S_6 , and S_8 in the gaseous phase using the data by Kelley (54).

Peter and Woy (84) calculated the equilibrium constant of the Claus reaction from the known thermodynamic data such as the standard entropy, enthalpy, and heat capacity of each component involved. In their calculation they considered S_2 to be the only sulfur specie in the product stream, which did not seem to be

realistic.

McGregor (72) and Liu (65) using the data by McBride et al. (71) calculated the equilibrium compositions in Claus reaction system assuming that there are only three species of sulfur molecule, S_8 , S_6 and S_2 , over temperature range of 550° to 1600°K.

Recently Detry et al. (29) obtained heat of reaction and entropy data for sulfur species association-dissociation reactions using the electrochemical Knudsen-cell with a mass spectrometer over temperature range of 200° to 400°C.

Rau et al. (91) derived a set of equations to calculate partial pressures of different sulfur species as a function of total pressure and temperature of the system by fitting their measured data of sulfur vapor density to equilibrium constants calculated from the thermodynamic properties given by Detry et al. (29) over the temperature range between 823 and 1273°K. In their calculation fugacity coefficients were included to correct equilibrium constants which described the equilibria between S_2 and all the other sulfur species when pressures are high. They found that partial pressures of S_6 , S_7 and S_8 showed, at low temperatures, a completely different variation with temperature to that found experimentally by Detry et al. (29). Bennett and Meisen (9) used the thermodynamic data for sulfur

species based on Detry's measurements (29) in their calculation of equilibrium compositions in the Claus furnace at temperatures as high as 2000°K. Their results were generally in good agreement with those of McGregor (72) or Gamson and Elkins (35) though the conversion level of H₂S was lower than that of McGregor but higher than Gamson and Elkins. In addition to the minimum conversion at approximately 850°K suggested by Gamson and Elkins (35), Bennett and Meisen (9) suggested that there could be maximum conversion at approximately 1700°K. This suggestion was based upon the possibility of the existence of HS or SO at the equilibrium state. The physical reason of this maximum conversion was attributed to the fact that elemental sulfur might undergo oxidation at elevated temperatures. For all their sophisticated arguments for including all the possible species involved in Claus process, Bennett and Meisen's results showed much larger discrepancies from the actual experimental data obtained in the present study than those predicted by McGregor. Regarding the controversial aspects on the morphology of the sulfur species, McGregor's simple approach was employed in this study to predict the equilibrium composition.

The equilibrium distribution of sulfur species between 400°K and 1100°K at the atmospheric pressure is shown in figure 1 computed by McGregor's method.

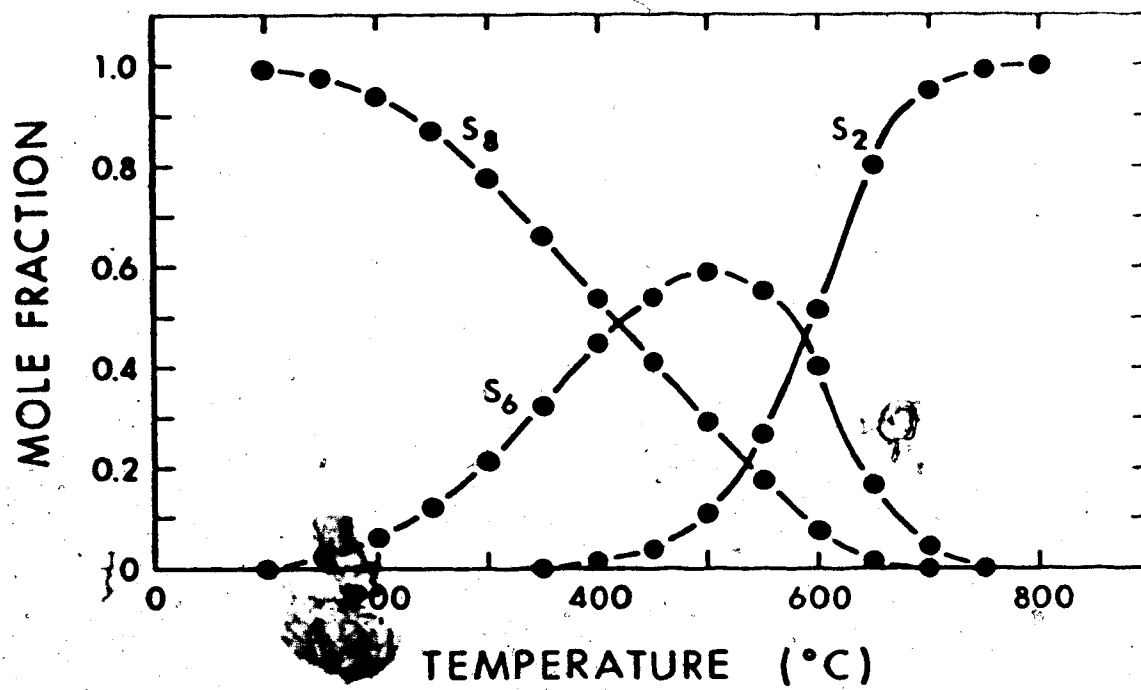


FIGURE 1: EQUILIBRIUM DISTRIBUTION BETWEEN SULFUR SPECIES AT ONE ATMOSPHERE (72)

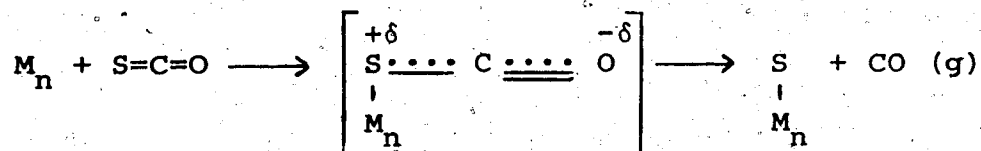
2.4 Catalysis By Some Transition Elements:

High activity of transition metals in the catalysts has been known for a long time (4) and transition metals have been applied as effective catalysts in many practical processes (40,87). Nickel or cobalt sulfides were found to be active catalysts for the Claus reaction by Griffith et al. (41), and any readily sulfidable metal was a suitable Claus catalyst according to Marsh and Newling (70) as cited by Pilgrim and Ingraham (87).

Haas et al. (44) investigated the activity patterns in the catalytic reduction of SO_2 by CO on some transition elements on alumina in an integral flow reactor. In their studies the pure alumina was found to be not so active as the alumina that contained transition metal. They tested the alumina catalyst impregnated with various kinds of transition metals such as titanium, vanadium, chromium, manganese, iron, cobalt, nickel and copper to find that chromium and iron on alumina were the two best catalysts for SO_2 -CO reaction. The impregnated alumina tablets they used contained between 2 and 3 percent transition metals.

The interaction of CO_2 , COS and CS_2 with an evaporated manganese surface was examined by Goodsel and Blyholder (40) using infrared and mass spectral techniques. Their observations indicated that the C=S

bond is more readily broken than the C=O bond on the manganese surface resulting in sulfidation of manganese. The reaction mechanism was given as



The failure of the manganese surface to adsorb CO after exposure to COS was assumed to occur because of the adsorbed sulfur.

Haas and Khalafalla (42,43) found that the addition of a transition metal to alumina inhibited the COS-SO₂ reaction and alumina alone was the most active catalyst for COS-SO₂ reaction. Khalafalla and Haas (56) attributed the decrease in activity of a transition metal-alumina catalyst to the partial loss of pellet internal surface area and porosity by sulfide formation and metal swelling since the molar volume of metal sulfide is greater than that of the metal alone.

2.5 Performance of a Claus Unit:

2.5.1 Importance of Combustion Chamber or Burner Design

As environmental protection requirements became more strict, sulfur recovery efficiencies greater than 99 percent are needed. Improper design of a burner may

cause side reactions like carbon formation when processing sour gases containing hydrocarbons (33). These side reactions disturb the process in the catalytic converter and impair operational safety and optimum sulfur recovery. Design of a combustion chamber or a burner are, therefore, of utmost importance in obtaining a high overall plant efficiency. Practical operational experience has shown that improper design of a combustion chamber on a burner may result in only 15 to 20 percent conversion where about 70 percent conversion should be obtainable based on the H_2S concentration in the sour gas. This difference in performance occurs partly due to the incomplete mixing of feed gas and air, and partly due to formation of carbon soot or ammoniacal sulfur compounds when processing sour gases containing hydrocarbons or ammonia (33). Maximum equilibrium conversion can be attained by mixing the required stoichiometric amount of air with the sour gas (9) before entering the combustion chamber such that the oxygen reacts with H_2S just behind the burner mouth (33). A multiburner system distributed over the entire cross section of the combustion chamber front wall has been shown to be very satisfactory for this purpose.

The formation of COS , CS_2 , H_2 and CO in the burner is dependent upon the CO_2 and CH_4 content in the

sour gas. The major problem with the burner design is related to the fact that measurement of the exact composition of the gas at the burner outlet is almost impossible with suitable measuring methods available at such high temperatures (33). For this reason the theoretical reaction equilibrium calculation is needed as the next best approximation method to predict combustion chamber performance and furthermore to estimate the overall Claus unit performance.

2.5.2 Performance of a Catalytic Converter

Catalytic converters of modern Claus type sulfur plants are mostly designed for space velocity of 650 to 900 SCFH of reactant gas mixture per cubic foot of catalyst bed volume. The catalyst is contained in horizontal drums of about 60 feet long and 13 feet in diameter with flow downward through the bed which is packed to a depth of 3 to 4 feet.

The efficiency of sulfur removal in Claus units has recently been reported to be improved by reducing the reaction temperature below the dew point of sulfur vapor (38). However, this low temperature operation has a disadvantage of sulfur deposition on the catalyst which may necessitate catalyst regeneration. In a conventional Claus plant, the reaction between H_2S and SO_2 occurs exothermically below about $800^\circ K$, thus being

avored by decreasing the reaction temperature, but occurs endothermically above about 800°K, thus being favored by increasing the reaction temperature. The reaction can be pushed to completion by removal of product sulfur from the product mixture. The operating conditions for each reactor are normally selected so that all sulfur formed by the reaction remains in the vapor state, i.e., the reaction mixture is always above the sulfur dew point. To obtain higher conversions, several successive reaction stages are usually provided with intermediate condensation and removal of sulfur product. The removal of sulfur permits a reduction of temperature in successive reactors which makes approach to the higher equilibrium conversion level attainable, while still remaining above the sulfur dew point.

As the desired conversion level in Claus reaction increases, the possible sulfur losses due to COS, CS₂ and elemental sulfur vapor play a more important role. Carbonyl sulfide and carbon disulfide are formed in the burner section of the sulfur plant, but can be hydrolysed and eventually converted to elemental sulfur by applying appropriate controlling conditions and catalysts in the catalytic reactor system (38). Increasing the temperature of the first reactor of a two-reactor system may decrease the loss of sulfur as

COS and CS₂ in the tail gas. However, the higher temperature may result in less favorable Claus reaction equilibrium and tend to increase the loss of sulfur as H₂S and SO₂ in the tail gas (38). Addition of a third reactor may reduce the loss of H₂S and SO₂, but have little effect on COS and CS₂.

One of the practical approach to minimize the loss of elemental sulfur formed in the converter is to operate the final condenser at low temperature and install an efficient mist extractor to reduce entrainment in the tail gas.

2.5.3 Claus Reactor Design

i) Catalytic Reactor Modeling

Various kinds of sophisticated models have been recently proposed in the literature for a heterogeneous catalytic reaction, which may largely be divided into two main categories; pseudo-homogeneous or heterogeneous models.

Pseudo-homogeneous models are employed to extend the mathematical simplicity which is used for a homogeneous reactor modeling. In this kind of model, material and energy balance equations are written separately for the catalyst particles and the interstitial fluid. However, these equations no longer reflect the

concept that discrete particles exist within the reactor bed. All the particles in the bed are treated as a continuous one.

In the heterogeneous models, a catalytic reactor is treated as a series of small continuous flow stirred-tank reactors.

For catalytic reactor analysis, pseudo-homogeneous models are more commonly employed in one- or two-dimensional modes. In this work a one-dimensional pseudo-homogeneous model was employed since the Claus catalytic converter is essentially an adiabatic operation in which radial concentration and temperature gradients are negligible. Even in one-dimensional pseudo-homogeneous models, two different approaches have been considered; a one-phase model and a two-phase model. In the one-phase model, the entire reactor is treated as a homogeneous empty reactor while in the two-phase model, it is assumed that there are two continuous phases, solid catalyst and fluid. As mentioned above, this continuous two-phase model still neglects the particulate aspects of catalyst pellets.

It has been customary to describe fixed-bed catalytic reactors in terms of the one-phase model (47,48). However, for strong exothermic reaction systems, this approach often yields unsatisfactory results because of the differences in the temperatures of the solid and

the fluid phases. In these cases, the two-phase model may be applied to take the gradients between phases into consideration although it involves a highly nonlinear set of differential equations. The behavior of the two phase model has been an interesting subject of many publications for a long period of time due to its importance in practical applications (16,62,102).

ii) One-dimensional Pseudo-homogeneous model

Liu and Amundson (62,63) developed a continuous two-phase model in their analysis of a packed bed reactor, in which the complex behavior in the reactor is concentrated in two homogeneous phases; in the flowing fluid phase and in the fixed catalyst solid phase. They improved Barkelew's simple model (5), which neglected axial and radial dispersion as well as interphase and intraparticle transport resistances, by introducing interphase resistance effects. However, Liu and Amundson still neglected intraparticle resistances so that the reaction was assumed to be controlled completely by interphase effects. They also assumed a uniform velocity profile over the cross-section of the bed and neglected the effects of length of the reactor bed and temperature on the velocity profile. The major purpose of their model was to check the existence of multiple

steady states in the catalytic bed depending upon the state of the individual catalyst particles. In their investigation the effects of the inlet gas temperature and the inlet partial pressure of reactants upon the concentration and temperature profiles were also examined, and the stability of the adiabatic packed bed reactor was found to be dependent upon the existence of multiple steady-states for single particles; if every particle along the bed axis had only one steady state, then the reactor would be stable, and unique concentration and temperature profiles would result for all initial particle temperatures and concentrations. On the other hand if a single particle in the reactor has multiple steady states, then, from continuity of the mathematical model, adjacent particles would undoubtedly exhibit multiple steady states.

Hlavacek et al. (49) investigated the effect of Peclet number for mass and heat transfer in the adiabatic tubular reactor using a dispersion one-phase model. Their results showed that higher ratio of mass transfer Peclet number to heat transfer Peclet number enlarged the domain of multiple solutions.

The effects of axial dispersion were checked by Liu and Amundson (64) to find that in the multiple steady state the profiles of temperature and concentration were appreciably more sensitive to axial dispersion

than in the single steady state. Eigenberger (30) extended the model by Liu and Amundson (62) by including the effect of effective heat conduction term in the catalyst phase heat balance equation. His computations indicated that the temperature maximum could move to the front of the reactor due to the backward conduction of heat; compared to the case without effective heat conduction in the catalyst phase.

Votruba et al. (102) used a piston flow model of a tubular adiabatic fixed bed reactor with external heat and mass transfer for description of temperature and concentration profiles along the reactor using the two-phase model developed by Liu and Anundson (62). They neglected axial dispersion and conduction through catalyst pellets as well as resistances within the porous catalyst structure. They only considered the convective mass and heat transfer in the axial direction and external heat and mass transfer on the catalyst surface as transport mechanism within the bed. Their computed results revealed that there could be multiple steady states within the reactor due to the external heat and mass transfer resistances over some range of parameter values.

Eigenberger (31) also investigated the effect of different boundary conditions in the frontal surface of the catalyst bed using the two-phase model taking

heat conduction into account. His boundary condition for the front end of the catalyst bed was

$$k_e \left(\frac{\partial T_s}{\partial Z} \right)_{Z=0} = C_R \left[(T_s)_{Z=0}^4 - \left\{ \frac{(T_s)_{Z=0} + T_{fo}}{2} \right\}^4 \right] \dots\dots (2.7)$$

According to Eigenberger's results the usual assumption of an adiabatic termination of the front of the catalyst phase had to be revised in cases where a high temperature excess of the catalyst phase can occur at the beginning of the reactor. His reasoning was that a certain amount of heat would leave the front end of the catalyst bed by radiation if the catalyst temperature at the entrance exceeds the fluid temperature considerably. Eigenberger also noted that the ignition zone, defined as the region where significant reaction takes place on the catalyst surface for the first time in the bed, was fixed at the entrance of the reactor when the fluid velocity is low while the ignition zone was located in the middle of the bed separated from the entrance when the fluid velocity is high.

Another interesting result shown by Eigenberger was that only one steady state existed with very small fluid velocities or very high fluid velocities. The moving velocity of the creeping profile of the

conversion was significantly affected by the fluid velocity but almost negligibly influenced by the different kind of model applied.

The importance of axial dispersion was considered by Karanth and Hughes (52), who recommended the criterion that there is no significant axial dispersion provided the bed depth be greater than 50 catalyst pellet diameters.

iii) External Transport Resistances

The concentration and temperature difference between the bulk fluid and the catalyst surface is dependent upon the mass - and heat-transfer coefficient between the two phases, the reaction rate constant, and the heat of reaction. The reaction rate constant and the heat of reaction have specific values corresponding to each specific reaction system. However, the values of the mass- or heat-transfer coefficients depend solely upon the kind of fluid and the flow pattern in the fluid phase near the catalyst surface.

Average transport coefficients between the bulk gas stream and the solid particle surface have been investigated by many researchers (13,34,68). Friedlander's approach (34) was to get mass transfer coefficients from the boundary layer analysis around a single solid spherical particle and obtained,

$$S_h = 0.89 S_c^{1/3} R_e^{1/2} \quad (2.8)$$

Froessling's correlation (8) used the method of dimensional analysis to correlate the mass transfer coefficient to the other important dimensionless groups to get

$$S_h = 2 + 0.6 S_c^{1/3} R_e^{1/2} \quad (2.9)$$

For a fixed-bed reactor, Chilton and Colburn (17) developed the correlation for the mass transfer coefficient,

$$j_D = \frac{k_m \rho_f}{G} S_c^{2/3} = f(R_e) \quad (2.10)$$

and by applying the analogy between mass- and heat-transfer phenomena the correlation for the heat transfer coefficient, showed

$$j_H = \frac{h}{C_{pf} G} P_r^{2/3} = f(R_e) \quad (2.11)$$

De Acetis and Thodos (27) have summarized the data available up to 1960 to get the relationship between j_D and R_e as well as between j_H and R_e ;

$$j_D = \frac{0.725}{R_e^{0.41} - 1.5} \quad (2.12)$$

$$j_H = \frac{1.10}{R_e^{0.41} - 1.5} \quad (2.13)$$

In this study De Acetis and Thodos' equations have been employed to estimate the external heat and mass transfer coefficients.

iv) Internal Transport Resistances

In order to obtain a reliable simulation of a fixed bed catalytic reactor performance, it is often necessary to consider the effect of the interaction between diffusion and reaction within a catalyst pellet as well as the effect of the external transport limitations between the fluid stream and the catalyst outside surface, particularly for highly exothermic catalytic reactions. The overall influence of these physical processes on the reaction rate is conveniently expressed by use of an effectiveness factor, which is defined by the ratio of the actual reaction rate to that which would be obtained were there no diffusion limitations. The determination of the effectiveness factor usually requires numerical integration of a rather complicated system of non-linear two-point boundary value ordinary differential equations. Numerous attempts have been made to simplify the equations into a more tractable form and in some instances semi-analytical solutions have been found.

For a spherical catalyst pellet the steady state material and energy balance equations may be written as

$$D_e \frac{d^2 C_p}{dr^2} + D_e \left(\frac{2}{r}\right) \frac{dC_p}{dr} - r_p = 0 \quad (2.14)$$

$$k_e \frac{d^2 T_p}{dr^2} + k_e \left(\frac{2}{r}\right) \frac{dT_p}{dr} + (-\Delta H) r_p = 0 \quad (2.15)$$

Converting the above two equations to dimensionless form by introducing the relationships,

$$y = \frac{C_p}{C_s}$$

$$\theta = \frac{T_p}{T_s}$$

$$x = \frac{r}{L_p}$$

$$\phi^2 = L_p^2 \left(\frac{r_s (P_s, T_s)}{D_e C_s} \right)$$

$$\beta = (-\Delta H) \frac{D_e C_s}{k_e T_s}$$

gives finally,

$$\frac{d^2 y}{dx^2} + \frac{2}{x} \frac{dy}{dx} - \phi^2 \left(\frac{r_p (P_p, T_p)}{r_s (P_s, T_s)} \right) = 0 \quad (2.16)$$

$$\frac{d^2\theta}{dx^2} + \frac{2}{x} \frac{d\theta}{dx} + \beta\phi^2 \left(\frac{r_p(P_p, T_p)}{r_s(P_s, T_s)} \right) = 0 \quad (2.17)$$

The boundary conditions for the above equations depend upon whether external transport resistances are included or neglected. When the latter case is assumed the boundary condition becomes the Dirichlet type

$$\begin{aligned} x = 0, \quad \frac{dy}{dx} = 0, \quad \frac{d\theta}{dx} = 0 \\ x = 1, \quad y = 1, \quad \theta = 1 \end{aligned} \quad (2.18)$$

Should the external transport resistance be taken into account, the boundary condition is of the Neumann type due to the finite rates of convective mass and heat transfer on the surface of the catalyst pellet.

$$\begin{aligned} x = 0, \quad \frac{dy}{dx} = 0, \quad \frac{d\theta}{dx} = 0 \\ x = 1, \quad y = 1 - \frac{1}{S_h} \frac{dy}{dx}, \quad \theta = 1 - \frac{1}{N_u} \frac{d\theta}{dx} \\ \dots\dots (2.19) \end{aligned}$$

For the Dirichlet boundary conditions, Weisz and Hicks (106) developed a simple transformation method to convert the problem into an initial value one which enabled a rapid evaluation of the effectiveness factor-Thiele modulus curve. However, they employed the Adams-Molton iteration technique without

checking the accuracy at the open end of the integration path.

Varma and Amundson (100) applied the maximal and minimal principle to compute the bounds of the effectiveness factor for the infinite slab geometry with Dirichlet boundary conditions.

For Neumann boundary conditions, McGuire and Lapidus (73) solved the problem using the Crank-Nicolson implicit method. However, the difficulties still remained with the large amount of computing time though the accuracy was satisfactory from the engineering point-of-view.

For the purpose of improving the conventional finite difference method in solving the problem related to diffusion with chemical reaction, an orthogonal collocation method has recently been developed by Villadsen and Stewart (101). They employed the interior collocation method in which orthogonality conditions were applied to select the optimum collocation points. The accuracy was found to be comparable to that of conventional methods but with a much simpler computation procedure.

For highly active catalysts, Petersen (85) developed an asymptotic method to solve the non-isothermal Dirichlet problem. The basic idea of this method was based upon the assumption that when the catalyst is

highly reactive, most of the reaction would be confined to a thin layer near the external surface of the catalyst pellet. The conservation equations, therefore, may be approximated by those for a slab, whatever the original pellet geometry may be, and the calculation of the effectiveness factor becomes relatively easy. But this approximation method is not applicable in general at low values of the Thiele modulus, usually below 2 (52).

To improve Petersen's approximation method, Paterson and Cresswell (82) developed the effective reaction zone method. In their proposal, it was assumed that at some point within the catalyst pellet the concentration of a reactant drops to zero value. A parabolic trial function was found to be quite adequate for engineering design purposes and the computational effort involved was very small by using the collocation technique. The major problem involved in this concept was how the appropriate optimum collocation point can be chosen.

Quite recently Van Den Bosch and Padmanabhan (99) examined the efficiencies of different kinds of collocation methods in their ability to predict the effectiveness factor for the Neumann type boundary condition. They recommended the collocation point of $\frac{1}{\sqrt{2}}$ for the high reactivity model instead of $\frac{1}{\sqrt{5}}$ proposed

by Villadsen and Stewart (101). It was found that the accuracy of the orthogonal collocation method could be improved by changing the optimum collocation point from $\frac{1}{\sqrt{5}}$ to $\frac{1}{\sqrt{2}}$ for the high reactivity model proposed by Paterson and Cresswell (82).

The effectiveness factor in the transition regime between the Knudsen and the bulk molecular diffusion in the micropore within the catalyst pellet was treated by Abramov (2,3) and Abed et al. (1) with consideration of the Poiseuille flow in the pores due to the change of the number of moles of the gas along the pore length.

v) Effective Diffusivity

To obtain a reasonable estimation of the effectiveness factor it is necessary to use accurate values of the effective diffusivity for the reactant concerned as well as the physical properties of the catalyst pellet. Satterfield (93) collected a considerable amount of experimental data on effective diffusivities and also proposed estimation methods for the situation where experimental data are not available. Since experimental data are still not sufficient for different reaction systems with different kinds of catalysts, it is frequently required to estimate an effective diffusivity from fundamental data on the reactant and the

catalyst pellet in the absence of the actual data.

To explain the complexity of the pore geometry of the catalyst voids in evaluating the effective diffusivity, some models have been proposed. Wheeler (107) proposed a parallel pore model to represent the monodispersed pore size distribution in a catalyst pellet. In his model, the effective diffusivity was described by

$$D_e = \left(\frac{\epsilon}{\tau}\right) D \quad (2.20)$$

where

$$D = \frac{1}{(1-\alpha y_A)/D_{AB} + 1/D_{KA}} \quad (2.21)$$

$$\alpha = 1 + \frac{N_B}{N_A} \quad (2.22)$$

$$D_{KA} = \frac{2}{3} \left(\frac{8 R_g T}{\pi M_A} \right)^{1/2} R_p \quad (2.23)$$

According to Satterfield (93) the tortuosity factor, τ , can be approximated as 4 for non-surface diffusion catalyst pellets. Here the tortuosity factor was defined by the ratio of the actual diffusion path to the average pore length.

Hideo Teshima (46) obtained experimental data on the effective diffusivity of carbon dioxide in porous chromia-alumina catalyst with average pore diameter of 50 Å and pellet porosity of 0.41 using an isotopic

exchange reaction method. His experimental values were in agreement with the parallel pore model when the tortuosity factor of 3.4 was employed.

Since information about the surface diffusion effect on the catalyst pellet is still limited due to inadequate experimental and theoretical aspects of surface transport phenomena (94), the value of 4.0 for the tortuosity factor for the Alon catalyst pellet was applied in this study.

Johnson and Stewart (51) exploited a model in which a porous material could be represented as a bundle of randomly oriented cylindrical capillaries with different radii. In this model the effective diffusivity was described as

$$D_e = \kappa \int D \, d\sigma(r) \quad (2.24)$$

where

$$\kappa = \frac{\int \cos^2 \theta \, dv(\theta)}{\int dv(\theta)} \quad (2.25)$$

The problem in the Johnson and Stewart model is related to experimental data for the geometric constant, κ , as defined by equation (2.21)

Upper and lower bounds for an effective diffusivity of a binary diffusion system were calculated by Petty (86) but the need for experimental determination of the geometric constant, κ , still could not be eliminated. The importance of the choice of statistics

which best characterizes the pore size distribution function $\sigma(r)$ was emphasized by Petty (86).

Wak and Smith (103,104) proposed a random pore model for a bidispersed catalyst pellet to get an expression for the effective diffusivity;

$$D_e = D_M \epsilon_M^2 + \frac{\epsilon_M^2 (1+3\epsilon_M)}{1-\epsilon_M} D_\mu \quad (2.26)$$

Wheeler's parallel pore model has been applied to estimate the effective diffusivity in the Alon catalyst for this study.

vi) Effective Thermal Conductivity

In addition to concentration gradients, a temperature gradient may also exist within individual catalyst pellets during gas-solid catalytic reactions. This temperature gradient may have a more significant effect on the reaction rate than concentration gradient may have, and hence on the effectiveness of the internal surface of the pellet.

Mischke and Smith (77) measured thermal conductivities of pellets of alumina particles as a function of macropore volume fraction. They found that the thermal conductivity of solid alumina decreases with temperature. The low thermal conductivities of alumina itself indicated that severe temperature gradient could be possible in porous catalysts for highly exothermic

reactions. But the large effects of density of pellets on the effective thermal conductivity suggested that the area of contact between particles in the pellet was a significant parameter which was more important than the conductivity of the solid phase itself.

According to their experimental results, the alumina catalyst pellet of void fraction of 0.4 filled with air at 120°F was found to have the thermal conductivity of 0.082 Btu/hr.ft.°F.

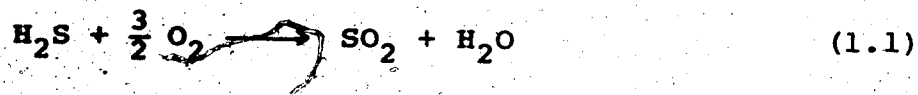
CHAPTER III

PREDICTION OF CLAUS UNIT PERFORMANCE

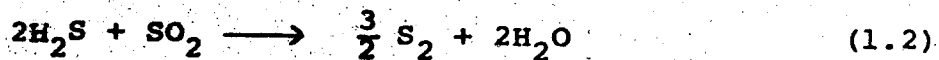
3.1 Performance of the Front-End Burner:

In a conventional Claus process unit, one-third of H_2S in the feed stream is converted to SO_2 in the front-end burner and the remaining two-thirds of H_2S is eventually converted to elemental sulfur in the catalytic converter according to two consecutive reaction schemes (1.1) and (1.2) described in Chapter 1. If an assumption is made that the acid-gas feed stream contains very small amounts of impurities like hydrocarbons, other reactions than reactions (1.1) and (1.2) may be ignored in the calculations to predict the performance of the front-end burner in a Claus unit.

The reaction stoichiometry may be written in terms of fractional conversions of H_2S , α and β , according to reaction schemes (1.1) and (1.2) respectively, in the following way when the two reactions occur in sequence and not in parallel.



$$3-\alpha \quad 1.5(1-\alpha) \quad \alpha \quad \alpha$$



$$3-\alpha-2\beta \quad \alpha-\beta \quad 1.5\beta \quad \alpha+2\beta$$

The assumption of a consecutive reaction scheme is quite reasonable since reaction (1.1) is a very fast combustion process while the reaction (2) is very slow in the absence of proper catalysts even at high temperatures. Furthermore the equilibrium constant is much larger in the reaction (1.1) than in the reaction (1.2) as shown in Table 2 (33).

TABLE 2
EQUILIBRIUM CONSTANTS FOR REACTIONS (1.1) and (1.2)

<u>Temperature, °C</u>	<u>Reaction (1.1)</u>	<u>Reaction (1.2)</u>
700	0.5562×10^{24}	0.9928×10^0
800	0.1388×10^{22}	0.1612×10^1
900	0.9608×10^{19}	0.2394×10^1
1000	0.1449×10^{18}	0.3320×10^1
1100	0.4018×10^{16}	0.4363×10^1
1200	0.1809×10^{15}	0.5495×10^1
1300	0.1205×10^{14}	0.6689×10^1

Since the formation of S_2 by the reaction (1.2) may lead to other forms of sulfur molecules such as S_6 or S_8 , it is necessary to include reactions (1.8) and (1.9) along with the reaction (1.2) to completely describe the reaction system.



$$1.5(1-v_1-v_2) \quad 0.5 \beta v_1$$



$$1.5 \beta(1-v_1-v_2) \quad 0.375 \beta v_2$$

Here v_1 and v_2 are defined as "fraction of the equivalent moles of S_2 which associated to form S_6 or S_8 ", and can be calculated from mole fractions X_2 , X_6 and X_8 obtained in the equilibrium calculation by using the following relationships.

$$v_1 = \frac{3 X_6}{X_2 + 3 X_6 + 4 X_8} \quad (3.1)$$

$$v_2 = \frac{4 X_8}{X_2 + 3 X_6 + 4 X_8} \quad (3.2)$$

$$v_0 = 1 - v_1 - v_2 \quad (3.3)$$

The computed results of values of v_1 and v_2 at different temperatures are shown on Figure 2 which was obtained by using the free energy minimization method.

In this reaction, the assumption of the existence of only three different molecular species of sulfur, S_2 , S_6 and S_8 was inevitable since the existence of other sulfur species was still controversial.

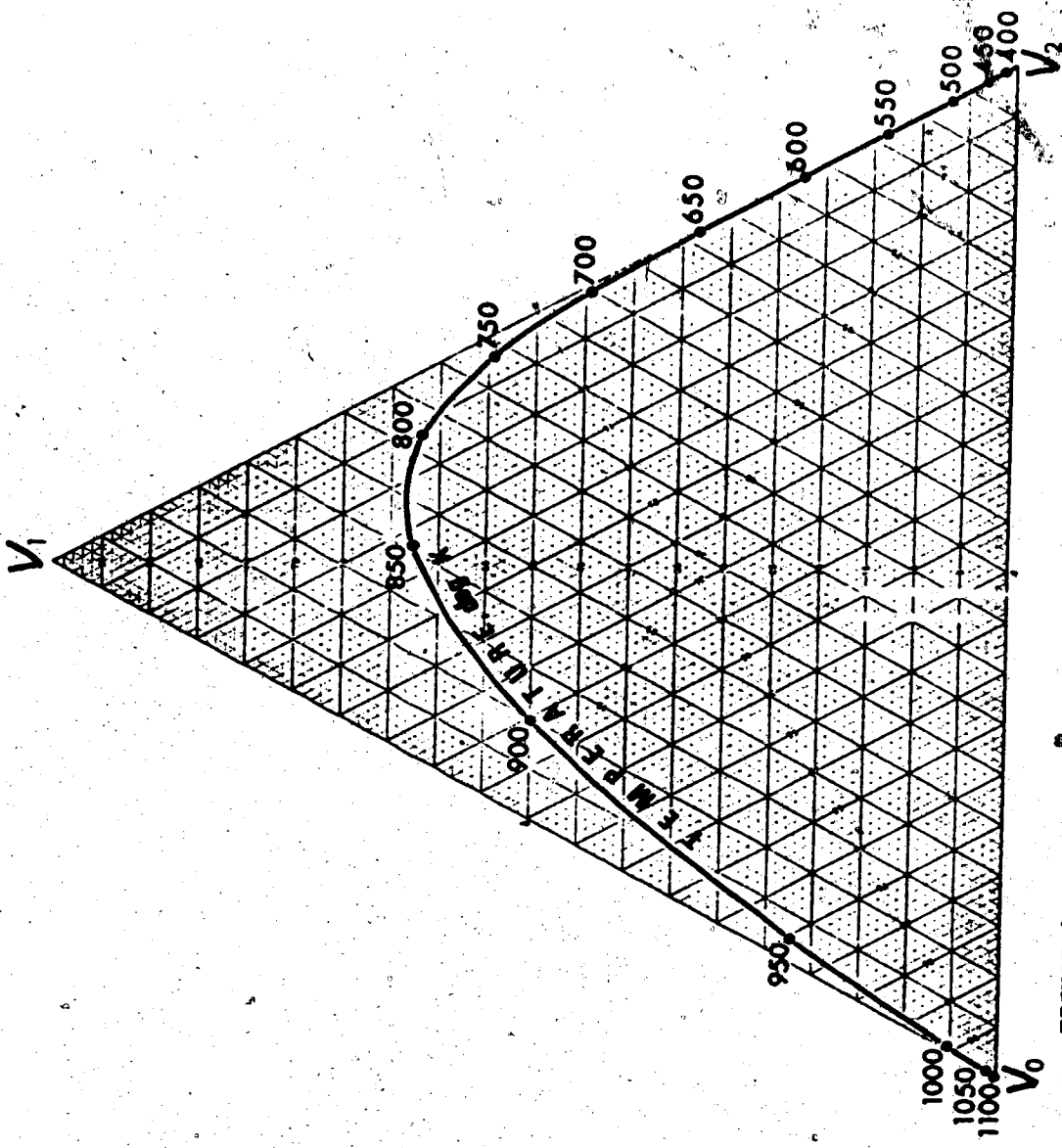


FIGURE 2: FRACTION OF THE EQUIVALENT MOLES OF S₂ ASSOCIATED TO S₆ OR S₈ AT ONE ATMOSPHERE

and no reliable data for them were available over the practical temperature range of the burner condition. In calculating the equilibrium composition of a particular gas mixture at a fixed temperature, the equilibrium distribution between S_2 , S_6 and S_8 was assumed. In tracing reaction paths which do not follow a sequence of equilibrium compositions, e.g. adiabatic reaction paths involving the reaction (1.2), the distribution of the S_n compounds may not be predicted because the reaction rate data are not available for these association-dissociation reactions between sulfur species. For this kind of situation it is often assumed to facilitate calculations along the reaction path that the various species of elemental sulfur will self-equilibrate along that path.

It was also assumed that the feed H_2S could be completely mixed with stoichiometric amount of air to form a uniform homogeneous reactant mixture right after the entrance of the burner. This condition may be easily achieved by modifying the burner chamber using some baffles or vanes in the path of the reactant stream.

All reaction components were assumed to be in the gas phase and to exhibit perfect gas behavior over the range of compositions and temperatures encountered. A constant pressure of one atmosphere was employed

throughout the calculations by neglecting the effect of change of the mole number within the reaction system. Quantitatively the increase of the total number of moles in reaction (1.1) is 0.5 mole per 10.14 moles of the feed mixture as illustrated in Figure 7. The change of the total number of moles due to reaction (1.2) depends upon the reaction temperature. After reaction (1.1) has been completed, the temperature in the front-end burner becomes high enough, as shown in Figure 4, to make the average number of atoms in sulfur species smaller than 3. Then a net increase in the total number of moles can be predicted due to reaction (1.2). Therefore, the approximate maximum pressure decrease due to reaction (1.1) and (1.2) is expected to be about 5 percent of the feed pressure.

The following data for heat of reaction (54) were used for reactions (1.1), (1.2), (1.8) and (1.9).

$$\Delta H_{298}^{\circ} (1) = -123,924 \text{ cal/gmole of H}_2\text{S}$$

$$\Delta H_{298}^{\circ} (2) = 5,625 \text{ cal/gmole of H}_2\text{S}$$

$$\Delta H_{298}^{\circ} (7) = -22,673 \text{ cal/gmole of S}_2$$

$$\Delta H_{298}^{\circ} (8) = -24,753 \text{ cal/gmole of S}_2$$

The product mixtures were assumed to contain N_2 , H_2S , SO_2 , O_2 , H_2 , S_2 , S_6 and S_8 . The thermodynamic

equilibrium compositions between different sulfur species along the reaction path were obtained using the free energy minimization method (72) and published thermodynamic data (71,105). The derivation of equations to get adiabatic reaction paths in the front-end burner and the related computer programs are presented in Appendix C.

Reference to the form and magnitude of the equilibrium constants for reaction (1.1) and (1.2) as tabulated in Table 1 and described in the following expressions

$$K_{p,1} = \frac{P_{SO_2} P_{H_2O}}{P_{H_2S} P_{O_2}^{3/2}} = \frac{y_{SO_2} y_{H_2O}}{y_{H_2S} y_{O_2}^{3/2}} \pi^{-1/2} \quad (3.4)$$

$$K_{p,2} = \frac{P_{S_n}^{3/n} P_{H_2O}^2}{P_{H_2S}^2 P_{SO_2}} = \frac{y_{S_n}^{3/n} y_{H_2O}^2}{y_{H_2S}^2 y_{SO_2}} \pi^{3/n-1} \quad (3.5)$$

shows that reaction (1.1) is essentially irreversible. Equations (3.4) and (3.5) also show that equilibrium compositions are relatively insensitive to pressure changes, and when the total pressure, π , equals one atmosphere, they are independent of reaction pressure.

The effect of the inert content on the equilibrium conversion can be predicted when the equilibrium constant is described in terms of conversion. Based upon the stoichiometric feed ratio of H_2S and SO_2

in the presence of I-moles of inerts per a-moles of SO_2 , the equilibrium constant for reaction (1.2) may be obtained in terms of the fractional conversion of SO_2 .

$$K_{p,2} = \left(\frac{x}{1-x}\right)^3 \left(\frac{3}{n}\right)^{3/n} \left\{ \left(\frac{N_0}{a}\right) \frac{1}{X} + \left(\frac{3}{n} - 1\right) \right\}^{(1-3/n)} \pi^{(3/n-1)} \quad \text{..... (3.6)}$$

where N_0 is the total initial number of moles in the feed mixture, which is equal to $(3a + I)$. From equation (3.6) it may be found that the equilibrium constant for the Claus reaction is a function of X and $\left(\frac{N_0}{a}\right)$ for a constant value of n at one atmospheric pressure. For the value of n equal to 3, $K_{p,2}$ appears to be constant for a fixed value of X , which means there is no dilution effect on the conversion level due to inert gases as long as the $\text{H}_2\text{S}-\text{SO}_2$ feed ratio is maintained at the stoichiometric 2 to 1 ratio. When n is not equal to 3, the value of $K_{p,2}$ may decrease or increase depending upon the values of $\left(\frac{N_0}{a}\right)$ and n . If n is less than 3, there is a net increase of the total number of moles due to the reaction while a net decrease for the value of n larger than 3. When n is much less than 3, the equilibrium conversion level will increase as the inert content increases. On the other hand, when n is much larger than 3, the equilibrium conversion

level will decrease with the increasing inert content. For the value of n which is around 3, the effect of the inert content on the conversion level cannot be easily predicted from equation (3.6).

The computed results plotted in Figure 3 shows the interesting behavior of the equilibrium conversion level depending upon the inert content and the average number of atoms in the sulfur vapor. Figure 3 really indicates that the conversion level of the Claus reaction can be improved or deteriorated by increasing the inert content in the feed stream depending upon the operating temperature. When the operating temperature is above 900°K , the conversion level increases with the increasing inert content, while the conversion level decreases with the increasing inert content in the temperature range below 750°K .

Figure 4 shows "fractional conversion of H_2S to S_n plus SO_2 " as a function of the reaction temperature where the conversion X is defined by

$$X = \frac{[\text{Moles of } \text{H}_2\text{S} \text{ in acid-gas}] - [\text{moles of } \text{H}_2\text{S} \text{ leaving the burner}]}{[\text{moles of } \text{H}_2\text{S} \text{ in acid-gas}]}$$

..... (3.7)

In Figure 4 the lines below the dotted level of 33.3% conversion level represent reaction paths according to

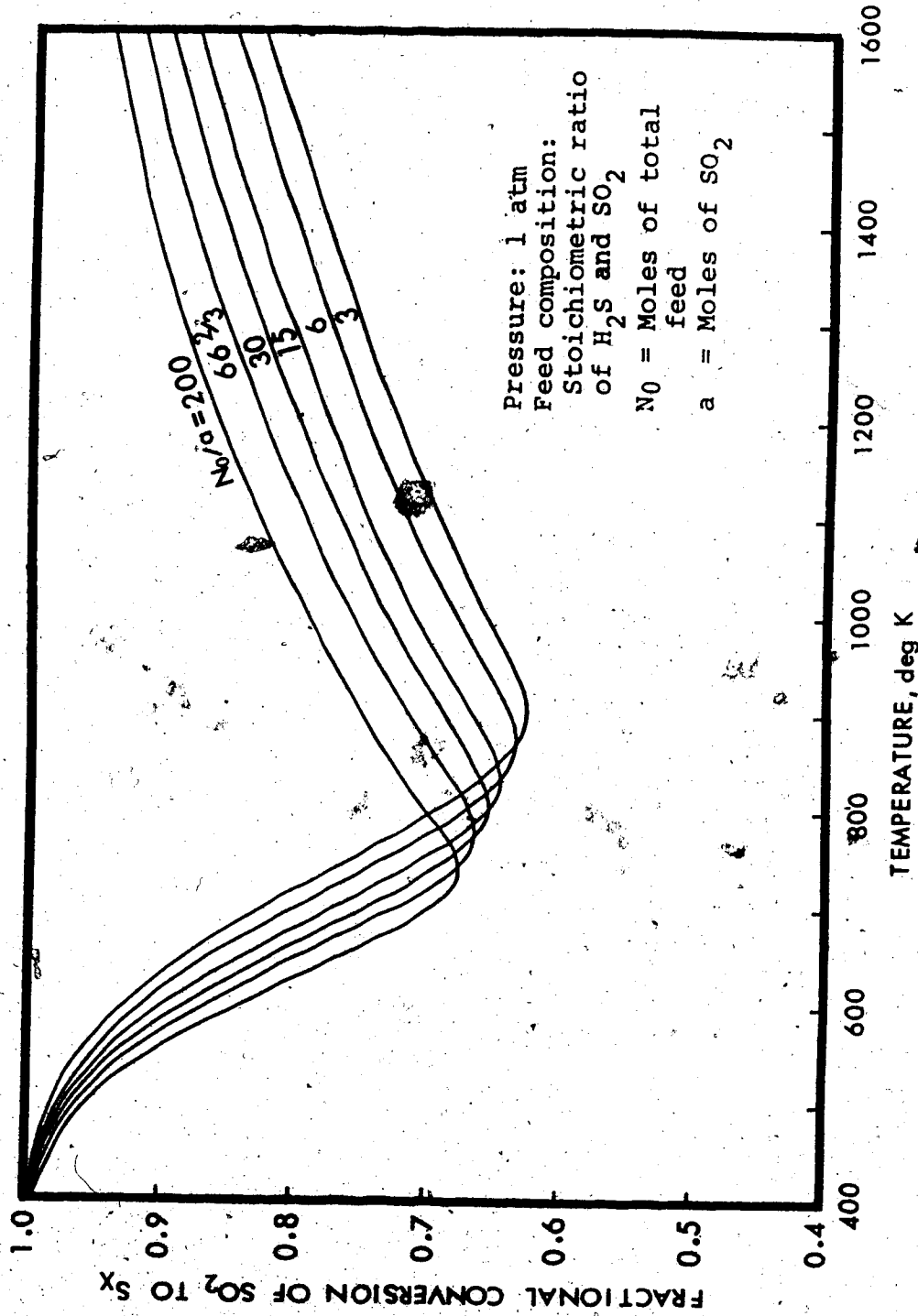


FIGURE 3: EFFECT OF THE INERT CONTENT ON EQUILIBRIUM CONVERSION OF THE CAUS REACTION AT ONE ATMOSPHERE

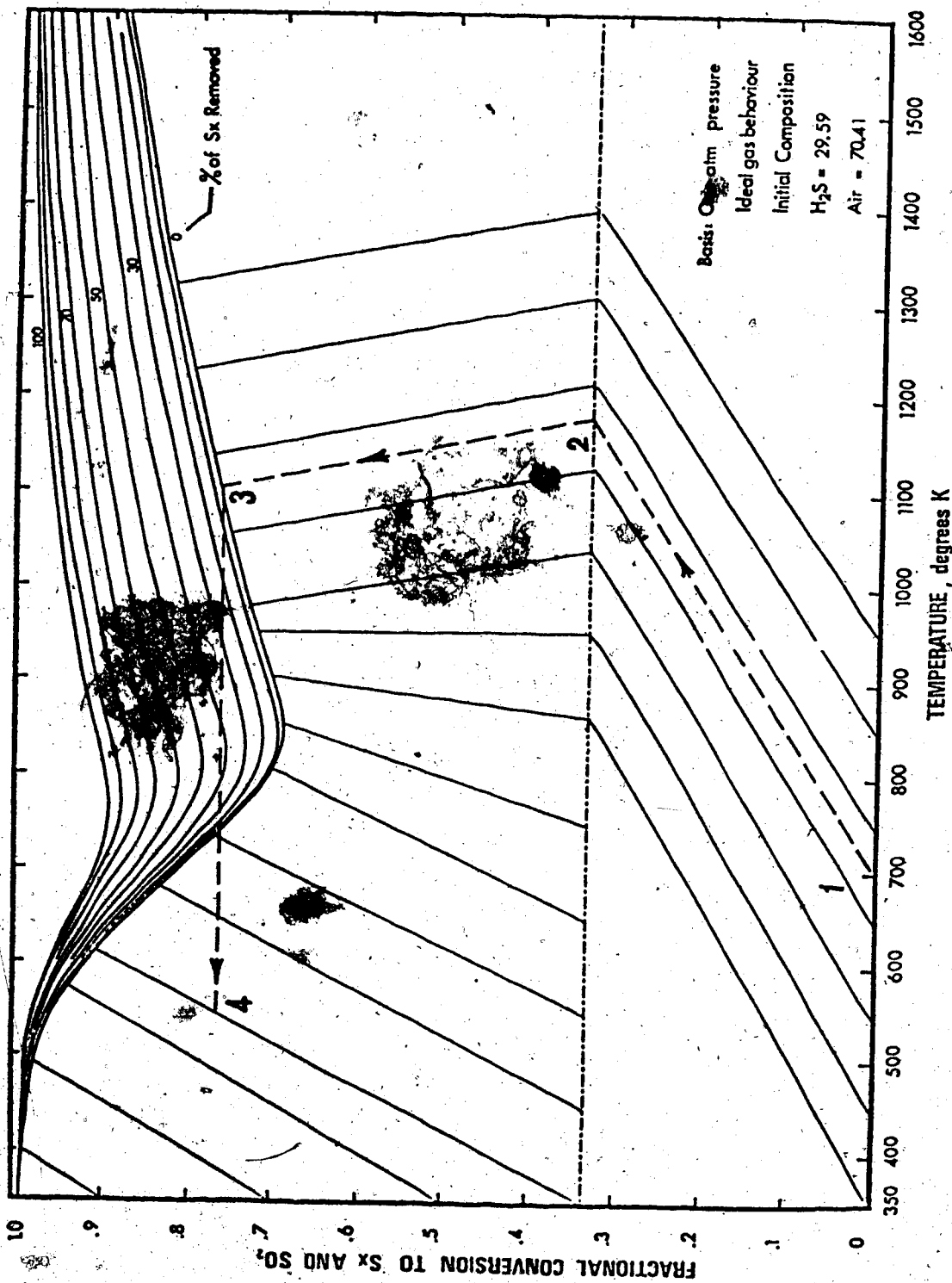


FIGURE 4: EQUILIBRIUM CONVERSION AND ADIABATIC REACTION PATH IN THE FRONT-END BURNER

the reaction (1.1) while the lines between the equilibrium curve and the 33.3% conversion level represent reaction paths according to the reaction (1.2). The bottom curve in the family of equilibrium curves in the upper part of Figure 4 shows an X-T plot for 100% H_2S content in the acid-gas, i.e. for no removal of produced sulfur, while the other curves represent the same gas but after increasing levels of sulfur removal.

Figure 4 shows that removal of 10% of produced equilibrium content of sulfur vapor followed by re-equilibration of the reaction mixture results in additional conversion of H_2S to S_x according to reaction (1.2) from the 0% sulfur removal curve to the 10% one. Thus the ordinates for the family of curves represent the cumulative conversion attainable after a number of process steps during which the reaction system remains closed except for the removal of sulfur.

Figure 5 shows a lower temperature portion of Figure 4 on an expanded scale to facilitate examination of reaction paths for reaction (1.2) in a catalytic converter. Figure 4 and Figure 5 will be useful for burner and catalytic converter calculations which involve reactions (1.1) and (1.2) occurring sequentially but under adiabatic flame conditions.

The equilibrium conversion of reaction (1.2) is temperature dependent at a fixed inert content as

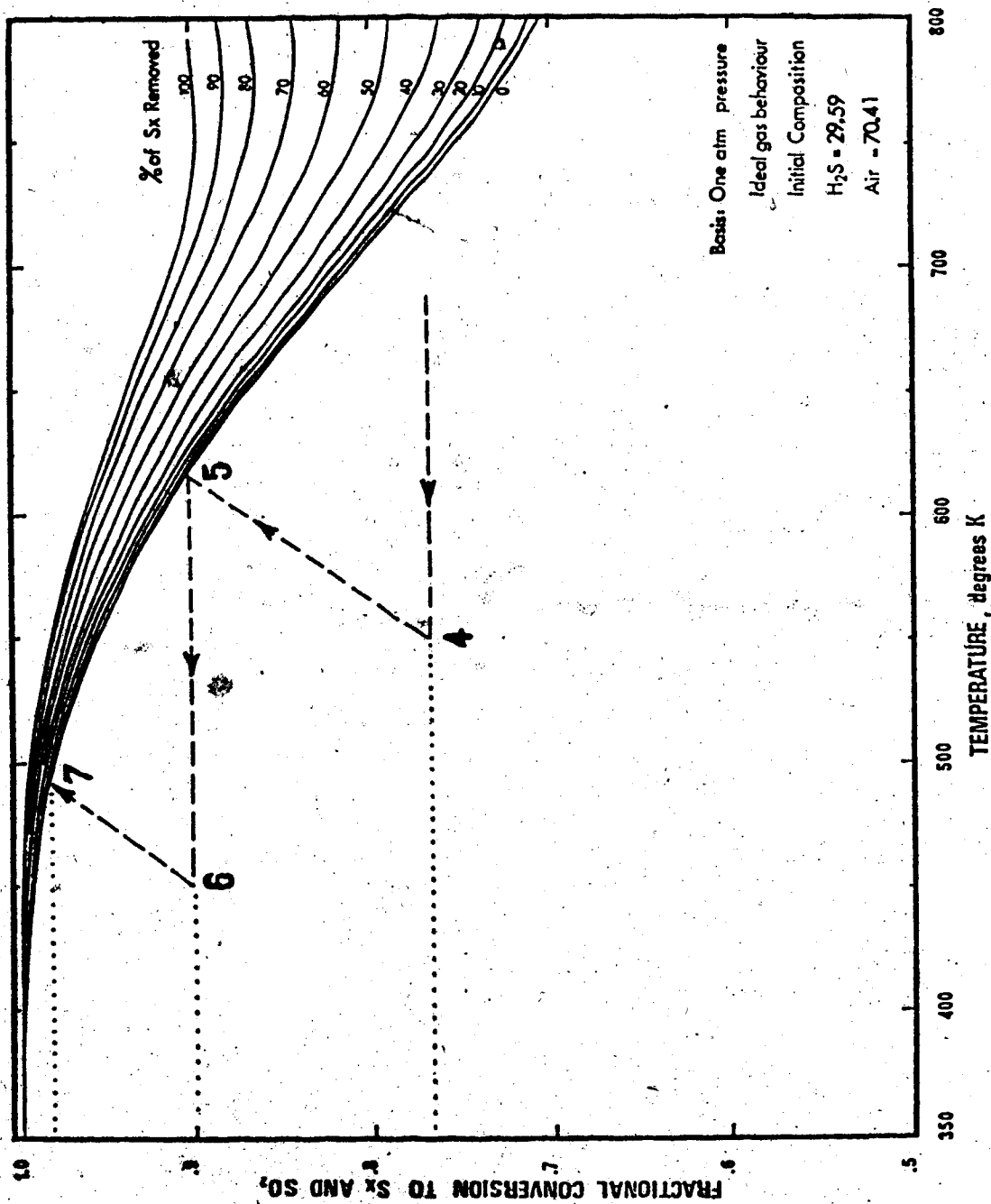


FIGURE 5: ILLUSTRATION OF A REACTION PATH IN THE WASTE-HEAT BOILER AND CATALYTIC CONVERTER

shown in Figure 4. At low temperature ranges of below 800°K, the equilibrium conversion decreases as the temperature increases, while at high temperature ranges of above 800°K the equilibrium conversion increases as the temperature increases. The minimum conversion occurs at the temperature range of about 800°K depending upon the level of sulfur removal as shown on Figure 4.

The existence of a minimum conversion point in the reaction (1.2) can be explained by the association-dissociation reaction between different sulfur species, which causes an exothermic reaction scheme at the low temperature range and an endothermic reaction scheme at the high temperature range. The plots in Figures 3, 4 and 5 are thus really characteristic of reactions (1.2), (1.8) and (1.9) rather than of the reaction (1.1).

Since adiabatic temperature rises are non-equilibrium reaction paths in which the X-T coordinates are uniquely related by the condition that the enthalpy of the system remains constant, equilibrium considerations in the reaction mixture, except for that between different sulfur species, are not required to get the X-T relationship. The magnitude of the slope $\frac{dX}{dT}$ at constant enthalpy of the system depends upon the sign and the magnitude of the heat of reaction as well

as upon the capacity of the reaction mixture to absorb the heat released, or vice-versa.

The effect of inert gases upon the dx/dt curve for reaction (1.1) was computed, as shown in Table 3, to estimate the inhibiting effect against a temperature rise for cases of 10% excess amount of N_2 , 20% and 40% of additional CO_2 contents in the acid-gas. The inertness of CO_2 was checked by using a feed acid-gas containing H_2S and CO_2 to get product distribution which might contain COS and CS_2 . The computed results in Figure 6 show that CO_2 contents in the acid-gas stream can be treated as an inert gas in this particular study to predict the adiabatic reaction path in the front-end burner since the conversion of CO_2 to COS and CS_2 is so small for the given temperature and pressure condition. The influence of other impurities present in the acid-gas in small amounts were neglected.

Figure 7 illustrates the basis on which the adiabatic temperature rises in the front-end burner may be predicted. The temperature rise, $(T_2 - T_1)$, results from reaction (1.1) occurring to completion, $X = 0.33$, along an adiabatic reaction path; $(T_3 - T_2)$ is the slight temperature drop arising from the further conversion via reactions (1.2), (1.8) and (1.9) to form an equilibrium composition of reactants (H_2S and SO_2), products (S_2 , S_6 , S_8 and H_2O) and an inert (N_2).

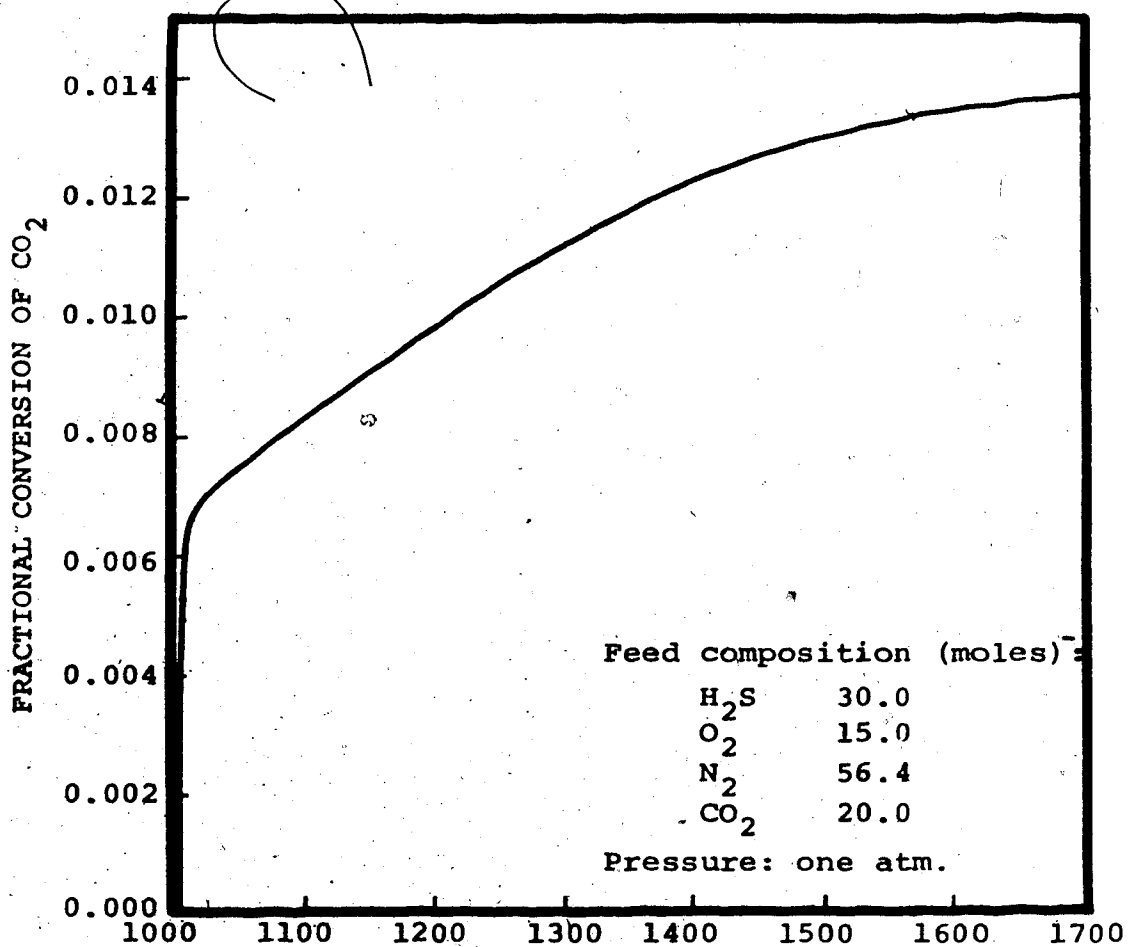
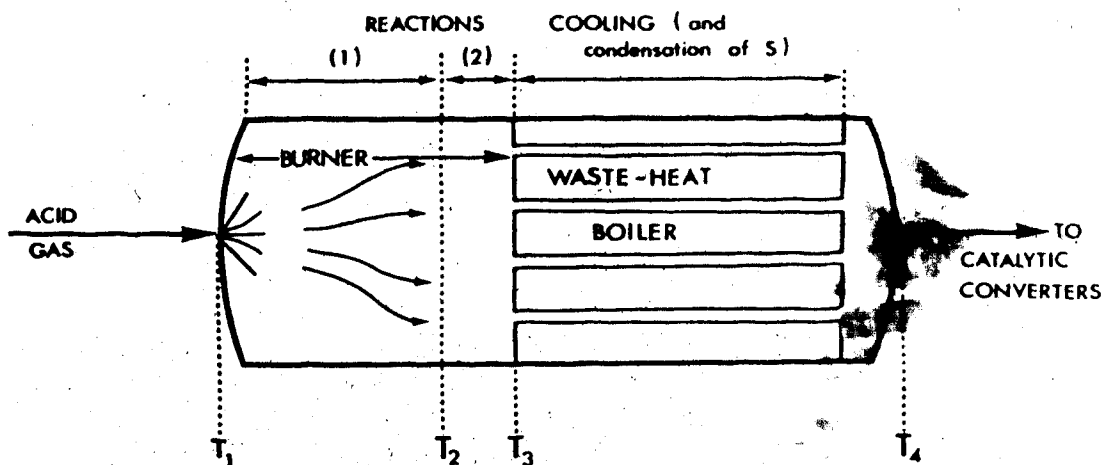


FIGURE 6: EQUILIBRIUM CONVERSION OF CO₂ IN THE FRONT-END BURNER



		MOLES OF COMPONENTS			
H_2S	3	2	$2(1-X)$	$2(1-X)$	
O_2	1.5	0	0	0	
N_2	5.64	5.64	5.64	5.64	
SO_2	0	1	$1-X$	$1-X$	
H_2O	0	1	$1+2X$	$1+2X$	
S_2	0	0	$(1-V_1-V_2)(1.5X)$	} Uncondensed fraction	
S_6	0	0	$V_1(1.5X)$		
S_8	0	0	$V_2(1.5X)$		

X = EQUILIBRIUM CONVERSION ATTAINABLE AT T_3

FIGURE 7: FRONT-END REACTION PATH

Further cooling occurs within the waste heat boiler and is assumed to produce either a cooled gaseous stream (in a once-through process) or a gas and liquid sulfur mixture at the vapor-liquid saturation temperature of sulfur. The actual location of the temperature, T_3 , may be conjectural. To predict the plant conversion levels use can be made of the above sequential reaction scheme.

Adiabatic X-T paths have been plotted in Figure 4 and 5 for various inlet temperatures T_1 . These paths all terminate at $X = 0.33$ as described above. Further adiabatic temperature changes via reactions (1.2), (1.7) and (1.8) are shown in the region above $X = 0.33$ and below the equilibrium curve labeled as "0% sulfur removal".

Each of the T_2 - T_3 paths will terminate on an $X^* - T^*$ equilibrium point. When the additional cooling occurs in the waste-heat boiler section, the reaction rate will be suppressed and the resulting change in state may be followed along the constant conversion line until the specified temperature T_4 is attained. The extent of cooling to T_4 along the constant conversion line will determine whether sulfur condenses or remains in vapor phase.

One point to be emphasized in Figure 4 is that the conversion X represents total conversion based on

the initial H_2S feed, i.e. conversion of H_2S to both SO_2 and S_x via two reactions (1.1) and (1.2). The dotted line labeled 1-2-3-4 in Figure 4 illustrates the reaction paths for a 100% H_2S acid-gas undergoing the process already described above. If 50% of the sulfur so formed is condensed in the waste-heat boiler and then separated from the reaction mixture, the curve in Figure 4 labeled "50%" would describe the subsequent equilibrium X^*-T^* compositions permitted for such a stream composition.

Here, the equilibrium calculations and estimated X-T paths do not indicate whether the predicted temperature rise is sufficient to maintain a stable flame temperature in the burner or not. This condition must be specified on the basis of plant experience.

The adiabatic reaction paths which have been calculated were found to be quite dramatically influenced by the equilibrium distribution between the sulfur species, S_2 , S_6 and S_8 , at some temperature ranges, especially between 700° and $1000^\circ K$.

The discontinuity in X-T paths at $X = 0.33$, strictly speaking, is not realistic, but appears of convenience in analytic calculations, because the overall temperature rise during the overall reaction paths would become the path from T_1 through T_3 . In this sense the slope of the reaction path has its

meaning ultimately to predict the terminating product temperature from the front-end burner just before the catalytic converter.

3.2 Performance of the Claus Catalytic Converter

Upon specifying an exit temperature and the corresponding composition, T_4 and X_4 in Figure 7, of the product stream from the particular waste-heat boiler, further reaction may be promoted by contacting the stream with a bed of catalysts.

The cooling process from T_3 to T_4 contributes not only for condensing of sulfur formed in the front-end burner but also for obtaining a higher equilibrium conversion level in the temperature range below 800°K . This additional sulfur formation and increasing the overall conversion level by alternately cooling the gas stream and then passing it through a bed of catalyst is the most popular scheme in a "once-through" sulfur recovery process. To predict the overall performance of a Claus unit a proper mathematical modeling of the catalytic converter is also required in addition to the front-end burner calculation.

Various kinds of mathematical models for a catalytic fixed bed reactor have already been discussed in the literature survey. In the case of a Claus catalytic converter the catalyst bed is very large in its

diameter (15 ~ 20 feet) and the depth is much shorter (3 ~ 4 feet) compared to its diameter. Therefore, the assumption of adiabatic operation is realistic, in which case the one-dimensional model is applicable in the absence of radial concentration and temperature gradients.

For the above reason, a homogeneous one-dimensional model was adopted to simulate the Claus catalytic converter, more particularly that originally developed by Liu and Amundson(62), their so-called two-phase model. According to this model, the general transport and reaction processes in the catalytic bed may be described by the following equations:

$$V_{int} \frac{dC_f}{dz} + \frac{A_m k_m}{\epsilon_B} (C_f - C_s) - D_L \frac{d^2 C_f}{dz^2} = 0 \quad (3.8)$$

$$\rho_f C_{pf} V_{int} \frac{dT_f}{dz} + \frac{A_h h}{\epsilon_B} (T_f - T_s) + \frac{A_B h}{\epsilon_B} (T_w - T_f) = 0 \quad (3.9)$$

$$A_m k_m (C_s - C_f) + \eta \rho_B r_s (P_s, T_s) = 0 \quad (3.10)$$

$$A_h h (T_s - T_f) + \eta \Delta H \rho_B r_s (P_s, T_s) - k_e \frac{d^2 T_s}{dz^2} = 0 \quad \dots\dots\dots (3.11)$$

In the above equations, the rate expression to be used herein is the one proposed by Liu (66) for the Alon catalyst. Actually the model by Liu and Amundson (62) is modified by including the internal transport resistances through the insertion of the effectiveness factor which was ignored by many investigators (30,49,102).

By assuming the following conditions:

- (1) Negligible axial dispersion
- (2) Negligible axial conduction
- (3) Uniform velocity profile across the bed
- (4) Adiabatic condition with surroundings
- (5) Constant pressure along the reactor
- (6) Stoichiometric feed ratio of H_2S and SO_2
- (7) Equilibrium distribution of sulfur species between S_2 , S_6 and S_8 at the given temperature along the reactor
- (8) Uniform concentration distribution on the catalyst external surface
- (9) No Poiseuille flow in the pores, i.e., a negligible change in the number of moles of the reaction mixture.

the general equations for heat and mass balances may be reduced to a simplified form as presented in Appendix E. The resulting simplified equations to be solved become, in terms of dimensionless variables,

$$\frac{dx_f}{dL} + A_1 (X_f - X_s) = 0 \quad (3.12)$$

$$A_2 (X_f - X_s) + \frac{A_3 (f_1 f_2)^{3/2}}{(A_4 - A_5 f_1 f_2)^2} \exp\left(\frac{A_6}{F_2}\right) = 0$$

..... (3.13)

Equations (3.12) and (3.13) were solved numerically by using the Newton-Raphson method in equation (3.13) and the standard Runge-Kutta-Gill integration method in equation (3.12) repetitively starting from the inlet up to the outlet of the reactor with the precalculated value of the effectiveness factor.

The most important consideration in this treatment arises with the effectiveness factor of the catalyst pellets, whose effect on the actual reaction rate is implicitly included in the parameter A_3 in equation (3.13). The various methods to calculate or estimate the effectiveness factor of the catalyst pellets have extensively been surveyed in the literature survey.

The appropriate choice of a calculation method for the catalyst effectiveness factor can reduce much of the computing time since the effectiveness factor should be repeatedly calculated along the reactor bed to obtain an accurate prediction of the reaction path through the bed. The first step to be taken before choosing any proper calculation procedure is to decide

whether the reaction involved is in the fast reaction regime or in the slow one. In the fast reaction regime the concentration of a reactant rapidly drops to zero before it can reach the center of the spherical catalyst pellet while it gradually decreases until it can reach the center of the pellet in the slow reaction regime.

To decide upon which reaction regime is applicable, the concept of the Thiele modulus was used. For spherical catalyst pellets, the Thiele modulus is defined by (94)

$$\phi_s = \frac{R}{3} \sqrt{\frac{\rho_p r_{s,p}(P_s, T_s)}{D_e C_s}} \quad (3.14)$$

For Thiele modulus of less than 0.5, most of the reaction occurs in the entire catalyst pellet in the slow reaction regime which means that the reaction rate is slow enough compared to the diffusion rate for the catalyst effectiveness factor to become approximately 1. On the other hand when the Thiele modulus becomes larger than 5 the reaction occurs in the fast reaction regime where the reaction rate is fast enough compared to the diffusion rate to make the effectiveness factor much smaller than unity (61).

In this study, the calculated value of the Thiele modulus (Appendix F) at the reactor inlet

conditions shows that the reaction occurs somewhere between the fast and the slow reaction regimes since the calculated Thiele modulus \sqrt{V} is about 5. This value of the Thiele modulus enables the asymptotic solution of the transport equations to be used to obtain the effectiveness factor with an error of less than 15%, as shown on Figure 8.

To make certain whether the reaction interface, X_I , defined as the point in the catalyst pore where the concentration of the reactant might drop to zero, falls in between the external catalyst surface and the center, Van Den Bosch's collocation method (90) was modified and applied to this reaction system. The collocation equation was derived for this particular reaction system (Appendix G), which was solved using the false position method to get X_I with the optimum collocation point of $\frac{1}{\sqrt{2}}$ as proposed by Van Den Bosch (99) for the high reactivity model. The calculated results showed that X_I was equal to zero implying that the positive concentration of the reactant could reach the center of the catalyst pellet.

Therefore, the accurate value of the effectiveness factor may not be expected by employing the shell model on a flat slab approximation in this particular situation. Judging from the above preliminary investigations, the Weiss and Hicks' conventional method (106)

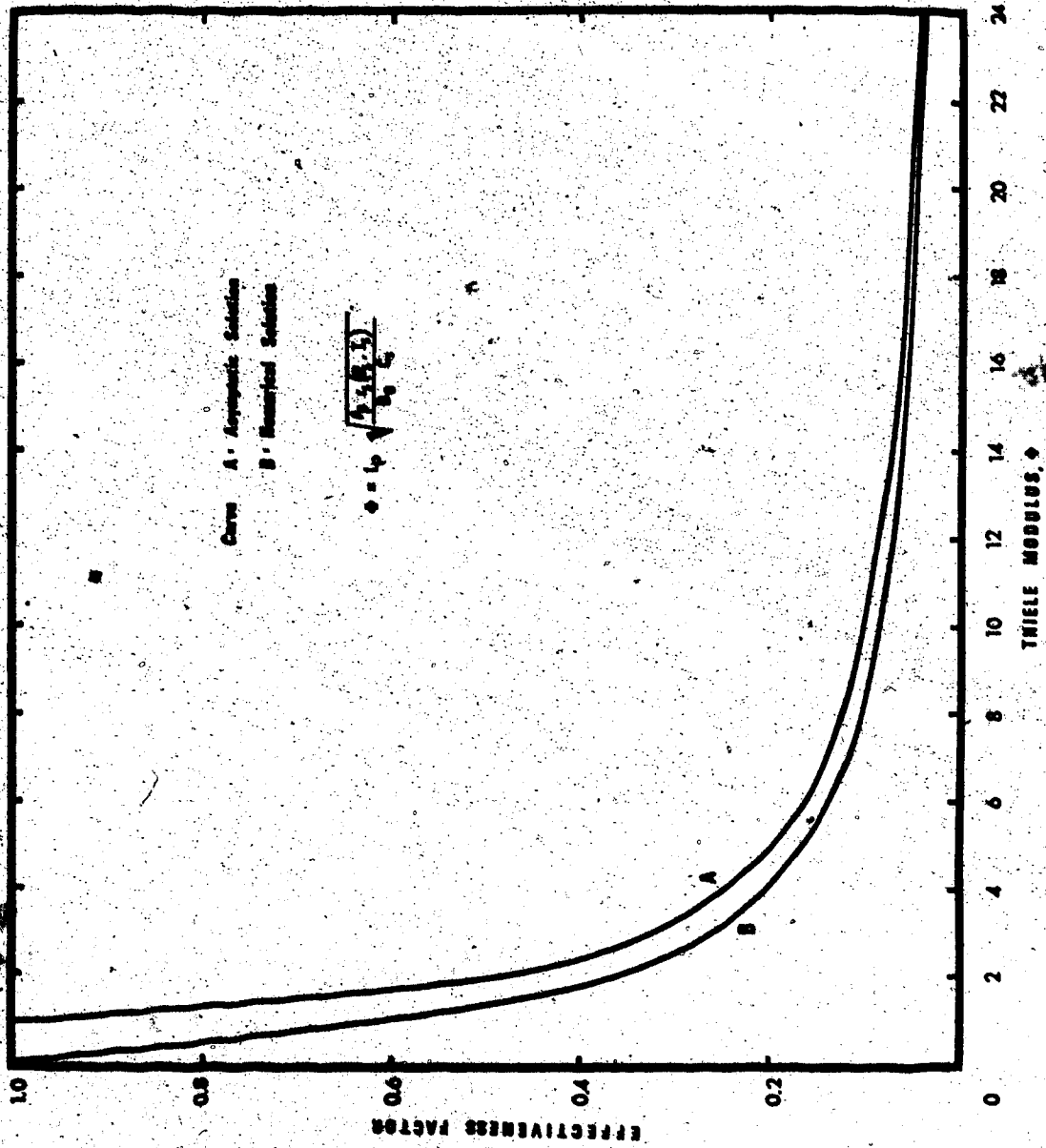


FIGURE 8: EFFECTIVENESS FACTOR AS A FUNCTION OF THIELE MODULUS FOR THE CLAUS REACTION ON Al_2O_3 CATALYST

was supposed to be the most proper method to calculate the effectiveness factor although it was a little slow and required a number of iteration.

The detailed derivation of equations to apply the Weiss and Hicks' method to this study is presented in Appendix H with the related computer program. For the purpose of comparison the asymptotic solution using the approximate flat-slab model was also obtained as presented in Appendix F. The calculated values of the effectiveness factor by both the conventional numerical method and the asymptotic method are shown in Figure 8 as a function of the Thiele modulus. In Figure 8 it can be found that the difference between the two methods is significant when the Thiele modulus is less than 10 and negligible when it is larger than 10. The Thiele modulus at the reactor inlet condition was calculated to be 4.4 and at the outlet condition 5.4. The calculation procedure was given in Appendix E and H. The corresponding effectiveness factor of 0.18 and 0.15 may be seen in Figure 8. The maximum percent deviation of the effectiveness factor is, therefore, about 8.3%. Furthermore the effectiveness factor is essentially a linear function between the Thiele modulus of 4.4 and 5.4 as may be recognized in Figure 8. As a result, the arithmetic average value of the effectiveness factor between the inlet and the

outlet condition was treated as an overall effectiveness factor for the whole length of the reactor bed. In further calculations to predict the characteristic performance data of the Claus converter the overall constant effectiveness factor with the value of 0.17 has been applied.

The effective diffusivity was calculated using the parallel pore model based upon Chuang's experimental data (18) for the pore size distribution of the Alon catalyst. The average pore size employed was 80 Å, in which range the diffusion phenomena certainly occurs in the Knudsen diffusion regime. The tortuosity factor was chosen as 4.0 in reference to data by Hideo Teshima (46) and the recommended value of Satterfield (93). The calculated value of the effective diffusivity was 0.001888 as shown in Appendix D.

The effective thermal conductivity data were very limited. Fortunately, however, the catalyst pellets concerned in this study have pore structures of small enough dimensions to be operating in the Knudsen diffusion regime. Furthermore the pore size distribution range around the average value was relatively narrow according to Chuang's data (18). Operation with this type of a catalyst would therefore be expected to be free of internal thermal effects within the catalyst pellet and justifies neglecting of these

effects even under the severe mass diffusion effects (106). Often the effect of the thermal conductivity becomes very important for the pore structures of non-Knudsen diffusion regime (106).

The data obtained by Mischke and Smith (77) gave the value of the effective thermal conductivity of alumina catalysts with macro void fraction of 0.4 equal to 0.082 But/hr.ft.²°F at 120°F under the atmospheric environment. This value was used in this work to predict the intraparticle thermal effects. The results of calculations indicated, as presented in Appendix F, that the internal thermal effect may be neglected.

For this kind of small pore structures, the above analysis implies that the effective diffusivity rather than the effective thermal conductivity may play a very decisive role. Because of the absence of the internal thermal effect the energy balance equation within the catalyst pellet does not need to be considered when computing the effectiveness factor, i.e. the mass balance equation is the only equation to be solved.

3.3 Results of Reactor Modeling

The temperature and the conversion profiles along the catalyst bed are plotted in Figure 9 for a feed temperature of 550°K and space velocity of

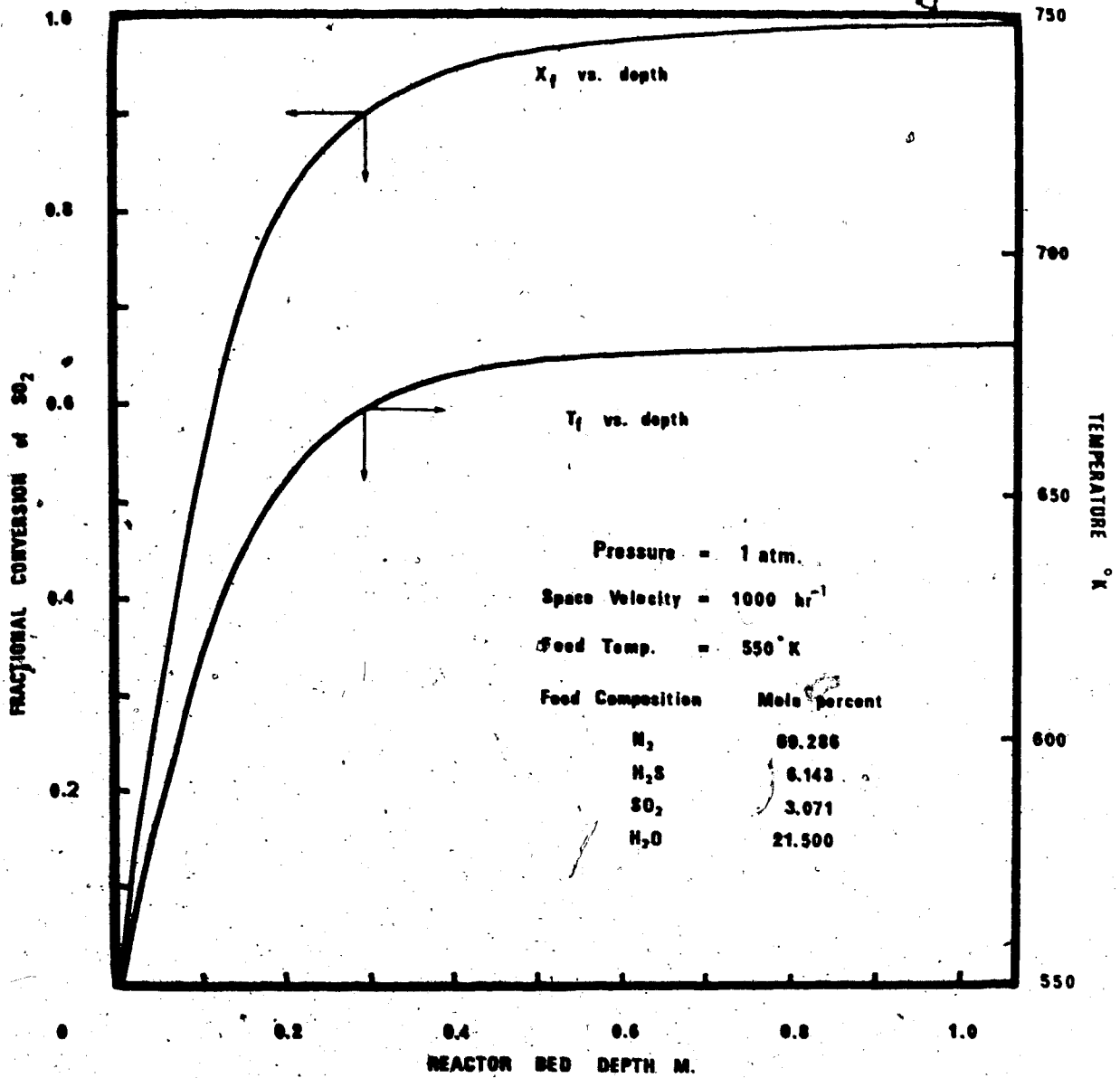


FIGURE 9: TEMPERATURE AND CONVERSION PROFILES ALONG THE CATALYST BED DEPTH

1000 hr^{-1} . The profiles indicate that a significant amount of reaction occurs at the entrance of the reactor bed and almost maximum conversion may be reached at the depth of about 2 feet. With this prediction it can be suggested that if the space velocity is increased to a higher level than 1000 hr^{-1} , a greater yield may be obtained without affecting the reactor efficiency.

In Figure 10, the effect of the external transport resistance is shown for the inlet section of the reactor since the inlet section can have the greatest gradient in temperature and concentration when the significant reaction occurs at the inlet section. According to Figure 10, the effect of the external diffusion effect is quite negligible even in the inlet section while the thermal resistance is considerable.

The negligible mass transport resistance in the external fluid film can provide a unique steady state solution of the transport equations (3.12) and (3.13) even with considerable thermal resistances. The possibility of the existence of multiple solutions due to the external resistance was checked by solving the equation (3.13) for X_g with X_f as a parameter using the false position method. The computed results are plotted in Figure 11. Obviously no multiple solutions may exist under the reaction conditions of this simulation and, of course, under the practical plant

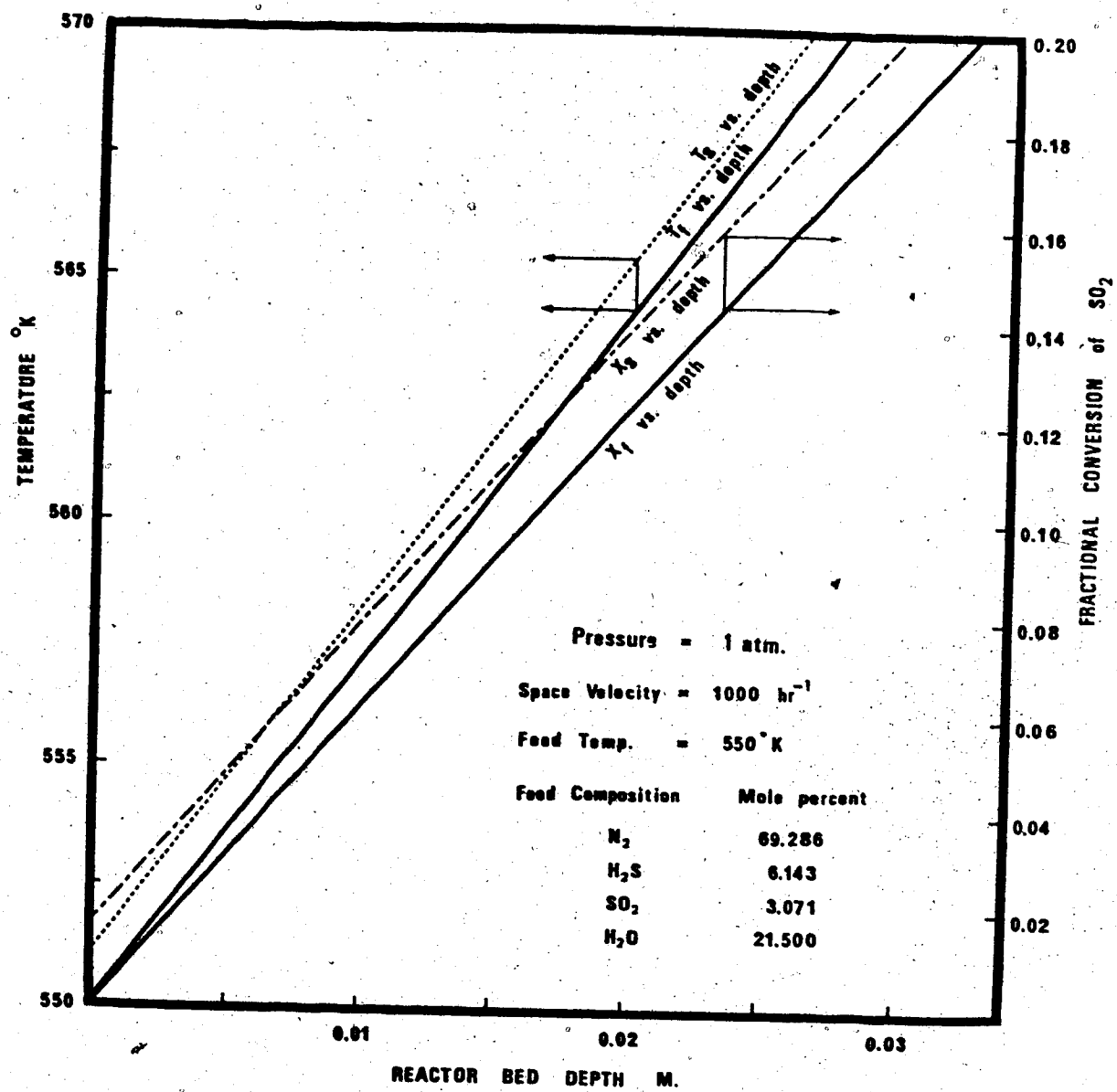


FIGURE 10: EFFECT OF EXTERNAL TRANSPORT RESISTANCES

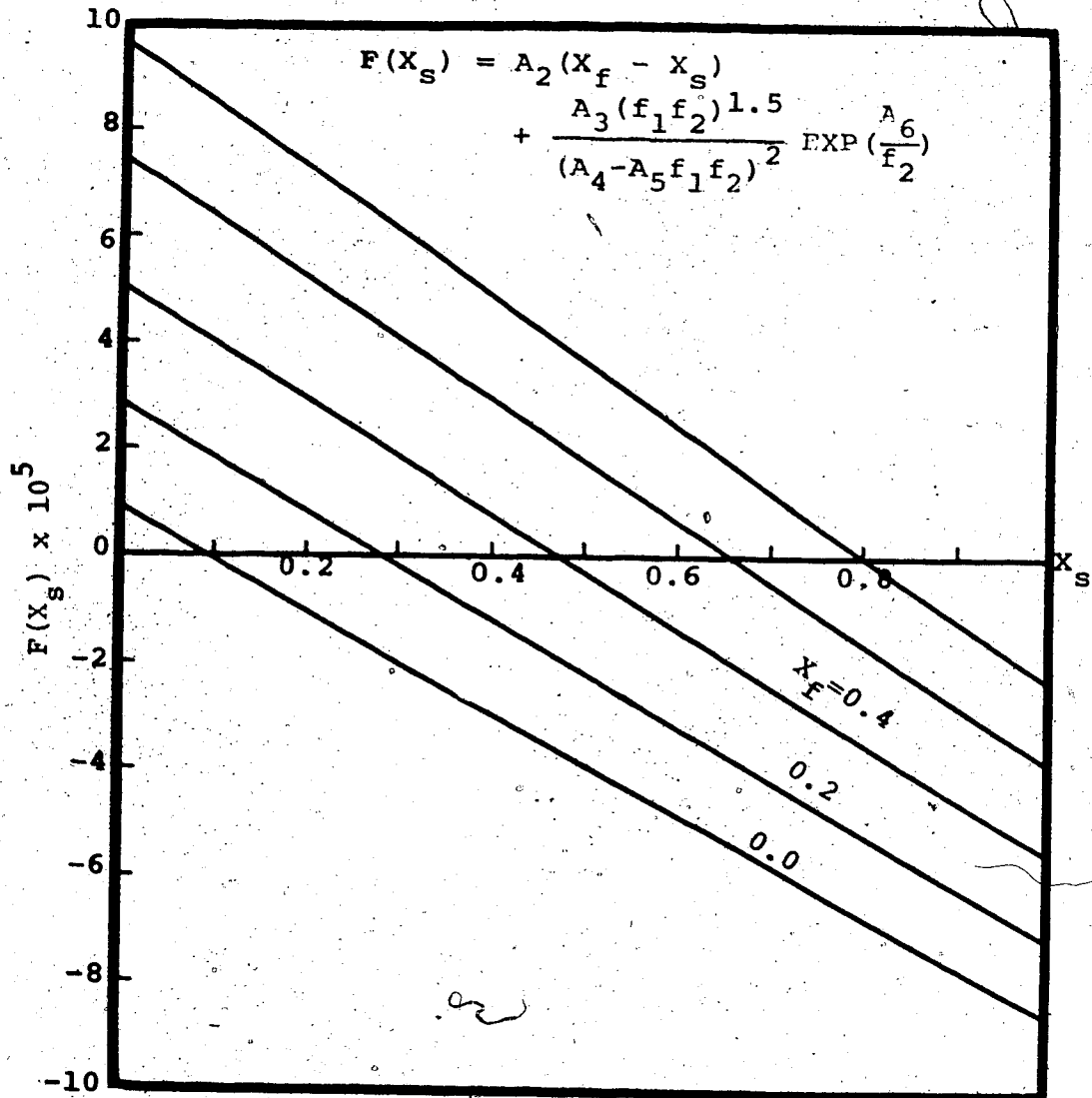


FIGURE 11: CHECK ON THE EXISTANCE OF MULTIPLE SOLUTIONS DUE TO EXTERNAL TRANSPORT RESISTANCES

operational condition.

Figure 12 has been plotted to evaluate the effect of the feed temperature on the X-T plot with a space velocity of 1000 hr^{-1} . The slope of $\frac{dX}{dT}$ appears to be almost constant for the different inlet temperatures.

Figure 13 represents the effect of the feed temperature on the temperature profile along the reactor with a constant space velocity of 1000 hr^{-1} . From the slopes of the temperature profiles it can be predicted that the feed temperature should be above 500°K to get high enough reaction rate right at the entrance of the catalyst bed.

Figure 14 shows the effect of the feed temperature on the conversion profile along the reactor with a constant space velocity of 1000 hr^{-1} . Judging from the slopes of the profiles it can be confirmed that the fast reaction rate right at the entrance of the catalyst bed can be achieved when the feed temperature is above 500°K . The difference in the conversion level appears to be negligible at the outlet of the reaction when the feed temperature becomes higher than 500°K .

Figure 15 indicates that the effect of the space velocity on the conversion level at the fixed feed temperature of 550°K is significant when the space velocity exceeds 2000 hr^{-1} , but negligible when

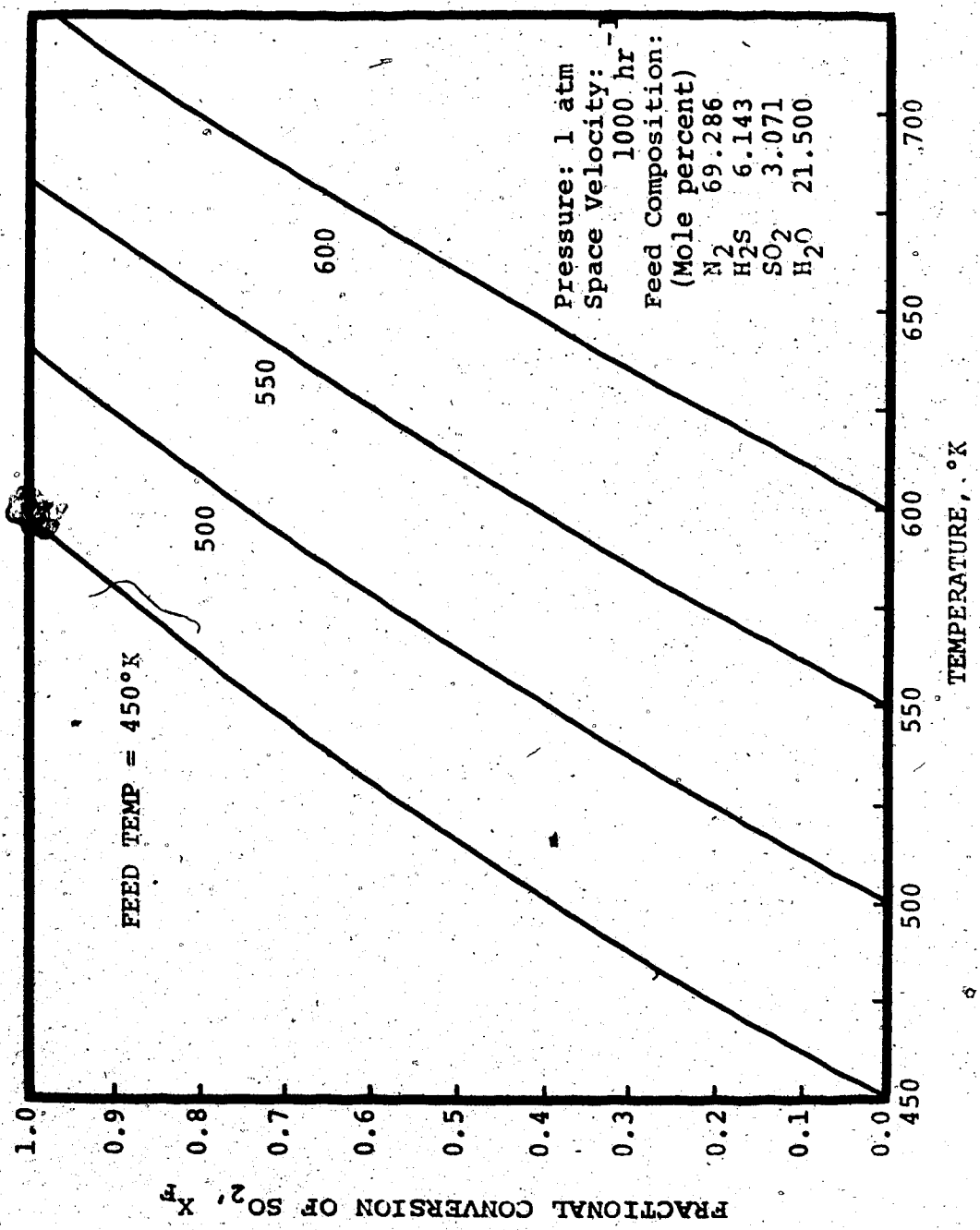


FIGURE 12: EFFECT OF THE FEED TEMPERATURE ON X-T PLOT

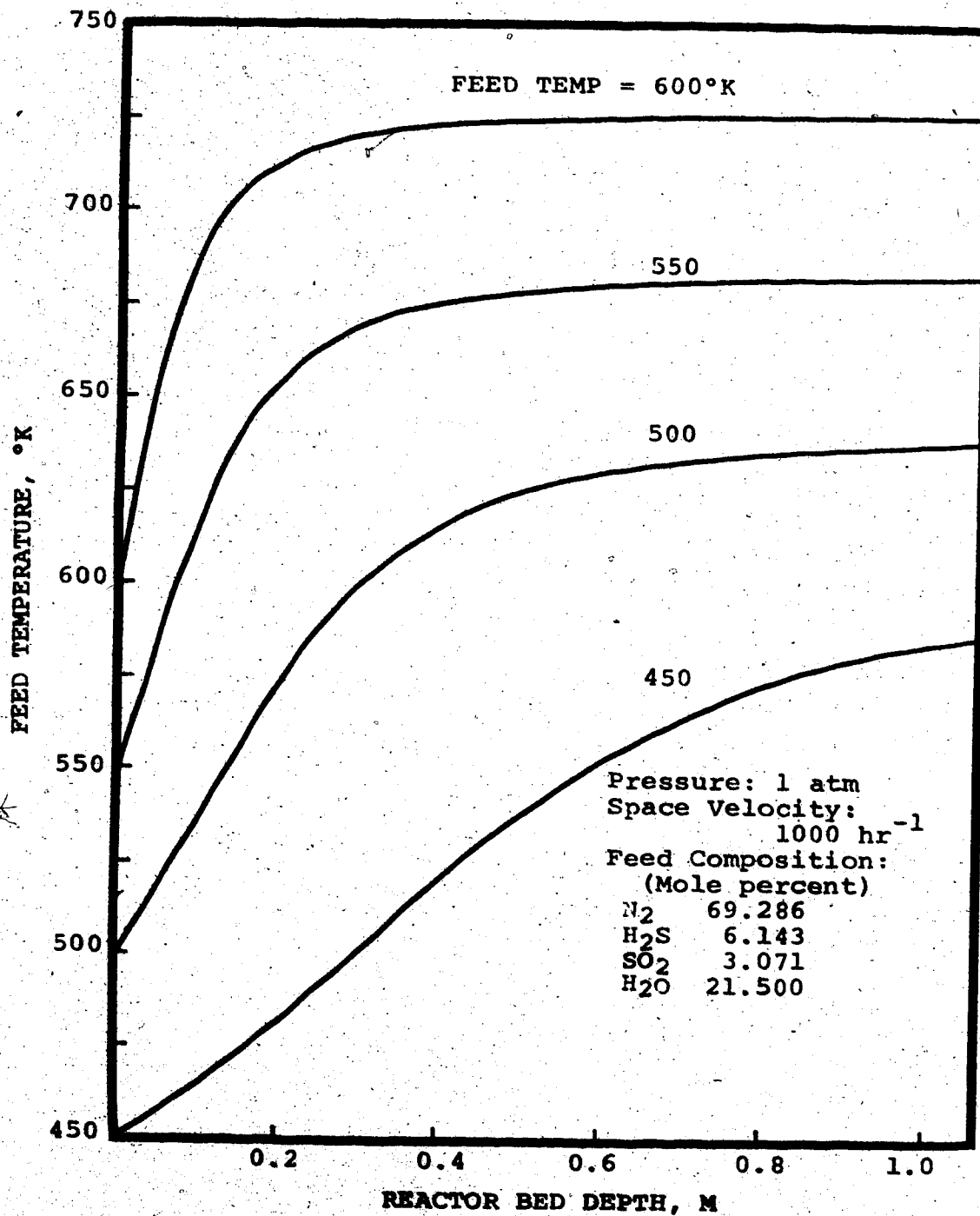


FIGURE 13: EFFECT OF THE FEED TEMPERATURE ON TEMPERATURE PROFILES

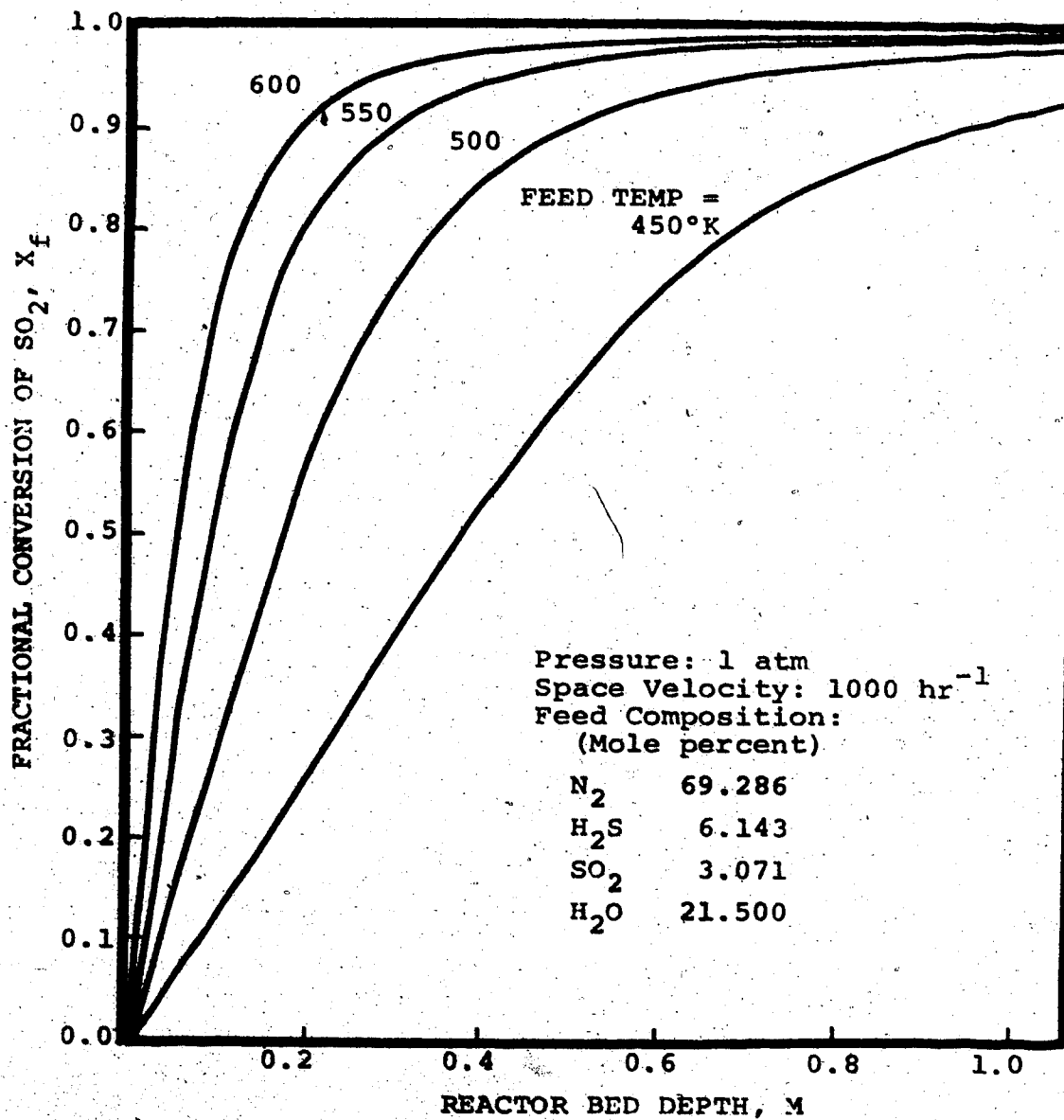


FIGURE 14: EFFECT OF THE FEED TEMPERATURE ON CONVERSION PROFILES

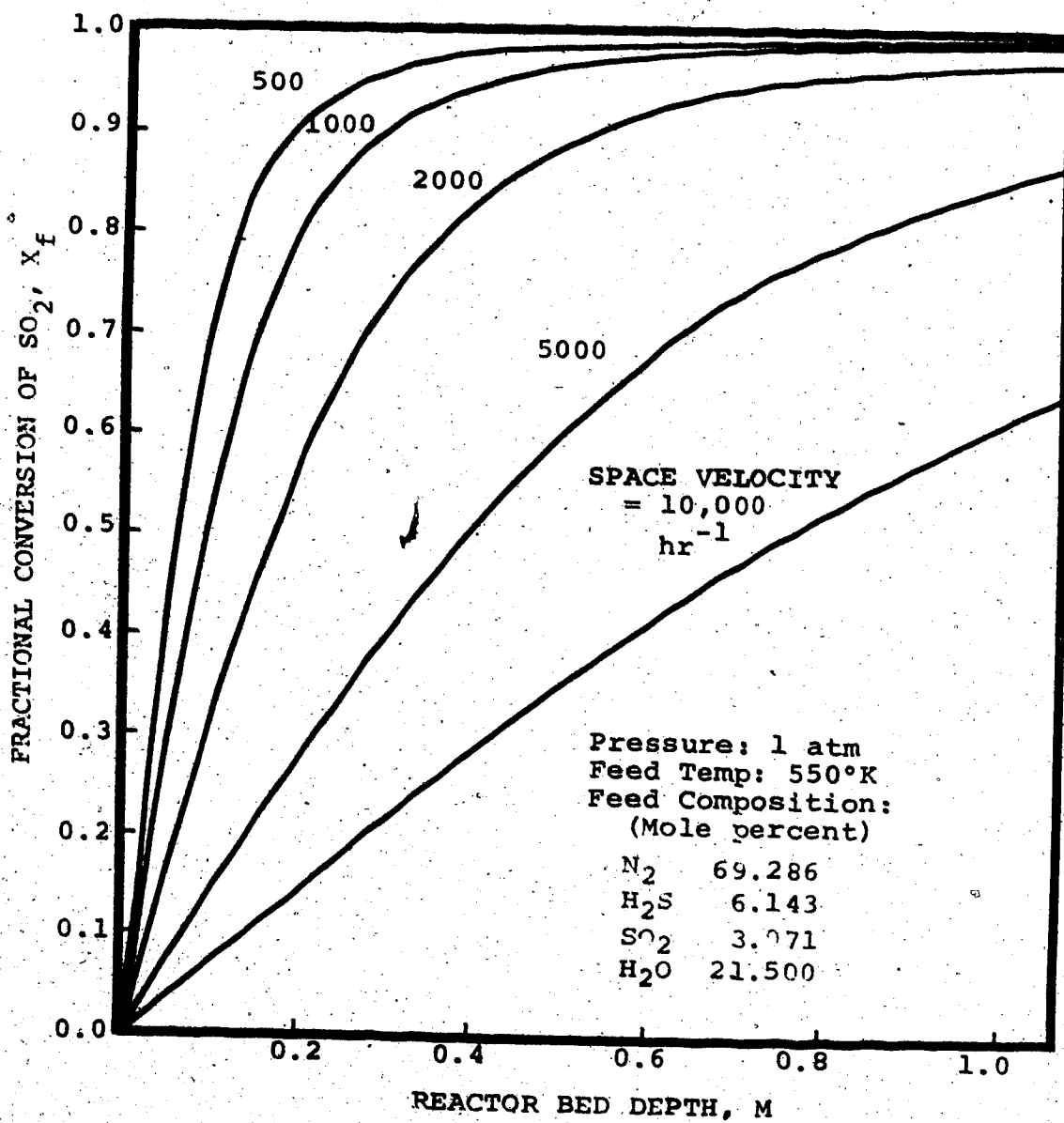


FIGURE 15: EFFECT OF THE SPACE VELOCITY ON CONVERSION PROFILES

it is below 1000 hr^{-1} .

What should be noted in this modeling results is the fact that the reverse reaction of the Claus process was not taken into account due to the lack of knowledge on the rate of the reverse reaction. However, the reverse reaction rate was found to be negligible compared to the forward reaction rate in its magnitude under industrial operation conditions according to Liu (66) in his statistical correlation of the rate data. Another point which should be made here is that simultaneous reactions which may possibly occur in the Claus reactor, for example the COS-SO_2 and $\text{COS-H}_2\text{O}$ reactions, have not been considered in this simulation work.

CHAPTER IV

DESCRIPTION OF EXPERIMENTAL SYSTEM

The experimental equipment consists of three major parts; a reactant feeding system, a reaction system and an analysis system. The reactant feeding system was originally designed and built by McGregor (72), to which an additional COS feeding line was installed in this work. In the reaction system, an integral bed reactor was employed instead of the differential recycle reactor which had been used by McGregor (72), Liu (65), and Karren (53) for their kinetic studies on the Claus reaction. To analyse the feed and the product streams a gas chromatograph was used.

4.1 Reactant Feeding System:

The schematic diagram of the reactant feeding system is presented in Figure 16. The feeding system starts from gas cylinders, each of which has been equipped with its own pressure regulator. In the nitrogen feed line a second pressure regulator was provided in series with the first to improve the control of nitrogen pressure upstream of the flow controller since the nitrogen cylinder pressure tended to drop much faster due to its much larger flow rate compared to other reactants.

Each gas stream except COS was dried with

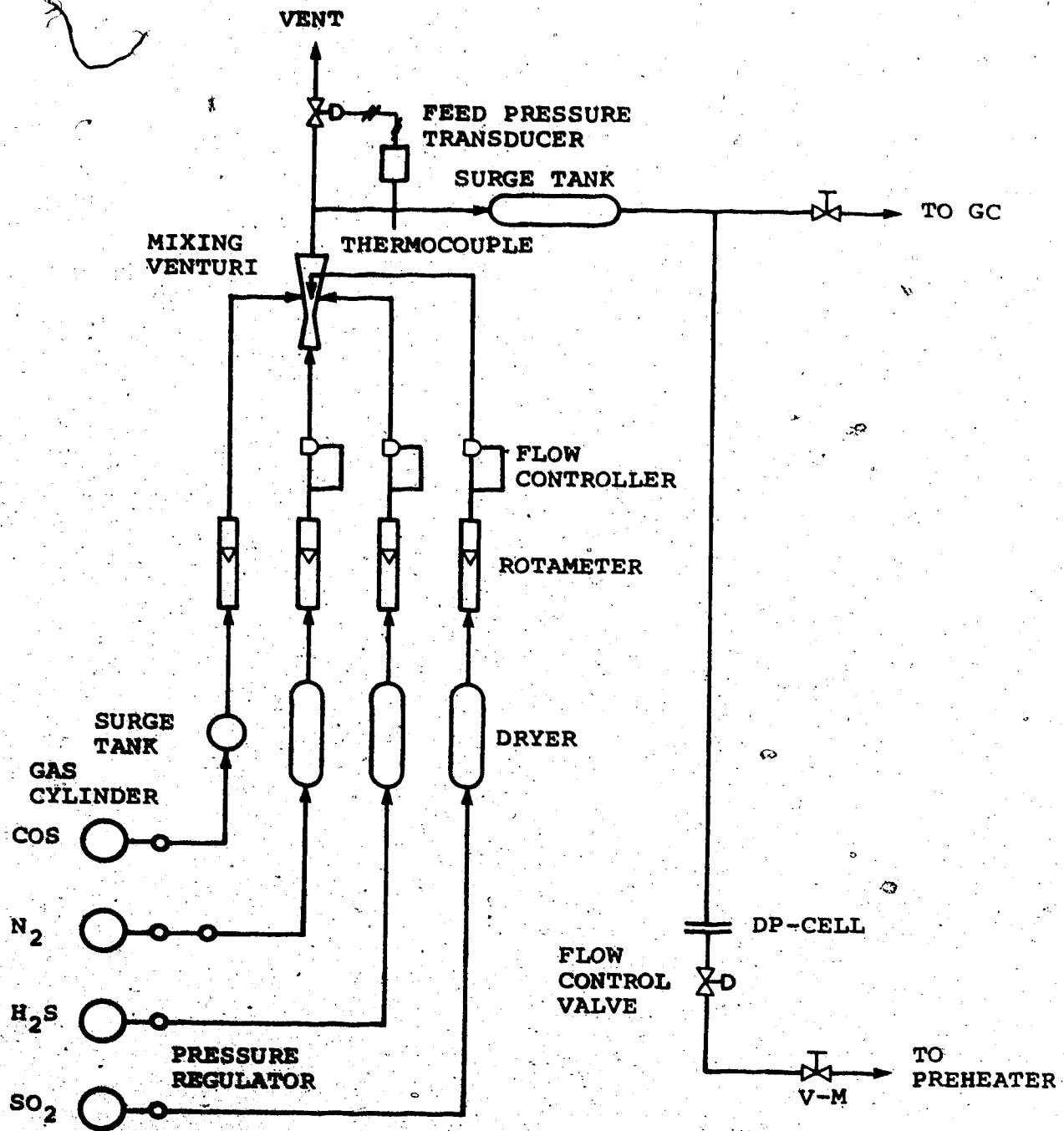


FIGURE 16: SCHEMATIC DIAGRAM OF THE REACTANT FEEDING SYSTEM

anhydrous calcium sulfate contained in a 500 ml stainless steel cylinder to prevent the homogeneous reaction between H_2S and SO_2 in the presence of condensed water vapor. The COS cylinder was checked for water impurities and in the absence of water content a COS drier was unnecessary.

Glass rotameters with stainless steel balls were used to control the flow rate of each reactant stream along with the flow controllers of diaphragm type. A surge tank was installed in the COS feeding line to improve the feed pressure control without using the diaphragm type controller. The rotameters did not give accurate readings of the flow rates, so they were used only as a visual indicator of whether the flow rate of reactant streams remained constant. The accurate flow rate of each reactant stream was obtained by the GC analysis results of the feed stream combined with the measured total flow rate.

The reactants were mixed in the mixing venturi to form the feed mixture of desired composition, whose total absolute pressure was measured by a Foxboro 66 FR-2 electronic absolute pressure transducer and whose temperature was measured by an iron-constantan thermocouple.

The total flow rate of the feed mixture was

measured by a Foxboro 613 DL differential pressure cell and controlled by a Foxboro Stabiflo 6R-V4 control valve. A surge tank with a volume capacity of 500 ml was used to ensure complete mixing of the reactants before they reach the control valve.

A variable portion of the feed mixture on the upstream side of the differential pressure cell was continuously vented depending upon the desired flow rate of the feed mixture through the reactor. Another small portion of the feed mixture was introduced continuously to the gas chromatographic detector for analysis of the feed composition.

4.2 Feed-Product Analysis System:

The composition of both feed and product streams was analysed by a gas chromatograph equipped with a Beckman - 320 programmer, Infotronics Aerograph 471 digital integrator, and Hewlett-Packard Model 17503 A recorder. The schematic flow diagram of the analysis system is presented in Figure 17.

4.2.1 Separation of components in GC Column

To separate all components in the gaseous reactant and product mixture the GC column was arranged in a three-column-in-series mode. All of the possible components, N_2 , CO_2 , H_2S , COS , SO_2 and H_2O were

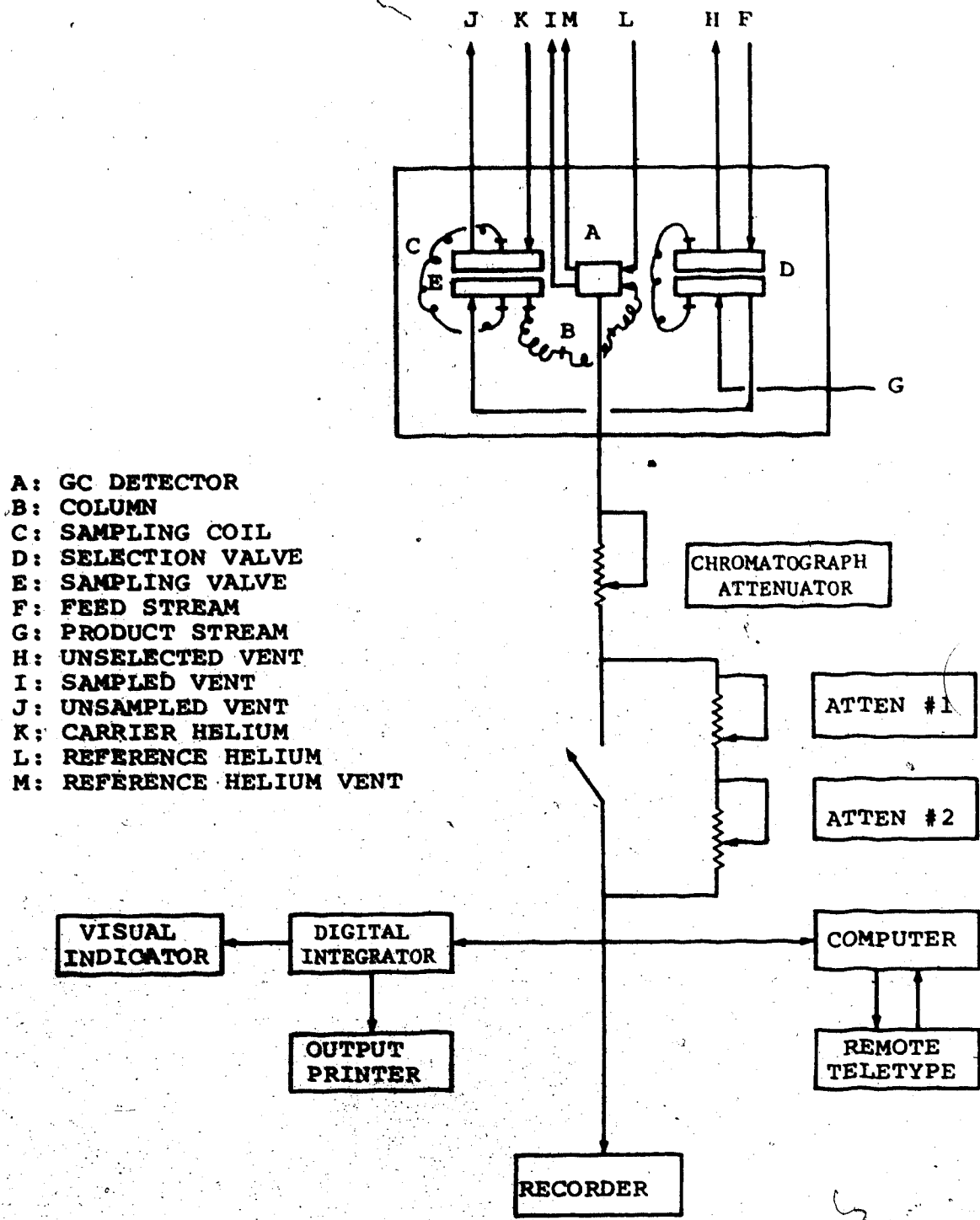


FIGURE 17: SCHEMATIC DIAGRAM OF THE ANALYSIS SYSTEM

separated using three columns in series; the first column was a 3-foot Chromosorb 104, the second a 6-foot Porapak QS in 50-80 mesh, and the third a 3-foot Porapak T. All of these columns were made of 1/8 inch diameter SS 316 stainless steel tubings.

According to experimental results for optimum column arrangements, the longer the Chromosorb 104 column became, the better was the resolution between SO_2 and H_2O peaks but the worse between COS and H_2S peaks. In the absence of the Porapak QS column H_2S and COS peaks completely fused into one large peak while the separation between SO_2 and H_2O peaks was excellent with almost the same elution time as obtained in the presence of that column. Porapak T column improved separation of H_2S and COS peaks but made the elution time of SO_2 and H_2O peaks longer causing excessive tailings in both peaks. With the optimum three-column-in-series arrangement, 3 feet of Chromosorb - 6 feet of Porapak QS - 3 feet of Porapak T, the total elution time was about 12 minutes with good separation between each peak at the column temperature of 190°F . The temperature control of the GC system was performed by Honeywell R 7161 temperature controller and displayed on Honeywell Elektronik 16 multipoint temperature recorder.

The experimental results showing a comparison between different column arrangements have been summarized in Table 4.

TABLE 4

COMPARISON BETWEEN DIFFERENT COLUMN ARRANGEMENTS

A = Chromosorb 104 column

B = Porapak QS column

C = Porapak T column

Numeric value = the length of
a column in feet

No.	Column Arrangement	Separation		Helium Flow Rate (ml/min)	Elution Time (min)	Column Temperature (°F)
		H ₂ S-COS	SO ₂ -H ₂ O			
1	4A + 6B	good	good	15	30	120
2	4A+6B+3C	good	good	35	16	200
3	6B + 3C	good	fused	35	excessive tailing	200
4	1A+6B+3C	good	fused	35	less tailing	200
5	3A+6B+3C	good	good	35	12	190

The feature of the separation of each peak is illustrated in Figure 18 using the selected optimum column, column No. 5.

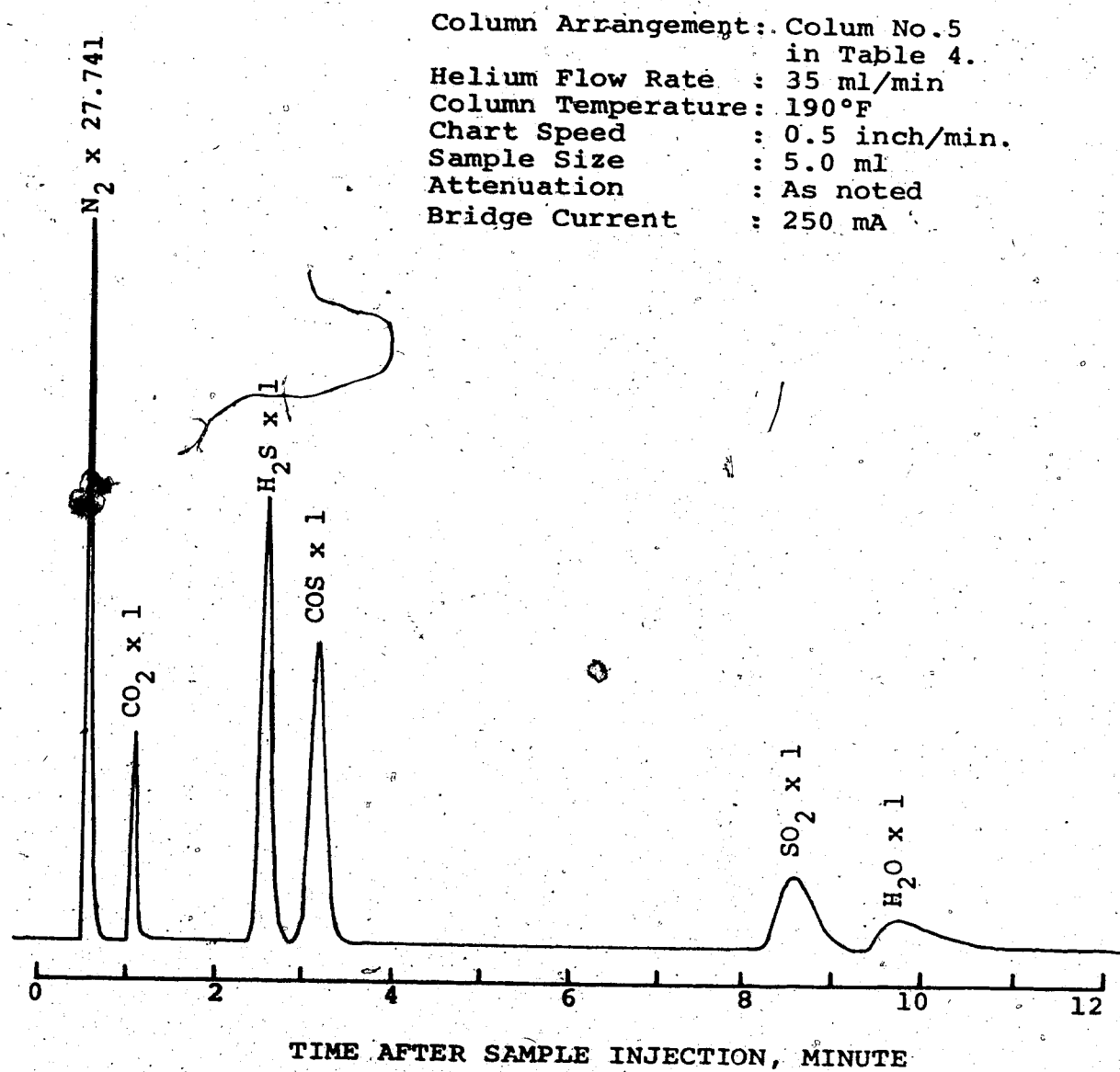


FIGURE 18: TYPICAL CHROMATOGRAM FOR SEPARATION OF N₂, CO₂, H₂S, COS, SO₂ AND H₂O

4.2.2 Selection Valve and Sampling Valve Mode

Two 6-way valves were used to select and sample the feed and product stream alternately. The structure and the detailed description of the operating condition of both valves were given by McGregor (72) and Liu (65). Both valves were actuated with air pressure of about 20 psi initiated by a manual push button on the control panel; the product stream was selected by pushing the button and the feed stream was selected when the push button was in the pulled-out position.

The sample injection button on the programmer chassis was pushed down manually for 13 seconds to sample the selected stream for GC analysis. The automatic sampling action by the cam adjustment had been employed by the former researchers (53,65,72) but was not used in this work because it was found to cause significant noise in the electrical circuit which extends from the GC output to the recorder, the integrator and the computer.

4.2.3 Attenuator Setting

The individual attenuator in the Beckmann-320 programmer which could be automatically actuated by adjusting the microswitch can also cause severe noises all through the electrical circuit when the cam

position changed. So the timer cam was not used throughout this work. Instead, three separate attenuators were installed; a chromatograph attenuator, attenuator I, and attenuator II.

The chromatograph attenuator was set to 10.0 which would give the maximum sensitivity while attenuators I and II were set to 10.0 and 5.0, respectively. These attenuator settings were determined by the condition that the maximum output of the largest peak (N_2 peak) from the GC should not exceed the maximum allowable input to the digital integrator at the maximum sensitivity range (50 mV).

The attenuator selection switch mode is shown on Figure A.4 in Appendix A. An on-off switch was provided in parallel with the attenuator I and II which were connected in series. When the switch was off, the attenuator I and II were connected to the output from the chromatograph attenuator giving the maximum attenuation ratio or minimum sensitivity. When the switch was on, the attenuator I and II were bypassed to obtain the maximum sensitivity or the minimum attenuation ratio. During the actual operation the switch was off for the nitrogen peak, and on for other peaks to obtain maximum sensitivity over the permissible input signal range to the integrator and the computer.

4.3 Reaction System:

The reaction system was comprised of the preheater, a reactor, a sulfur condenser, a water condenser and a sulfur trap. The schematic diagram of the reaction system is shown in Figure 19.

4.3.1 Feed Preheater

The feed mixture was preheated from room temperature to the desired reaction temperature by passing through the preheater. The preheater was constructed from a solid stainless steel block. Two high-resistance heating elements were inserted in holes drilled within the block, and stainless steel 316 tubing was wrapped helically about the exterior of the solid block in 20 pre-machined helical grooves. The entire assembly was insulated with a glass wool blanket. The power supply to the preheater was adjusted manually by a Variac. The temperature was measured and recorded by an iron-constantan thermocouple located at the top of the preheater and a Honeywell Elektronik 16 temperature recorder. An auxiliary U-shaped heating element was installed between the feed preheater and the reactor to compensate for the heat loss from the line. The temperature of this element was controlled by an on-off temperature controller fabricated by the shop in the Department of Chemical Engineering.

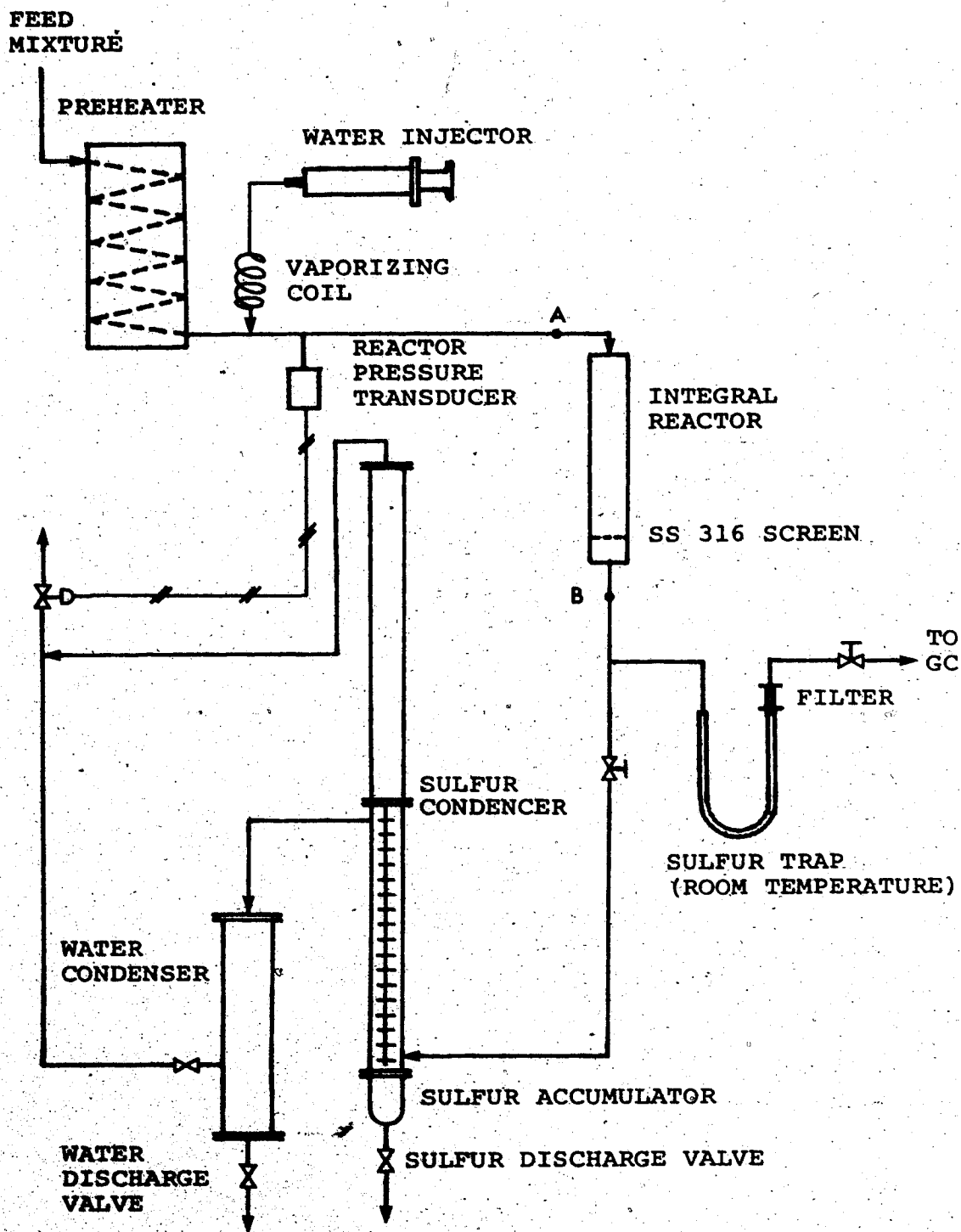


FIGURE 19: SCHEMATIC DIAGRAM OF THE REACTION SYSTEM

4.3.2 Reactor

An integral fixed bed reactor was used in this study. The reactor assembly was fabricated using a stainless steel 316 tube of 1 inch diameter and 9 inches long. A stainless steel 316 screen of 30 mesh size was fixed at the depth of 7 7/8 inch from the top of the reactor tube, which was connected to the reaction system by 1 inch Swagelok fittings. The reactor assembly was easily removable from the system by disconnecting at points A and B in Figure 19 whenever new catalyst was to be charged.

The temperature of the feed stream at the reactor inlet was measured just above the top of the catalyst bed and that of the product stream at the reactor outlet was measured just below the bottom of the bed by iron-constantan thermocouples which were precalibrated according to the procedure presented in Appendix B.

The reactor outlet temperature was controlled manually by adjusting the input current to the reactor wall heating element by means of a Variac. The reactor wall heating element was made of the nichrome wire wound uniformly around the reactor wall.

The pressure in the reactor during the reaction period was measured upstream of the reactor and controlled by a Statham electronic gauge pressure

transducer connected to a Foxboro V4A pressure control valve. The pressure transducer was precalibrated by the procedure described in Appendix B.

A water injection coil made of a stainless steel 316 tube of 1/16 inch diameter and 2 feet long was connected to the feed line between the preheater and the reactor. The water injected to the injection coil by a syringe pump was vaporized in the injection coil by heat supplied by the auxiliary heating element.

4.3.3 Sulfur Condenser and Water Condenser

The product stream from the reactor was divided into two streams; the first portion entered the sulfur condenser and then the water condenser before being vented, while the remainder of the stream entered the sulfur trap to remove the product sulfur vapor before reaching the GC analysis system.

The sulfur condenser originally designed by Liu (65) was found to be smaller than required for this study so that another additional one-pass condenser was added on the top of the original condenser to increase the holding time of the condenser system. The additional sulfur condenser was made of stainless steel tube of 3/4 inch in diameter and 20 inches in length with no interior baffles.

The temperature of the first condenser was maintained at around 350°C at the inlet and 110°C at the outlet so that the product sulfur might be condensed into the liquid phase, which helped to maintain a steady flow of the gaseous product mixture without any serious plugging. The second condenser was kept at the room temperature to completely knock-out the sulfur vapor which would not be condensed in the first condenser.

The water condenser was made of stainless steel pipe of 2 inch diameter and 10 inches in length, and packed with glass wool. The condensed water was allowed to flow by gravity into the bottom of the condenser to be accumulated before discharge through the vent valve attached to the bottom of the condenser. The product stream stripped of the sulfur and water vapor passed through the side opening to reach the reactor pressure control valve on the vent line.

Since the product stream entered the condenser system merely for disposal by venting, the design and operational conditions were not so critical as those required in the previous studies (53,65,72). The only performance requirement for the condenser system was to keep the reactor pressure constant while maintaining steady flow. Actually, however, the downstream part of the condenser system was gradually plugged with

entrained sulfur dust making it necessary to clean out the lines every week. The pressure buildup due to the accumulation of the sulfur dust in the line was compensated by gradually increasing the opening of the reactor pressure control valve.

The lines from the reactor to the sulfur condenser and to the sulfur trap as well as from the sulfur condenser to the water condenser were kept heated by wrapping with nichrome wire to prevent sulfur vapor from condensing in the lines. The first sulfur condenser itself was also heated with nichrome wire windings. To control the input current to each heater, separate Variacs were used.

A sulfur accumulator was attached to the bottom of the first condenser to receive the condensed liquid sulfur flowing downward by gravity. In addition a vent valve was installed at the bottom of the sulfur accumulator to avoid the replacement of the sulfur accumulator by regularly removing the accumulated liquid sulfur through the vent valve.

A detailed description of the structure of the first sulfur condenser was presented elsewhere (65).

4.3.4 Sulfur Trap

A sulfur trap was designed to remove the

product sulfur vapor before the product stream entered the GC analysis system. The first sulfur trap was made of a stainless steel 316 tube of 1/2 inch in diameter and 10 inches in length with a U-shape. No baffle was provided in the sulfur trap to reduce the dead zone around the base of the baffles which could cause the broader residence time distribution of the product stream in the trap. The second sulfur trap was made of 3/4 inch diameter stainless steel tube of 7 inches in length and V-shaped, with no baffles inside. Each sulfur trap was alternately used while the other was undergoing cleaning of the accumulated sulfur.

The temperature of the sulfur trap was kept just above the water vapor condensing temperature in the product stream, usually at the room temperature. This was to prevent absorption of H_2S and SO_2 in the condensed water with resulting chemical reaction which could cause incorrect GC analysis results of the product stream. The inlet temperature to this sulfur trap was measured by an iron-constantan thermocouple and recorded on the Honeywell 24 point electronic recorder. The outlet temperature from the sulfur trap to the GC system was also monitored by an iron-constantan thermocouple and recorded on the recorder.

Just next to the outlet of the sulfur trap, a

sponge filter made of polystyrene foam was packed in the line in about 1/2 inch depth to avoid any entrainment of dusty sulfur particles upstream to the GC.

4.4 Process Measuring and Control System:

All temperatures were measured by stainless steel-shielded iron-constantan thermocouples. The voltage signal from each thermocouple was adjusted by a Acromag model 323 electronic 0°C reference and then recorded on a Honeywell 24 point electronic recorder. The recorder was equipped with an integral solid state calibrator, a chart span selector of 5 to 5000 mV span and a voltage range suppressor of 0 to 1000 mV. The recorder was precalibrated using a potentiometer and occasionally checked when any malfunctioning was revealed. In almost all the experimental run, the 20 mV span was employed.

The total absolute pressure of the feed stream was measured by a Foxboro model 66 FR-2 electronic absolute pressure transducer while the feed flow rate by a Foxboro model 613 DL electronic differential pressure cell. The reactor pressure was measured by a Statham gauge pressure transducer. The signals from the feed and reactor pressure transducer were recorded

on the Foxboro 6430 HF electronic control recorder and controlled by the Foxboro V4A control valve.

The feed flow rate was controlled manually by the Foxboro 69 PA-1 control valve in combination with the valve V-M on the schematic flow diagram in Figure 16.

The reactor inlet and outlet temperatures, the sulfur condenser inlet and outlet temperatures, the sulfur trap inlet and outlet temperatures, the pre-heater temperature and the auxiliary heater temperature were controlled manually by adjusting the input current through the variacs. The temperature of the gas chromatograph oven was automatically controlled by a Honeywell R 7161 temperature controller.

The gas chromatograph and the process measuring devices were calibrated through the procedures described in Appendix A and B.

CHAPTER V

EXPERIMENTAL PROCEDURES AND RESULTS

The experimental work to be described herein deals mainly with improvements in the procedures employed in measuring conversions for reaction (1.2) using an integral fixed-bed reactor and then with evaluation of the performances of a number of catalysts over a variety of conditions. The latter experiments involve three main objectives; a comparison of activities between the newly developed bifunctional catalyst and a commercial alumina catalyst, a determination of the influence of ratio of mass of activating agent to mass of γ -alumina "support" upon the catalyst performance, and finally, an evaluation of maximum attainable conversions in the laboratory reactor.

5.1 General Experimental Procedures:

5.1.1 Startup of the System:

A known amount of a catalyst was loaded into the reactor, which was then gently vibrated to obtain a more uniform packing of the catalyst bed. After the reactor was reassembled, all of the threaded joints and fittings were checked for leakage using the soap

bubble test method with positive nitrogen pressure of around 30 psi within the system. When the system was gas-tight, the auxiliary heater and the reactor were insulated by a box-type covering made of a blanket of ceramic wool.

The nitrogen cylinder valve was then opened to start a flow of nitrogen through the system, and then all heating elements were switched on. The temperature of the catalyst bed was raised at the rate of approximately 3°C per minute until the feed temperature reached 570°K. With both the nitrogen flow and heating started, the flow of helium was initiated through carrier and reference sides in the GC system at the rate of 35 ml/min through each side. After switching on the GC systems which included the GC oven and the detector filament, it took about 3 hours to raise the GC oven temperature to 190°F and more than 12 hours to get a stable baseline.

5.1.2 Experimental Measurement of Integral

Conversions:

All newly charged catalysts were activated by heating continuously with first the nitrogen flow through the reactor, and then with the N₂ - H₂S mixture of about 3 mole percent in H₂S concentration.

The feed temperature during activation and reduction with H_2S was maintained at $570^\circ K$ for more than 3 hours, respectively, which was slightly higher than the normal operating temperature.

After checking the functioning of process measuring and controlling systems, the heaters about product lines leading to the GC and to the sulfur condenser, were started. The gas chromatograph base-line on the recorder was readjusted by manipulating the zero setting on the Beckman programmer panel. Then, the base-line for the digital integrator was adjusted separately by manipulating the zero knob on the Infotronic digital integrator. During the gas chromatograph base-line adjustment, the attenuation ratio was set at the maximum sensitivity, i.e. at the minimum attenuation ratio, on both the gas chromatograph and the recorder. The base-line adjustment could be checked visually on the recorder reading as well as numerically on the integrator printout.

Having finished the checking of the system behavior and readjusting the base lines of the GC and the integrator as needed, the feed mixture was introduced to the reaction system. To obtain desired flow rates and composition of the feed mixture, all the individual rotameters and the feed control valve were

adjusted to the proper level. After getting the results of the feed GC analysis, the component flow rates and the total flow rate of the feed stream were readjusted by manipulating the rotameters and the feed control valve until the desired composition and the flow rate were obtained. The total flow rate and the pressure of the feed stream were checked and readjusted by means of the differential pressure cell and the feed pressure transducer as described in Chapter IV.

To prevent disturbances in the analytical system which might occur due to the change of sample selection between the product and the feed stream, the same flow rate of the feed or the product stream through the GC detector was maintained by keeping the differential pressure constant on the mercury manometer which was installed in the sample vent line from the GC detector. Throughout this experimental work the differential pressure of this sample vent line has been kept at about 1 inch of mercury for both the feed and the product sample vent.

When the reactant mixture was fed into the reactor, the temperature of the catalyst bed increased quickly due to the exothermic nature of the reaction between H_2S and SO_2 . As a result, to

maintain a constant temperature in the catalyst bed the input current to the reactor wall heating element had to be readjusted.

After the reactor outlet temperature became stabilized, the feed and the product stream were alternately analysed by the gas chromatograph until more than three consecutive reproducible results for both streams were obtained. If the feed and the product compositions had remained unchanged, it was assumed that the reaction system had reached a steady state with a steady catalyst activity. Generally, when a new catalyst was introduced, a startup time of roughly one day was required because of the activation period required. In making consecutive runs in which temperature of the reactor or space velocity were changed, a new steady state could be obtained within roughly 2 days for the reactor temperature change and 3 hours for the change of the space velocity.

The experimental data thus obtained included the reactor inlet and outlet temperatures, and feed and reactor pressure, the feed flow rate, the atmospheric pressure, the room temperature and the GC area results by the digital integrator printouts.

5.1.3 Shutdown Procedure:

The reactant flows with the exception of nitrogen were stopped when a complete set of runs for one type of a catalyst was obtained. The nitrogen was kept flowing through the system for more than 5 hours to completely purge remaining reactants and products which might undergo additional reaction while standing within the closed system for prolonged periods. After complete purging, which could be checked by the H_2S smell in the product vent line, all power supplied to the system was switched off to cool the system to room temperature.

Before another new fresh catalyst batch could be charged, the reactor assembly was disconnected from the system. The batch of the used catalyst was carefully discharged from the reactor and examined for any changes during the reaction period before being stored.

5.1.4 Materials:

i) Feed Gases

All gaseous reactants, H_2S , SO_2 and CO_2 were obtained from Matheson Co. Nitrogen was obtained from Alberta Oxygen Ltd. Carbon dioxide was used for the

gas chromatograph calibration and was also obtained from the Matheson Co. The purities specified by the suppliers are listed in Table 5.

TABLE 5
PURITIES OF GASES

N ₂	99.99 % min.
H ₂ S	99.50 % min.
COS	97.50 % min.
SO ₂	99.98 % min.
CO ₂	99.995 % min.

However, the oxygen contamination in the nitrogen cylinder was frequently detected and so, every nitrogen cylinder newly delivered was always checked for oxygen content using Molecular Sieve 5A column of 16 foot by 1/4 inch O.D. preconditioned in vacuum at 250°C for 20 hours. The thermal conductivity cell was kept at 220°C and the bridge current was 150 mA. The column temperature was kept at 135°C with the helium flow rate of 80 ml/min. The purity of H₂S or SO₂ was checked from the feed GC analysis data. The resulting feed GC data never showed peaks other than N₂, H₂S or SO₂ peak, which meant that no detectable amount of impurities existed in the H₂S or SO₂ cylinder. In the COS cylinder carbon dioxide was.

always detected in very low concentration, but water vapor was not detected. Since carbon dioxide can be treated as an inert gas, which was demonstrated in Chapter III, the COS cylinder was used without any further purification of COS.

ii) Catalysts

The standard catalyst employed in this study for the purpose of comparison between different catalysts was S-201 γ -alumina manufactured by Kaiser Aluminum and Chemical Sales Inc. The properties of the S-201 catalyst specified by the manufacturer are presented in Table 6.

TABLE 6

STANDARD CATALYST PROPERTIES (S-201)

Surface area:	380 m ² /gm
Chemical composition on dry basis:	
SiO ₂	0.020 %
Fe ₂ O ₃	0.020 %
TiO ₂	0.002 %
Na ₂ O ₃	0.300 %
Al ₂ O ₃	93.600 %
Ignition loss	6.000 %

The developed bifunctional catalyst evaluated in the present study were prepared by crushing Kaiser S-201 alumina catalyst in the size range of -3 to +8 mesh and selecting the -12 to +24 mesh fraction through the use of standard sieves. This was followed by chemical treatment with various concentrations of $\text{Cu}(\text{NO}_3)_2 \cdot 3 \text{H}_2\text{O}$ before heat treatment in an oven for 20 hours at a temperature of 550°F. Heat treatment resulted in the evolution of oxides of nitrogen (109).

2 Data Reduction Procedure:

The experimental measurements of temperatures, pressures and flow rates were obtained in terms of the percentage of full scale readings on the electronic recorder except for those of the atmospheric pressure and room temperature. The reactor inlet and outlet temperature data were converted to the actual temperature scale in degree centigrade using the calibration equation presented in Appendix B. The pressure data were converted to absolute pressure in mm Hg for the feed, and to gauge pressure in mm Hg for the reactor pressure according to the calibration equations presented in Appendix B. The feed flow rate data were converted to the actual flow rate in

SCFH by means of the calibration equation for the differential pressure cell obtained through the procedure described in Appendix B.

The feed and product compositions were calculated from the gas chromatographic peak areas using the calibration equation for each component as described in Appendix A. To calculate the molar feed rate of each feed component from the calculated feed composition and flow rate, the assumption of ideal gas behavior was applied for all gaseous components. In calculating the product stream composition, the nitrogen flow rate was taken to be the same in both the feed and the product streams since nitrogen was an inert gas in this reaction system. From the calculated nitrogen flow rate and the composition of the product stream, the molar flow rate of each of the reactants in the product stream was obtained.

The fractional conversion was then obtained from the difference between the molar flow rate of a reference reactant in the feed and the product stream. As a reference reactant, H_2S was chosen for the H_2S-SO_2 reaction, and COS for the $COS-SO_2$ reaction.

The partial pressure of each component over the catalyst bed in the reactor was calculated from

7

the product composition and the total pressure in the reactor, taking into account equilibrium distribution of elemental sulfur species.

A computer program for calculation of the material balance was written to process the experimental raw data into the calculated conversion of H_2S and COS simultaneously. The detailed calculation procedure for a particular run is shown in Appendix I, accompanied by the listings of the corresponding computer program, MTBAL, which was stored in the disc core memory.

Input of the raw data to the IBM 1800 computer system and output from the computer in the form of printing of the computed results were performed on the remote teletype located in the laboratory.

5.3 Experimental Results and Discussions:

5.3.1 Preliminary Investigations:

i) Performance Test of the Sulfur Trap

To check whether significant additional reaction due to the catalysing effect of the liquid sulfur occurred during the condensing within the trap of sulfur vapor in the product stream, two

different methods were tested.

The first method used an ice-bath. The U-shaped sulfur trap was immersed in a cold bath filled with ice-salt mixture to maintain a constant bath temperature of -20°C . When the product stream was introduced through the sulfur trap, both sulfur and water vapors were condensed into the solid phase near the entrance of the sulfur trap. This resulted in frequent plugging of the line, which necessitated frequent cleaning of the sulfur trap.

In the second method, a high flow-rate method, the U-shaped sulfur trap was kept just above the water vapor condensing temperature, around 20 to 30°C depending upon the water content in the product stream. In this method, only sulfur vapor was condensed in the trap.

In these tests the feed to the reactor contained 3 percent of H_2S , 1.5 percent of SO_2 and the balance N_2 on the molar basis, and the temperature of the product stream at the inlet to the sulfur trap was around 500°K . The tests were carried out over flow-rates of the product stream through the sulfur trap ranging from 20 to 500 ml/min.

Figure 20 shows the comparison between the performances of the two methods. For the high

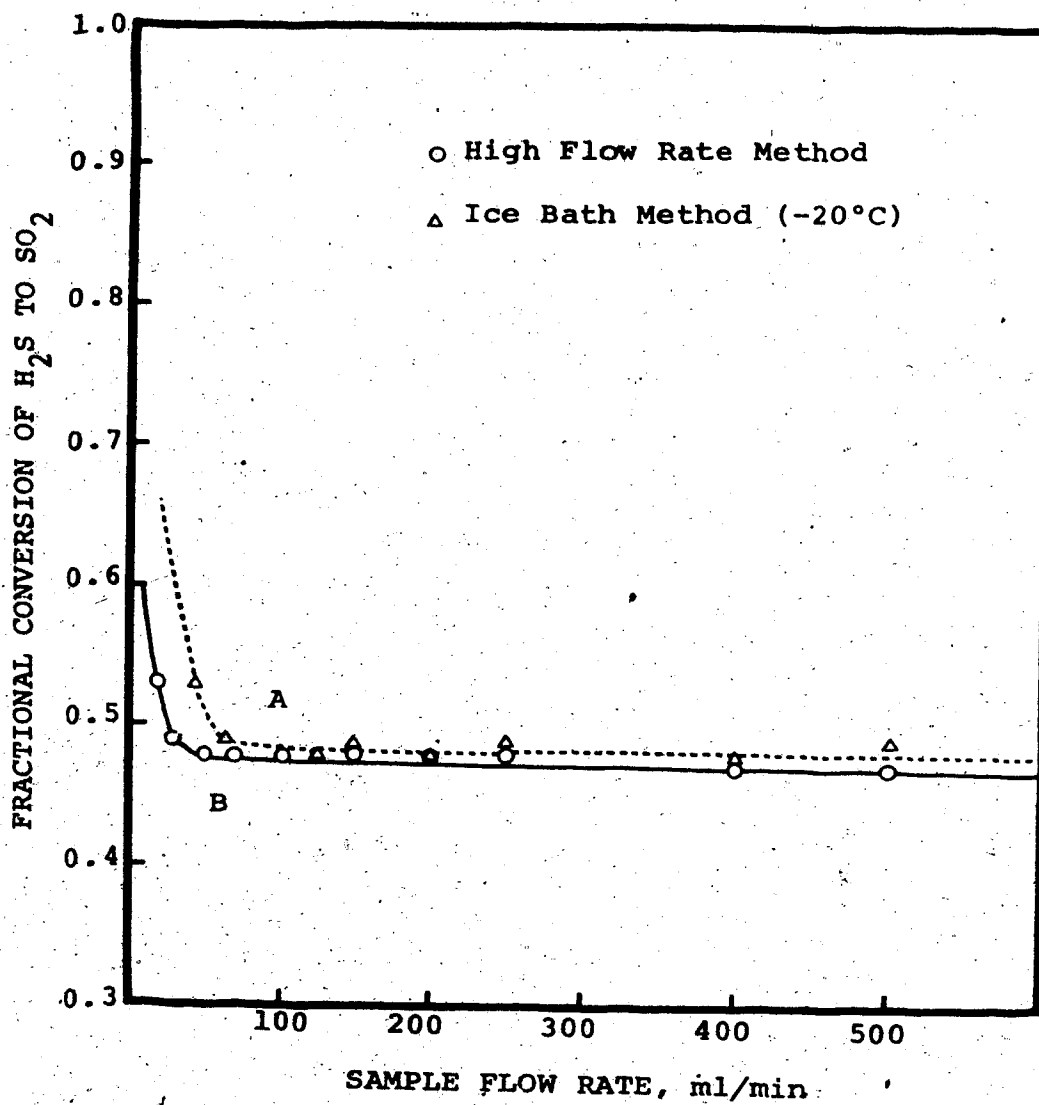


FIGURE 20: SULFUR TRAP PERFORMANCE TEST

flow-rate method the effect of the additional reaction due to the catalysing effect of the condensed liquid sulfur appeared to be significant at a flow rate below 30 ml/min of the product stream as shown in curve B. In the ice-bath method the high conversion level of H_2S at the low flow-rate range of below 50 ml/min, as shown in curve A, seemed not to be the results of any additional reaction but to be the result of physical absorption of H_2S in condensed water during the condensing period of water vapor. To check the effect of physical absorption of H_2S in liquid water the sulfur trap was kept at a temperature below the saturation temperature of water vapor. The resulting data showed that the H_2S and SO_2 peaks in the product stream decreased. Sometimes H_2S peaks completely disappeared from the product stream. The physical absorption effect was much more significant for H_2S peaks than for SO_2 peaks under the same condition.

In the high flow-rate method, because of the smaller temperature gradient between the wall of the sulfur trap and the product stream compared to the ice-bath method, the condensing rate of sulfur vapor might be supposed to be slower, and the condensing zone in the trap to be longer than those in the ice-bath method. In spite of these phenomena, the resulting data shown in Figure 20 revealed that the high

flow-rate method at room temperature gave lower conversion of H_2S than the ice-bath method. It should be noted here that the lower the conversion of H_2S which was obtained during a steady-state run, the better the performance of the sulfur trap.

As a result, no convincing advantage is apparent for using the ice-bath method when the flow-rate of the product stream exceeds 100 ml/min. The disadvantage of the ice-bath method, therefore, was found to be the difficulty of eliminating the H_2S absorption in condensed water while that of the high flow-rate method was the entrainment of sulfur mist downstream from the sulfur trap.

By considering these performance test results and disadvantages of each method, it was decided that the high flow-rate method would be employed for this research but with a modification of the sulfur trap. The modification was done by packing a dust filter, made of styrene foam, right near the outlet of the sulfur trap to provide sulfur demisting. A flow-rate of 200 ml/min through the sulfur trap was employed throughout this study.

ii) Homogeneous Reaction Test in the Preheater

The effect of homogeneous reaction between H_2S and SO_2 in the preheater was checked before making kinetic runs. When the flow rate of the feed mixture

was above 2.0 SCFH, the effect of homogeneous reaction in the preheater at 600°K was found to be negligible. However, when the preheater was contaminated with the product liquid sulfur, the effect of homogeneous reaction was quite significant. This sulfur contamination occurred due to condensation and accumulation of the product sulfur in the preheater when the preheater was not completely purged out before shut-down of the heating system after each run.

Considering the above preliminary investigations the preheater was completely purged out using pure nitrogen for more than 5 hours after each kinetic run to prevent any possible condensation or accumulation of the product sulfur due to the slow homogeneous reaction in the preheater. Since the effect of the homogeneous reaction was found to be significant when the feed flow rate was below 2.0 SCFH, the feed flow rate above 2.0 SCFH was adopted throughout this study except for runs K and L for the test of the maximum obtainable conversion level of the Claus reaction.

iii) Calibration of the Gas Chromatograph

The gas chromatograph was calibrated according to the procedures presented in Appendix A.

The first calibration, whose results were shown in Figure 21, was based upon the no-individual attenuation scheme in which only one general purpose attenuator (chromatograph attenuator) was used. In this calibration, the reliabilities of the digital integrator and the computer were examined by comparing their results with that of the disc integrator which could be supposed to be the most correct. In Figure 22, the integrated results from the digital integrator and the disc integrator shows good consistency while those obtained by the computer are very much scattered. This scattering may be attributed to an improper input signal to the computer system without any attenuation of the output signal from the GC detector since the attenuation scheme II has been employed throughout the first calibration procedure. The results from the digital integrator in the first calibration were applied in data reduction calculation for suns A, B, C, D, E and J.

A second calibration was carried out as above but using different attenuation ratios for the N_2 -peak and other peaks. Since the digital integrator performance proved to be quite reliable in the first calibration, the disc integrator was not used to check the accuracy of the second calibration. The attenuation scheme III was employed for this calibration. The

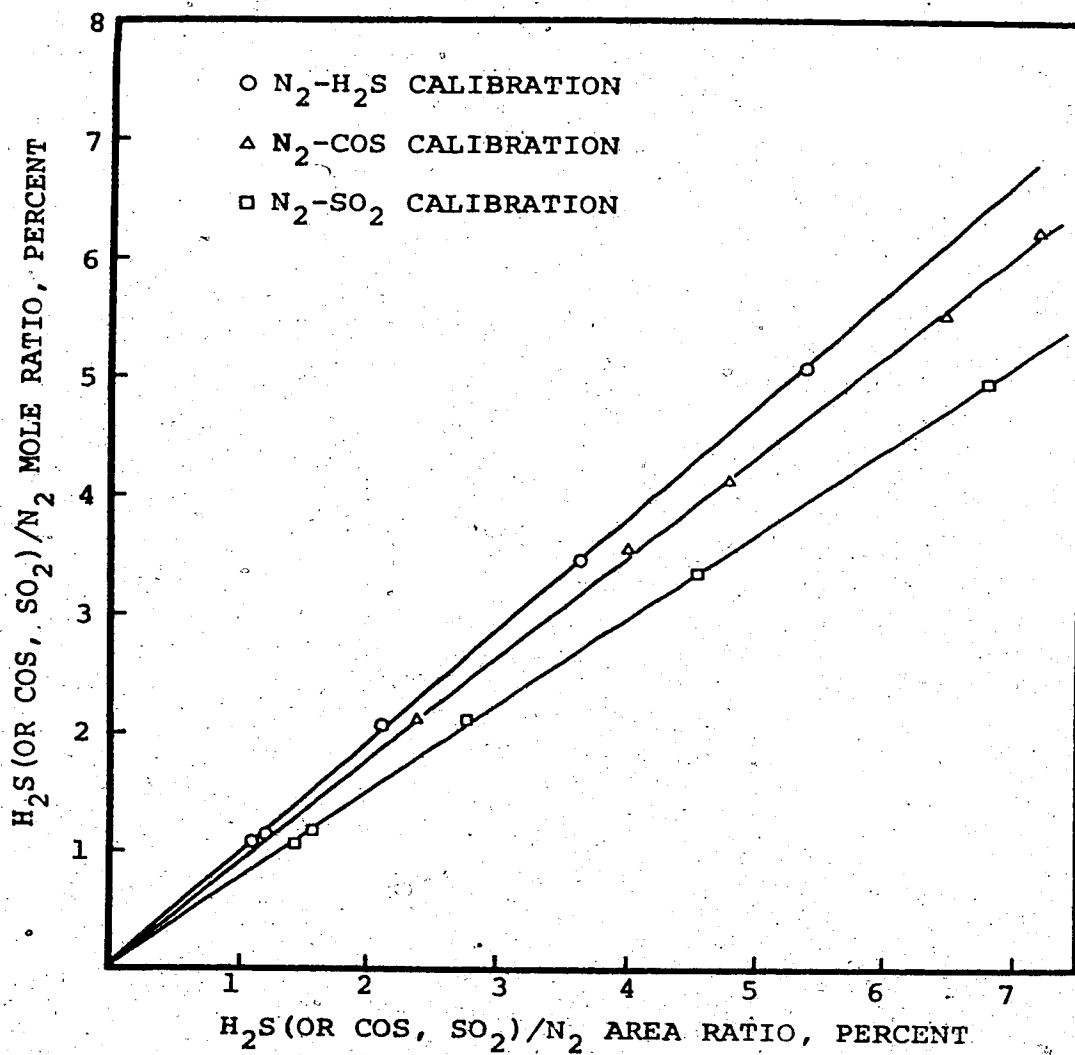


FIGURE 21: FIRST CALIBRATION OF GAS CHROMATOGRAPH

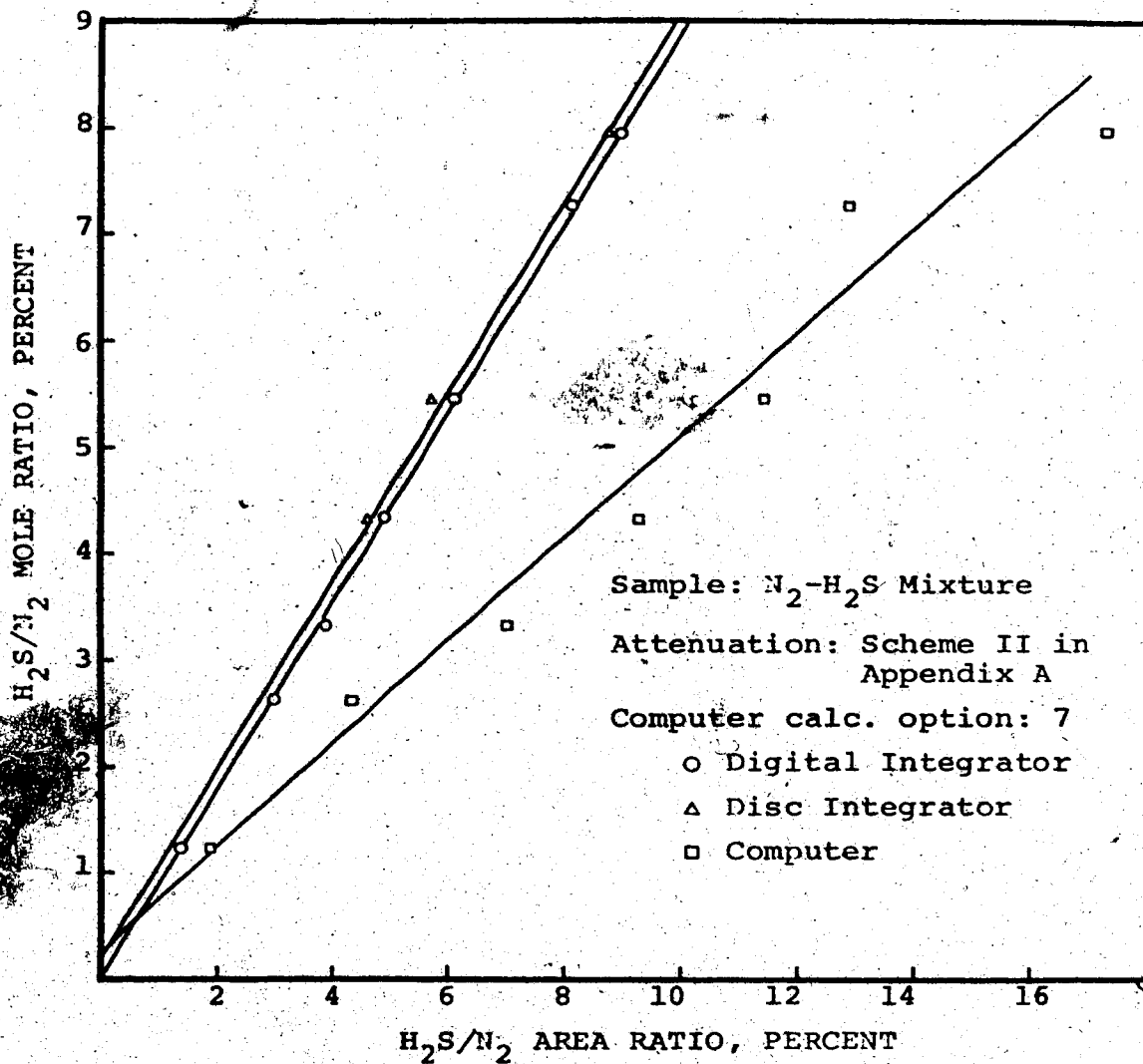


FIGURE 22: PERFORMANCE COMPARISON OF DIFFERENT INTEGRATING SYSTEMS

results in Figure 23 show a very good consistency between the digital integrator and the computer. The second calibration results by the digital integrator was used in data reduction calculation for runs F, G, H, I, K and L.

Reproducibility of the computer and the digital integrator has been compared for a calibration run in Table 7.

TABLE 7

COMPARISON OF REPRODUCIBILITY

Peak	<u>Digital Integrator</u>		<u>Computer</u>	
	<u>Ave. Area</u>	<u>Avg. % Deviation</u>	<u>Avg. Area</u>	<u>Avg. % Deviation</u>
N ₂	198768	0.0039845	5319610	0.0042479
H ₂ S	73196	0.0054839	1939811	0.0079665
COS	97239	0.0034246	2587350	0.0041820
SO ₂	18646	0.0375630	456142	0.0128670

In the above comparison the calculation option 2 was employed in GCJOB definition because the calculation option 7 required a detailed elution time data for each peak. These were not conveniently available because the status of the equipment at the

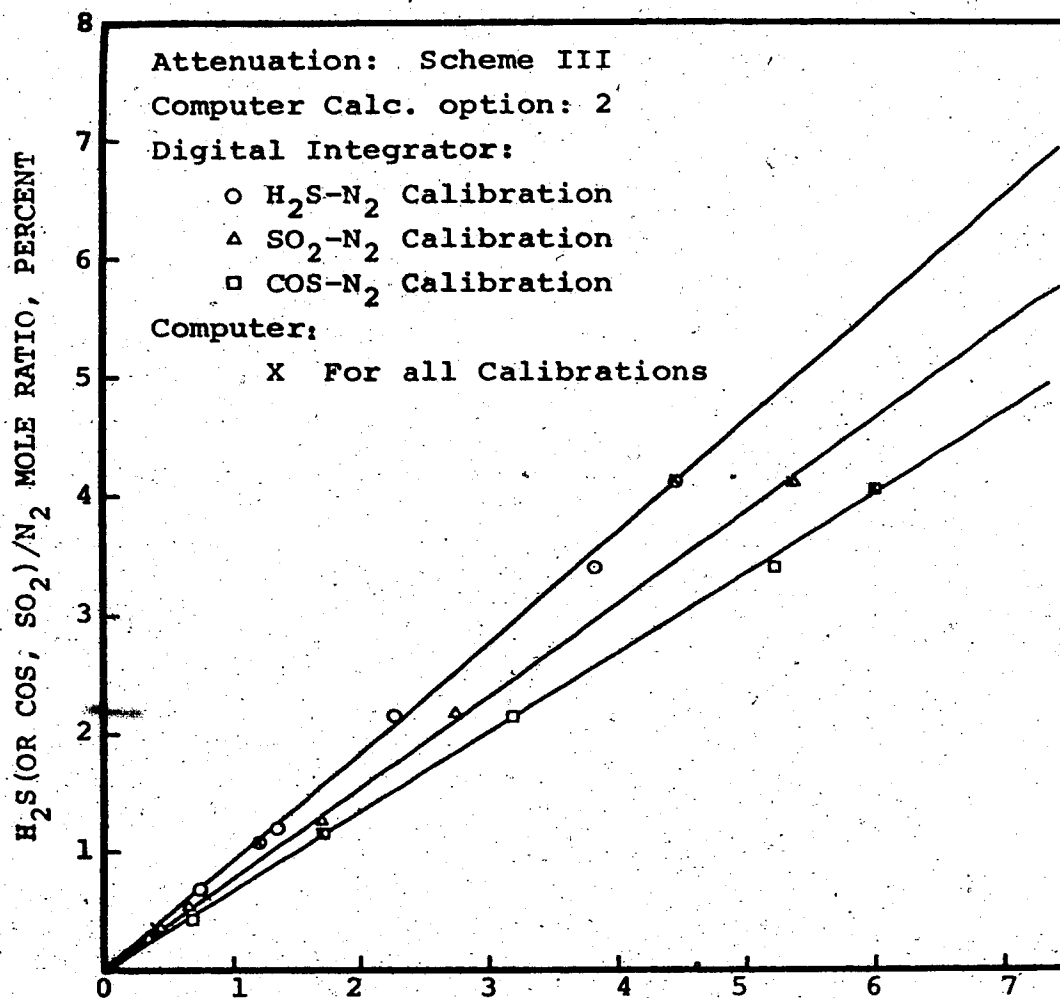


FIGURE 23: SECOND CALIBRATION OF GAS CHROMATOGRAPH

time of this study was still not fixed. Detailed descriptions on the calculation option can be found elsewhere (110).

Table 7 shows that reproducibility of the digital integrator is better than the computer for N_2 , H_2S and COS peaks but worse for the SO_2 peak. The less reproducible result for the SO_2 peak of the digital integrator seemed to be due to base line readjustment to correct drifting during the experimental run. The SO_2 peak is very sensitive to the base line adjustment due to its flat Gaussian shape and a long elution time. However, the need for SO_2 peak areas could be eliminated by using areas of other components in the sulfur balance calculation for the reaction system. Thus, it was decided to use the digital integrator rather than the computer. The lower reproducibility in the computer results seemed to originate with the interfering effect of signal transmission noises along the electrical circuits leading to the computer input terminal, and also to the absence of detailed information on the elution time of each peak. This missing information prevented the computer from starting action at the right instants during the GC cycle.

The integrated results from the digital integrator or from the computer were printed on a Victor

digit-matic printer, or on a teletype, respectively, at the end of each peak.

5.3.2 Comparison of Catalyst Activities

i) Effect of Catalyst Promoter Upon Simultaneous Reactions

Simultaneous conversions of both the $\text{H}_2\text{S-SO}_2$ and the COS-SO_2 reactions on four catalysts were measured in the integral-bed reactor to evaluate the dual activities of each catalyst. The catalysts tested included pure γ -alumina (S-201), 5.4 % Cu-on-alumina, 12.08 % Cu-on-alumina, and 16.07 % Cu-on-alumina. The weight of a batch of catalyst approximated 1.0 gram in the particle size range of -12 to +24 mesh. Each catalyst was preconditioned in the same way using the procedure described in the general experimental procedure of section 5.1. Before starting to obtain kinetic data, this procedure included an initial heating period with nitrogen flow for about 3 hours, then maintaining the bed with nitrogen flow at the temperature of 290°C for a further 3 hours, finally followed by the reduction period with combined N_2 and H_2S flow for another 3 hours.

The feed mixture was usually composed of 3 mole percent of both H_2S and COS , 1.5 mole percent of

SO₂, and the balance, N₂. Keeping the feed composition and reactor inlet and outlet temperatures constant, only the feed flow rate was changed to get conversion-space velocity data for each catalyst. After obtaining one data point at a fixed space velocity, it took about 3 hours to reach a new steady state at a different space velocity.

Here it should be noted that the size of catalyst particles used in this study averaged around 5 times smaller than that for catalyst pellets used in the field plant, making the external surface per unit catalyst volume also about 5 times larger than that of the plant catalyst pellet. To compensate for this increased external surface area per unit volume of the catalyst bed, a space velocity of 5000 hr⁻¹ would be expected to be reasonable to simulate the field plant space velocity of 1000 hr⁻¹. However, upon considering the external transport resistances existing at a space velocity of 1000 hr⁻¹ as shown in Chapter III, a higher space velocity appears to be desirable in comparing the catalytic activities of different catalysts since the true activities might be disguised by the effect of the external resistances. Furthermore, a better discrimination between activities of different catalysts may be obtained at higher space velocity region as may be seen in Figure 24. Therefore,

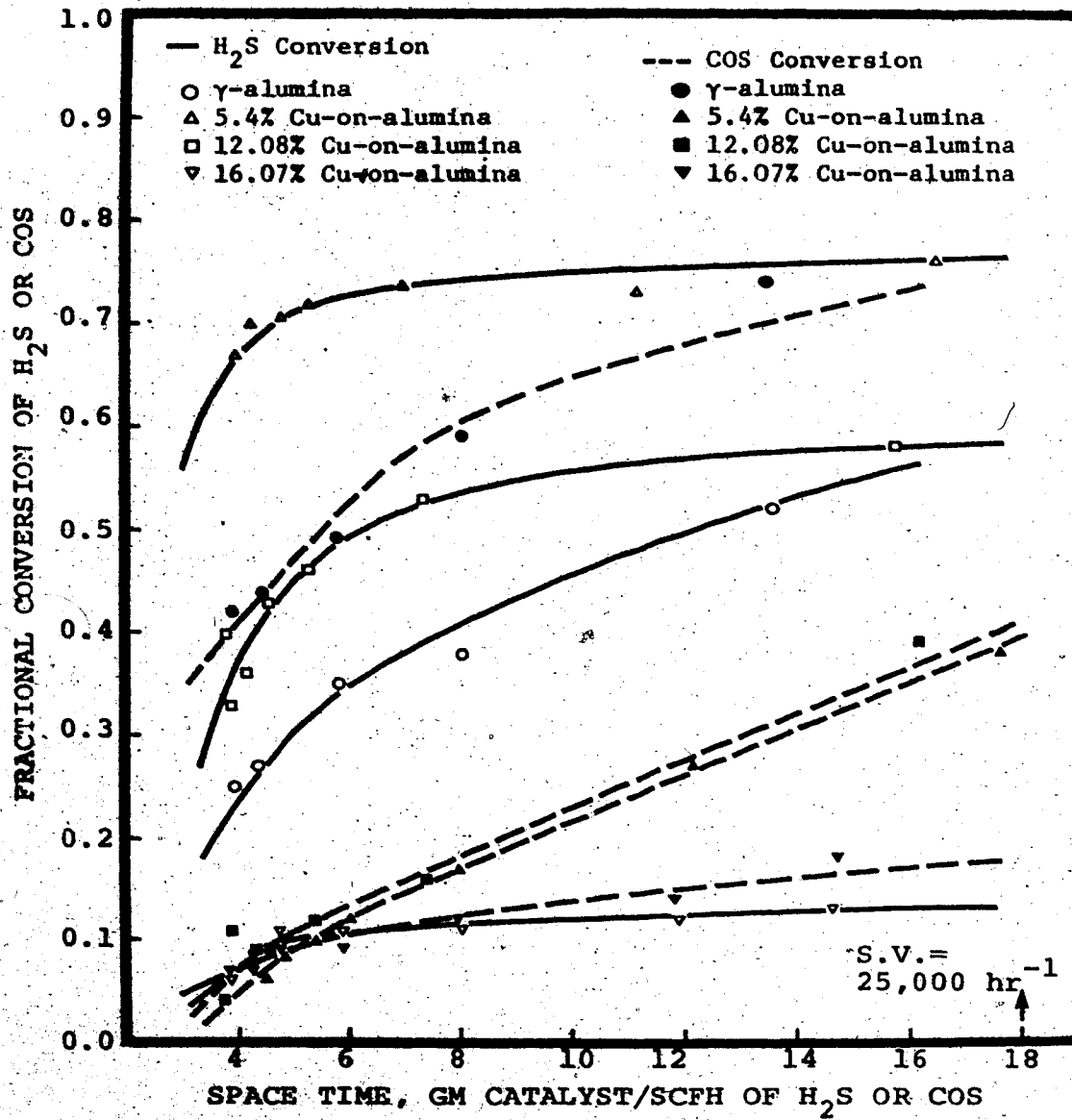


FIGURE 24: SIMULTANEOUS CONVERSIONS USING DIFFERENT CATALYSTS

a space velocity ranging from 25,000 hr^{-1} to 150,000 hr^{-1} was used throughout this study, which averages about 17 times larger than the plant operational condition.

For each experimental run, the space time, $W/F_{\text{H}_2\text{S}}$ (or W/F_{COS}), was calculated and plotted versus the fractional conversion of H_2S (or COS) as shown in Figure 24. The computer program "MTBAL" presented in Appendix I was used in these calculations and data processing was initiated through the input terminal (teletype) connected to the IBM 1800 computer system.

The conversion of H_2S and COS in the simultaneous reaction system, $\text{H}_2\text{S}-\text{SO}_2$ and $\text{COS}-\text{SO}_2$, is shown in Figure 24 for each catalyst tested. It can be seen that 5.4% Cu-on-alumina is most active for the $\text{H}_2\text{S}-\text{SO}_2$ reaction while pure γ -alumina (S-201) is most active for the $\text{COS}-\text{SO}_2$ reaction. Figure 25 has been plotted from Figure 24 at fixed space-times of 8.0 and 14.0 (gm-catalyst/SCFH of H_2S or COS) to isolate the effect of copper content on the conversion level of both $\text{H}_2\text{S}-\text{SO}_2$ and $\text{COS}-\text{SO}_2$ reactions. It shows that the maximum catalytic activity for the $\text{H}_2\text{S}-\text{SO}_2$ reaction appears to be at a copper content of around 5%. Figure 25 also shows that the addition of copper markedly reduces the catalytic activity for the $\text{COS}-\text{SO}_2$ reaction. A clear explanation for this effect of copper content

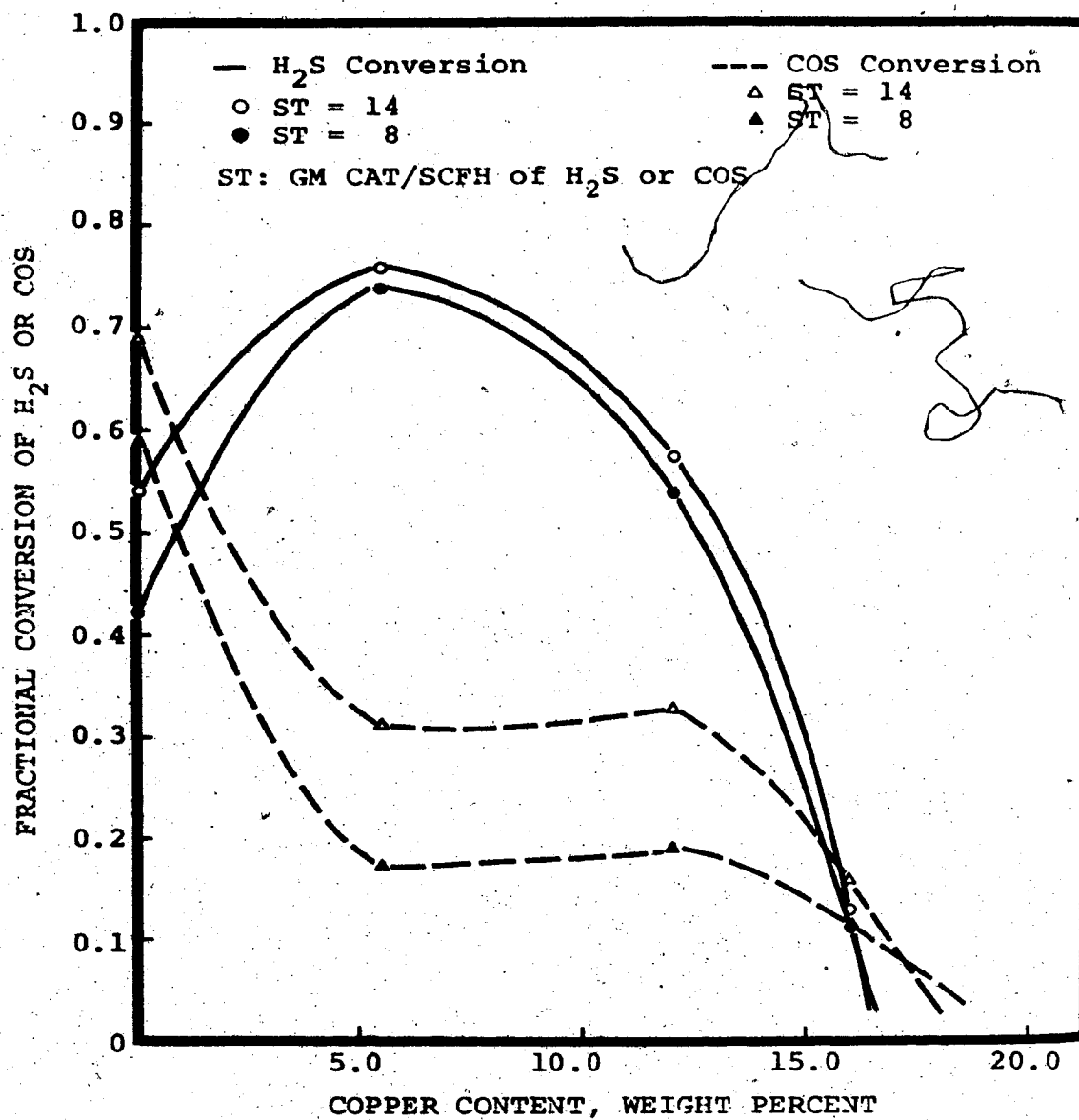


FIGURE 25: EFFECT OF COPPER CONTENT ON THE CONVERSION LEVEL

upon the catalytic activity for the two reactions is not available at this stage of the study. However, one may conjecture that the role of copper in the bifunctional catalyst may be explained by the donation of its 4s-electron to an electrophilic Lewis-acid site on the alumina surface. Furthermore, since the energy level of 3d-orbital is only slightly lower than that of 4s-orbital in a copper atom, a 3d-electron of the copper atom may easily be attracted to H_2S or SO_2 molecules promoting the adsorption of H_2S or SO_2 on the copper surface. Then copper on the Lewis-acid site is presumably sulfided by H_2S and SO_2 to form CuS (which was recognized by the color change of the catalyst particles from deep blue to black). When the copper surface is sulfided, the catalytic activity becomes stabilized and reaction conversion steadies. This additional catalytic effect by the sulfided copper for H_2S-SO_2 reaction enhances the H_2S conversion level to some extent as shown in Figure 25 at a copper content below 5.4%. Up to 5.4% copper content, most of the copper may be sited on the Lewis-acid site as an electron donor, but when the copper content exceeds about 5.4%, the basic sites may also be occupied by copper, but now as an electron acceptor. This could inhibit the H_2S-SO_2 reaction since Liu(67) has shown basic sites to be necessary for the reaction to

proceed.

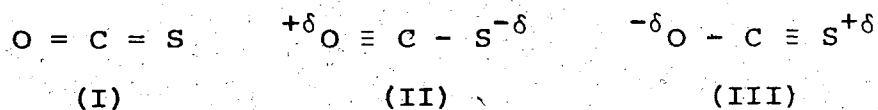
The above hypothesis may be strengthened by considering the effect of the copper content on the COS-SO₂ reaction conversions. As the copper content increases for COS-SO₂ reaction, the activity of the alumina catalyst decreases almost linearly up to roughly the same copper content of 5.4%. Then the activity becomes almost stabilized with increasingly larger copper contents up to a copper content of approximately 12% as shown in Figure 25. When the copper content exceeds 12%, the activity decreases again with the increasing copper content. From the above observations it may be assumed that excess copper could be sited on both the remaining Lewis-acid sites and basic sites when the copper content exceeds 12%.

To explain the above observations, the adsorption and reaction mechanism of H₂S, SO₂ and COS on the pure γ -alumina surface as well as on the Cu-on-alumina catalyst surface should be discussed.

On the pure γ -alumina surface, both H₂S and SO₂ were found to be adsorbed on the Lewis-acid sites in the latest results of Liu's study (66). For the adsorbed H₂S and SO₂ to react, basic sites were vitally important (67). Carbonyl sulfide was also found to be adsorbed on the Lewis-acid sites (19). Therefore, the Lewis-acid sites on the pure γ -alumina surface may be

competed by H_2S , SO_2 and COS making two reactions, $\text{H}_2\text{S}-\text{SO}_2$ and $\text{COS}-\text{SO}_2$, competitive rather than independent. From the above reasoning the pure γ -alumina may not be considered to be a bifunctional catalyst for the above two reactions. However, the individual reaction conversion is substantially high for both of the reactions as shown in Figure 24. This may be due to the low coverage of Lewis-acid sites by reaction components at the reaction temperature of about 285°C .

A COS adsorption mechanism on the alumina surface may be proposed on the basis of the balance bond formalism. Carbonyl sulfide is a hybrid of three resonance structures (32) as shown below:

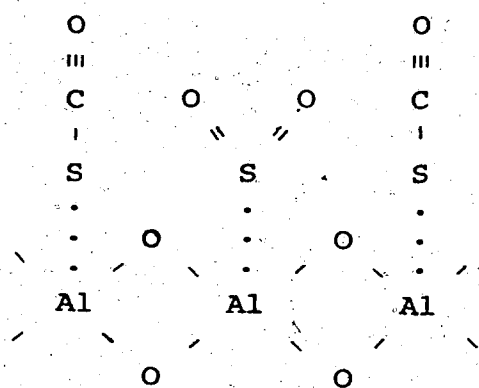


Although resonance structure I and II predominate (32), resonance structure III, in which oxygen has a residual negative charge, is probably more favored to the Lewis-acid site than the other structures because the oxygen atom is more electronegative than the sulfur atom.

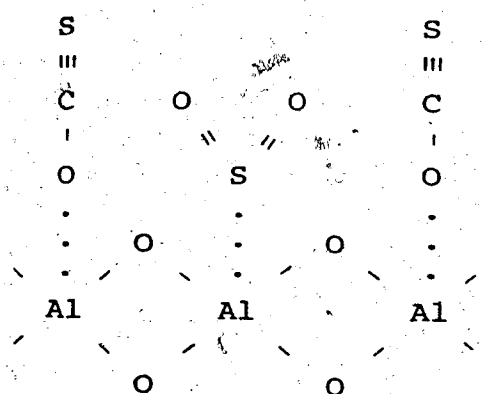
Since carbonyl sulfide may be considered a stronger base than H_2S or SO_2 , it should be chemisorbed on the Lewis-acid site on the alumina surface, which has already been demonstrated by Liu (65). Chuang et al. (19) proposed a mechanism in which COS was adsorbed

on the Lewis-acid site with the sulfur atom on the alumina surface but it is more likely that the adsorption of COS on the Lewis-acid site is also a hybrid of the two mechanisms; the sulfur atom on the Lewis-acid site or the oxygen atom on the Lewis-acid site. When COS adsorption occurs according to the former mechanism, chemisorbed COS on the Lewis-acid site could readily react with a chemisorbed SO_2 or H_2O on a neighboring Lewis-acid site by a Langmuir-Hinshelwood dual-site mechanism and leave an adsorbed sulfur atom on the alumina surface. On the other hand if COS adsorption occurs according to the latter mechanism, reversible adsorption of COS may occur without reaction with neighboring SO_2 .

From the above analysis, an adsorption and reaction model may be proposed as follows:



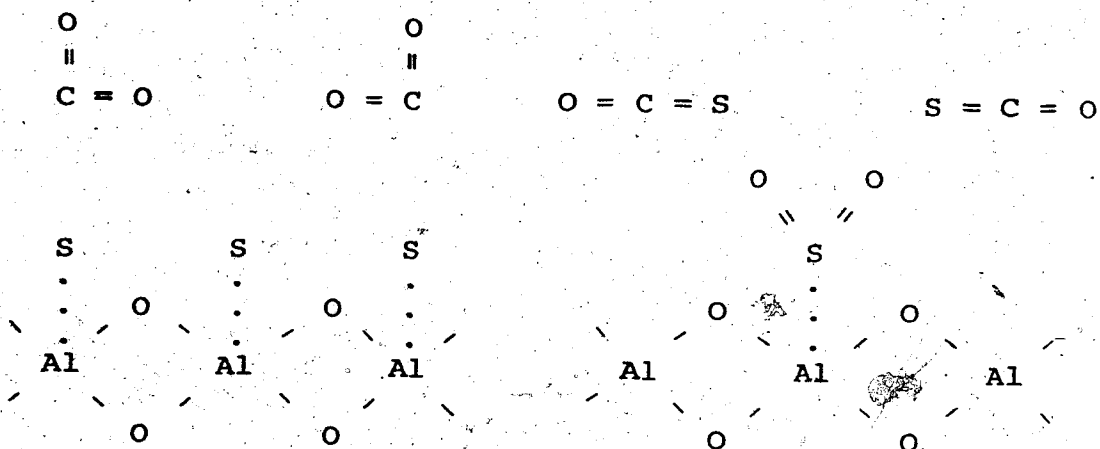
(adsorption I)



(adsorption II)

◻ reaction

◻ no reaction



On the Cu-on-alumina catalyst, the mechanism of COS-SO₂ reaction may be the same as on the pure γ-alumina, but most of the H₂S-SO₂ reaction may occur on the copper surface rather than on the alumina surface. Increasing the copper content affects both of the reactions as may be seen in Figure 25. Blocking of the Lewis-acid sites with copper atoms may reduce the number of adsorption sites for COS causing the activity to decrease for the COS-SO₂ reaction because Lewis-acid sites are critically important for this reaction. Therefore, the inhibiting effect of copper on the COS conversion level may be explained by the blocking of the Lewis-acid sites with copper even if the COS-SO₂ reaction could be bypassed by the faster COS-H₂O reaction. The hydrolysis reaction of COS will be discussed in more detail in a later section.

On the other hand, adsorption and reaction of H₂S and SO₂ may be enhanced by the sulfided copper on the Cu-on-alumina catalyst. Therefore, the reaction conversion increases when the copper content increases to some extent, beyond which copper may occupy basic sites to suppress the reaction rate as shown in Figure 25.

Therefore, it may be concluded, for the Cu-on-alumina catalyst, that the H₂S-SO₂ reaction may proceed largely on the sulfided copper surface rather

than on the Lewis-acid sites of the alumina surface, while the COS-SO₂ reaction proceeds on the Lewis-acid sites according to the same mechanism as on the γ -alumina catalyst; the Cu-on-alumina acts as a bi-functional catalyst for two reactions, H₂S-SO₂ and COS-SO₂, which may be confirmed by the data in Figure 28.

Unfortunately, however, the reason why sulfided copper could promote the rate of H₂S-SO₂ reaction is not fully understood in this study. Presumably it may be due to the change of the electronic configuration of copper making the accessibility of H₂S and SO₂ easier.

ii) Comparison of Individual Reaction Rates
During Simultaneous Reactions

Individual reaction rates were compared for one selected catalyst, 5.4% Cu-on-alumina, by varying the space velocity. When water was introduced with the feed stream, distilled water was injected through the vaporizing coil by means of the water injection pump shown in Figure 19. The water injection pump was precalibrated through the procedure described in Appendix B. All of the other experimental procedures were identical to those described in (i), and the experimental results are shown in Figure 26.

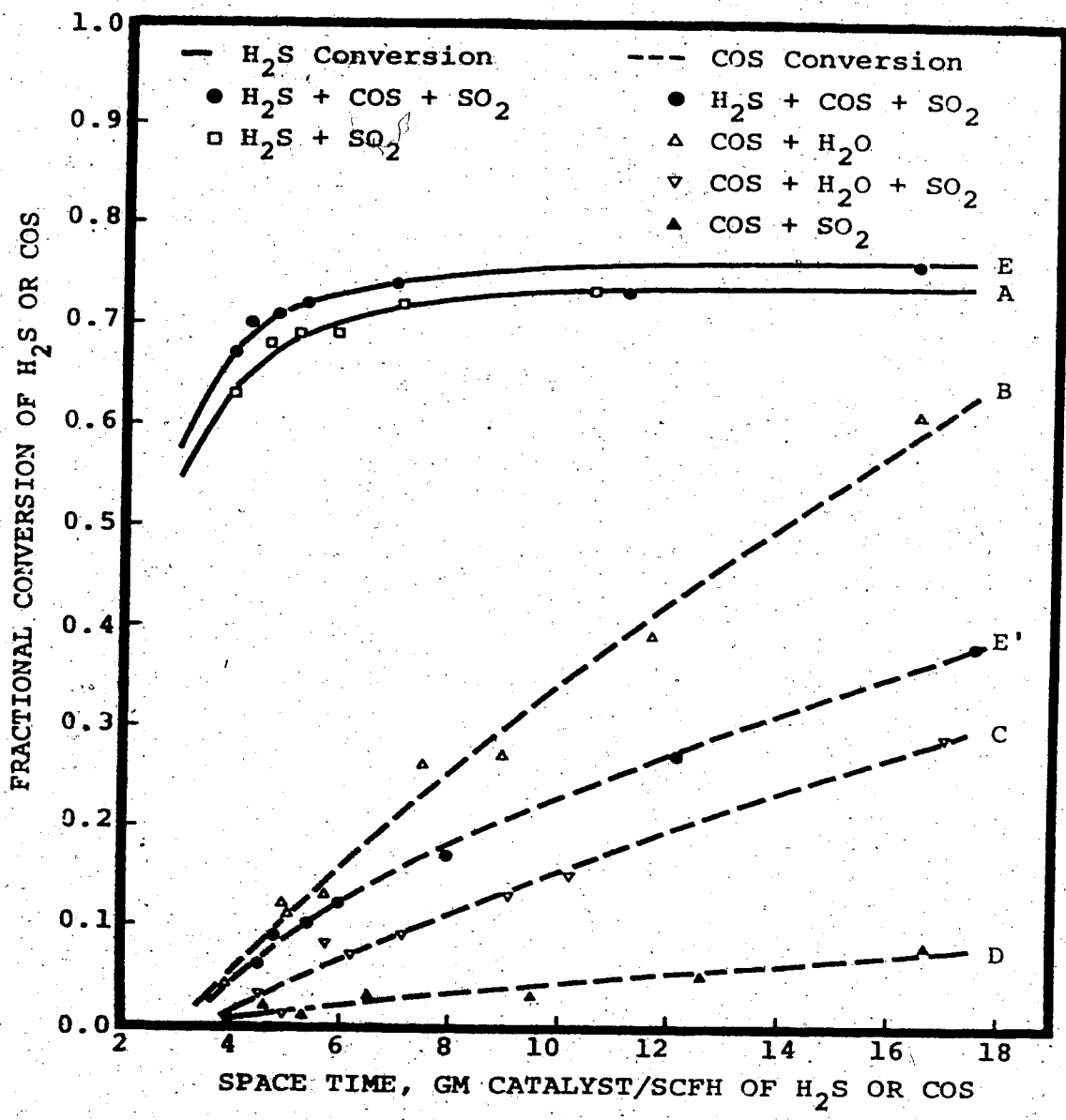


FIGURE 26: COMPARISON OF INDIVIDUAL REACTION RATE ON 5.4% CU-ON-ALUMINA CATALYST

A slight difference in the level of the H_2S conversion may be seen between curves A and E in Figure 26. This small difference in the conversions may be explained by the effect of the difference of the heat of reaction between the two reaction systems. In the reaction system E, the total heat of reaction is slightly larger than that for the reaction system A due to the combined effect of both exothermic reactions, H_2S-SO_2 and $COS-SO_2$. The resulting slightly higher bed temperature may cause a higher conversion of H_2S . If the above reasoning correctly explains the observed phenomena, a bifunctional activity of this catalyst for both H_2S-SO_2 and $COS-SO_2$ reactions is quite evident. This combined heat of reaction effect can also be seen in the reaction systems C and E'. A slightly higher conversion in the reactions system E' can be explained by its combined heats of reaction being larger than that from the reaction system C.

From curves B and E' it may be concluded that the hydrolysis reaction of COS is inhibited by the presence of SO_2 , which means that SO_2 competes with H_2O for adsorption sites on the alumina surface. That is, H_2O (or SO_2) adsorbed on the Lewis-acid sites reacts with COS adsorbed on the neighboring Lewis-acid sites.

The conversion in the reaction system D indicates that no CO_2 -poisoning occurs in 5.4% Cu-on-alumina catalyst during COS-SO_2 reaction period, which is in contrast to the findings by Liu (65) for pure γ -alumina in the absence of water vapor. The reason for this contrast is not yet evident but it may be due to the residual amount of water vapor presumably present on the catalyst or to an independent catalytic role of copper for the COS-SO_2 reaction.

The effect of water content in the feed stream upon the rate of COS hydrolysis has been investigated using pure γ -alumina catalyst and the results are shown in Figure 27. When the water content becomes higher than 1.5 mole percent of the feed stream, which is one-half the stoichiometric amount for 3.0 mole percent of COS content in the feed, the hydrolysis reaction appears to be zero order with respect to water. On the other hand, when the water content remains below one-half the stoichiometric amount, the reaction rate increases as the water content increases. For stoichiometric amount of water content, the results in this study agree with other investigations (37,79) reporting that the hydrolysis of COS is of zero order with respect to water concentration for both γ -alumina and Co-Mo-alumina catalysts. However, no published

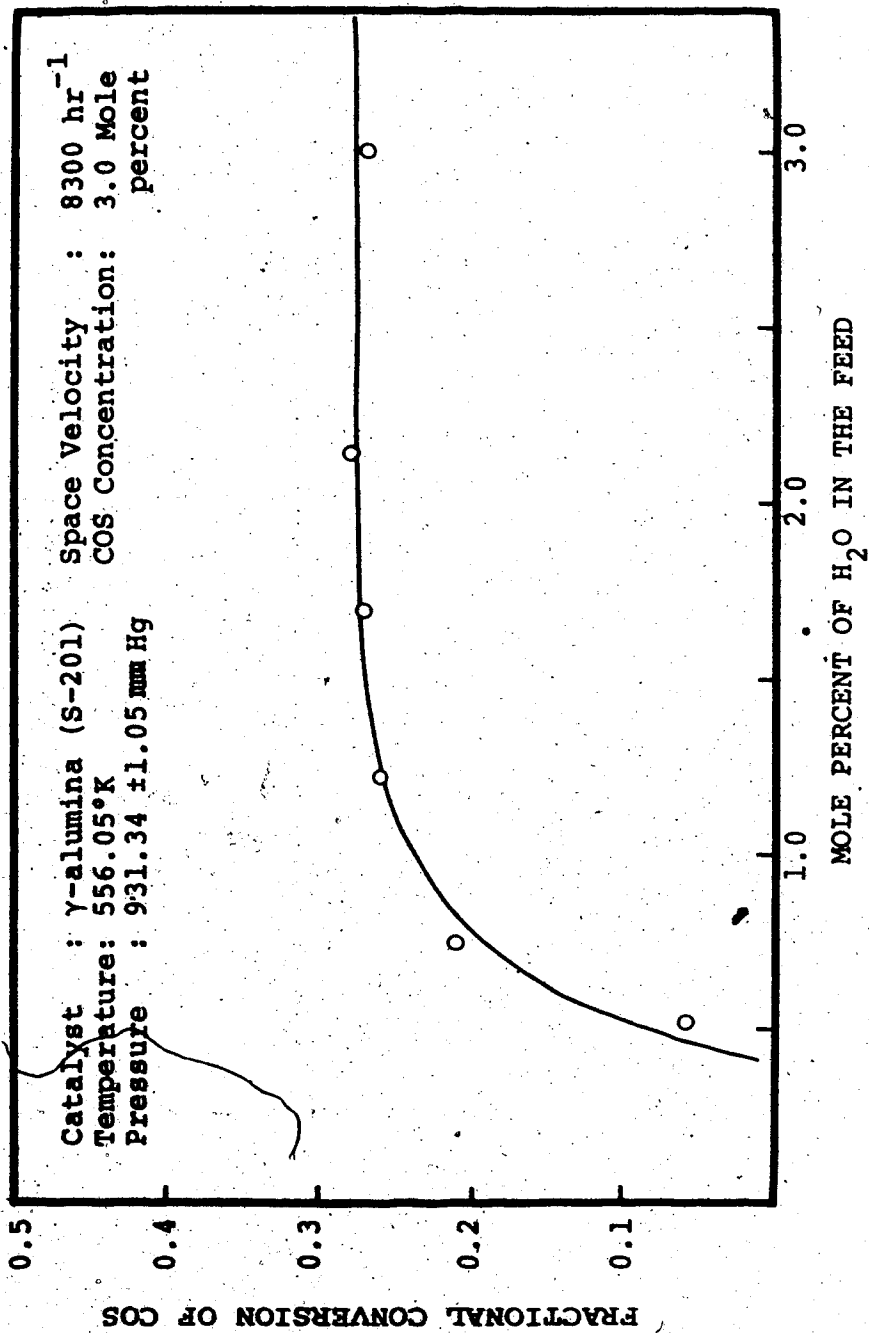


FIGURE 27: EFFECT OF WATER CONTENT IN THE FEED ON HYDROLYSIS OF COS ON γ -ALUMINA

data seems to be available for low concentrations of water in the feed.

5.3.3 Performance Test on the Bifunctional Activity:

To demonstrate more clearly the bifunctional characteristics of the catalyst for the simultaneous reactions, H_2S-SO_2 and $COS-SO_2$, a 12.08% Cu-on-alumina catalyst was used. While this composition is not an "optimal" composition for the bifunctional catalyst, reference to Figure 25 shows that the result will still apply to the "optimal" composition of about 5.4% Cu.

The amount of catalyst tested was 1.0213 gm with a space time of around 6.0 gm-catalyst per SCFH of H_2S (or COS). The observed results are shown in Figure 28. The conversion levels A and AA represent the conversion of H_2S and COS respectively when the feed mixture contains H_2S , SO_2 and COS in 3:3:1.5 mole percent with the balance N_2 . Then, the COS feed line was cut off and the conversion level B1 was obtained for the single reaction between H_2S and SO_2 . After measuring the conversion level B1 for about one hour, the H_2S feed line was closed and then the COS feed line was opened to make the $COS-SO_2$ reaction proceed without being interrupted by H_2S-SO_2 reaction.

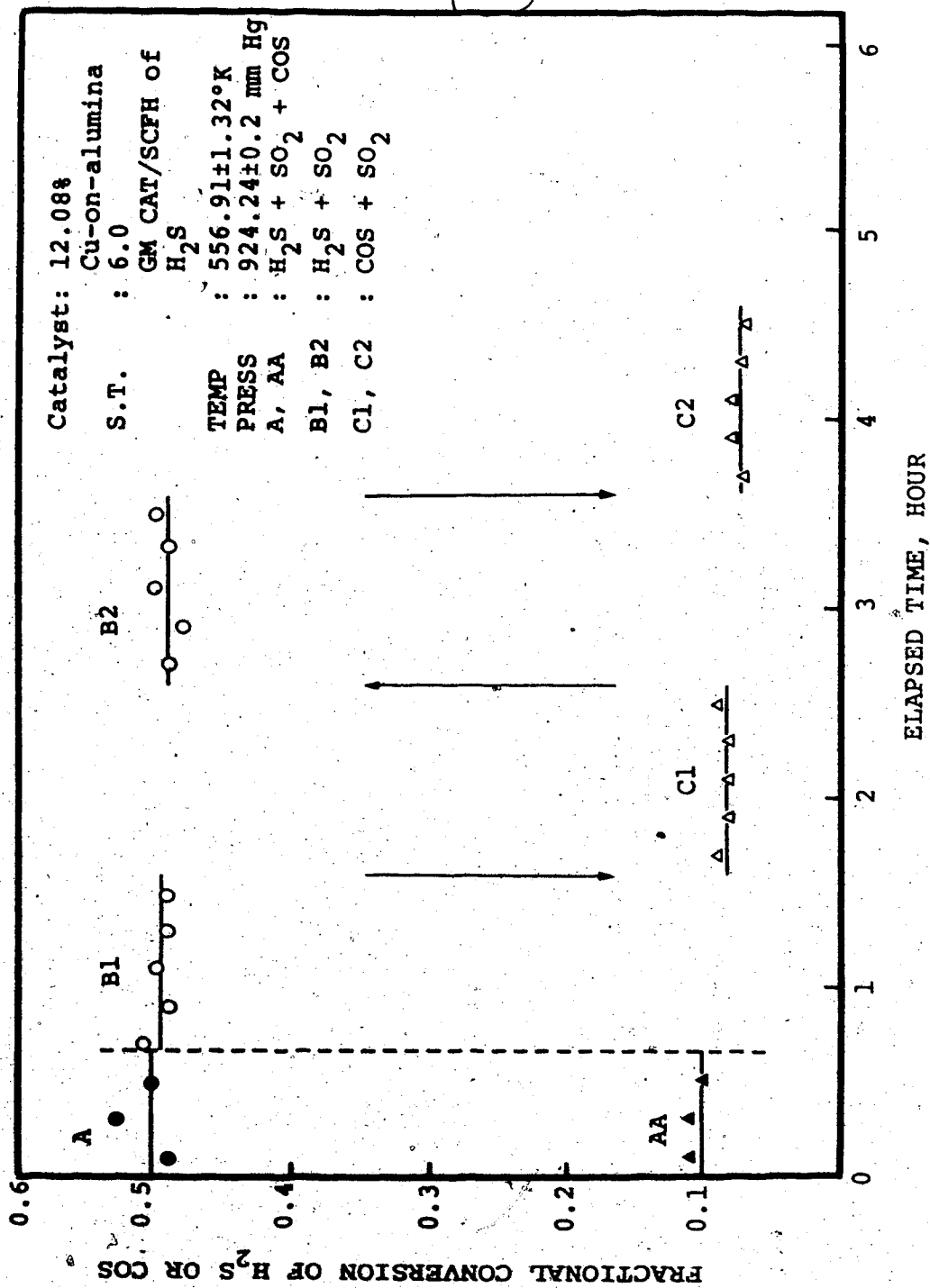


FIGURE 28: TEST OF BIFUNCTIONAL CHARACTERISTICS OF CU-ON-ALUMINA CATALYST

The resulting conversion level of C1 was obtained. The conversion levels B2 and C2 were then obtained through the same procedure as was done to obtain B1 and C1.

The conversion levels of H_2S in A, B1 and B2 in Figure 28 are nearly the same, which means that the catalyst tested essentially acts as a bifunctional catalyst without interaction from the other reaction. The small difference in the conversion level between the reaction system A and B1 (or B2) since the combined heat of reaction in the reaction A is slightly higher than that in the reaction B1 (or B2) which may cause a slightly higher reaction rate. The same analysis may be applied to the conversion level AA and C1 (or C2), for COS conversion in the $COS-SO_2$ reaction, confirming the bifunctional characteristics of this catalyst.

5.3.4 Maximum Obtainable Conversion Level:

Pure γ -alumina (S-201) was chosen to investigate the maximum obtainable conversion level for comparison with the theoretical thermodynamic equilibrium conversion level. The feed mixture consisted of 3 mole percent of H_2S , 1.5 mole percent of SO_2 and the balance, N_2 . The amount of the catalyst

charged was 35 gram packed in a bed depth of roughly 6 inches. The feed temperature to the catalyst bed and the reactor outlet temperature were kept the same and varied from 550°K up to 700°K.

Before examining the conversion data as a function of the reactor outlet temperature, the relationship between conversion and the space velocity was examined at a fixed reactor outlet temperature of 700°K. From the results shown in Figure 29, it can be seen that in the region below the space velocity of 20 hr⁻¹ (or above the space time of 0.05 hour) the conversion has almost leveled off but is still rising slowly with decreasing space velocity (or increasing space-time). The asymptotic experimental conversion level may be found to be 89.5% at 700°K in Figure 29, while the thermodynamic equilibrium conversion is 72.5%.

In additional experimental runs, the space velocities of 100 hr⁻¹ and 4 hr⁻¹ were fixed to examine the upper limit of the obtainable conversion level in the Claus reaction. The resulting experimental data are plotted in Figure 30 where they may be compared with the computed thermodynamic equilibrium conversions by Gamson and Elkins (35), and McGregor (72) as well as with the experimental data

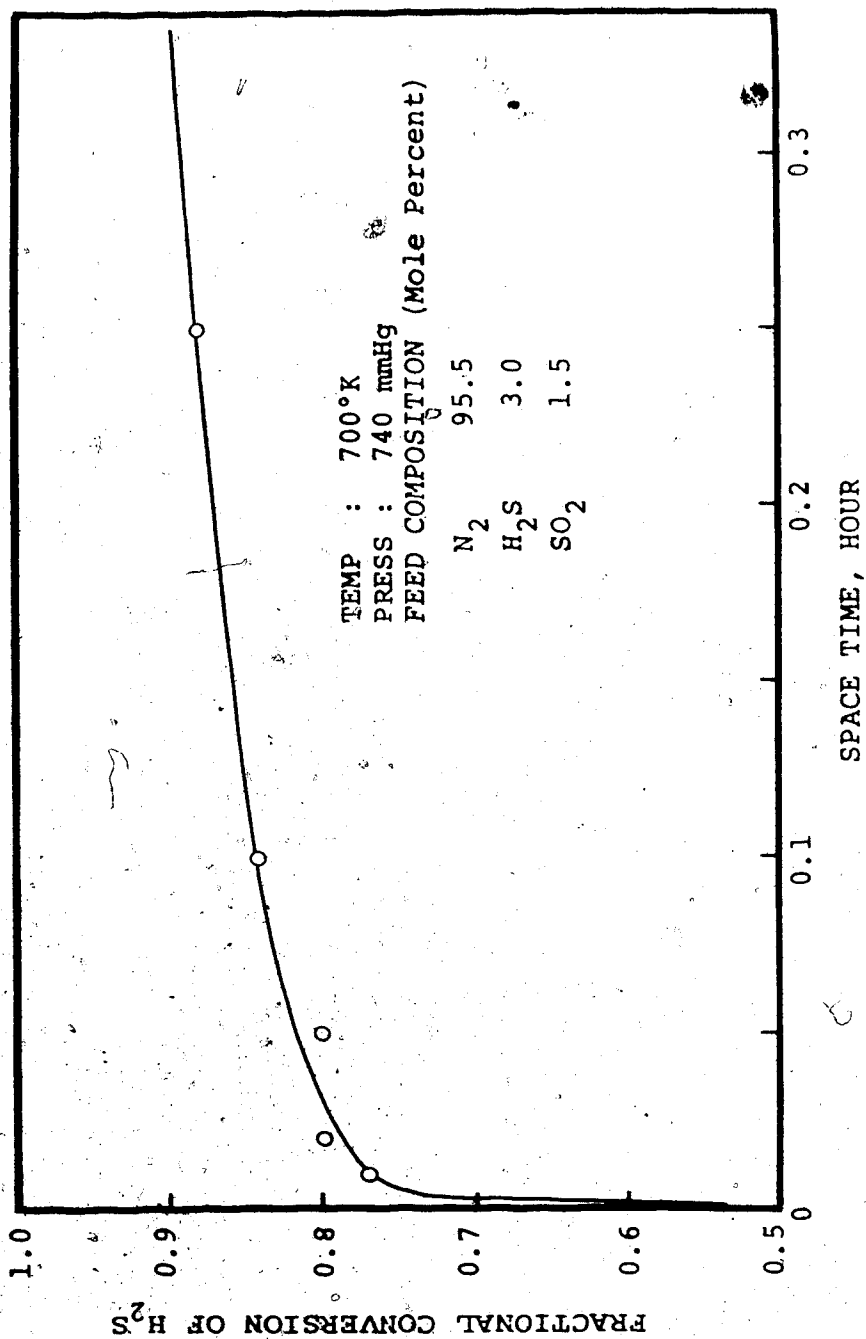


FIGURE:29: CONVERSION LEVEL AS A FUNCTION OF SPACE TIME

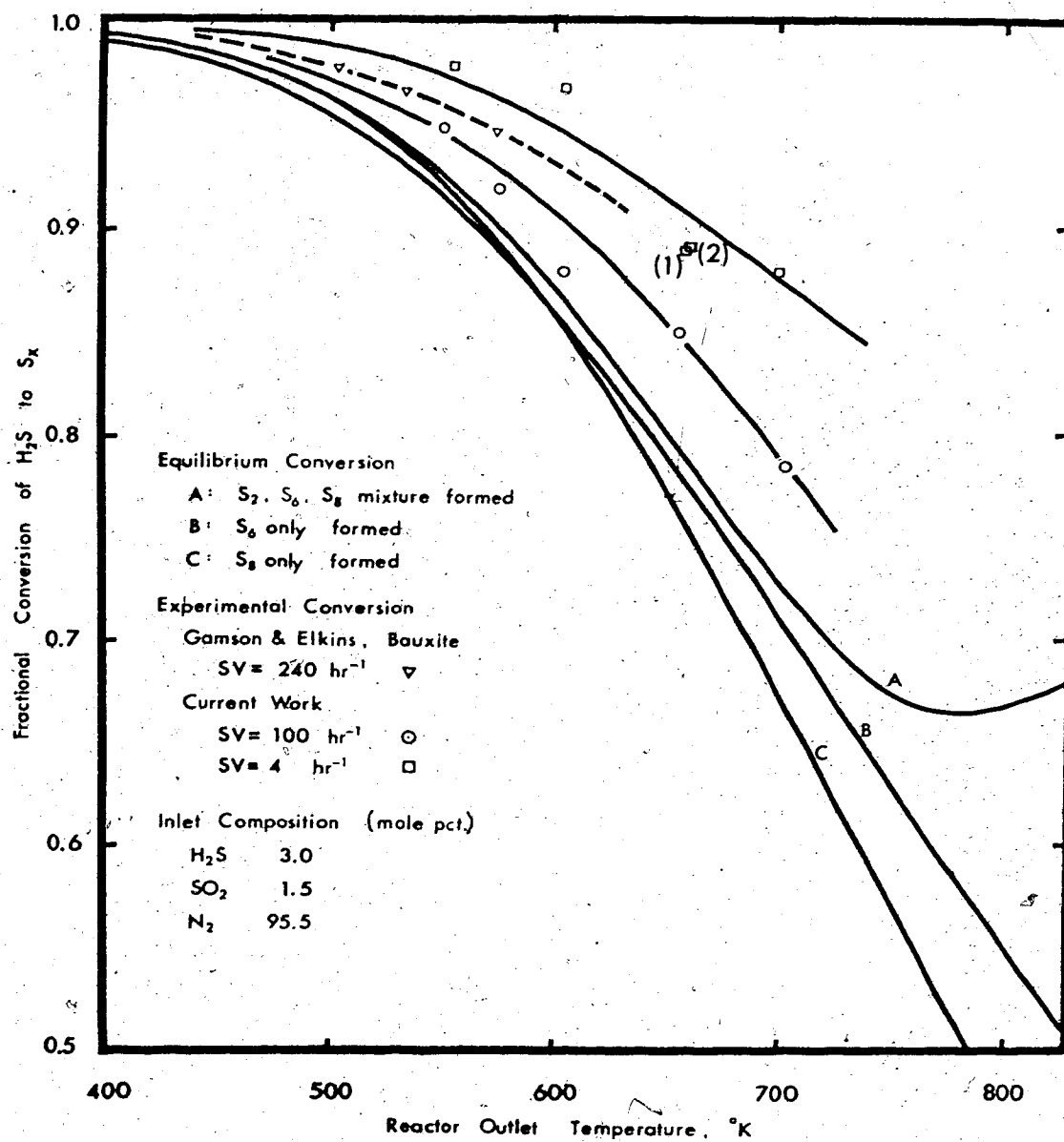


FIGURE 30: COMPARISON BETWEEN PREDICTED AND EXPERIMENTAL CONVERSIONS AS A FUNCTION OF REACTOR OUTLET TEMPERATURE

Gamson and Elkins (35).

In Figure 30 curve C represents the thermodynamic equilibrium conversion at different reaction temperatures computed on the assumption that the product sulfur exists only as S_8 , while curve B shows the computed results based upon the product sulfur in the form of S_6 . On the other hand, with an equilibrium distribution between S_2 , S_6 and S_8 species the equilibrium conversion curve A was predicted.

In these experimental runs it required more than 24 hours to reach a steady-state conversion level. It was found that the smaller the space velocity the longer the time to reach a steady state. In Figure 30 the data point (1) was obtained after 24 hours while the data point (2) was obtained after 72 hours since the flow condition and the reactor temperature had been stabilized. The two data points show essentially the same conversion indicating that the steady-state condition had been reached in about 24 hours.

Quite unexpected but very interesting results were obtained in this experimental run as may be seen in Figure 30. The experimental conversion level at the space velocity of 100 hr^{-1} is well above the equilibrium conversion level for all the temperature

range between 550° and 700°K. The overshooting of the experimental conversions beyond those for the equilibrium curve is even higher in the case of the space velocity of 4 hr⁻¹ than in 100 hr⁻¹. These results are compared with those Gamson and Elkins (35) obtained at a space velocity of 240 hr⁻¹.

This large discrepancy between the experimental and theoretical equilibrium conversions cannot be fully explained at this stage. However, the following suggestions might be pertinent.

First, possible inaccuracies in temperature measurement may result in misplotting of the data points above the equilibrium conversion curve. However, this possibility is very small considering the well-equipped experimental apparatus and measuring devices used in this study in contrast with the rather large discrepancies between the experimental and the equilibrium conversion level. Actually it may be seen in Figure 30 that an incorrect measurement of the reactor outlet temperature of 50°K higher than the true temperature, is required in shifting the equilibrium curve to the experimental curve for the space velocity of 100 hr⁻¹. Furthermore, for the space velocity of 4 hr⁻¹, a temperature deviation larger than 80°K is needed to shift the equilibrium

curve to the experimental one. These large deviations in temperature measurement are quite improbable even after considering the effect of radiative heat transfer from the reactor wall to the thermocouple.

Secondly, the higher experimental conversion could imply that a shift of the theoretical equilibrium conversion to the forward direction of the reaction (1.2) is occurring. This shift could result from a lower sulfur partial pressure on the surface of the catalyst pores than that in the bulk gas stream. This lower partial pressure of the sulfur vapor on the catalyst surface might be caused by polymerization of the product sulfur on the catalyst surface forming new species with longer chains like S_{10} , S_{20} , S_{100} and so on. This polymerization phenomena on the alumina surface, while speculative, might be one of the characteristic properties of sulfur species distribution. In such circumstances, additional reaction beyond the expected equilibrium conversion for the condition of the bulk gas stream could occur within the pore.

Thirdly, the experimental conversion level could be higher than the equilibrium conversion level if the data were taken before the reaction system reached a steady-state. This seems to be due to the

non-equilibrated adsorption and desorption of sulfur species in the catalyst pore (55) before the partial pressure of sulfur vapor could reach a saturation point which could result in capillary condensation.

Another possibility, but one which seems to be improbable, is that the thermodynamic data used in the calculation of the sulfur species equilibrium distribution are incorrect.

It should be emphasized here that Figure 30 shows that the conversion level decreases as the temperature increases, which means that reverse reaction in the $\text{H}_2\text{S}-\text{SO}_2$ reaction is occurring. Unfortunately, however, this reverse reaction has not been isolated for study to date. With the type of the equipment used in this report, it was not possible to evaluate more clearly the influence of the reverse reaction.

CHAPTER VI

CONCLUSIONS AND RECOMMENDATIONS

6.1 Performance of Equipment

The experimental apparatus used in this study encountered difficulties for the first few months, but after various repairs it functioned fairly well in most respects. Feed and reactor pressure controls, total feed flow-rate control, and temperature control of the preheater operated satisfactorily. Residual problems still existed in the feed composition control, GC analysis system and reactor temperature control. The feed composition fluctuated severely with an average deviation of $\pm 3\%$ due to malfunctioning of the gas cylinder pressure regulator and the flow controller.

In the GC analysis system, base-line adjustment within the Infotronic digital integrator was difficult. Because the SO_2 -peak area was very sensitive to these base-line changes, considerable error in the GC analysis for this component resulted. Therefore, consistency between conversions based upon H_2S (or COS) and those upon SO_2 could not be expected.

The manual control scheme for the reactor inlet and out temperatures was inconvenient and inaccurate with a control error of around $\pm 3^\circ\text{K}$.

To obtain more precise control of the reactor pressure, an absolute pressure transducer should be used instead of the gauge pressure transducer used in this study.

After initiating some improvements, GC monitoring by the computer was found to be consistent with results from both the digital integrator and a disc integrator. Thus, development of an on-line data processing system becomes possible after devising an automatic sample injection scheme to get accurate elution time data for each peak. In addition, a new gas chromatograph equipped with a temperature programmer will be very helpful to shorten the cycle of each analysis, which is 12 minutes at present.

6.2 Prediction of a Claus Unit Performance

The calculation of equilibrium conversions for a Claus unit revealed that the reaction conversion may be increased or decreased by changing the inert gas content depending upon the temperature level. When the equilibrium temperature is above 900°K , the conversion level increases with increasing inert content, while the conversion level decreases with increasing inert content in the temperature range below 750°K . For the operating temperature range between 750° and 900°K , the conversion level of the Claus reaction depends upon both the operating temperature and the inert content. Most Claus

plant furnaces or converters operate at temperatures outside this middle range.

In the calculation of the adiabatic reaction path in the front-end burner it was assumed that the reaction (1.1) and (1.2) occurred consecutively and reached an equilibrium condition. However, the actual condition in the front-end burner may not be in equilibrium condition. Therefore, accurate reaction kinetics combined with mass transfer rate in the front-end burner is required to understand the actual dynamic behavior of the reaction path. The literature suggests that the mixing efficiency at the entrance of the front-end burner should also be experimentally investigated for various geometrical configurations since the mass transfer rate depends largely upon the mixing efficiency.

From the simulation of a Claus catalytic converter employing the one-dimensional two-phase model (62) and Liu's rate expression for reaction (1.2) for an Alon catalyst (66), the rate of reaction has been found to be sufficiently fast to proceed significantly right at the entrance of the catalyst bed. The maximum obtainable conversion may be reached within 2 feet bed-depth when the feed temperature is 550°K and the space velocity is 1000 hr⁻¹. At a space velocity of 1000 hr⁻¹ and a feed temperature of 550°K, the external mass transfer resistance was found to be negligible compared to the

internal resistance, while the external heat transfer resistance was found to be significant compared to the internal resistance. On the above results, it is recommended that the space velocity should be larger than 1000 hr^{-1} and the catalyst particle size should be less than $1/8$ inch in diameter, which was employed for this simulation, to eliminate the effect of the external and internal transport resistance in investigating the intrinsic rate expression or in evaluating the catalytic activity in the laboratory reactor. In using smaller catalyst particles, the observed rate per unit weight of catalysts will increase because of the larger external area. Also it was observed in experiments that the performance of various catalysts could be best compared at lower conversion levels. For this reason, a much larger space velocity between $25,000$ and $150,000 \text{ hr}^{-1}$ and smaller catalyst particle sizing -12 to $+24$ mesh, were used throughout this study.

To extend the applicability of the reactor simulation to Alon catalysts with different physical properties, the effectiveness factor-Thiele modulus relationship was computed. The calculated value of the effectiveness factor, 0.17 , indicated that the rate of the Claus reaction is so fast even at such a low concentration of the feed reactants, 6.14 percent of H_2S and 3.07 percent of SO_2 with the balance N_2 and H_2O , that most of the reaction occurred in the thin shell near the

external surface of the catalyst particle. This result agrees with other observations (45, 72).

However, for a more practical simulation of the Claus converter, it may be necessary to consider the effect of simultaneous reactions, like COS-SO_2 and $\text{COS-H}_2\text{O}$, which possibly occur in the Claus converter. Here the need for knowledge of the reaction kinetics of such pertinent minor reactions, including the reverse reaction in reaction (1.2), arises. In addition, physical properties of various kinds of catalyst particles, like effective diffusivity, effective thermal conductivity or pore size distributions, should be critically investigated to provide an improved basis for prediction of actual performance of a Claus converter.

3 Evaluation of a Bifunctional Catalyst

The bifunctional activity of the newly developed catalyst, Cu-on-alumina, was proven experimentally. The copper on the γ -alumina surface was shown to improve the $\text{H}_2\text{S} - \text{SO}_2$ reaction rate to some extent but with some deterioration of the simultaneous $\text{COS} - \text{SO}_2$ reaction rate relative to the γ -alumina used in preparing this catalyst. The optimum content of copper for maximum reaction conversion of the $\text{H}_2\text{S} - \text{SO}_2$ reaction was found to be somewhere around 5%. Possible adsorption and reaction mechanisms for the two reactions, $\text{H}_2\text{S} - \text{SO}_2$ and $\text{COS} - \text{SO}_2$, on both the γ -alumina and the Cu-on-alumina

catalyst were discussed in terms of the experimental data observed and the latest mechanistic model developed by Liu (66) for the $H_2S - SO_2$ reaction on γ -alumina.

Summarizing, on pure γ -alumina catalyst, H_2S , COS and SO_2 individually appear to compete for the Lewis-acid sites. To account for bifunctional activity on the Cu-on-alumina catalyst, H_2S and SO_2 are believed to be adsorbed on the sulfided copper surface more easily than on the Lewis-acid sites, while COS may be adsorbed on the Lewis-acid sites in the same mechanism as on the γ -alumina. However, adsorbed H_2S and SO_2 on the sulfided copper surface are believed to react more readily in the presence of neighboring basic sites. The complementary role of the basic sites for the $H_2S - SO_2$ reaction on γ -alumina, which is to stretch the $H-S$ bond by the electrostatic attractive force between the basic oxide ion and the H-atom of H_2S (66), may be similar on the Cu-on-alumina surface. The decreasing conversion of the $H_2S - SO_2$ reaction beyond the copper content of 5% may be explained by the blocking effect of copper on the basic sites. Therefore, the basic sites appear to be vitally involved in the $H_2S - SO_2$ reaction mechanism on both the γ -alumina and Cu-on-alumina catalysts. On the above postulations, it may be concluded that, on the Cu-on-alumina catalyst surface, the $H_2S - SO_2$ reaction

proceeds mainly on the sulfided copper surface in the presence of neighboring basic sites, while the COS - SO₂ reaction proceeds exclusively on the Lewis-acid sites.

To confirm the above explanation, an infrared spectroscopic study on the adsorption mechanism of H₂S, SO₂ and COS on Cu-on-alumina catalyst is recommended.

4. Maximum Obtainable Conversion in the Claus Reaction

The maximum obtainable conversion level of the Claus reaction was investigated and found to be above the theoretical thermodynamic equilibrium conversion level for the same temperature, pressure and feed composition. This highly unexpected result and some possible explanations were discussed. No clear evidence is available at present to explain this discrepancy. To test whether surface adsorption equilibria for elemental sulfur are responsible, it is recommended that a long-term operation (for around one week) of the reactor be used to provide enough time to ensure that such equilibrium states are reached for the adsorption-desorption phenomena of sulfur vapor within the catalyst pores.

5. Reversible Reaction in the Claus Reaction

During the investigation of the maximum obtainable conversion level in the Claus reaction, it was noted on

figure 30 that the conversion level decreased as the temperature increased from 550° up to 700°K. From this observation, it may be concluded that the reverse reaction in the Claus reaction is significant even though its visible rate is negligible. Therefore, it is recommended that the reverse reaction kinetics for the Claus reaction should be investigated.

NOMENCLATURE

<u>Symbol</u>	<u>Meaning</u>
A_1, A_2	constant estimated by curve-fitting conversion-space velocity data
A_B	external wall area of catalyst bed ($\text{cm}^2/\text{bed volume}$)
A_h	heat transfer area ($\text{cm}^2/\text{bed volume}$)
A_m	mass transfer area ($\text{cm}^2/\text{bed volume}$)
C_f	concentration in the fluid phase (gmole/ml)
C_p	concentration within the catalyst pellet (gmole/ml)
C_s	concentration on the external surface of the catalyst (gmole/ml)
C_{pf}	heat capacity of the fluid phase ($\text{cal/gmole} \cdot ^\circ\text{K}$)
C_R	radiation constant
D	molecular diffusivity (cm^2/sec)
D_{AB}	bulk diffusivity (cm^2/sec)
D_e	effective diffusivity (cm^2/sec)
D_{KA}	Knudsen diffusivity (cm^2/sec)
D_M	diffusivity in the macropore (cm^2/sec)
D_μ	diffusivity in the micropore (cm^2/sec)
d_p	diameter of the catalyst pellet (cm)
F	volumetric flow rate of the fluid stream (cu.ft./hr)
F_{H_2S}	volumetric flow rate of the fluid stream (cu.ft./hr)

F_{COS}	volumetric flow rate of COS (cu.ft./hr)
G	mass flux (gm/cm ² -sec)
ΔH	heat transfer coefficient (cal/cm ² ·hr·°K)
j_D	j-factor for mass transfer
j_H	j-factor for heat transfer
K_p	equilibrium constant
k	reaction rate constant
k_e	effective thermal conductivity (cal/cm·hr·°K)
k_f	thermal conductivity of the fluid phase (cal/cm·hr·°K)
k_m	mass transfer coefficient (cm/sec)
l	total depth of the catalyst bed (cm)
L	dimensionless length
L_p	characteristic pore length, $L_p = R/3$ for a spherical pellet $L_p = R$ for a flat slab pellet
M_A	molecular weight of species A
M_B	molecular weight of species B
n	average number of atoms in a sulfur molecule
N_A	mole flux of component A (gmole/cm ² ·sec)
N_B	mole flux of component B (gmole/cm ² ·sec)
Nu	Nusselt number (= $h dp/k_f$)
$P_{\text{H}_2\text{O}}$	partial pressure of H ₂ O (mm Hg)
$P_{\text{H}_2\text{S}}$	partial pressure of H ₂ S (mm Hg)
P_{SO_2}	partial pressure of SO ₂ (mm Hg)

Pr	Prandtl number ($= C_{pf} \mu_f / k_f$)
R	radius of a catalyst pellet (cm)
R_g	gas constant
Re	Reynold number ($= dpG / \mu_f$)
R_p	radius of a pore (\AA)
r	distance from the center of the spherical catalyst pellet (cm)
r_{H_2S}	rate of disappearance of H_2S (gmole/sec-gm catalyst)
r_{SO_2}	rate of disappearance of SO_2 (gmole/sec-gm catalyst)
r_p	global rate expression
$r_s(P_s, T_s)$	intrinsic rate expression on the external surface of a catalyst
$r_p(P_p, T_p)$	intrinsic rate expression within the catalyst pellet
Sc	Schmidt number ($= \mu_f / \rho_f \cdot D$)
Sh	Sherwood number ($= k_m dp / D$)
T	temperature ($^{\circ}K$)
T^*	equilibrium temperature ($^{\circ}K$)
T_f	temperature of the fluid phase ($^{\circ}K$)
T_{fo}	temperature of the fluid phase at the reactor inlet ($^{\circ}K$)
T_p	temperature within the catalyst pellet ($^{\circ}K$)
T_s	temperature of the external surface of the catalyst pellet ($^{\circ}K$)
V_{int}	interstitial velocity (cm/sec)
W	weight of catalyst (gm)

X	conversion
X^*	equilibrium conversion
X_f	conversion in the fluid phase
X_s	conversion on the external surface of catalysts
x	dimensionless length
Y	dimensionless concentration
Y_A	mole fraction of a component A
z	reactor bed depth (cm)

Greek Letters

β	dimensionless variable
ϵ	void fraction
ϵ_μ	void fraction due to micropores
ϵ_M	void fraction due to macropores
η	effectiveness factor
θ	dimensionless temperature
θ_f	dimensionless temperature difference in the fluid phase
θ_s	dimensionless temperature difference on the external surface of catalysts
κ	geometrical constant of catalyst pores
μ_f	viscosity of fluid phase (gm/cm \cdot sec)
$\nu(\theta)$	pore orientation distribution function
ξ	dimensionless length
π	total pressure

ρ_B	density of the catalyst bed (gm/ml)
ρ_f	density of fluid phase (gm/ml)
ρ_p	density of the catalyst pellet (gm/ml)
$\sigma(r)$	pore size distribution function
τ	tortuosity factor
ϕ	Thiele modulus in general definition
ϕ_s	Thiele modulus for a spherical pellet
ϕ_f	Thiele modulus for a flat slab pellet
ψ	dimensionless concentration

BIBLIOGRAPHY

1. Abed, R., and Rinker, R. G., *AIChE J.*, 19(3), 618 (1973).
2. Abramov, A. A., *Teor. Osn. Khim. Tekh.*, 8(1), 116 (1974).
3. Abramov, A. A., and Zhdanov, V. M., *Teor. Osn. Khim. Tekh.*, 7(3), 365 (1973).
4. Balandin, A. A., "Catalysis and Chemical Kinetics", pp 255, Academic Press, New York, 1964.
5. Barkelew, C., *Chem. Eng. Progr. Symp. Ser.*, 37(25), 55 (1959).
6. Barry, C. B., *Hydro. Proc.*, 51(4), 102 (1972).
7. Bartlett, P. D., Lohaus, G., and Weis, C. D., *J. Am. Chem. Soc.*, 80, 5064 (1958).
8. Bennett, C. O., and Myers, J. E., "Momentum, Heat and Mass Transfer", 2nd ed., pp 509, McGraw-Hill, New York, 1974.
9. Bennett, H. A., and Meisen, A., *Can. J. Chem. Eng.*, 51(12), 720 (1973).
10. Berkowitz, J., and Chupka, W. A., *J. Chem. Phys.*, 40(2), 287 (1964).
11. Berkowitz, J., and Marquart, J. R., *J. Chem. Phys.*, 39, 275 (1963).
12. Braune, H., Peter, S., and Neveling, V., *Z. Naturforsch.*, 6a, 32 (1951).
13. Brian, P. L. T., and Hales, H. B., *AIChE J.*, 15, 419 (1969).
14. Buchböck, G., *Z. Phys. Chem.*, 23, 123 (1897).
15. Cameron, D. J., and Beavon, D. K., Paper presented at CNGPA meeting, Edmonton, February, 1970.
16. Carnova, E. A., *Theor. Found. Chem. Tech.*, 4, 367 (1970).
17. Chilton, T. C., and Colburn, A. P., *I & EC*, 26, 1183 (1934).

18. Chuang, T. T., Ph.D. thesis, University of Alberta, Edmonton, Alberta, 1971.
19. Chuang, T. T., Dalla Lana, I. G., and Liu, C. L., J. Chem. Soc., Faraday Trans., 69, 643 (1973).
20. Claus, C. F., Brit. Pat., 5958 (1883).
21. Cormode, D. A., M.Sc. thesis, University of Alberta, Edmonton, Alberta, 1965.
22. Dalla Lana, I. G., Gas Proc. Canada, Jan/Feb, 36 (1971).
23. Dalla Lana, I. G., Gas Proc. Canada, Mar/Apr, 20 (1973).
24. Dalla Lana, I. G., Cho, B. K., and Liu, C. L., Paper presented in CNGPA research seminar, Calgary, November, 1974.
25. Dalla Lana, I. G., McGregor, D. E., Liu, C. L., and Cormode, A. E., Proc. 5th Europ./2nd Int. Symp. Chem. Reaction Engg., B2-9, 1972.
26. Davis, J. C., Chem. Eng., 79, 66 (1972).
27. De Acetis, J., and Thodos, G., I & EC, 52, 1003 (1960).
28. Deo, A. V., Dalla Lana, I. G., and Habgood, H. W., J. Catal., 21, 1270 (1971).
29. Detry, D., Drowast, J., Goldfinger, P., Keller, H., and Pickert, H., Z. Phys. Chem., N. F., 55, 314 (1967).
30. Eigenberger, G., Chem. Eng. Sci., 27, 1909 (1972).
31. Eigenberger, G., Chem. Eng. Sci., 27, 1917 (1972).
32. Ferm, R. J., Chem. Rev., 57, 621 (1957).
33. Fischer, H., Hydro. Proc., 10, 125 (1974).
34. Friedlander, S. K., AIChE J., 3, 43 (1957).
35. Gamson, B. W., and Elkins, R. H., Chem. Eng. Progr., 49, 203 (1953).
36. George, S. M., J. Catal., 35, 218 (1974).
37. George, S. M., J. Catal., 32, 261 (1974).
38. Goddin, C. S., Hunt, E. B., and Palm, J. W., Hydro. Proc., 10, 122 (1974).

39. Goetz, V. W., Sood, A., and Kittrell, J. R., I & EC, Prod. Res. Develop., 13(2), 110 (1974).
40. Goodsel, A. J., and Blyholder, G., J. Catal., 26, 11 (1972).
41. Griffith, R. H., Marcom, A. R., and Newling, W. B. S., Brit. Pat., 600118 (1948).
42. Haas, L. A., and Khalafalla, S. E., J. Catal., 29, 264 (1973).
43. Haas, L. A., and Khalafalla, S. E., ~~IEEE~~ paper selection A73-6, 1973..
44. Haas, L. A., McCormick, T. H., and Khalafalla, S. E., U.S. Bur. Mines Report Invest., No.7647, 1972.
45. Hammer, B. G. G., Doktorsavhandling, Chalmers Tek. Hogskola, No.14, 166 (1957).
46. Hideo Teshima, and Norigoshi Morida, J. Catal., 31, 1 (1973).
47. Hlavacek, V., and Hofmann, H., Chem. Eng. Sci., 25, 173 (1970).
48. Hlavacek, V., and Hofmann, H., Chem. Eng. Sci., 25, 187 (1970).
49. Hlavacek, V., Hofmann, H., Votruba, J., and Kubicek, M., Chem. Eng. Sci., 28, 1897 (1973).
50. Hyne, J. B., Oil Gas J., August 28, 64 (1972).
51. Johnson, M. F., and Stewart, W. E., J. Catal., 4, 248 (1965).
52. Karanth, N. G., and Hughes, R., Catal. Review, 9(2), 169 (1974).
53. Karren, B., M.Sc. thesis, University of Alberta, Edmonton, Alberta, 1972.
54. Kelley, K., U.S. Bur. Mines Bull., 406 (1937).
55. Kerr, R., Private communications.
56. Khalafalla, S. E., and Haas, L. A., J. Catal., 24, 121 (1972).

57. Khalafalla, S. E., and Haas, L. A., J. Catal., 24, 115 (1972).
58. Krill, Helmut, and Klaus, Storp, Chem. Engg., July 23, 84 (1973).
59. Landau, M., Molyneux, A., and Houghton, R., I & EC, Symp. Ser., No.27 (1968).
60. Lepsoe, R., I & EC, 30, 92 (1938).
61. Levenspiel, O., "Chemical Reaction Engineering", 2nd ed., pp 473, John Wiley & Sons, New York, 1972.
62. Liu, S. L., and Amundson, N. R., I & EC, Fundls, 1, 200 (1962).
63. Liu, S. L., and Amundson, N. R., I & EC, Fundls, 2, 12 (1963).
64. Liu, S. L., and Amundson, N. R., I & EC, Fundls, 2, 183 (1963).
65. Liu, C. L., M.Sc. thesis, University of Alberta, Edmonton, Alberta, 1971.
66. Liu, C. L., Unpublished research results, 1975.
67. Liu, C. L., and Dalla Lana, I. G., Paper presented at Canadian Sulfur Symposium, Calgary, May, 1974.
68. Lochiel, A. C., and Calderbank, P. H., Chem. Eng. Sci., 19, 471 (1964).
69. Lovett, W. D., and Cunniff, F. T., Chem. Eng. Progr., 70(5), 43 (1974).
70. Marsh, J. D. F., and Newling, W. B. S., Brit. Pat., 867,853 (1961).
71. McBride, B. J., Heimel, S., Ehlers, J. G., and Gordon, S., NASA SP-3001 (1963).
72. McGregor, D. E., Ph.D. thesis, University of Alberta, Edmonton, Alberta, 1971.
73. McGuire, M. L., and Lapidus, L., ALChE J., 11, 85 (1965).
74. Neisen, A., and Bennett, H. A., Hydro. Proc., 53(11), 171 (1974).

75. Meyer, B., "Elemental Sulfur", Interscience, New York, 1965.
76. Mezaki, R., and Kittrell, J. R., Can. J. Chem. Eng., 44, 285 (1966).
77. Mischke, R. A., and Smith, J. H., I & EC Fundls., 1(4), 288 (1962).
78. Naber, J. E., Wesselingh, J. A., and Groenendaal, W., Chem. Eng. Progr., 69(12), 29 (1973).
79. Namba Seitaro, and Shiba Tadao, Kogyo Kagaku Zasshi, 71(1), 93 (1968).
80. Neumann, K. K., Erdöl und Kohle-Erdgas-Petrochem. Brennstoff Chem., 25(11), 656 (1972).
81. Okay, V. C., and Short, W. L., I & EC Process Des. Develop., 12(3), 291 (1973).
82. Paterson, W. R., and Cresswell, D. L., Chem. Eng. Sci. 26, 605 (1971).
83. Pearson, M. J., Hydro. Proc., 52(2), 81 (1973).
84. Peter, S., and Woy, H., Chem. Ing. Technik, 41, 979 (1969).
85. Petersen, E. E., "Chemical Reaction Analysis", Prentice-Hall, Englewood Cliffs, New Jersey, 1965.
86. Petty, L. A., Chem. Eng. Sci., 28, 119 (1973).
87. Pilgrim, R. F., and Ingraham, T. R., Mines Branch Information Circular IC 243, June, 1970.
88. Preuner, G., Z. Phys. Chem. 44, 733 (1903).
89. Preuner, G., and Schupp, W., Z. Phys. Chem., 68, 129 (1909).
90. Querido, R., and Short, W. L., I & EC Process Des. Develop., 12(1), 10 (1973).
91. Rau, H., Kutty, T. R. N., and Guedes de Carvalho, J. R. F., J. Chem. Thermodynamics, 5, 833 (1973).
92. Ross, R. A., and Jeanes, M. R., I & EC Prod. Res. Develop., 13(2), 102 (1974).

93. Satterfield, C. N., "Mass Transfer in Heterogeneous Catalysis", pp 56, MIT Press, Cambridge, Mass., 1970.
94. Smith, J. M., "Chemical Engineering Kinetics", 2nd ed., pp 420, 430, McGraw-Hill, New York, 1970.
95. Stecher, P. G., "Hydrogen Sulfide Removal Process", Noyes Data Corporation, New Jersey, 1972.
96. Steijns, M., and Mars, P., J. Catal., 35, 11 (1974).
97. Taylor, H. A., and Wesley, W. A., J. Chem. Phys., 31, 216 (1957).
98. Thompson, Kearton, C. F., and Lamb, S. A., J. Chem. Sci., 1033 (1935).
99. Van Den Bosch, B., and Padmanabhan, L., Chem. Eng. Sci., 29, 1217 (1974).
100. Varma, A., and Amundson, N. R., Chem. Eng. Sci., 28, 91 (1973).
101. Villadsen, J. V., and Stewart, W. E., Chem. Eng. Sci., 22, 1483 (1967).
102. Votruba, J., Kubicek, M., and Hlavacek, V., Chem. Eng. Sci., 29, 2333 (1974).
103. Wakao, N., and Smith, J. M., Chem. Eng. Sci., 17, 825 (1962).
104. Wakao, N., and Smith, J. M., I & EC Fundls. Quart., 3, 123 (1964).
105. Wayman, D. D., et al, NBS Technical Note 270-3, U.S. Government Printing Office, 1968.
106. Weiss, P. B., and Hicks, J. S., Chem. Eng. Sci., 17, 265 (1962).
107. Wheeler, A., "Advances in Catalysis", Vol.III, pp 250, Academic Press, New York, 1951.
108. White, W. B., Johnson, S. M., and Danzig, G. B., J. Chem. Phys., 28, 751 (1958).
109. Moser, J. P., Personal communications.
110. Nagy, J. N., and Moser, J. P., "Users Manual for the Monitoring and Control of Gas Chromatographs by the IBM 1800 Computer", Dept. of Chem. Eng., University of Alberta, Edmonton, Alberta, 1973.

APPENDIX A

CALIBRATION OF THE GAS CHROMATOGRAPHIC SYSTEM

A-1. Calibration Procedure:

The gas chromatograph was calibrated using sample gas mixtures the composition of which was known from the volumetric mixing ratio. The apparatus used for sample preparation is illustrated in Figure A.1, which was originally fabricated by McGregor (72).

The sample mixing chamber was made of a 5 liter lucite cylinder equipped with a movable piston and a mixing fan beneath the top cover of the cylinder. The lucite cylinder had been calibrated by McGregor (72) to describe the volume of the gas mixture in the cylinder as a function of the piston position.

Before preparing the sample mixture the cylinder was initially purged with nitrogen for about 2 hours. Then the cylinder filled with pure nitrogen through the line A was allowed to equilibrate to the atmospheric pressure and temperature. Then the gas burette and the line B were purged with one of the calibration gases and a volume of the gas was trapped in the burette by lowering the mercury reservoir. The pressure of the trapped gas being not equal to the atmospheric pressure, the elevation of the mercury reservoir was manipulated to get the atmospheric pressure which was confirmed by the water manometer.

Then the trapped gas was compressed to about 30 psi by raising the elevation of the mercury reservoir and

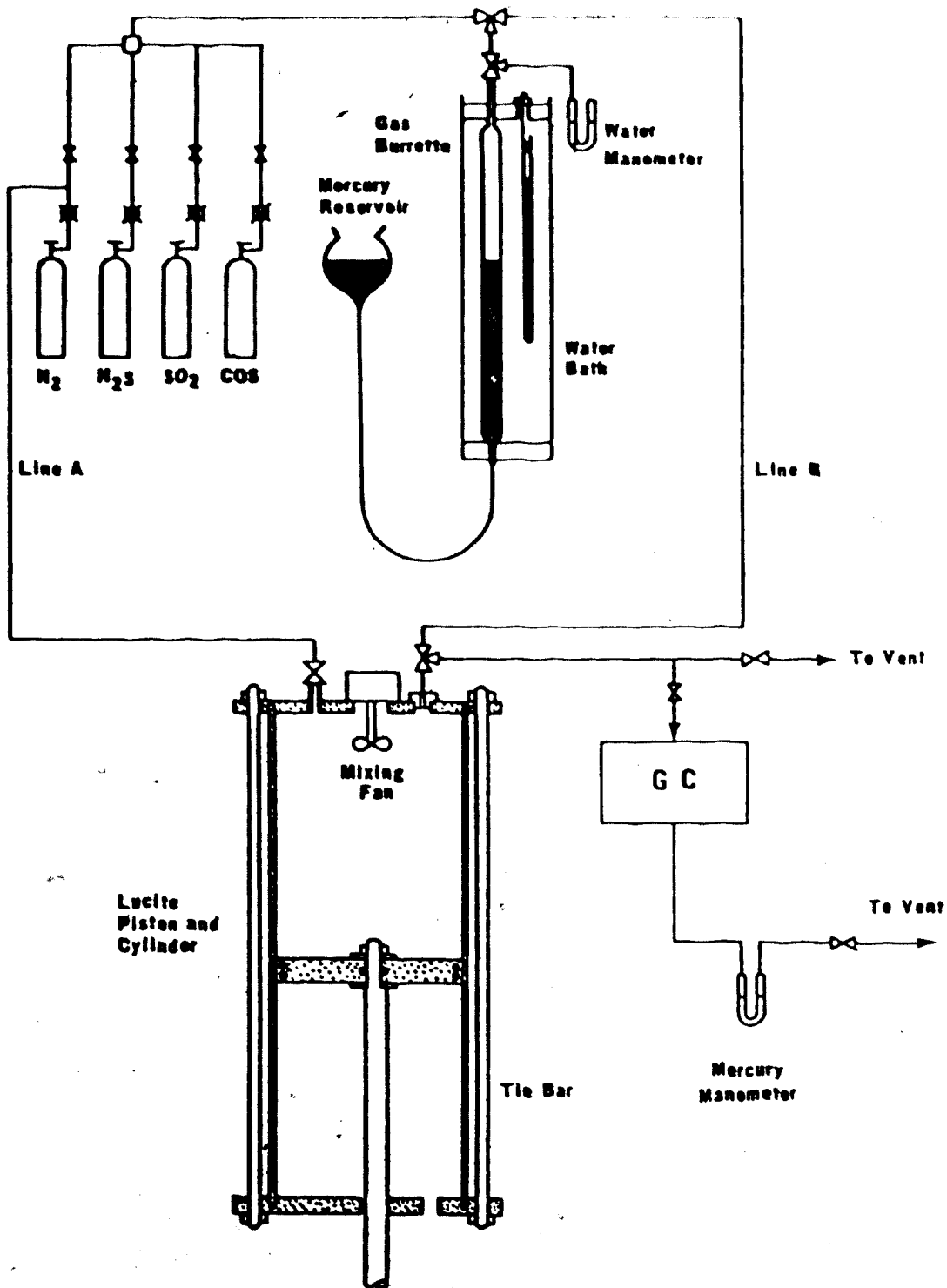


FIGURE A.1: GC CALIBRATION APPARATUS

forcing it into the cylinder through the line B with a sufficient positive pressure. The residual volume of the trapped gas was brought to the atmospheric condition by manipulating the elevation of the mercury reservoir again. The difference of the gas volume between the initial and the residual at atmospheric condition was recorded as the introduced gas volume to the mixing cylinder.

While the first calibration gas was being mixed with the nitrogen in the mixing cylinder by the mixing fan, the line B and the gas burette was purged with the nitrogen and then by the second calibration gas. Then the second calibration gas was trapped in the burette, equilibrated to the atmospheric condition and then forced into the cylinder in the same way as the first calibration gas. The third calibration gas was also introduced into the cylinder in the same way as the first one.

After the final sample was mixed for one hour by the mixing fan, it was forced into the GC sampling loop with a positive pressure head of 1 inch mercury, which was measured by a mercury manometer on the vent line from the GC, by lifting the cylinder position.

The sample introduced to the GC sampling loop was injected to the sampling coil by pushing the injection lamp on the GC programmer panel for 13 seconds.

A-2. Attenuation System Design:

The individual attenuation system originally installed on the GC programmer panel was found to be malfunctioning due to the excessive electrical noise causing the unstable base line whenever each microswitch changed its electrical connection on the timer control cam. The schematic diagram of the individual attenuation system used by the former investigators (53,65,72) is illustrated in Figure A.2.

So the previous individual attenuating system was not employed throughout this study, and the first GC calibration was done at a fixed attenuation for all peaks as shown on Figure A.3. With this attenuation scheme, the GC calibration results by the computer and the integrators were not consistent as described in Chapter 5.

Finally it was found that another installation of attenuation system was still possible. The newly installed attenuation system is illustrated in Figure A.4. The attenuation scheme III was calibrated by measuring the output signal from each attenuator at a arbitrarily assigned input signal. The voltage signal was measured using a potentiometer. The results of the calibration of the three attenuators are listed in Table A.1 through A.3. The GC calibration results using the attenuation scheme III by the computer and the integrator were in a very good

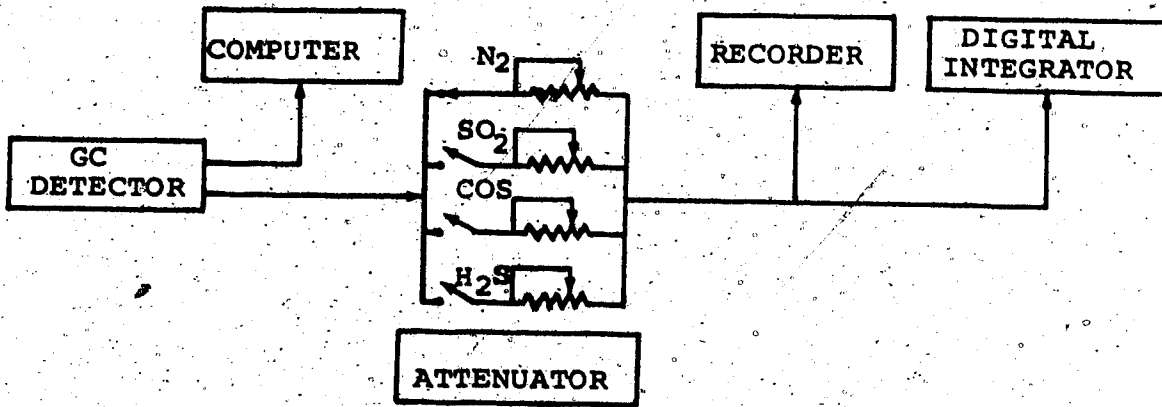


FIGURE A.2 ATTENUATION SCHEME I

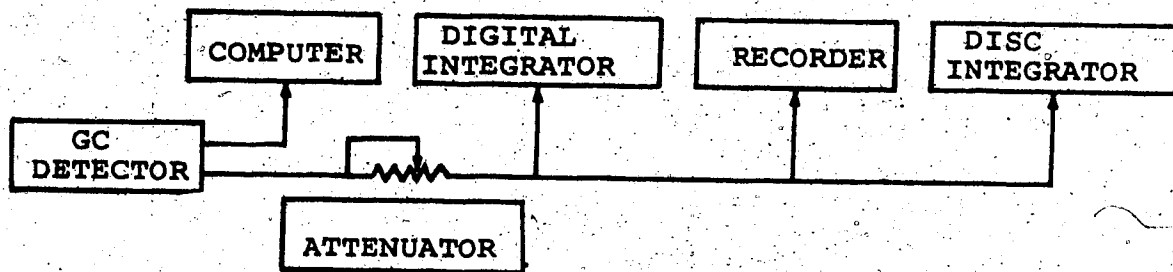


FIGURE A.3 ATTENUATION SCHEME II

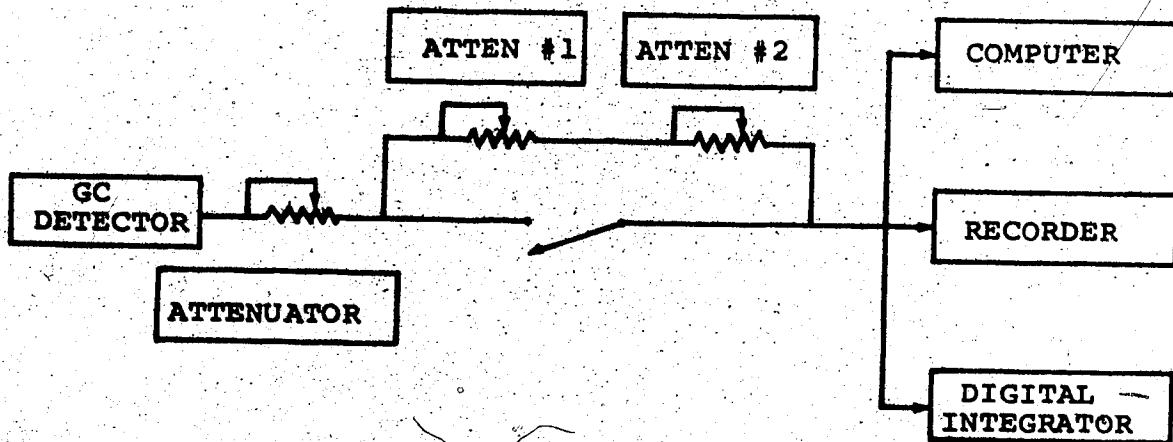


FIGURE A.4 ATTENUATION SCHEME III

TABLE A. 1

CALIBRATION OF CHROMATOGRAPH ATTENUATOR

X = ATTENUATOR SETTING
Y = ATTENUATION RATIO

THE COEFFICIENTS OF THE POLYNOMIAL ARE

A0 = 19.95917

A1 = -1.88738

REGENERATED DATA

X MEASURED	Y OBSERVED	Y CALCULATED	PCT ERROR
1.000	18.069	18.071	0.013
2.000	16.008	16.184	1.097
3.000	14.202	14.297	0.666
4.000	12.586	12.409	1.403
5.000	10.735	10.522	1.984
6.000	8.690	8.634	0.640
7.000	6.759	6.747	0.174
8.000	4.740	4.860	2.527
9.000	2.920	2.972	1.804
10.000	1.073	1.085	1.095

VARIANCE = 0.015210

STANDARD DEVIATION = 0.123330

MAXIMUM PCT ERROR = 2.527461

TABLE A. 2

CALIBRATION OF ATTENUATOR #1

X = ATTENUATOR SETTING
Y = ATTENUATION RATIO

THE COEFFICIENTS OF THE POLYNOMIAL ARE

A0 = 1.07781

A1 = 0.17031

REGENERATED DATA

X MEASURED	Y OBSERVED	Y CALCULATED	PCT ERROR
1.000	1.210	1.248	3.119
2.000	1.398	1.418	1.396
3.000	1.687	1.588	5.833
4.000	1.784	1.759	1.425
5.000	1.893	1.929	1.880
6.000	2.073	2.099	1.266
7.000	2.254	2.269	0.704
8.000	2.431	2.440	0.370
9.000	2.613	2.610	0.126
10.000	2.797	2.780	0.603

VARIANCE = 0.001636

STANDARD DEVIATION = 0.040452

MAXIMUM PCT ERROR = 5.833227

TABLE A. 3

CALIBRATION OF ATTENUATOR #2

X = ATTENUATOR SETTING
Y = ATTENUATION RATIO

THE COEFFICIENTS OF THE POLYNOMIAL ARE

A0 = 1.17312

A1 = 1.76047

REGENERATED DATA

X MEASURED	Y OBSERVED	Y CALCULATED	PCT ERROR
1.000	2.811	2.933	4.343
2.000	4.635	4.694	1.271
3.000	6.471	6.454	0.265
4.000	8.365	8.215	1.802
5.000	10.147	9.975	1.699
6.000	11.706	11.735	0.251
7.000	13.450	13.496	0.338
8.000	15.244	15.256	0.081
9.000	16.980	17.017	0.219
10.000	18.743	18.777	0.185

VARIANCE = 0.008538

STANDARD DEVIATION = 0.092401

MAXIMUM PCT ERROR = 4.343668

agreement as described in Chapter 5.

A-3. Homogeneous Reaction Effects In The Mixing Cylinder:

To check the homogeneous reaction effects during the mixing period of the sample gas mixture in the mixing cylinder, the calibration results for SO₂ component both in the COS-H₂S-SO₂-N₂ mixture and in the SO₂-N₂ mixture were compared as illustrated in Figure A.5.

Figure A.5 indicates that there was no homogeneous reaction during the mixing period of the sample gas mixture. The calibration data for the SO₂-N₂ mixture are listed in Table A.4.

The first calibration results of the gas chromatograph using attenuation scheme II, are listed in Table A.5 and the second calibration results using attenuation scheme III are listed in Table A.6. A listing of the program GCCAL, used to reduce the calibration data to usable results, is also included.

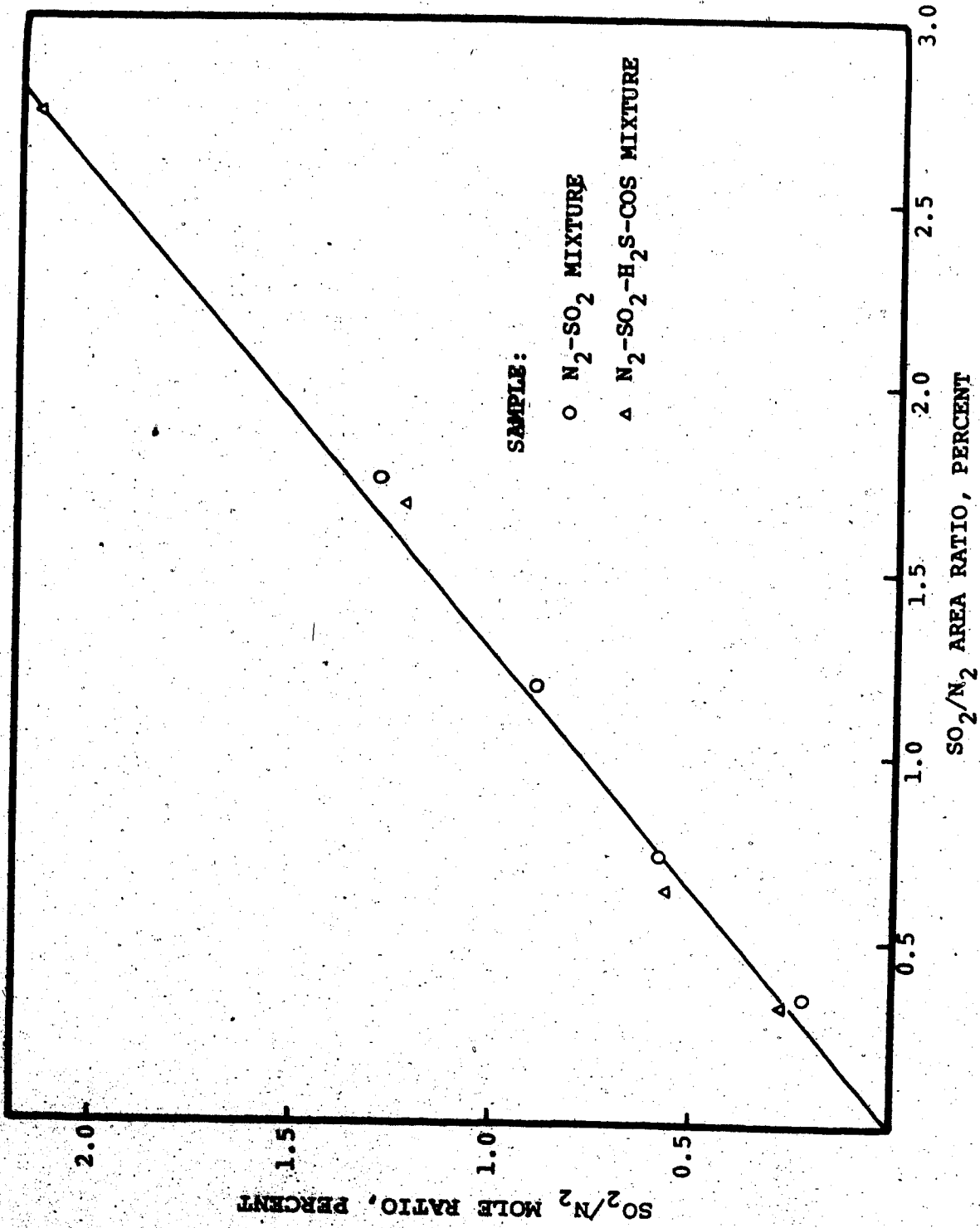


FIGURE A.5: HOMOGENEOUS REACTION EFFECTS IN THE MIXING CHAMBER DURING THE CALIBRATION PERIOD

TABLE A.4

CALIBRATION SAMPLE NUMBER 1

SAMPLE PREPARATION CONDITIONS

ROOM TEMPERATURE..... 292.5 DEG K
 BATH TEMPERATURE..... 291.7 DEG K
 ATMOSPHERIC PRESSURE..... 697.6 MM HG
 VOLUME OF NITROGEN..... 4619.3 CC
 VOLUME OF SULFUR DIOXIDE .. 56.2 CC

SAMPLE COMPOSITION (MOLE PERCENT)

NITROGEN..... 98.7675
 SULFUR DIOXIDE ... 1.2324
 100X MOLAR RATIO... 1.2478

INTEGRATOR AREA RESULTS (THE LAST SET IS THE AVERAGE)

NITROGEN		SULFUR DIOXIDE		100X
INTEGRATED AREA	PCT OF TOTAL	INTEGRATED AREA	PCT OF TOTAL	AREA RATIO
0.543787E 07	98.35	0.910210E 05	1.64	1.6738
0.543654E 07	98.33	0.920240E 05	1.66	1.6926
0.544517E 07	98.35	0.912500E 05	1.64	1.6757
0.544201E 07	98.32	0.928330E 05	1.67	1.7058
0.545233E 07	98.31	0.934960E 05	1.68	1.7147
0.544278E 07	98.33	0.921248E 05	1.66	1.6925

TABLE A.4 (CONTINUED)

CALIBRATION SAMPLE NUMBER 2

SAMPLE PREPARATION CONDITIONS

ROOM TEMPERATURE..... 291.5 DEG K
 BATH TEMPERATURE..... 290.8 DEG K
 ATMOSPHERIC PRESSURE..... 697.8 MM HG
 VOLUME OF NITROGEN..... 4619.3 CC
 VOLUME OF SULFUR DIOXIDE .. 12.6 CC

SAMPLE COMPOSITION (MOLE PERCENT)

NITROGEN..... 99.7211
 SULFUR DIOXIDE ... 0.2788
 100X MOLAR RATIO... 0.2796

INTEGRATOR AREA RESULTS (THE LAST SET IS THE AVERAGE)

NITROGEN		SULFUR DIOXIDE		100X
INTEGRATED AREA	PCT OF TOTAL	INTEGRATED AREA	PCT OF TOTAL	AREA RATIO
0.549638E 07	99.67	0.179220E 05	0.32	0.3260
0.555189E 07	99.65	0.190600E 05	0.34	0.3433
0.553106E 07	99.68	0.176200E 05	0.31	0.3185
0.549580E 07	99.64	0.193090E 05	0.35	0.3513
0.549491E 07	99.64	0.193210E 05	0.35	0.3516
0.551400E 07	99.66	0.186464E 05	0.33	0.3381

TABLE A.4 (CONTINUED)

CALIBRATION SAMPLE NUMBER 3

SAMPLE PREPARATION CONDITIONS

ROOM TEMPERATURE..... 293.0 DEG K
 BATH TEMPERATURE..... 292.2 DEG K
 ATMOSPHERIC PRESSURE..... 702.1 MM HG
 VOLUME OF NITROGEN..... 4619.3 CC
 VOLUME OF SULFUR DIOXIDE .. 25.5 CC

SAMPLE COMPOSITION (MOLE PERCENT)

NITROGEN..... 99.4370
 SULFUR DIOXIDE ... 0.5630
 100X MOLAR RATIO... 0.5661

INTEGRATOR AREA RESULTS (THE LAST SET IS THE AVERAGE)

NITROGEN		SULFUR DIOXIDE		100X
INTEGRATED AREA	PCT OF TOTAL	INTEGRATED AREA	PCT OF TOTAL	AREA RATIO
0.532763E 07	99.31	0.365880E 05	0.68	0.6867
0.524177E 07	99.34	0.343750E 05	0.65	0.6557
0.553896E 07	99.43	0.314710E 05	0.56	0.5681
0.531029E 07	99.32	0.359030E 05	0.67	0.6761
0.535077E 07	99.37	0.334400E 05	0.62	0.6249
0.535388E 07	99.36	0.343554E 05	0.63	0.6423

TABLE A.4 (CONTINUED)

CALIBRATION SAMPLE NUMBER 4

SAMPLE PREPARATION CONDITIONS

ROOM TEMPERATURE..... 292.0 DEG K
 BATH TEMPERATURE..... 291.5 DEG K
 ATMOSPHERIC PRESSURE..... 706.6 MM HG
 VOLUME OF NITROGEN..... 4619.3 CC
 VOLUME OF SULFUR DIOXIDE .. 98.0 CC

SAMPLE COMPOSITION (MOLE PERCENT)

NITROGEN:..... 97.8725
 SULFUR DIOXIDE ... 2.1274
 100X MOLAR RATIO... 2.1737

INTEGRATOR AREA RESULTS (THE LAST SET IS THE AVERAGE)

NITROGEN		SULFUR DIOXIDE		100X
INTEGRATED AREA	PCT OF TOTAL	INTEGRATED AREA	PCT OF TOTAL	AREA RATIO
0.539304E 07	97.35	0.146565E 06	2.64	2.7176
0.541332E 07	97.42	0.143307E 06	2.57	2.6473
0.533457E 07	97.28	0.149082E 06	2.71	2.7946
0.537665E 07	97.30	0.149103E 06	2.69	2.7731
0.541047E 07	97.31	0.149222E 06	2.68	2.7580
0.538561E 07	97.33	0.147455E 06	2.66	2.7381

TABLE A.5

GC CALIBRATION FOR N₂-H₂S MIXTURE
ATTENUATION SCHEME II

X = AREA RATIO (100XH₂S/N₂)
Y = MOLE RATIO (100XH₂S/N₂)

THE COEFFICIENTS OF THE POLYNOMIAL ARE

A0 = 0.02159

A1 = 0.94687

REGENERATED DATA

X MEASURED	Y OBSERVED	Y CALCULATED	PCT ERROR
1.104	1.084	1.067	1.542
1.212	1.111	1.169	5.175
2.106	2.060	2.016	2.136
3.619	3.463	3.449	0.401
5.363	5.083	5.100	0.336

VARIANCE = 0.001503

STANDARD DEVIATION = 0.038772

MAXIMUM PCT ERROR = 5.175019

TABLE A. 5 (CONTINUED)

GC CALIBRATION FOR N₂-CO₂ MIXTURE
ATTENUATION SCHEME II

X = AREA RATIO (100XCOS/N₂)
 Y = MOLE RATIO (100XCOS/N₂)

THE COEFFICIENTS OF THE POLYNOMIAL ARE

A₀ = 0.03809

A₁ = 0.72771

REGENERATED DATA

X MEASURED	Y OBSERVED	Y CALCULATED	PCT ERROR
1.431	1.048	1.080	3.022
1.571	1.168	1.181	1.150
2.761	2.101	2.047	2.538
4.526	3.343	3.331	0.332
6.784	4.956	4.975	0.389

VARIANCE = 0.001131

STANDARD DEVIATION = 0.033639

MAXIMUM PCT ERROR = 3.02273

TABLE A.5 (CONTINUED)

GC CALIBRATION FOR N₂-SO₂ MIXTURE
ATTENUATION SCHEME II

X = AREA RATIO (100XSO₂/N₂)
Y = MOLE RATIO (100XSO₂/N₂)

THE COEFFICIENTS OF THE POLYNOMIAL ARE

A₀ = 0.11839

A₁ = 0.84600

REGENERATED DATA

X MEASURED	Y OBSERVED	Y CALCULATED	PCT ERROR
2.382	2.117	2.134	0.799
3.998	3.554	3.500	1.525
4.768	4.133	4.152	0.472
6.452	5.516	5.577	1.103
7.176	6.232	6.189	0.692

VARIANCE = 0.002294

STANDARD DEVIATION = 0.047904

MAXIMUM PCT ERROR = 1.525091

TABLE A.6

GC CALIBRATION FOR N₂-H₂S MIXTURE
ATTENUATION SCHEME III

X = AREA RATIO (100XH₂S/N₂)
Y = MOLE RATIO (100XH₂S/N₂)

THE COEFFICIENTS OF THE POLYNOMIAL ARE

A₀ = 0.00733

A₁ = 0.89491

REGENERATED DATA

X MEASURED	Y OBSERVED	Y CALCULATED	PCT ERROR
0.742	0.638	0.672	5.338
1.327	1.179	1.195	1.351
2.277	2.138	2.045	4.357
3.838	3.398	3.442	1.270

VARIANCE = 0.003989

STANDARD DEVIATION = 0.063159

MAXIMUM PCT ERROR = 5.338395

TABLE A.6(CONTINUED)

GC CALIBRATION FOR N₂-COS MIXTURE
ATTENUATION SCHEME III

X = AREA RATIO (100XCOS/N₂)
Y = MOLE RATIO (100XCOS/N₂)

THE COEFFICIENTS OF THE POLYNOMIAL ARE

A₀ = -0.00149

A₁ = 0.65325

REGENERATED DATA

X MEASURED	Y OBSERVED	Y CALCULATED	PCT ERROR
0.670	0.431	0.436	1.155
1.765	1.138	1.151	1.167
3.188	2.115	2.081	1.598
5.212	3.388	3.403	0.458

VARIANCE = 0.000528

STANDARD DEVIATION = 0.022987

MAXIMUM PCT ERROR = 1.598227

TABLE A.6(CONTINUED)

GC CALIBRATION FOR N₂-SO₂ MIXTURE
ATTENUATION SCHEME III

X = AREA RATIO (100XSO₂/N₂)
Y = MOLE RATIO (100XSO₂/N₂)

THE COEFFICIENTS OF THE POLYNOMIAL ARE

A₀ = 0.02466

A₁ = 0.77038

REGENERATED DATA

X MEASURED	Y OBSERVED	Y CALCULATED	PCT ERROR
0.338	0.279	0.285	1.979
0.642	0.566	0.519	8.234
1.692	1.247	1.328	6.470
2.738	2.173	2.134	1.824

VARIANCE = 0.003431

STANDARD DEVIATION = 0.058579

MAXIMUM PCT ERROR = 8.234605

TABLE A.6 (CONTINUED)

GC CALIBRATION FOR N₂-CO₂ MIXTURE
ATTENUATION SCHEME III

X = AREA RATIO (100XCO₂/N₂)
 Y = MOLE RATIO (100XCO₂/N₂)

THE COEFFICIENTS OF THE POLYNOMIAL ARE

A₀ = -0.03191

A₁ = 0.86214

REGENERATED DATA

X MEASURED	Y OBSERVED	Y CALCULATED	PCT ERROR
0.350	0.263	0.269	2.442
0.694	0.570	0.566	0.625
1.056	0.887	0.879	0.988
1.607	1.347	1.353	0.438

VARIANCE = 0.000055

STANDARD DEVIATION = 0.007439

MAXIMUM PCT ERROR = 2.442953

```

*****
*
*           MAINLINE GCCAL
*
* THIS PROGRAM REDUCES THE PEAK AREA DATA TAKEN FROM *
* THE DIGITAL INTEGRATOR TO CALCULATED RESULTS USEFUL *
* FOR THE INTERNAL STANDARD PROCEDURE FOR THE CALIBR- *
* ATION OF THE GAS CHROMATOGRAPH
*
*
* ****INPUT DATA
*
*   NSET  = NUMBER OF SETS OF DATA
*   NCOPY = NUMBER OF COPIES OF OUTPUT DESIRED
*   NRUN  = CALIBRATION RUN NUMBER
*   NCRUM = NUMBER OF CHROMATOGRAM TAKEN
*   IPEAK = PEAK NUMBER CALIBRATED
*           ...2=H2S
*           ...3=SO2
*           ...4=CDS
*           ...5=CO2
*
*   RTEM  = ROOM TEMPERATURE(DEG C)
*   BTEM  = WATER BATH TEMPERATURE(DEG C)
*   APRES = ATMOSPHERIC PRESSURE(MM HG)
*   V(1)  = DISTANCE BETWEEN PISTON AND END OF
*           CYLINDER(CM)
*
*   V(2)  = VOLUME OF CALIBRATION GAS(CU CM)
*   ATN1  = ATTENUATOR #1 SETTING
*   ATN2  = ATTENUATOR #2 SETTING
*   AR(1) = AREA OF NITROGEN PEAK
*   AR(3) = AREA OF CALIBRATION GAS PEAK
*
*****

```

```

DIMENSION SNAM(4,4),SMV(5),V(2), AR(5),AVG(5),STORE(6
1,5)
DATA SMV/22402.10,22176.10,21901.63,22417.51,22346.34/
DATA SNAM/'HYDR','OGEN','SUL','FIDE','SULF','UR D',
1'IOXI','DE ','CARB','ONYL','SUL','FIDE','CARB',
2'ON ','DIOX','IDE '/
READ(5,1) NSET,NCOPY,NPAGE
DO 2 ISET=1,NSET
READ(5,1) NRUN,NCRUM,IPEAK
READ(5,3) RTEM,BTEM,APRES,V(1),V(2),ATN1,ATN2
STEMP=273.
SPRES=760.
RTEM=RTEM+STEMP
BTEM=BTEM+STEMP

```

C CALCULATION OF SAMPLE COMPOSITION

... (CONT'D)

```

C
XMN2=(11.+151.192*V(1))*STEMP/RTEM*APRES/SPRES/SMV(1)
V(1)=(11.+151.192*V(1))
XMCAL=V(2)*STEMP/BTEM*APRES/SPRES/SMV(IPEAK)
TOTM=XMN2+XMCAL
XMN2=XMN2/TOTM*100.
XMCAL=XMCAL/TOTM*100.
RMDL=XMCAL/XMN2*100.
KPEAK=IPEAK-1

```

```

C
C
READ AND PROCESS PEAK AREA DATA

```

```

NCAT=0
DO 4 I=1,5
4 AVG(I)=0.0
DO 5 ICROM=1,NCROM
NCAT=NCAT+1
READ (5,33) AR(1),AR(3)

```

```

C
C
CORRECTED PEAK AREA OF NITROGEN PEAK

```

```

AR(1)=AR(1)*(1.76947*ATN2 + 1.17312)*(0.17031*ATNI +
* 1.07781)
TOTA= AR(1)+ AR(3)
AR (2)= AR(1)/TOTA*100.
AR (4)= AR(3)/TOTA*100.
AR (5)= AR(3)/ AR(1)*100.

```

```

C
C
CALCULATION OF THE AVERAGES

```

```

DO 6 I=1,5
6 AVG(I)= AR(I)+AVG(I)
DO 20 J=1,5
20 STORE(NCAT,J)= AR(J)
5 CONTINUE
DO 7 I=1,5
7 AVG(I)=AVG(I)/NCROM
NCAT=NCAT+1
DO 21 J=1,5
21 STORE(NCAT,J)=AVG(J)
NN=NCROM+1
DO 23 IC=1,NCOPY
WRITE(6,17) NPAGE
IF(NRUN-1) 51,51,52
51 WRITE(6,37)
GO TO 53

```

... (CONT'D)

```

52 WRITE(6,38)
53 WRITE(6,10) NRUN,RTEM,BTEM
   WRITE(6,9) APRES,V(1),(SNAM(J,KPEAK),J=1,4),V(2)
   WRITE(6,11) XMN2,(SNAM(J,KPEAK),J=1,4),XMCAL,RMOL
   WRITE(6,12)
   WRITE(6,13) (SNAM(J,KPEAK),J=1,4)
   WRITE(6,15) ((STORE(I,J),J=1,5),I=1,NN)
23 CONTINUE
   NPAGE=NPAGE+1
   2 CONTINUE
   1 FORMAT(5I5)
   3 FORMAT(7F10.5)
33 FORMAT(2F10.2)
10 FORMAT( / 15X , 'CALIBRATION SAMPLE NUMBER',I3,///10X,
  * 'SAMPLE PREPARATION CONDITIONS' //12X, 'ROOM TEMPERATUR
  1, 'E', '.....',F7.1, ' DEG K', //12X, 'BATH TEMPERATU
  *, 'RE.....',F7.1, ' DEG K', /)
  9 FORMAT(//12X, 'ATMOSPHERIC PRESSURE.....',F7.1, ' MM HG'
  *, //12X, 'VOLUME OF NITROGEN.....',F7.1, ' CC', //12X,
  1 'VOLUME OF ',4A4, '...',F5.1, ' CC')
11 FORMAT( //,10X, 'SAMPLE COMPOSITION (MOLE PERCENT)' /
  */12X, 'NITROGEN.....',F8.4, //12X,4A4, '...',F8.4,
  1 //12X, '100X MOLAR RATIO...',F8.4)
12 FORMAT(//10X, 'INTEGRATOR AREA RESULTS (THE LAST SET ',
  1 'IS THE AVERAGE)') /)
13 FORMAT( 19X, 'NITROGEN',13X,4A4,9X, '100X', //11X,
  * 'INTEGRATED',6X, 'PCT OF',5X, 'INTEGRATED',6X, 'PCT OF',
  17X, 'AREA' / 15X, 'AREA',8X, 'TOTAL',10X, 'AREA',8X, 'TOTAL'
  *,6X, 'RATIO' /)
15 FORMAT( 9X,E13.6,3X,F6.2,6X,E13.6,3X,F6.2,5X,F7.4 /)
17 FORMAT('1', ///66X, 'A-',I2, //)
37 FORMAT(20X, 'TABLE A.4' / )
38 FORMAT(20X, 'TABLE A.4 (CONTINUED)' / )
   CALL EXIT
   END

```

APPENDIX B

CALIBRATION OF PROCESS MEASURING DEVICES

B-1. Differential Pressure Transducer:

The electronic differential pressure transducer was calibrated using a pre-calibrated dry test meter with pure nitrogen flow at room temperature. A Foxboro 6430 HF electronic control recorder was used to record the pressure difference in the cell. The calibration data were obtained at three different feed pressure levels of 20, 25 and 30 psia and were fitted to the calibration equation of the following form.

$$Y = a_0 + a_1X + a_2X^2$$

where

Y = volumetric flow rate (SCFH)

X = square root of percent reading on the recorder

a_0, a_1, a_2 = calibrated parameters

by applying the linear least-square curve fitting technique assuming that the flow behavior was in the region between laminar and turbulent flow. The calibration results are listed in Table B.1, B.2 and B.3.

B-2. Feed Absolute Pressure Transducer:

The Foxboro 611 AH absolute pressure transducer was calibrated at room temperature with pure nitrogen flow in the feed line using a mercury manometer as a reference. The absolute pressure signal was recorded on the

TABLE B. 1

DP-CELL CALIBRATION
(FEED PRESSURE AT 30 PSIA)

X = RECORDER READING (SQRT OF PER CENT)
Y = FEED FLOW RATE (SCFH)

THE COEFFICIENTS OF THE POLYNOMIAL ARE

A0 = -0.00814

A1 = 1.05586

A2 = 0.00003

REGENERATED DATA

X MEASURED	Y OBSERVED	Y CALCULATED	PCT ERROR
9.920	10.492	10.469	0.212
9.099	9.560	9.602	0.441
8.075	8.502	8.520	0.216
7.457	7.929	7.867	0.775
6.066	6.368	6.398	0.472
4.528	4.790	4.773	0.342
3.592	3.771	3.785	0.371
2.408	2.539	2.534	0.173

VARIANCE = 0.001113

STANDARD DEVIATION = 0.033366

MAXIMUM PCT ERROR = 0.775749

TABLE B. 2

DP-CELL CALIBRATION
(FEED PRESSURE AT 25 PSIA)

X = RECORDER READING (SQRT OF PER CENT)
Y = FEED FLOW RATE (SCFH)

THE COEFFICIENTS OF THE POLYNOMIAL ARE

A0 = 0.08793

A1 = 0.94999

A2 = -0.00099

REGENERATED DATA

X MEASURED	Y OBSERVED	Y CALCULATED	PCT ERROR
9.894	9.403	9.390	0.137
9.050	8.588	8.604	0.188
7.937	7.589	7.565	0.308
6.892	6.559	6.588	0.445
6.253	5.978	5.989	0.191
4.950	4.762	4.766	0.086
3.240	3.234	3.155	2.426
2.387	2.296	2.349	2.348

VARIANCE = 0.001578

STANDARD DEVIATION = 0.039724

MAXIMUM PCT ERROR = 2.426989

TABLE B. 3

DP-CELL CALIBRATION
(FEED PRESSURE AT 20 PSIA)

X = RECORDER READING (SQRT OF PER CENT)
Y = FEED FLOW RATE (SCFH)

THE COEFFICIENTS OF THE POLYNOMIAL ARE

A0 = -0.06161

A1 = 0.87416

A2 = -0.00318

REGENERATED DATA

X MEASURED	Y OBSERVED	Y CALCULATED	PCT ERROR
9.818	8.208	8.213	0.069
9.311	7.791	7.801	0.133
8.438	7.098	7.087	0.145
7.064	5.977	5.954	0.377
5.899	4.990	4.984	0.116
4.837	4.076	4.092	0.396
3.479	2.915	2.941	0.892
2.098	1.778	1.758	1.105

VARIANCE = 0.000302

STANDARD DEVIATION = 0.017382

MAXIMUM PCT ERROR = 1.105066

Foxboro 6430 HF electronic control recorder. The reference absolute pressure for the calibration was obtained by adding the barometric pressure to the mercury manometer reading. The calibration data were fitted to a straight line by means of a linear least-square fitting technique and the results are listed in Table B.4.

B-3 Reactor Gauge Pressure Transducer:

The reactor gauge pressure transducer (Statham PG-732TC-10-350) was calibrated in the same way as described for the feed absolute pressure transducer calibration. The data which represent the relation between the percent reading on the recorder and the mercury manometer reading was obtained after the reactor system reached steady state through which pure nitrogen was flowing. Since the normal operational condition of the reactor system was in the high temperature range of around 250°K, the reactor pressure transducer was calibrated at elevated temperatures of 480°K, 500°K and 560°K. A frequent malfunctioning of the reactor pressure transducer was found. Whenever any malfunctioning was detected, the transducer was checked and recalibrated for next runs. The results of calibration #1 were used for runs A, B, C, D, E and J. The calibration equation #2 was used for runs F and G, while the calibration equation #3 was used for other runs. The calibration results are shown in Table B.5 through B.9.

TABLE B. 4

FEED ABSOLUTE PRESSURE TRANSDUCER CALIBRATION

X = RECORDER READING (PER CENT)
 Y = ABSOLUTE PRESSURE (MM-HG)

THE COEFFICIENTS OF THE POLYNOMIAL ARE

A0 = 744.61367

A1 = 12.71505

REGENERATED DATA

X MEASURED	Y OBSERVED	Y CALCULATED	PCT ERROR
2.900	781.100	781.487	0.049
5.900	820.500	819.632	0.105
13.800	921.900	920.081	0.197
20.500	1004.900	1005.272	0.037
29.400	1115.500	1118.436	0.263
38.900	1237.200	1239.229	0.163
52.300	1413.800	1409.610	0.296
65.500	1576.300	1577.449	0.072

VARIANCE = 5.136350

STANDARD DEVIATION = 2.266351

MAXIMUM PCT ERROR = 0.296308

TABLE B. 5

REACTOR GAUGE PRESSURE TRANSDUCER CALIBRATION #1
(AT 480 DEGREE K)

X = RECORDER READING (PER CENT)
Y = GAUGE PRESSURE (MM-HG)

THE COEFFICIENTS OF THE POLYNOMIAL ARE

A0 = 8.92106

A1 = 4.41818

REGENERATED DATA

X MEASURED	Y OBSERVED	Y CALCULATED	PCT ERROR
6.100	36.300	35.871	1.179
11.300	59.500	58.846	1.098
22.150	106.900	106.783	0.108
35.150	163.300	164.220	0.563
50.500	230.700	232.039	0.580
77.500	352.000	351.330	0.190
90.600	409.600	409.208	0.095

VARIANCE = 0.644358

STANDARD DEVIATION = 0.802719

MAXIMUM PCT ERROR = 1.179151

TABLE B. 6

REACTOR GAUGE PRESSURE TRANSDUCER CALIBRATION #1
(AT 500 DEGREE K)

X = RECORDER READING (PER CENT)
Y = GAUGE PRESSURE (MM-HG)

THE COEFFICIENTS OF THE POLYNOMIAL ARE

A0 = 14.52163

A1 = 4.33165

REGENERATED DATA

X MEASURED	Y OBSERVED	Y CALCULATED	PCT ERROR
6.000	40.500	40.511	0.028
14.300	77.100	76.464	0.824
26.000	126.600	127.144	0.430
43.150	201.400	201.432	0.016
58.800	269.100	269.222	0.045
73.500	332.600	332.897	0.089
95.600	429.000	428.627	0.086

VARIANCE = 0.157432

STANDARD DEVIATION = 0.396778

MAXIMUM PCT ERROR = 0.824627

TABLE B. 7

REACTOR GAUGE PRESSURE TRANSDUCER CALIBRATION #1
(AT 560 DEGREE K)

X = RECORDER READING (PER CENT)
Y = GAUGE PRESSURE (MM-HG)

THE COEFFICIENTS OF THE POLYNOMIAL ARE

A0 = 15.83784

A1 = 4.32817

REGENERATED DATA

X MEASURED	Y OBSERVED	Y CALCULATED	PCT ERROR
4.200	34.500	34.016	1.402
11.500	66.200	65.611	0.888
17.000	89.600	89.416	0.204
28.400	138.300	138.758	0.331
39.700	186.700	187.666	0.517
58.100	266.400	267.304	0.339
73.200	333.000	332.660	0.102
91.500	412.600	411.865	0.177

VARIANCE = 0.461480

STANDARD DEVIATION = 0.679323

MAXIMUM PCT ERROR = 1.402393

TABLE B. 8

REACTOR GAUGE PRESSURE TRANSDUCER CALIBRATION #2
(AT 560 DEGREE K)

X = RECORDER READING (PER CENT)
Y = GAUGE PRESSURE (MM-HG)

THE COEFFICIENTS OF THE POLYNOMIAL ARE

A0 = 1.81379

A1 = 4.05037

REGENERATED DATA

X MEASURED	Y OBSERVED	Y CALCULATED	PCT ERROR
15.100	63.000	62.974	0.040
26.800	108.000	110.363	2.188
33.300	135.000	136.691	1.252
39.000	160.000	159.778	0.138
50.000	207.000	204.332	1.288
61.600	254.000	251.316	1.056
63.300	261.000	258.202	1.071
80.800	326.000	329.083	0.945
92.200	374.000	375.258	0.336

VARIANCE = 5.216590

STANDARD DEVIATION = 2.283985

MAXIMUM PCT ERROR = 2.188647

TABLE B. 9

REACTOR GAUGE PRESSURE TRANSDUCER CALIBRATION #3
(AT 560 DEGREE K)

X = RECORDER READING (PER CENT)

Y = GAUGE PRESSURE (MM-HG)

THE COEFFICIENTS OF THE POLYNOMIAL ARE

A0 = 27.66422

A1 = 4.19851

REGENERATED DATA

X MEASURED	Y OBSERVED	Y CALCULATED	PCT ERROR
20.000	112.000	111.634	0.326
31.700	161.000	160.757	0.150
42.800	207.000	207.360	0.174
47.800	231.000	228.353	1.145
54.000	252.000	254.384	0.946
64.000	294.000	296.369	0.805
83.000	378.000	376.141	0.491

VARIANCE = 3.680093

STANDARD DEVIATION = 1.918356

MAXIMUM PCT ERROR = 1.145756

B-4. Thermocouples:

The thermocouples for measuring the reactor inlet and outlet temperatures were calibrated using a platinum resistance thermometer as the temperature standard in a fluidized sand bath at the instrument shop. The calibrated results are shown in Table B.10 and B.11.

B-5. Water Feeder:

The syringe pump for water injection (Sage model - 355) was calibrated by a gravimetric method. The flow range of the syringe was set at the scale of 1/100. The water sample was received in a 5 ml weighing bottle. To eliminate evaporation loss during the calibration period a capillary tube stopper was used to connect the syringe outlet to the weighing bottle. The weight of the sampled water received for a certain time interval was converted to the volume of water by dividing it with its density. The data for water density (1) was corrected for different temperatures as shown in Table B.12. The calibration results are shown in Table B.13.

1. Perry, J.H., "Chemical Engineers Handbook", 4th ed., New York, 3-70, 1963.

TABLE B.10

THERMOCOUPLE CALIBRATION FOR REACTOR INLET TEMP.

X = RECORDER READING (MILLIVOLT)
 Y = TEMPERATURE (DEGREE CENTIGRADE)

THE COEFFICIENTS OF THE POLYNOMIAL ARE

A0 = 1.40878

A1 = 18.31152

REGENERATED DATA

X MEASURED	Y OBSERVED	Y CALCULATED	PCT ERROR
1.034	20.510	20.342	0.814
2.075	37.950	39.405	3.834
7.970	149.350	147.351	1.338
14.211	261.510	261.633	0.047
20.254	371.610	372.290	0.183
26.238	481.960	481.866	0.019

VARIANCE = 1.325184

STANDARD DEVIATION = 1.151166

MAXIMUM PCT. ERROR = 3.834459

TABLE B.11

THERMOCOUPLE CALIBRATION FOR REACTOR OUTLET TEMP.

X = RECORDER READING (MILLIVOLT)
 Y = TEMPERATURE (DEGREE CENTIGRADE)

THE COEFFICIENTS OF THE POLYNOMIAL ARE

A0 = 2.51827

A1 = 18.21650

REGENERATED DATA

X MEASURED	Y OBSERVED	Y CALCULATED	PCT ERROR
1.034	20.510	21.354	4.115
1.949	37.950	38.022	0.190
7.969	149.350	147.685	1.114
14.234	261.510	261.812	0.115
20.296	371.610	372.240	0.169
26.309	481.960	481.776	0.038

VARIANCE = 0.802073

STANDARD DEVIATION = 0.895585

MAXIMUM PCT ERROR = 4.115689

TABLE B.12

CALIBRATION OF WATER FEED PUMP

X = ADJUSTMENT READING (PER CENT AT 1/100 SCALE)
 Y = FEED RATE (CC H₂O/HR)

THE COEFFICIENTS OF THE POLYNOMIAL ARE

A₀ = 0.31009

A₁ = 0.52032

REGENERATED DATA

X MEASURED	Y OBSERVED	Y CALCULATED	PCT ERROR
10.000	5.388	5.513	2.315
20.000	10.849	10.716	1.221
30.000	16.107	15.919	1.165
50.000	25.993	26.326	1.279
70.000	36.869	36.732	0.371

VARIANCE = 0.049418

STANDARD DEVIATION = 0.222303

MAXIMUM PCT ERROR = 2.315128

TABLE B.13

DENSITY CORRECTION OF FEED WATER

X = FEED WATER TEMP. (DEG. C)
 Y = DENSITY OF WATER (GM/CC)

THE COEFFICIENTS OF THE POLYNOMIAL ARE

A0 = 1.00244

A1 = -0.00022

REGENERATED DATA

X MEASURED	Y OBSERVED	Y CALCULATED	PCT ERROR
10.000	0.999	1.000	0.043
15.000	0.999	0.999	0.010
20.000	0.998	0.997	0.034
25.000	0.997	0.996	0.033
30.000	0.995	0.995	0.007
35.000	0.994	0.994	0.041

VARIANCE = 0.000000

STANDARD DEVIATION = 0.000346

MAXIMUM PCT ERROR = 0.043511

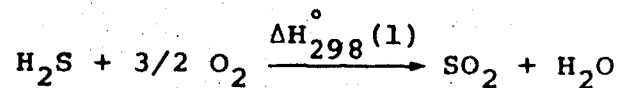
APPENDIX C

DERIVATION OF EQUATIONS FOR ADIABATIC REACTION PATHS IN
THE FRONT-END BURNER

C-1. Adiabatic Reaction Path in the Front-End Burner

Section (1):

The oxidation reaction between H_2S and air to form SO_2 and H_2O is assumed to be the only reaction to occur in the burner section (1) in Figure 6.



No. of moles, initial:	3	1.5	0	0
final:	(3-X)	1.5(1-X)	X	X

..... (A.1)

where X is the number of moles of H_2S converted to SO_2 .

Since the adiabatic condition during the reaction period in the burner may be assumed, the total enthalpy of the system should remain constant before and after the reaction. Then the following energy balance equation can be written by referring to Figure 6.

$$\int_{T_1}^{298} \{ 3 C_{P,H_2S} + 1.5 C_{P,O_2} + (5.64 + Z) C_{P,N_2} + Y C_{P,CO_2} \} dT + X \cdot \Delta H_{298}^{\circ}(1)$$

$$+ \int_{298}^{T_2} \{ (3-X) C_{P,H_2S} + 1.5 (1-X) C_{P,O_2} + (5.64 + Z) C_{P,N_2} + X C_{P,SO_2}$$

$$+ X C_{P,H_2O} + Y C_{P,CO_2} \} dT = 0 \quad \dots \quad (A.2)$$

where Y and Z represent the number of moles of CO_2 and the excess nitrogen present in the feed stream as inert gases.

The heat capacity of the gaseous component i may be described as a function of temperature (70) such as

$$C_{p,i} = R_g \sum_{j=1}^5 A_{ij} T^{(j-1)} \quad (\text{A.3})$$

where A_{ij} = temperature coefficients for the thermodynamic property function

and $i = 1$ for H_2S

$i = 2$ for SO_2

$i = 3$ for S_8

$i = 4$ for S_6

$i = 5$ for S_2

$i = 6$ for H_2O

$i = 7$ for N_2

$i = 8$ for H_2

$i = 9$ for O_2

$i = 10$ for CO_2

Then equation (A.2) can be integrated to give

$$\text{conversion in the burner section (1)} = \frac{X}{3} \quad (\text{A.4})$$

$$\text{where } X = R_g \cdot \text{FHT} / \{ \Delta H_{298}^\circ(1) - R_g \cdot \text{PHEAT} \} \quad (\text{A.5})$$

$$PHT = \sum_{j=1}^5 \{A_{1j} + 1.5 A_{9j} + (5.64 + Z) A_{7j} + Y A_{10j}\} \left(\frac{T_1^j - T_2^j}{j} \right) \dots \dots \dots (A.6)$$

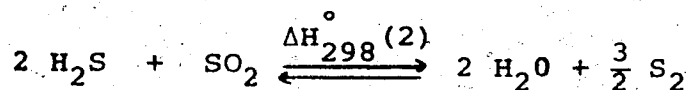
$$PHEAT = \sum_{j=1}^5 \{A_{1j} + 1.5 A_{9j} - A_{2j} - A_{6j}\} \left\{ \frac{298^j - T_2^j}{j} \right\} \dots \dots \dots (A.7)$$

The computer program BURN1 was used to solve the above equations and also listed.

C-2. Adiabatic Reaction Path in the Front-End Burner

Section (2):

In the burner section (2) in Figure 6, the reaction between H_2S and SO_2 occurs according to equation (A.8) following reaction (A.1) in the burner section (1).



No. of moles, initial:	2	1	1	0
final:	2(1-X)	(1-X)	(1+2X)	1.5X
			(A.8)

where X is the conversion of H_2S to elemental sulfur.

Furthermore the association-dissociation reactions between sulfur species are assumed to occur simultaneously with reaction (A.8).



$$(1-v_1-v_2)(1.5X) \quad v_1(1.5X)$$



$$(1-v_1-v_2)(1.5X) \quad v_2(1.5X)$$

Then the following energy balance equation can be derived by referring to Figure 6 on the basis of the adiabatic condition of the reaction system within the burner.

$$\int_{T_2}^{298} \{ 2 C_{P,H_2S} + C_{P,SO_2} + C_{P,H_2O} + (5.64 + Z) C_{P,N_2} + Y C_{P,CO_2} \} dT$$

$$+ 2X \Delta H_{298}^{\circ}(2) + v_1(1.5X) \Delta H_{298}^{\circ}(8) + v_2(1.5X) \Delta H_{298}^{\circ}(9)$$

$$+ \int_{298}^{T_3} \{ 2(1-X) C_{P,H_2S} + (1+X) C_{P,SO_2} + (1+2X) C_{P,H_2O} + (1-v_1-v_2)(1.5X) C_{P,S_2}$$

$$+ v_1(1.5X) C_{P,S_6} + v_2(1.5X) C_{P,S_8} + (5.64+Z) C_{P,N_2} + Y C_{P,CO_2} \} dT = 0$$

..... (A.11)

By the same procedures as in (C-1) the following results can be obtained.

Total conversion in the front-end burner

$$= (1 + 2X)/3 \quad (\text{A.12})$$

where

$$X = R_g \cdot \text{FHT} / (\text{DH} - R_g \cdot \text{PHEAT}) \quad (\text{A.13})$$

$$\text{FHT} = \sum_{j=1}^5 \{ 2 A_{1j} + A_{2j} + (5.64 + Z) A_{7j} + Y A_{10j} + A_{6j} \} \left(\frac{T_2^j - T_3^j}{j} \right) \quad (\text{A.14})$$

$$\text{DH} = 2 \Delta H_{298}^{\circ}(2) + 1.5 v_1 \cdot \Delta H_{298}^{\circ}(8) + 1.5 v_2 \cdot \Delta H_{298}^{\circ}(9) \quad (\text{A.15})$$

$$\text{PHEAT} = \sum_{j=1}^5 \{ 2 A_{1j} + A_{2j} - 2 A_{6j} - 1.5 (1 - v_1 - v_2) A_{5j} - 0.5 v_1 \cdot A_{4j} - 0.375 v_2 \cdot A_{3j} \} \left(\frac{298^j - T_3^j}{j} \right) \quad (\text{A.16})$$

A listing of the computer program BURN2, used to solve the above equations, is included.

... (CONT'D)

```

TF(1)=TFD
TT(1)=298.
DO 78 I=1,4
TF(I+1)=TFD*TF(I)
78 TT(I+1)=298.*TT(I)
DO 99 NC=1,30
TPR=TFD+50.*NC
FHT =0.
PHEAT=0.
TP(1)=TPR
DO 31 I=1,4
31 TP(I+1)=TPR*TP(I)
DO 74 I=1,5
74 TPP(I)=TP(I)
DO 81 I=1,N
DO 81 J=1,5
81 C(I,J)=A(I,J)
IF(TPR-1000.) 64,64,55
55 DO 61 J=1,5
61 TP(J)=TR(J)
L=1
64 DO 22 J=1,5
FHT=FHT+(3.*C(1,J)+1.5*C(9,J) +(5.64+Z)*C(7,J) +Y*C(10
1,J))*(TP(J) -TF(J))/J
22 PHEAT=PHEAT +(C(1,J)+1.5*C(9,J) -C(2,J)-C(6,J))*(TP(J)
*-TT(J))/J
IF(TPR-1000.) 91,91,92
92 IF(L-1) 93,93,91
93 DO 95 I=1,N
DO 95 J=1,5
95 C(I,J)=AA(I,J)
DO 39 I=1,5
TT(I)=TR(I)
TF(I)=TR(I)
39 TP(I)=TPP(I)
L=L+1
GO TO 64

```

C. CALCULATION OF CONVERSION AT THE EXIT TEMPERATURE

```

91 X1=1.987*FHT/(123924.9+1.987*PHEAT)
DXDT= (X1-XX1)/50.
XX1=X1
WRITE(6,102) TPR,X1,DXDT
102 FORMAT(30X,F10.1,5X,F10.3,20X,E12.5)
IF(X1-1.0) 96,96,88
96 IF(TPR-1000.) 99,99,94
94 TF(1)=TFD
TT(1)=298.
DO 777 I=1,4.

```

... (CONT'D)

```
TT(I+1)=298.*TT(I)
777 TF(I+1)=TFD*TF(I)
99 CONTINUE
88 CONTINUE
CALL EXIT
END
```

```

C *****
C *
C *                               *
C *                               *
C *                               *
C * THIS PROGRAM COMPUTES THE ADIABATIC REACTION PATH *
C * IN THE FRONT-END BURNER SECTION (2) OF A CLAUS UNIT *
C * ACCORDING TO REACTION (1.2) ASSUMING EQUILIBRIUM *
C * DISTRIBUTION OF SULFUR SPECIES *
C *
C * N = NUMBER OF COMPOUNDS IN THE REACTION *
C * MIXTURE *
C * A = TEMPERATURE COEFFICIENTS OF A THERMODYNA- *
C * MIC FUNCTION FOR HEAT CAPACITY(FOR LOWER *
C * THAN 1000 DEG K) *
C * AA = TEMPERATURE COEFFICIENTS OF A THERMODYNA- *
C * MIC FUNCTION FOR HEAT CAPACITY(FOR HIGHER *
C * THAN 1000 DEG K) *
C * Y = NUMBER OF MOLES OF CARBON DIOXIDE IN THE *
C * FEED *
C * Z = NUMBER OF MOLES OF EXCESS NITROGEN IN *
C * THE FEED *
C * DH2 = HEAT OF REACTION IN H2S-SO2 REACTION *
C * DH3 = HEAT OF REACTION IN 3S2-S6 REACTION *
C * DH4 = HEAT OF REACTION IN 4S2-S8 REACTION *
C * TFD = FEED TEMPERATURE *
C * PT = TOTAL PRESSURE IN MM HG *
C *
C *****

```

```

DIMENSION A(20,5),AA(20,5),TF(5),TT(5),TP(5),TR(5),
1FH TL(5),FH TH(5),PH TL(5),PH TH(5)
READ(5,1) N
1 FORMAT(1I5)
DO 3 I=1,N
3 READ(5,5) (A(I,J),J=1,5)
5 FORMAT(5E15.7)
DO 4 I=1,N
4 READ(5,5) (AA(I,J),J=1,5)
TR(1)=1000.
DO 77 I=1,4
77 TR(I+1)=1000.*TR(I)
DO 88 NN=1,23
READ(5,8) Z,Y,DH2,DH3,DH4
8 FORMAT(5F10.2)
WRITE(6,10)
10 FORMAT(1H1,25X,'ADIABATIC TEMPERATURE-CONVERSION
* CALCULATION')
READ(5,54) TFD,PT
54 FORMAT(2F10.2)

```

... (CONT'D)

```

WRITE(6,11) TFD
11 FORMAT(///28X,'INITIAL TEMPERATURE = ',F6.1/)
WRITE (6,101)
101 FORMAT(30X,'FINAL TEMP',5X,'CONVERSION',15X,'DX/DT'/)
XX2=0.33333
TF(1)=TFD
TT(1)=298.
DO 78 I=1,4
  TF(I+1)=TFD*TF(I)
78 TT(I+1)=298.*TT(I)
DO 600 J=1,5
  FHTL(J)=2.*A(1,J)+A(2,J)+(5.64+Z)*A(7,J)+Y*A(10,J)
  *+A(6,J)
600 FHTH(J)= 2.*AA(1,J)+AA(2,J)+(5.64+Z)*AA(7,J)+Y*AA(10
  *,J)+AA(6,J)
M=1
DO 99 NC=1,30
  TPR=TFD+10.*NC*(-1.)*M
  FHT =0.
  PHEAT=0.
  TP(1)=TPR
  DO 31 I=1,4
31 TP(I+1)=TPR*TP(I)
  PS2=PT/760.
  CALL FREM(PS2,TPR,XN1,XN2)
  DH=2.*DH2 +1.5* XN1 *DH3 +1.5* XN2 *DH4
  DO 500 J=1,5
  PHTL(J)=2.*A(1,J)+A(2,J)-2.*A(6,J)-1.5*(1.-XN1-XN2)*A
  1(5,J)-0.5*XN1*A(4,J)-0.375*XN2*A(3,J)
500 PHTH(J)= 2.*AA(1,J)+AA(2,J)-2.*AA(6,J)-1.5*(1.-XN1-XN2
  1)*AA(5,J)-0.5*XN1*AA(4,J)-0.375*XN2*AA(3,J)
C   FOR BOTH TFD AND TPR LOWER THAN 1000 DEG K
IF (TFD-1000.) 335,335,426
335 IF (TPR-1000.) 336,336,691
336 DO 337 J=1,5
  FHT=FHT+FHTL(J) *(TF(J)-TP(J))/J
337 PHEAT=PHEAT+PHTL(J)*(TP(J)-TT(J))/J
GO TO 91
C   FOR TFD HIGHER THAN 1000 DEG K AND TPR LOWER THAN
C   1000 DEG K
426 IF (TPR-1000.) 427, 427,560
427 DO 428 J=1,5
  FHT=FHT+(FHTH(J)*(TF(J)-TR(J)) +FHTL(J)*(TR(J)-TP(J)))
  */J
428 PHEAT=PHEAT+PHTL(J)*(TP(J)-TT(J))/J
GO TO 91

```


... (CONT'D)

C FOR BOTH TFD AND TPR HIGHER THAN 1000 DEG K

```
560 DO 561 J=1,5
      FHT=FHT + (FHTH(J)*(TF(J)-TP(J)))/J
561 PHEAT=PHEAT + (PHTH(J)*(TP(J)-TR(J)) + PHTL(J)*(TR(J)
      *-TT(J)))/J
      GO TO 91
```

C FOR TFD LOWER THAN 1000 DEG K AND TPR HIGHER THAN
C 1000 DEG K

```
691 DO 692 J=1,5
      FHT=FHT + (FHTH(J)*(TR(J)-TP(J)) + FHTL(J)*(TF(J)
      *-TR(J)))/J
692 PHEAT=PHEAT + (PHTH(J)*(TP(J)-TR(J)) + PHTL(J)*(TR(J)
      *-TT(J)))/J
```

C CALCULATION OF CONVERSION AT THE EXIT TEMPERATURE

```
91 X2=1.987*FHT/( DH -1.987*PHEAT)
   X2=0.33333+2.*X2/3.
   DXDT = (X2-XX2) / (10.*(-1.)*M)
   XX2=X2
   WRITE(6,102) TPR,X2,DXDT
102 FORMAT(30X,F10.1,5X,F10.3,12X,E12.5)
   IF(TFD-950.) 1000,999,999
1000 M=2
      GO TO 998
999 M=1
998 IF (X2-1.0) 99,99,88
   99 CONTINUE
   88 CONTINUE
   CALL EXIT
   END
```

APPENDIX D

ESTIMATION OF EFFECTIVE DIFFUSIVITY

D-2. Molecular Diffusivity of SO₂:

To estimate the molecular diffusivity of SO₂ through N₂, Wilke-Lee correlation (1) can be used.

$$D_{AB} = \frac{\left(0.00107 - 0.000246 \sqrt{\frac{1}{M_A} + \frac{1}{M_B}}\right) T^{3/2} \sqrt{\frac{1}{M_A} + \frac{1}{M_B}}}{\pi (r_{AB})^2 I_D} \dots \dots \dots (D.1)$$

where

$$M_A = \text{molecular weight of SO}_2 = 64$$

$$M_B = \text{molecular weight of N}_2 = 28$$

$$r_{AB} = \text{collision diameter, } \text{\AA} = \frac{r_A + r_B}{2}$$

$$r_A \text{ for SO}_2^{(2)} = 4.290 \text{ } \text{\AA}$$

$$r_B \text{ for N}_2 = 3.681 \text{ } \text{\AA}$$

$$I_D = \text{collision integral for diffusion} = f \left(\frac{kT}{\epsilon_{AB}} \right)$$

$$\frac{\epsilon_{AB}}{k}^{(2)} = \sqrt{\frac{\epsilon_A}{k} \frac{\epsilon_B}{k}} = \sqrt{(91.5)(252)} = 151.8486$$

At

$$T = 550^\circ\text{K},$$

$$\frac{kT}{\epsilon_{AB}} = 3.612, \text{ then } I_D^{(2)} \approx 0.45$$

For $T = 550^\circ\text{K}, \pi = 1 \text{ atm},$

(1) Wilke, C.R., and Lee, C.Y.; I & EC, 47, 1253 (1955).

(2) Perry, J.H.; "Chemical Engineers Handbook" 4th ed., 14-20, 21, 1963.

$$D_{AB} = \frac{\left(0.00107 - 0.000246 \sqrt{\frac{1}{28} + \frac{1}{64}}\right) (550)^{3/2} \sqrt{\frac{1}{28} + \frac{1}{64}}}{(3.9855)^2 (0.45)}$$

$$\approx 0.4215 \text{ cm}^2/\text{sec}$$

The above estimated value was used as the molecular diffusivity of SO_2 in the Claus reactant mixture by assuming the Claus feed gas as a binary mixture of SO_2 and N_2 .

D-2. Knudsen Diffusivity of SO_2 :

From equation (2.23)

$$D_{KA} = 9.7 \times 10^3 R_p \left(\frac{T}{M_A}\right)^{1/2} \quad (2.23)$$

where R_p = average radius of a pore = 80 \AA from the data of Chuang (18).

Then at $T = 550^\circ\text{K}$

$$D_{KA} = (9.7 \times 10^3) (80 \times 10^{-8}) \left(\frac{550}{64}\right)^{1/2}$$

$$= 0.02275 \text{ cm}^2/\text{sec.}$$

D-3. Effective Diffusivity:

To estimate the combined diffusivity, equation (2.21) can be used,

$$\frac{1}{D} = \frac{1 - \alpha y_A}{D_{AB}} + \frac{1}{D_{KA}} \quad (2.21)$$

where

$$\alpha = \frac{N_B}{N_A} = 0 \quad \text{by assuming } N_2 \text{ component is stagnant.}$$

Then

$$\frac{1}{D} = \frac{1}{D_{AB}} + \frac{1}{D_{KA}} = \frac{1}{0.4215} + \frac{1}{0.02275} = 46.3285$$

or

$$D = 0.02158 \text{ cm}^2/\text{sec.}$$

Now the effective diffusivity can be estimated by applying the parallel pore model or equation (2.20),

$$D_e = D \left(\frac{\epsilon}{\tau} \right) \quad (2.20)$$

where

ϵ = void fraction of a catalyst pellet, taken as 0.35,

τ = tortuosity factor, taken as 4.0.

Then

$$D_e = (0.02158) \left(\frac{0.35}{4.0} \right) = 0.001888 \text{ cm}^2/\text{sec.}$$

APPENDIX E

SIMPLIFICATION OF MODELING EQUATIONS

E-1. Modeling Equations:

General modeling equations are presented in Chapter III.

$$V_{int} \frac{dC_f}{dz} + \frac{A_m k_m}{\epsilon_B} (C_f - C_s) - D_L \frac{d^2 C_f}{dz^2} = 0 \quad (3.8)$$

$$\rho_f C_{pf} V_{int} \frac{dT_f}{dz} + \frac{A_h h}{\epsilon_B} (T_f - T_s) + \frac{A_B h}{\epsilon_B} (T_w - T_f) = 0$$

..... (3.9)

$$A_m k_m (C_s - C_f) + \eta \cdot \rho_B \cdot r_s (P_s, T_s) = 0 \quad (3.10)$$

$$A_h h (T_s - T_f) + \eta \cdot \Delta H \cdot \rho_B r_s (P_s, T_s) - k_e \frac{d^2 T_s}{dz^2} = 0$$

..... (3.11)

where

$$r_s (P_s, T_s) = 1.28 \times 10^{-4} \frac{P_{H_2S} P_{SO_2}^{1/2}}{(1 + 0.006 P_{H_2O})^2} \exp \left[\frac{-7350}{R_g T_s} \right] \quad (1.7)$$

E-2. Simplification of Modeling Equations:

- i) Assume the axial dispersion is negligible compared to the convective mass transfer due to bulk motion, then the last term can be neglected in equation (3.8).
- ii) Assume the axial conduction through catalyst pellets is negligible compared to the convective heat transfer due to bulk motion in the fluid phase, then the last term in equation (3.11) can be neglected.
- iii) Assume adiabatic condition in the reactor system, then the last term in equation (3.9) can be neglected.
- iv) Assume the stoichiometric feed ratio of H_2S and SO_2 , then the reaction rate expression can be rearranged by the following relations.

$$P_{H_2S} = 2 P_{SO_2}$$

$$P_{H_2O} = P_{H_2O,i} + 2 (P_{SO_2,i} - P_{SO_2})$$

where the subscript i represents the initial condition in the feed stream. The reaction rate expression, therefore, becomes

$$r_s (P_s, T_s) = 2.56 \times 10^{-4} \frac{P_{SO_2}^{3/2}}{\{1 + 0.006(P_{H_2O,i} + 2 P_{SO_2,i} - 2 P_{SO_2})\}^2} \exp\left(\frac{-7350}{R T_s}\right) \quad (E.1)$$

Now introduce dimensionless variables to simplify the general modeling equations with the above assumptions.

Let

$$L = \frac{Z}{\ell} \quad (\text{E.2})$$

$$X_f = \frac{C_{fi} - C_f}{C_{fi}}, \quad X_c = \frac{C_{fi} - C_s}{C_{fi}} \quad (\text{E.3})$$

$$\theta_f = \frac{T_{fi} - T_f}{T_{fi}}, \quad \theta_c = \frac{T_{fi} - T_s}{T_{fi}} \quad (\text{E.4})$$

Then

$$C_f = C_{fi} (1 - X_f), \quad C_s = C_{fi} (1 - X_c) \quad (\text{E.5})$$

$$T_f = T_{fi} (1 - \theta_f), \quad T_s = T_{fi} (1 - \theta_c) \quad (\text{E.6})$$

By combining equations (3.8) and (3.9),

$$A_m k_m (C_s - C_f) \Delta H - A_h h (T_s - T_f) = 0$$

or

$$A_m k_m (C_s - C_f) = \frac{A_h h (T_s - T_f)}{\Delta H} \quad (\text{E.7})$$

From equations (3.6), (3.7) and (E.7),

$$\begin{aligned} \epsilon_B V_{int} \frac{dC_f}{dz} &= A_m k_m (C_s - C_f) \\ &= \frac{A_h h (T_s - T_f)}{\Delta H} = \frac{1}{\Delta H} \rho_f C_{pf} \epsilon_B V_{int} \frac{dT_f}{dz} \end{aligned}$$

$$\text{or} \quad \frac{dC_f}{dz} = \frac{\rho_f C_{pf}}{\Delta H} = \frac{dT_f}{dz} \quad (\text{E.8})$$

By using equations (E.5) and (E.6), equation (E.8) can be integrated to get a $X_f - \theta_f$ relationship.

$$\int_0^{X_f} C_{fi} dx_f = \frac{\rho_f C_{pf} T_{fi}}{\Delta H} \int_0^{\theta_f} d\theta_f$$

$$C_{fi} X_f = \frac{\rho_f C_{pf} T_{fi}}{\Delta H} \theta_f$$

$$\text{or } \theta_f = \frac{\Delta H C_{fi}}{\rho_f C_{pf} T_{fi}} X_f \quad (\text{E.9})$$

Equation (3.6) can be described in terms of conversion by employing equation (E.5).

$$\epsilon_B V_{int} \frac{d}{dz} C_{fi} (1 - X_f) =$$

$$A_m k_m \{C_{fi} (1 - X_s) - C_{fi} (1 - X_f)\}$$

$$\therefore \frac{dX_f}{dz} = \frac{A_m k_m}{\epsilon_B V_{int}} (X_s - X_f)$$

$$\text{or } \frac{dX_f}{dL} = A_1 (X_s - X_f) \quad (3.12)$$

$$\text{where } A_1 = \frac{l \cdot A_m \cdot k_m}{\epsilon_B V_{int}} \quad (\text{E.10})$$

From equations (E.7), (E.5) and (E.6),

$$A_m k_m C_{fi} (1 - X_s) - C_{fi} (1 - X_f) =$$

$$\frac{A_h h}{\Delta H} T_{fi} (1 - \theta_s) - T_{fi} (1 - \theta_f)$$

$$\therefore \theta_f - \theta_s = \frac{A_m k_m C_{fi}}{A_h h T_{fi}} (X_f - X_s) \Delta H \quad (\text{E.11})$$

By introducing equation (E.9) to equation (E.11),

$$\frac{\Delta H C_{fi}}{\rho_f C_{pf} T_{fi}} X_f - \theta_s = \frac{A_m k_m C_{fi}}{A_h h T_{fi}} (X_f - X_s) \Delta H$$

$$\therefore \theta_s = (A_7 - A_8) X_f + A_8 X_s \quad (\text{E.12})$$

$$\text{where } A_7 = \frac{\Delta H C_{fi}}{\rho_f C_{pf} T_{fi}} \quad (\text{E.13})$$

$$A_8 = \frac{A_m k_m C_{fi} \Delta H}{A_h h T_{fi}} \quad (\text{E.14})$$

Now equation (3.8) can be described in terms of conversion only since P_s and T_s can be expressed in terms of conversion.

$$\begin{aligned} P_s &= R_g T_s C_s = R_g T_{fi} (1 - \theta_s) C_{fi} (1 - X_s) \\ &= P_{fi} (1 - \theta_s) (1 - X_s) \\ &= P_{fi} \{1 - (A_7 - A_8) X_f - A_8 X_s\} (1 - X_s) \end{aligned} \quad (\text{E.15})$$

$$\begin{aligned} T_s &= T_{fi} (1 - \theta_s) \\ &= T_{fi} \{1 - (A_7 - A_8) X_f - A_8 X_s\} \end{aligned} \quad (\text{E.16})$$

Then the reaction rate expression becomes -

$$r_s (P_s, T_s) \rho_B \eta = \frac{A_3 (f_1 f_2)^{3/2}}{(A_4 - A_5 f_1 f_2)^2} \exp \left(\frac{A_6}{T_2} \right) \quad (\text{E.17})$$

where $A_2 = A_m k_m C_{fi}$ (E.18)

$$A_3 = (2.56 \times 10^{-4}) \rho_B \eta P_{fi}^{3/2} \quad (\text{E.19})$$

$$A_4 = 1 + 0.006 (P_{H_2O,i} + 2 P_{fi}) \quad (\text{E.20})$$

$$A_5 = 0.012 P_{fi} \quad (\text{E.21})$$

$$A_6 = \frac{-7350}{R_g T_{fi}} \quad (\text{E.22})$$

$$f_1 = 1 - X_s \quad (\text{E.23})$$

$$f_2 = 1 - (A_7 - A_8) X_f - A_8 X_s \quad (\text{E.25})$$

Finally equation (3.8) becomes,

$$A_2 (X_f - X_s) + \frac{A_3 (f_1 f_2)^{3/2}}{(A_4 - A_5 f_1 f_2)^2} \exp\left(\frac{A_6}{f_2}\right) = 0 \quad (\text{3.13})$$

The computer program MODEL, used to solve equations (3.12) and (3.13) simultaneously, is listed.

... (CONT'D)

```

RR=82.06*760.
VINT=VS/EB
WMOL= 28.*(1.-XHS-XSO-XHO-XS) +34.*XHS +64.*XSO +18.*
1XHO +64.*XS
PFO=PT*XSO
PHO=PT*XHO
CFO=PFO/RR/TF0
PS=PT*XS
A3=1. +0.006*(PHO+2.*PFO)
PF=PFO
PS2=PT/760.
TO=298.
TR(1)=298.
DO 20 J=1,4
20 TR(J+1)=298.*TR(J)
WRITE(6,27)
27 FORMAT(1H1,///,14X,'LENGTH',8X,'XF',8X,'XC',7X,'THF',
17X,'THC',8X,'TF',8X,'TC',7X,'XN1',7X,'XN2',8X,'DH'//)
XF=0.
DO 1000 III=1,1001
TT(1)=TF
DO 77 J=1,4
77 TT(J+1)=TF*TT(J)
DENST=PT*WMOL/RR/TF
VISCO=0.00025+0.000034*(TF-473.)/100.
CPF= AL(7,1)
DO 21 L=1,4
21 CPF=CPF+AL(7,L+1)*TT(L)
CPF=R*CPF/28.
XK=0.2976/3600.
D=0.010996*TF**1.5/PT/0.44
G=DENST*VS
SC=VISCO/DENST/D
PR=VISCO*CPF/XK
RE=G*DP/VISCO
RRE=RE**0.41-1.5
XJD=0.725/RRE
XJH=1.10/RRE
XKM=XJD*G/DENST*SC**(-2./3.)
H=XJH*CPF*G*PR**(-2./3.)
IF(III-1) 88,88,44
44 CALL FREM (PS2,TF,XN1,XN2 )
CALL HTORN (TF,XN1,XN2, R, TT,TR,DH)
GO TO 55
88 XN1=0.135
XN2=0.865
DH=11250.-1.5*(XN1*22673. +XN2*24753.)
55 C1=AM*XKM*CFO
C2=DB*PFO**1.5*0.17 * 2.56E-04
C3=1.+0.006*(PHO+2.*PFO)

```

... (CONT'D)

```

C4=0.012*PFO
C5=-7350./R/TFO
A1=XL*AM*XKM/VINT/EB
A2=DH*CFO/DENST/CPF/TFO
A3=C1*DH/AT/H/TFO
CALL NEWTN(XF,A2,A3,C1,C2,C3,C4,C5,XC)
Z=DZ*(LII-1)
THF=A2*XF
THC=(A2-A3)*XF+A3*XC
TF=TFO*(1.-THF)
TC=TFO*(1.-THC)
WRITE(6,25) Z, XF, XC, THF, THC, TF, TC, XN1, XN2, DH
25 FORMAT( 10X, 9F10.5, F10.2 )

```

C CALCULATE BULK FLUID CONDITION

```

CALL RKGS (A1,DZ,XC,XF)
CHK=1.0-XF
IF( ABS(CHK) -1.0E-07) 1001,1001,1000
1000 CONTINUE
1001 CALL EXIT
END

```

```

C *****
C *
C *          SUBROUTINE HTORN
C *
C * THIS SUBROUTINE CALCULATES THE STANDARD HEAT OF RE
C * -ACTION OF THE CLAUS REACTION CONSIDERING THE EFFE
C * -CT OF EQUILIBRIUM DISTRIBUTION OF SULFUR SPECIES
C * AT A DIFFERENT TEMPERATURE
C *
C *****

SUBROUTINE HTORN (T,XN1,XN2, R, TT,TR,DH)
DIMENSION TT(5),TR(5),AH(7,5), AL(7,5)
COMMON AL,AH
N=5
HR=11250.-XN1*22673.*1.5-XN2*24753.*1.5
IF(T-1000.) 20,20,30
20 DO 50 J=1,N
50 HR=HR+(2.*AL(6,J)+1.5*(1.-XN1-XN2)*AL(5,J)+0.5*XN1*AL
1(4,J) +0.375*XN2*AL(3,J)-2.*AL(1,J)-AL(2,J)) *(TT(J)-
2TR(J)) /J*R
GO TO 100
30 DO 40 J=1,N
40 HR=HR+(2.*AH(6,J)+1.5*(1.-XN1-XN2)*AH(5,J)+0.5*XN1*AH
1(4,J) +0.375*XN2*AH(3,J)-2.*AH(1,J)-AH(2,J)) *(TT(J)-
2TR(J)) /J*R
100 DH=HR
RETURN
END

```



```

C *****
C *
C *           SUBROUTINE NEWTN
C *
C * THIS SUBROUTINE IS TO SOLVE MODELLING EQUATION
C * (3.13) AND GET THE CONVERSION ON THE CATALYST SUR-
C * FACE AT A GIVEN CONVERSION IN THE BULK FLUID USING
C * NEWTON-RAPHSON ITERATION TECHNIQUE
C *
C *****

SUBROUTINE NEWTN(XF,A2,A3,C1,C2,C3,C4,C5,XMM)
DIMENSION X(500)
F1(X)=1.-X
F2(X)=1.-XF*(A2-A3)-A3*X
F3(X)=F1(X)*F2(X)
F4(X)=C3-C4*F3(X)
F5(X)=EXP(C5/F2(X))
F(X)=C1*(XF-X) +C2*F3(X)**1.5*F5(X) /((F4(X))**2.
DF(X)= -C1 +C2*F5(X)*(1.5*(F3(X))**0.5*(-F2(X)-A3*F1(X)
1) /((F4(X))**2. -(F3(X))**1.5*2.*(C4*F2(X)+A3*C4*F1(X)
2) /((F4(X))**3. +A3*C5*(F1(X))**1.5/(F4(X))**2./(F2(X))
3**0.5 )
G(X)=X-F(X)/DF(X)

C     INITIAL GUESS OF X

X(1)=XF+0.002

C     CALCULATE CONVERSION AT CATALYST SURFACE

DO 99 I=1,499
X(I+1)=G(X(I))
ESP=ABS((X(I+1)-X(I)) / X(I+1))
IF(ESP-0.0001) 100,100,99
99 CONTINUE
100 IF(I-499) 88,55,55
55 WRITE(6,77)
77 FORMAT(/10X,'NO CONVERGE'/)
88 XMM=X(I+1)
RETURN
END

```

```

C *****
C *
C *          SUBROUTINE RKGS          *
C *
C * THIS SUBROUTINE IS TO INTEGRATE THE MODELLING EQU- *
C * ATION (3.12) FROM THE INLET TO THE OUTLET OF THE *
C * REACTOR USING RUNGE-KUTTA-GILL FOURTH ORDER INTE- *
C * GRATION PROCEDURE *
C *
C *****

SUBROUTINE RKGS(A1,DZ,XC,Y)
F(Y)=A1*(XC-Y)
D1=DZ*F(Y)
D2=DZ*F(Y+D1/2. )
D3=DZ*F(Y+0.207107*D1 +0.292893*D2 )
D4=DZ*F(Y-0.707107*D2+1.707107*D3 )
Y=Y + (D1+D4)/6. +0.0976310*D2 +0.569035*D3
RETURN
END

```

APPENDIX F

ASYMPTOTIC SOLUTION FOR EFFECTIVENESS FACTOR

F-1. Check the Validity of the Isothermal Catalyst Pellet

Assumption:

The validity of the assumption of an isothermal catalyst pellet may be checked by the value of the heat of reaction parameter, β , at the inlet condition of the catalyst bed.

$$\begin{aligned}\beta &= (-\Delta H) \frac{D_e C_s}{k_e T_s} \\ &\approx (26000) \left(\frac{0.001888}{3.39 \times 10^{-4}} \right) \left(\frac{6.7 \times 10^{-7}}{556} \right) \\ &\quad \left(\frac{\text{cal}}{\text{mole SO}_2} \right) \left(\frac{\text{cm}^2/\text{sec}}{\text{cal}/\text{cm}^{\circ}\text{K}\cdot\text{sec}} \right) \left(\frac{\text{mole}/\text{cm}^3}{\text{K}} \right) \\ &= 1.7449 \times 10^{-4} \\ &\approx 0\end{aligned}$$

Therefore the whole pellet can be treated in a isothermal condition, and there is no need for an energy balance equation to calculate the effectiveness factor.

F-2. Modeling Equation for the Effectiveness Factor;

A general material balance equation within a catalyst pellet can be written as

$$\frac{d^2 C_p}{dr^2} + \frac{a}{r} \frac{d C_p}{dr} - \frac{\rho_p}{D_e} r_p (P_p, T_p) = 0 \quad (\text{F.1})$$

where $a = 0$ for a flat slab pellet
 $a = 1$ for a cylindrical pellet
 $a = 2$ for a spherical pellet

To check the validity of the asymptotic solution, the concept of Thiele-modulus, ϕ , can be employed for this particular reaction condition.

$$\phi_s = \frac{R}{3} \sqrt{\frac{\rho_p r_s (P_s, T_s)}{D_e C_s}} \quad (3.14)$$

$$\begin{aligned} \text{where } r_s (P_s, T_s) &= \frac{(2.56 \times 10^{-4}) P_s^{1.5}}{[1 + 0.006 (P_{H_2O,i} + 2 P_{f,i} - 2 P_s)]^2} \\ &\quad \text{EXP} \left(- \frac{7350}{R_g T_s} \right) \\ &= \frac{(2.56 \times 10^{-4}) (20.6545)^{1.5}}{(2.2604 - 0.012 \times 20.6545)^2} \\ &\quad \text{EXP} \left(\frac{-7350}{1.987 \times 556} \right) \\ &= 7.6047 \times 10^{-6} \text{ (g mole SO}_2\text{/} \\ &\quad \text{sec-gm catalyst)} \end{aligned}$$

$$R = \left(\frac{0.3175}{2} \right) \text{ cm}$$

$$\text{Then } \phi_s = \frac{1}{3} \left(\frac{0.3175}{2} \right) \sqrt{\frac{1.53 \times 7.6047 \times 10^{-6}}{0.001888 \times 5.957 \times 10^{-7}}} = 5.3823$$

Since the estimated value of Thiele modulus is larger than 5.0, the catalyst pellet may be approximated by

a flat slab model. The modeling equation can be obtained from equation (F.1) by letting a equal to zero.

$$\frac{d^2 C_p}{dr^2} - \frac{\rho_p}{D_e} r_p (P_p, T_p) = 0 \quad (\text{F.2})$$

In a dimensionless form,

$$\frac{d^2 \psi}{d\xi^2} - \phi_f^2 \frac{r_p (P_p, T_p)}{r_s (P_s, T_s)} = 0 \quad (\text{F.3})$$

where $\psi = \frac{C_p}{C_s} = \frac{P_p}{P_s}$ (F.4)

$$\xi = \frac{r}{R} \quad (\text{F.5})$$

$$\phi_f^2 = R^2 \frac{\rho_p r_s (P_s, T_s)}{D_e C_s} \quad (\text{F.6})$$

Furthermore,

$$\begin{aligned} \frac{r_p (P_p, T_p)}{r_s (P_s, T_s)} &= \frac{(2.56 \times 10^{-4}) P_p^{1.5}}{\{1 + 0.006(P_{H_2O,i} + 2P_{f,i} - 2P_p)\}^2} \text{EXP} \left(\frac{-7350}{R_g T_p} \right) \\ &= \frac{(2.56 \times 10^{-4}) P_s^{1.5}}{\{1 + 0.006(P_{H_2O,i} + 2P_{f,i} - 2P_s)\}^2} \text{EXP} \left(\frac{-7350}{R_g T_s} \right) \\ &= \frac{\psi^{1.5}}{(C_3 - C_2 \psi)^2} (C_3 - C_2)^2 \quad (\text{F.7}) \end{aligned}$$

where $C_1 = 1 + 0.006 (P_{H_2O,i} + 2 P_{f,i})$

$$C_2 = 0.012$$

$$C_3 = C_1/P_s$$

Now equation (F.3) becomes,

$$\frac{d^2\psi}{d\xi^2} - \phi_f^2 (C_3 - C_2)^2 \frac{\psi^{1.5}}{(C_3 - C_2\psi)^2} = 0 \quad (F.8)$$

with boundary conditions

$$\psi = 0 \quad \text{at} \quad \xi = 0$$

$$\frac{d\psi}{d\xi} = 0 \quad \text{at} \quad \xi = 0 \quad (F.9)$$

$$\psi = 1 \quad \text{at} \quad \xi = 1$$

F-3. Asymptotic Solution for the Effectiveness Factor:

An asymptotic solution of equation (F.1) can be obtained from the solution of equation (F.8). To solve equation (F.8), let

$$y = \frac{d\psi}{d\xi}$$

Then equation (F.8) becomes,

$$\frac{dy}{d\xi} = \phi_f^2 (C_3 - C_2)^2 \frac{\psi^{1.5}}{(C_3 - C_2\psi)^2} \quad (F.10)$$

After multiplying both sides of equation (F.10) by $d\psi$ and rearranging, equation (F.10) can be integrated such as

$$\int_{y(\xi=0)}^{y(\xi=1)} y dy = \phi_f^2 (C_3 - C_2)^2 \int_{\psi=0}^{\psi=1} \frac{\psi^{1.5}}{(C_3 - C_2\psi)^2} d\psi \quad (F.11)$$

The integration on the right hand side of equation (F.11) can be done analytically to obtain a value of 50.008. Then

$$\begin{aligned} Y_{(\xi=1)}^2 &= 2 \phi_f^2 (C_3 - C_2)^2 (50.008) \\ &= 2 \phi_f^2 (0.1094 - 0.012)^2 (50.008) \\ &= 0.94885 \phi_f^2 \end{aligned}$$

$$\text{or } Y_{(\xi=1)} = 0.9741 \phi_f$$

The effectiveness factor can be calculated according to its definition.

$$\eta = \frac{\text{Actual diffusion rate into the pores}}{\text{Reaction rate within the catalyst pellet}}$$

$$\begin{aligned} \text{Here actual diffusion rate} &= (D_e \frac{dC}{dr}) \left(\frac{6}{d_p \rho_p} \right) \\ &= D_e \left(\frac{C_s}{R} \right) \left(\frac{d\psi}{d\xi} \right)_{\xi=1} \left(\frac{6}{d_p \rho_p} \right) \\ &= \frac{3}{\phi_f} r_s (P_s, T_s) Y_{(\xi=1)} \end{aligned}$$

$$\text{reaction rate} = r_s (P_s, T_s)$$

Therefore

$$\begin{aligned} \eta &= \frac{\frac{3}{\phi_f} Y_{(\xi=1)}}{r_s} = \frac{\frac{3}{\phi_f} (0.9741 \phi_f)}{r_s} \\ &= \frac{2.9223}{\phi_f} = \frac{2.9223}{16.1468} = 0.1858 \end{aligned}$$

APPENDIX G

DERIVATION OF COLLOCATION EQUATION
FOR INTERNAL RESISTANCE OF CATALYST PELLETS

The general material balance equation for an isothermal spherical catalyst pellet becomes

$$\frac{d^2 C_p}{dr^2} + \frac{2}{r} \frac{dC_p}{dr} - \frac{\rho_p}{D_e} r_p (P_p, T_p) = 0 \quad (G.1)$$

By introducing dimensionless variables

$$\psi = \frac{C_p}{C_s} = \frac{P_p}{P_s} \quad (G.2)$$

$$\xi = \frac{r}{R} \quad (G.3)$$

equation (G.1) becomes

$$\frac{d^2 \psi}{d\xi^2} + \frac{2}{\xi} \frac{d\psi}{d\xi} - 9 \phi_s^2 \frac{r_p (P_p, T_p)}{r_s (P_s, T_s)} = 0 \quad (G.4)$$

where ϕ_s represents Thiele modulus defined by

$$\phi_s = \frac{R}{3} \sqrt{\frac{\rho_p r_s (P_s)}{D_e C_s}}$$

But as was shown in Appendix E,

$$\frac{r_p (P_p, T_p)}{r_s (P_s, T_s)} = \frac{\psi^{1.5}}{(C_3 - C_2)^2} (C_3 - C_2)^2 \quad (G.5)$$

where $C_1 = 1 + 0.006 (P_{H_2O,i} + 2 P_{fi})$

$$C_2 = 0.012$$

$$C_3 = C_1/P_s$$

Now equation (G.5) becomes

$$\frac{d^2 \psi}{d\xi^2} + \frac{2}{\xi} \frac{d\psi}{d\xi} - 9 \phi_s^2 (C_3 - C_2)^2 \frac{\psi^{1.5}}{(C_3 - C_2 \psi)^2} = 0 \quad (G.6)$$

To check the validity of the flat slab model for a spherical catalyst in solving equation (G.6), an approximation method can be applied for the steeply descending concentration profiles within the catalyst pellet, which was originally proposed by Paterson and Cresswell (76) in terms of the effective reaction zone defined by the region beyond which the reactant concentration becomes essentially zero where no reaction can occur as a consequence. To apply this reaction zone concept the reaction interphase ξ_I is defined as

$$x = \frac{\xi - \xi_I}{1 - \xi_I} \quad (\text{G.7})$$

In equation (G.7) x varies from zero to one for the value of ξ between ξ_I and one. Now equation (G.6) can be described in terms of the reaction interphase by using equation (G.7).

$$\frac{1}{(1 - \xi_I)^2} \frac{d^2 \psi}{dx^2} + \frac{2}{\xi_I + (1 - \xi_I)x} \left(\frac{1}{1 - \xi_I} \frac{d\psi}{dx} - \psi \right) - 9 \phi_B^2 (C_3 - C_2)^2 \frac{\psi^{1.5}}{(C_3 - C_2 \psi)^2} = 0 \quad (\text{G.8})$$

Boundary conditions are

$$\psi = 1 \quad \text{at} \quad x = 1 \quad (\text{G.9})$$

$$\psi = 0, \quad \frac{d\psi}{dx} = 0 \quad \text{at} \quad x = 0 \quad (\text{G.10})$$

It should be noted here that the boundary condition (G.9) is the Dirichlet type rather than the Neumann type in this problem. That is because the approximate value of the

Sherwood number in this particular case is

$$Sh = \frac{k_m d_p}{D_e} \approx \frac{10 \times 0.3}{0.0018} = 166$$

So the ratio of the convective mass transfer effect in the external film to the diffusive mass transfer effect within the pore is around 166. Therefore the external resistance is 166 times less than the internal resistance. Here the assumption that the bulk gas concentration can be rigorously used as the catalyst surface concentration to calculate the effectiveness factor. Actually the bulk gas phase concentration is different from the catalyst surface concentration as was indicated in the study on the effect of the external resistances. However, this difference has negligible effects on the calculated value of the effectiveness factor on that assumption since the major resistance exists in the inner part of the catalyst.

By employing the Paterson and Cresswell's collocation technique (76) improved by Van Den Bosch and Padmanabhan (90), the concentration profile in the reaction zone can be approximated by a parabola.

$$\psi = \psi_s x^2 \quad (G.11)$$

As expected in the internal collocation technique, equation (G.11) already satisfies the boundary conditions (G.9) and (G.10). From the boundary condition (G.9), ψ_s becomes one in equation (G.11) to make

$$\psi_i = x_i^2 \quad (G.12)$$

for any collocation point i . By substituting equation (G.12) into equation (G.8) the collocation equation can be obtained.

$$\frac{2}{(1 - \xi_I)^2} + \frac{4}{(1 - \xi_I)} \frac{x_i}{\xi_I + (1 - \xi_I) x_i} - 9 \phi_s^2 (C_3 - C_2)^2 \frac{x_i^3}{(C_3 - C_2 x_i)^2} = 0 \quad (G.13)$$

The optimum collocation point can be taken as $x_i = \frac{1}{\sqrt{2}}$ recommended by Van Den Bosch and Padmanabhan (90) for the high reactivity model.

For the value of $x_i = \frac{1}{\sqrt{2}}$ and calculated value of ϕ_s , ξ_I can be obtained from equation (G.13) to see the applicability of the high reactivity model using the false position iteration method. If the high reactivity model is really applicable, then the effectiveness factor can be calculated as

$$\eta = \frac{D_e \left(\frac{C_s}{R}\right) \left(\frac{d\psi}{d\xi}\right)_{\xi=1}}{r_s (P_s \cdot T_s)} \frac{6}{d_p \rho_p} = \frac{1}{3 \phi_s^2} \left(\frac{d\psi}{d\xi}\right)_{\xi=1} \quad (G.14)$$

But

$$\left(\frac{d\psi}{d\xi}\right)_{\xi=1} = \left(\frac{d\psi}{dx}\right)_{x=1} \left(\frac{dx}{d\xi}\right)_{\xi=1} = \frac{2}{1 - \xi_I} \quad (G.15)$$

By combining equations (G.14) and (G.15)

$$\eta = \frac{2}{3 \phi_s^2} \left(\frac{1}{1 - \xi_I}\right) \quad (G.16)$$

Then the concentration profiles become using equations (G.11) and (G.6),

$$\Psi = \left(\frac{\xi - \xi_I}{1 - \xi_I} \right)^2 = (A\xi + B)^2 \quad (\text{G.17})$$

A listing of the computer program COLLO, used to calculate the reaction interface ξ_I , is included.

```

C *****
C *
C *           MAINLINE COLLO
C *
C * THIS PROGRAM COMPUTES THE EFFECTIVENESS FACTOR OF
C * A ALON CATALYST FOR THE CLAUS REACTION UNDER CON-
C * DITIONS WHERE THE REACTION INTERFACE IS GREATER
C * THAN ZERO USING A INTERNAL COLLOCATION METHOD.
C *
C *       PT = TOTAL PRESSURE
C *       XHO = MOLE FRACTION OF H2O
C *       XSO = MOLE FRACTION OF SO2
C *
C *****

```

```

      READ(5,10) PT
10  FORMAT(1F10.5)
      READ(5,12) XHO,XSO
12  FORMAT(2F10.5)
      PHO=PT*XHO
      PFO=PT*XSO

```

```

C       ASSUME NEGLIGIBLE CONCENTRATION DIFFERENCE IN
C       EXTERNAL FILM

```

```

      PC=PFO
      C1=1.+0.006*(PHO+2.*PFO)
      C2=0.012
      C3=C1/PC
      DO 100 J=1,16
      H=4.0 +J
      CALL FALS2 (C2,C3,H,ZI)
      IF(ZI) 77,77,90
90  WRITE(6,60)
60  FORMAT(1H1,///19X,'THIELE',7X,'REACTION',2X,
1  'EFFECTIVENESS',/18X,'MODULUS',6X,'INTERFACE',9X,
2  'FACTOR' /)
      EFACT=2./H**2./(1.-ZI)/3.
100 WRITE(6,20) H,ZI,EFACT
20  FORMAT(//10X,3F15.4)
      GO TO 99
77  WRITE(6,88)
88  FORMAT(1H1,///10X,'THE REACTION INTERFACE IS NOT',
1  ' GREATER THAN ZERO.' /)
99  CALL EXIT
      END

```

```

C *****
C *
C *           SUBROUTINE FALS2
C *
C * THIS SUBROUTINE COMPUTES THE REACTION INTERFACE
C * FROM THE COLLOCATION EQUATION USING THE FALSE-
C * POSITION ITERATION METHOD.
C *
C *****

SUBROUTINE FALS2 (C2,C3,H,XMM)
DIMENSION XM(500)
F(X)=2./(1.-X)**2. +4./(1.-X)*XI/(X+(1.-X)*XI)-(H*(C3
1-C2)*XI**1.5/(C3-C2*X)**2.)*9.
XI=0.707107
XL=0.0
XR=1.0
XM(1)=0.
DO 99 I=1,499
XM(I+1)=(XL*F(XR)-XR*F(XL)) / (F(XR)-F(XL))
IF(F(XM(I+1)) *F(XL)) 22,33,44
22 XR=XM(I+1)
GO TO 70
33 XR=XM(I+1)
44 XL=XM(I+1)
70 ESP=ABS((XM(I+1)-XM(I)) /XM(I+1))
IF(ESP-0.001) 100,100,99
99 CONTINUE
100 IF(I-499) 88,55,55
55 WRITE(6,77)
77 FORMAT(/10X,'NO CONVERGE'/)
88 XMM=XM(I+1)
RETURN
END

```


APPENDIX H

NUMERICAL SOLUTION FOR EFFECTIVENESS FACTOR

BY WEISZ AND HICKS' METHOD

H-1. Numerical Solution for the Effectiveness Factor:

Use can be made of the equation (G.6)

$$\frac{d^2\psi}{d\xi^2} + \frac{2}{\xi} \frac{d\psi}{d\xi} - 9 \phi_s^2 (C_3 - C_2)^2 \frac{\psi^{1.5}}{(C_3 - C_2\psi)^2} = 0 \quad (\text{G.6})$$

with the boundary conditions of

$$\psi = 1 \quad \text{at} \quad \xi = 1$$

$$\frac{d\psi}{d\xi} = 0 \quad \text{at} \quad \xi = 0$$

Equation (G.6) can be transformed by introducing a new variable

$$x = \frac{\xi}{a} \quad (\text{H.1})$$

Then equation (G.6) becomes

$$\frac{d^2\psi}{dx^2} + \frac{2}{x} \frac{d\psi}{dx} - 9 a^2 \phi_s^2 (C_3 - C_2)^2 \frac{\psi^{1.5}}{(C_3 - C_2\psi)^2} = 0 \quad (\text{H.2})$$

Equation (H.2) can be numerically solved by the open-end method with a known initial value instead of treating it as a two-point boundary value problem, which was originally proposed by Weisz and Hicks (97).

The computing procedures are

- (1) Choose an arbitrary value of a ϕ_s
- (2) Assume an initial value of $\psi=0$ at $x=0$.
- (3) Integrate the equation up to $\psi=1$, and get the value of x at that point.
- (4) Solve for a using $a = \frac{\xi}{x} = \frac{1}{x}$ at $\psi=1$ from the boundary conditions.

(5) Solve for ϕ_s using condition (1).

(6) Solve for effectiveness factor by the relation

$$\eta = \frac{x}{3\phi_s^2} \left(\frac{d\psi}{dx} \right)_{x=\frac{1}{a}}$$

The condition (6) can be derived from the definition of the effectiveness factor;

$$\eta = \frac{D_e \left(\frac{C_s}{R} \right) \left(\frac{d\psi}{d\xi} \right)_{\xi=1}}{r_s(P_s, T_s)} \left(\frac{6}{d_p \rho_p} \right) = \frac{D_e C_s}{r_s(P_s, T_s) \cdot R^2 \rho_p} \cdot 3 \left(\frac{d\psi}{d\xi} \right)_{\xi=1}$$

since

$$\frac{D_e C_s}{r_s(P_s, T_s) R^2 \rho_p} = \frac{1}{(3\phi_s)^2} \quad \text{and} \quad \left(\frac{d\psi}{d\xi} \right)_{\xi=1} = \left(\frac{d\psi}{adx} \right)_{x=\frac{1}{a}}$$

$$\eta = \frac{3}{(3\phi_s)^2} \frac{1}{a} \left(\frac{d\psi}{dx} \right)_{x=\frac{1}{a}}$$

$$= \frac{x}{3\phi_s^2} \left(\frac{d\psi}{dx} \right)_{x=\frac{1}{a}}$$

Equation (H.2) can be transformed into two first order differential equations by letting

$$\frac{d\psi}{dx} = y \quad (\text{H.3})$$

Then

$$\frac{dy}{dx} + \frac{2}{x} y - 9 a^2 \phi_s^2 (C_3 - C_2)^2 \frac{\psi^{1.5}}{(C_3 - C_2 \psi)^2} = 0 \quad (\text{H.4})$$

Equation (H.3) and (H.4) can be solved simultaneously using the Runge-Kutta-Gill integration procedure. To determine the value of the indeterminate form of $\frac{2y}{x}$ on the left

hand side in equation (H.4) use can be made of the L'hospital's theorem at $x=0$.

$$\lim_{x \rightarrow 0} \frac{2y}{x} = \frac{2dy}{dx} \quad (\text{H.5})$$

Now equation (H.4) becomes, at $x=0$

$$\frac{dy}{dx} = 3 a^2 \phi_s^2 (C_3 - C_2)^2 \frac{\psi^{1.5}}{(C_3 - C_2 \psi)^2} \quad (\text{H.6})$$

For other points than $x=0$, equation (H.4) still applies.

The computer program CHOWH was used to calculate the effectiveness factor by applying Weisz and Hicks' method to the Claus reaction system and also listed.

H-2. Difference in Thiele Modulus Between At the Inlet and At the Outlet Condition:

The ratio of the Thiele modulus at the reactor bed outlet condition to that at inlet condition can be written as

$$\frac{\phi_o}{\phi_i} = \sqrt{\frac{r_o (P_s, T_s) C_{si}}{r_i (P_s, T_s) C_{so}}} \quad (\text{H.7})$$

by using the definition of the Thiele modulus, equation (3.14), and assuming constant pellet density and effective diffusivity along the bed. In equation (H.7) subscripts o and i represent the outlet and the inlet condition respectively.

If the denominator change in the reaction rate expression may be ignored equation (H.7) can be described in terms of concentration and temperature at the inlet and outlet of the catalyst bed.

$$\frac{\phi_o}{\phi_i} = \sqrt{\left(\frac{C_{so}}{C_{si}}\right)^{0.5} \left(\frac{T_{so}}{T_{si}}\right)^{1.5} \text{EXP} \left\{ \frac{E}{R_g} \left(\frac{1}{T_{si}} - \frac{1}{T_{so}} \right) \right\}} \quad (\text{H.8})$$

Assuming 98 percent conversion and $T_{si} = 550^\circ\text{K}$, $T_{so} = 680^\circ\text{K}$, equation (H.8) gives

$$\begin{aligned} \frac{\phi_o}{\phi_i} &= \sqrt{\left(\frac{1}{50}\right)^{0.5} \left(\frac{680}{550}\right)^{1.5} \text{EXP} \left\{ \frac{7350}{1.987} \left(\frac{1}{550} - \frac{1}{680} \right) \right\}} \\ &= 0.839 \end{aligned}$$

Therefore, from the calculated value of ϕ_i in Appendix F

$$\phi_o = 0.839 \phi_i = (0.839) (5.3823) = 4.4$$

... (CONT'D)

```
40 IF(KK-24) 50,60,60
50 Y(1)= 0.05-0.01*(KK-19)
   GO TO 90
60 IF(KK-33) 70,80,80
70 Y(1)=0.01-0.001*(KK-23)
   GO TO 90
80 Y(1)=0.001-0.0001*(KK-32)
90 Y(2)=0.
   DERY(1)=0.5
   DERY(2)=0.5
   CALL RUNGE(PRMT,Y,DERY,NDIM,IHLF,FCT,OUTP,AUX)
100 CONTINUE
    CALL EXIT
    END
```

```

C *****
C *
C *
C *
C *
C *
C *
C *
C *****

```

```

SUBROUTINE FCT

```

```

* THIS SUBROUTINE GIVES THE ORDINARY DIFFERENTIAL
* EQUATIONS TO BE SOLVED TO THE SUBROUTINE RUNGE.

```

```

SUBROUTINE FCT(X,Y,DERY)
DIMENSION Y(2),DERY(2)
COMMON C2,C3,AH
DERY(1)=Y(2)
IF(X) 20,20,30
30 DERY(2) = -2.*Y(2)/X+(AH*(C3-C2)/(C3-C2*Y(1)) )**2.*9.*
1Y(1)**1.5
GO TO 40
20 DERY(2)=(AH*(C3-C2) /(C3-C2*Y(1)) )**2.*Y(1)**1.5*3.
40 RETURN
END

```



```

C *****
C *
C *           SUBROUTINE RUNGE
C *
C * THIS SUBROUTINE SOLVES THE SYSTEMS OF ORDINARY
C * DIFFERENTIAL EQUATIONS SIMULTANEOUSLY BY THE RUNGE-
C * KUTTA-GILL METH WITH THE TEST OF ACCURACY
C *
C *****
C SUBROUTINE RUNGE (PRMT,Y,DERY,NDIM,INLP,FCT,OUTP,AUX)

```

```

C
C DIMENSION Y(2),DERY(2),AUX(8,2),A(4),B(4),C(4),PRMT(5)
C DO 1 I=1,NDIM
1 AUX(8,I)=0.06666667*DERY(I)
X=PRMT(1)
XEND=PRMT(2)
H=PRMT(3)
PRMT(5)=0.
CALL FCT(X,Y,DERY)

```

```

C ERROR TEST
C IF(H*(XEND-X) ) 38,37,2

```

```

C PREPARATIONS FOR RUNGE-KUTTA METHOD

```

```

2 A(1)=0.5
A(2)=0.2928932
A(3)=1.707107
A(4)=0.1666667
B(1)=2.
B(2)=1.
B(3)=1.
B(4)=2.
C(1)=0.5
C(2)=0.2928932
C(3)=1.707107
C(4)=0.5

```

```

C PREPARATION OF FIRST RUNGE-KUTTA STEP

```

```

DO 3 I=1,NDIM
AUX(1,I)=Y(I)
AUX(2,I)=DERY(I)
AUX(3,I)=0.
3 AUX(6,I)=0.

```

... (CONT'D)

```

IREC=0
H=H+H
IHLF=-1
ISTEP=0
IEND=0

```

```

C
C   START OF A RUNGE-KUTTA STEP

```

```

4 IF((X+H-XEND)*H) 7,6,5
5 H=XEND-X
6 IEND=1

```

```

C   RECORDING OF INITIAL VALUES OF THIS STEP

```

```

7 CALL OUTP(X,Y,DERY,IREC,NDIM,PRMT)
  IF(PRMT(5)) 40,8,40
8 ITEST=0
9 ISTEP=ISTEP+1

```

```

C
C   START OF INNERMOST RUNGE-KUTTA LOOP

```

```

      J=1
10  AJ=A(J)
     BJ=B(J)
     CJ=C(J)
     DO 11 I=1,NDIM
        R1=H*DERY(I)
        R2=AJ*(R1-BJ*AUX(6,I))
        Y(I)=Y(I)+R2
        R2=R2+R2+R2
11  AUX(6,I)=AUX(6,I)+R2-CJ*R1
     IF(J-4) 12,15,15
12  J=J+1
     IF(J-3) 13,14,13
13  X=X+0.5*H
14  CALL FCT(X,Y,DERY)
     GO TO 10

```

```

C   END OF INNERMOST RUNGE-KUTTA LOOP

```

```

C
C   TEST OF ACCURACY

```

```

15 IF(ITEST) 16,16,20

```

```

C   IN CASE ITEST=0 THERE IS NO POSSIBILITY FOR TESTING
C   OF ACCURACY

```

... (CONT'D)

```

16 DO 17 I=1,NDIM
17 AUX(4,I)=Y(I)
   ITEST=1
   ISTEP=ISTEP+ISTEP-2
18 IHLF=IHLF+1
   X=X-H
   H=0.5*H
   DO 19 I=1,NDIM
   Y(I)=AUX(1,I)
   DERY(I)=AUX(2,I)
19 AUX(6,I)=AUX(3,I)
   GO TO 9

```

C IN CASE ITEST=1 TESTING OF ACCURACY IS POSSIBLE

```

20 IMOD=ISTEP/2
   IF(ISTEP-IMOD) 21,23,21
21 CALL FCT(X,Y,DERY)
   DO 22 I=1,NDIM
   AUX(5,I)=Y(I)
22 AUX(7,I)=DERY(I)
   GO TO 9

```

C COMPUTATION OF TEST VALUE DELT

```

23 DELT=0.
   DO 24 I=1,NDIM
24 DELT=DELT+AUX(8,I)*ABS(AUX(4,I)-Y(I))
   IF(DELT-PRNT(4)) 28,28,25

```

C ERROR IS TOO GREAT

```

25 IF(IHLF-10) 26,36,36
26 DO 27 I=1,NDIM
27 AUX(4,I)=AUX(5,I)
   ISTEP=ISTEP+ISTEP-4
   X=X-H
   IEND=0
   GO TO 18

```

C RESULT VALUES ARE GOOD

```

28 CALL FCT(X,Y,DERY)
   DO 29 I=1,NDIM
   AUX(1,I)=Y(I)
   AUX(2,I)=DERY(I)
   AUX(3,I)=AUX(6,I)
   Y(I)=AUX(5,I)
29 DERY(I)=AUX(7,I)
   CALL OUTP(X,Y,DERY,IHLF,NDIM,PRNT)

```

... (CONT'D)

```
IF (PRMT(5)) 40,30,40
30 DO 31 I=1,NDIM
  Y(I)=AUX(1,I)
31 DERY(I)=AUX(2,I)
  IREC=IHLF
  IF(IEND) 32,32,39
```

C INCREMENT GETS DOUBLED

```
32 IHLF=IHLF-1
  ISTEP=ISTEP/2
  H=H+H
  IF(IHLF) 4,33,33
33 IMOD=ISTEP/2
  IF(ISTEP-IMOD-IMOD) 4,34,4
34 IF(DELT-0.02*PRMT(4)) 35,35,4
35 IHLF=IHLF-1
  ISTEP=ISTEP/2
  H=H+H
  GO TO 4
```

C RETURNS TO CALLING PROGRAM

```
36 IHLF=11
  CALL FCT(X,Y,DERY)
  GO TO 39
37 IHLF=12
  GO TO 39
38 IHLF=13
39 CALL OUTP(X,Y,DERY,IHLF,NDIM,PRMT)
40 RETURN
  END
```

```

C *****
C *
C *          SUBROUTINE OUTP          *
C *
C * THIS SUBROUTINE SPECIFIES THE OUTPUT OF THE *
C * SUBROUTINE RUNGE                *
C *
C *     EFACT = EFFECTIVENESS FACTOR *
C *     H     = THIELE MODULUS      *
C *
C *****

```

```

SUBROUTINE OUTP (X,Y,DERY,IHLF,NDIM,PRMT)
DIMENSION Y(2),DERY(2),PRMT(5)
COMMON C2,C3,AH
WRITE(6,40) X,Y(1),Y(2),IHLF
40 FORMAT( 10X,3F10.5, 110 )
IF(1.-Y(1)) 200,100,50
200 Y(2)=Y2 + (Y(2)-Y2)*(1.0-Y1) / (Y(1)-Y1)
X= XX+(X-XX)*(1.0-Y1) / (Y(1)-Y1)
100 H=AH*X
EFACT=X*Y(2)/3./H**2.
WRITE (6,80) H,EFACT
80 FORMAT( //20X,2F10.5/ )
PRMT(5)=1.
XX=0.
Y1=0.
Y2=0.
GO TO 60
50 XX=X
Y1=Y(1)
Y2=Y(2)
60 RETURN
END

```

APPENDIX I

SAMPLE CALCULATION OF DATA REDUCTION

I-1. Input Data:

Input data were entered on request after keyboard queuing the material balance program; MTBAL, on the remote teletype. A typical input request sequence is listed in Table I.1. All entered input data were preceded by a ">" and each input request precedes the input data. A typical output of the processed data is also listed in Table I.2.

I-2. Reduction of Input Data:

I-2.1 Temperature (°C)

- a) Treactor inlet = $1.40878 + 18.31152 \times (\text{M.V.})$
- b) Treactor outlet = $2.51827 + 18.21650 \times (\text{M.V.})$

I-2.2 Pressure (mm Hg)

- a) $P_{\text{feed}} (\text{abs.}) = 744.61367 + 12.71505 \times (\text{PCT})$
- b) $P_{\text{reactor}} (\text{gauge}) = 1.81379 + 4.05037 \times (\text{PCT})$
for runs F and G.
- $P_{\text{reactor}} (\text{gauge}) = 27.66422 + 4.19851 \times (\text{PCT})$
for runs H, I, K and L
- $P_{\text{reactor}} (\text{gauge}) = 15.83784 + 4.32817 \times (\text{PCT})$
for runs A, B, C, D, E and J.

I-2.3 Feed Flow Rate (SCFH)

- a) $FF_{N_2} = 0.08793 + 0.94999 \sqrt{\text{PCT}} - 0.00099 \times (\text{PCT})$
- b) composition correction for the feed mixture

$$P_{\text{MIX}} = \frac{\sum_{i=1}^4 \text{FDCOM}_i \times \text{MW}_i}{\sum_{i=1}^4 \text{FDCOM}_i \times V_i}$$

		<u>MW_i</u>	<u>(1) V_i (ml/gmole)</u>
i = 1	N ₂	28	22402.10
i = 2	H ₂ S	34	22176.10
i = 3	COS	60	22417.51
i = 4	SO ₂	64	21901.63

$$\rho_{N_2} = 28/V_i$$

$$FF_{MIX} = FF_{N_2} \left(\frac{\rho_{N_2}}{\rho_{MIX}} \right)^{1/2}$$

I-2.4 Gas Chromatograph Data

a) ATN 1 = 1.07781 + 0.17031 x (ATTEN #1 Setting)

ATN 2 = 1.17312 + 1.76047 x (ATTEN #2 Setting)

b) corrected area of N₂ - peak

i) For runs A, B, C, D, E and J

corrected area = measured area

ii) For runs F, G, H, I, K and L

corrected area = measured area x (ATN 1) x
(ATN 2)

c) calculate average area for each component

d) calculate area ratios, A_{H_2O}/A_{N_2} , A_{COS}/A_{N_2} and

A_{SO_2}/A_{N_2}

(1) Braker, W., and Mossman, A.L., "Matheson Gas Data Book", 5th ed., Matheson Gas Products, East Rutherford, N.J., 1971

e) calculate molar ratios from GC calibration

equations:

i) For runs A, B, C, D, E and J

$$M_{\text{H}_2\text{S}}/M_{\text{N}_2} = 0.01259 + 0.94687 \times (A_{\text{H}_2\text{S}}/A_{\text{N}_2}) \times 100$$

$$M_{\text{COS}}/M_{\text{N}_2} = 0.03809 + 0.72771 \times (A_{\text{COS}}/A_{\text{N}_2}) \times 100$$

$$M_{\text{SO}_2}/M_{\text{N}_2} = 0.11839 + 0.84600 \times (A_{\text{SO}_2}/A_{\text{N}_2}) \times 100$$

ii) For runs F, G, H, I, K and L

$$M_{\text{H}_2\text{S}}/M_{\text{N}_2} = 0.00733 + 0.89481 \times (A_{\text{H}_2\text{S}}/A_{\text{N}_2}) \times 100$$

$$M_{\text{COS}}/M_{\text{N}_2} = 0.00149 + 0.65325 \times (A_{\text{COS}}/A_{\text{N}_2}) \times 100$$

$$M_{\text{SO}_2}/M_{\text{N}_2} = 0.02466 + 0.77038 \times (A_{\text{SO}_2}/A_{\text{N}_2}) \times 100$$

f) calculate mole fractions

$$\text{FDCOM}_1 \text{ or } \text{PRCOM}_1 = 100 / (100 + M_{\text{H}_2\text{S}}/M_{\text{N}_2} + M_{\text{COS}}/M_{\text{N}_2} + M_{\text{SO}_2}/M_{\text{N}_2})$$

$$\text{FDCOM}_2 = \text{FDCOM}_1 \times (M_{\text{H}_2\text{S}}/M_{\text{N}_2}) / 100$$

$$\text{FDCOM}_3 = \text{FDCOM}_1 \times (M_{\text{COS}}/M_{\text{N}_2}) / 100$$

$$\text{FDCOM}_4 = \text{FDCOM}_1 \times (M_{\text{SO}_2}/M_{\text{N}_2}) / 100$$

I-2.5 Water Feeder

a) ml/HR = 0.31009 + 0.52032 x (dial setting)

b) gm/HR = (ml/HR) / (1.00244 - 0.00022 x T_{H₂O})

I-2.6 Component Flow Rates

a) average molar volume (ft^3/mole)

$$\text{AVGMV} = \sum_{i=1}^4 (y_i \times \text{FDCOM}_i) / 28317.016$$

where 28317.016 is a conversion factor from ft^3 to ml.

b) component flow rate (gmole/HR)

$$\text{FF}_{\text{N}_2} = \text{FDCOM}_1 \times (\text{FF}_{\text{MIX}} / \text{AVGMV})$$

$$\text{FF}_{\text{H}_2\text{S}} = \text{FDCOM}_2 \times (\text{FF}_{\text{MIX}} / \text{AVGMV})$$

$$\text{FF}_{\text{COS}} = \text{FDCOM}_3 \times (\text{FF}_{\text{MIX}} / \text{AVGMV})$$

$$\text{FF}_{\text{SO}_2} = \text{FDCOM}_4 \times (\text{FF}_{\text{MIX}} / \text{AVGMV})$$

$$\text{FF}_{\text{H}_2\text{O}} = (\text{gm H}_2\text{O}/\text{HR}) / 18.0588$$

c) component flow rate (SCFH)

$$F_{\text{H}_2\text{S}} = \text{FDCOM}_2 \times \text{FF}_{\text{MIX}}$$

$$F_{\text{COS}} = \text{FDCOM}_3 \times \text{FF}_{\text{MIX}}$$

$$F_{\text{SO}_2} = \text{FDCOM}_4 \times \text{FF}_{\text{MIX}}$$

I-2.7 Product Flow Rates (gmole/HR)

$$P_{\text{N}_2} = \text{FF}_{\text{N}_2}$$

$$P_{\text{H}_2\text{S}} = P_{\text{N}_2} \times (\text{PRCOM}_2 / \text{PRCOM}_1)$$

$$P_{\text{COS}} = P_{\text{N}_2} \times (\text{PRCOM}_3 / \text{PRCOM}_1)$$

$$P_{\text{SO}_2} = P_{\text{N}_2} \times (\text{PRCOM}_4 / \text{PRCOM}_1)$$

$$P_{CO_2} = FF_{COS} - P_{COS}$$

$$P_{Sn} = 1.5 \times (FF_{H_2S} + P_{H_2S} + FF_{COS} - P_{COS})/n$$

where n is the average number of atoms in a sulfur molecule.

I-2.8 Space Velocity (SCFH/gm cat.) and Space Time (gm cat./SCFH)

$$SV_{MIX} = FF_{MIX}/WC \quad ST_{MIX} = 1/SV_{MIX}$$

$$SV_{H_2S} = F_{H_2S}/WC \quad ST_{H_2S} = 1/SV_{H_2S}$$

$$SV_{COS} = F_{COS}/WC \quad ST_{COS} = 1/SV_{COS}$$

$$SV_{SO_2} = F_{SO_2}/WC \quad ST_{SO_2} = 1/SV_{SO_2}$$

where WC is the weight of catalyst in gram.

I-2.9 Fractional Conversions

$$H_2SCM = (FF_{H_2S} - P_{H_2S})/FF_{H_2S}$$

$$CoSCN = (FF_{COS} - P_{COS})/FF_{COS}$$

$$SO_2CN = (FF_{SO_2} - P_{SO_2})/FF_{SO_2}$$

I-2.10 Correction of Feed Composition for Water Injection

$$FDCOM_i = \frac{FF_i}{\sum_{i=1}^5 FF_i}$$

I-2.11 Partial Pressures in the Reactor (mm Hg)

$$pp_i = \frac{P_i \times P_{reactor}}{\sum_{i=1}^7 P_i}$$

where $i = 1$ for N_2
 $i = 2$ for H_2S
 $i = 3$ for COS
 $i = 4$ for SO_2
 $i = 5$ for H_2O
 $i = 6$ for CO_2
 $i = 7$ for Sn

I-3. Sample Calculation for Run F-6:

I-3.1 Gas Chromatograph Data

a) attenuator settings

ATTEN #1 = 10.0

ATTEN #2 = 5.0

b) feed analysis

	<u>N_2</u>	<u>H_2S</u>	<u>COS</u>	<u>SO_2</u>
Measured area	201267	203878	279190	117223
	200960	200308	278458	114565
	201201	203233	276263	122204
Corrected area	5583325	203878	279190	117223
	5574808	200308	278458	114565
	5581494	203233	276263	122204
Avg. corrected area	5579876	202473	277970	117997

c) product analysis

	<u>N₂</u>	<u>H₂S</u>	<u>COS</u>	<u>SO₂</u>
Measured area	199037	133398	244301	62466
	199785	131616	244920	63089
	200025	132677	243946	62988
Corrected area	5521462	133398	244301	62466
	5542213	131616	244920	63089
	5548870	132677	243946	62988
Avg. corrected area	5537515	132564	244389	62848

d) area ratios

	<u>Feed</u>	<u>Product</u>
A_{H_2S}/A_{N_2}	0.036286	0.023939
A_{COS}/A_{N_2}	0.049817	0.044133
A_{SO_2}/A_{N_2}	0.021147	0.011349

e) mole ratios (percent)

	<u>Feed</u>	<u>Product</u>
M_{H_2S}/M_{N_2}	3.254238	2.149416
M_{COS}/M_{N_2}	3.252806	2.881498
M_{SO_2}/M_{N_2}	1.653783	0.898964

f) mole fractions

	<u>Feed</u>	<u>Product</u>
N ₂	0.924549	0.944021
H ₂ S	0.030087	0.020291
COS	0.030074	0.027202
SO ₂	0.015290	0.008486

I-3.2 Temperatures (°C)

- a) T_{reactor inlet} = 1.40878 + 18.31152 (15.40)
= 283.41
- b) T_{reactor outlet} = 2.51827 + 18.21650 (15.40)
= 283.05

I-3.3 Pressure (mm Hg)

- a) P_{feed} (abs.) = 744.61367 + 12.71505 (40)
= 1253.22
- b) P_{reactor} (gauge) = 1.81379 + 4.05037 (55)
= 224.58
- c) Atmospheric pressure = 705.6

I-3.4 Feed Flow Rate (SCFH)

- a) $FF_{N_2} = 0.08793 + 0.94999 \sqrt{91} - 0.00099$ (90)
= 9.052247
- b) $P_{MIX} = (.092455 \times 28 + .03009 \times 34 + .03007 \times 60 +$
 $.01529 \times 64) / (.92455 \times 22402.1 +$
 $.03009 \times 22176.1 + .03007 \times 22417.51 +$
 $.01529 \times 21901.63)$
= 0.001326

$$\rho_{N_2} = 28/22402.1 = 0.00125$$

$$FF_{MIX} = 9.05225 \times (.00125/.001326)^{.5} = 8.789$$

I-3.5 Component Flow Rates

$$\begin{aligned} \text{a) } AVGMV &= (.92455 \times 22402.1 + .03009 \times 22176.1 + \\ &\quad .03007 \times 22417.51 + .01529 \times 21901.63) \\ &\quad / 28317.016 \\ &= 0.790624 \text{ (ft}^3/\text{gmole)} \end{aligned}$$

b) component flow rates (gmole/HR)

$$FF_{N_2} = 0.92455 \times 8.789 / 0.790624 = 10.2778$$

$$FF_{H_2S} = 0.03009 \times 8.789 / 0.790624 = 0.3345$$

$$FF_{COS} = 0.03007 \times 8.789 / 0.790624 = 0.3343$$

$$FF_{SO_2} = 0.01529 \times 8.789 / 0.790624 = 0.1700$$

c) component flow rates (SCFH)

$$F_{H_2S} = 0.03009 \times 8.789 = 0.26446$$

$$F_{COS} = 0.03007 \times 8.789 = 0.26429$$

$$F_{SO_2} = 0.01529 \times 8.789 = 0.13438$$

I-3.6 Product Flow Rates (gmole/HR)

$$P_{N_2} = 10.2778$$

$$P_{H_2S} = 10.2778 \times (0.020291/0.944021) = 0.22091$$

$$P_{COS} = 10.2778 \times (0.027202/0.944021) = 0.29616$$

$$P_{SO_2} = 10.2778 \times (0.008486/0.944021) = 0.09239$$

$$P_{H_2O} = 0 + (0.3345 - 0.2209) = 0.1136$$

$$P_{CO_2} = 0.3343 - 0.29616 = 0.0381$$

$$P_{Sn} = 1.5 \times (0.3345 - 0.2209 + 0.3343 - 0.29616) \\ 7.27$$

$$= 0.0313$$

I-3.7 Space Velocity (SCFH/gm cat) and Space Time
(gm cat/SCFH)

$$SV_{MIX} = 8.789/1.0213 = 8.6057$$

$$SV_{H_2S} = 0.26446/1.0213 = 0.2589$$

$$SV_{COS} = 0.26429/1.0213 = 0.2588$$

$$SV_{SO_2} = 0.13438/1.0213 = 0.1316$$

$$ST_{MIX} = 1/8.6057 = 0.1162$$

$$ST_{H_2S} = 1/0.2589 = 3.8625$$

$$ST_{COS} = 1/0.2588 = 3.8640$$

$$ST_{SO_2} = 1/0.1316 = 7.5988$$

I-3.8 Fractional Conversions

$$H_2SCN = (0.3345 - 0.22091)/0.3345 = 0.3396$$

$$COSCN = (0.3343 - 0.29616)/0.3343 = 0.1140$$

$$SO_2CN = (0.1700 - 0.09239)/0.1700 = 0.4565$$

I-3.9 Partial Pressures in the Reactor

$$\sum_{i=1}^7 P_i = 11.07026$$

$$\begin{aligned}
 PP_{N_2} &= (10.2778 \times 930.18) / 11.07026 = 863.59 \\
 PP_{H_2S} &= (0.22091 \times 930.18) / 11.07026 = 18.56 \\
 PP_{COS} &= (0.29616 \times 930.18) / 11.07026 = 24.88 \\
 PP_{SO_2} &= (0.09239 \times 930.18) / 11.07026 = 7.76 \\
 PP_{H_2O} &= (0.1136 \times 930.18) / 11.07026 = 9.55 \\
 PP_{CO_2} &= (0.0381 \times 930.18) / 11.07026 = 3.20 \\
 PP_{Sn} &= (0.0313 \times 930.18) / 11.07026 = 2.63
 \end{aligned}$$

The processed data in Table I.2 were based upon the following units:

weight of catalyst : gram
 temperature : degrees Kelvin
 pressure : mm Hg absolute
 space velocity : SCFH/gm catalyst
 space time : gm catalyst/SCFH
 feed rate : SCFH
 conversion : fractional conversion

```

*****
*
*           MAINLINE MTBAL
*
* THIS PROGRAM COMPUTES THE MATERIAL BALANCE IN THE
* INTEGRAL BED REACTOR FOR H2S-SO2-COS-H2O REACTION
* SYSTEM. INPUT IS REQUESTED ON THE TELETYPE IN A
* FREE FORMAT INPUT STYLE. THE RAW DATA AND THE
* PROCESSED DATA MAY BE ENTERED IN USER DEFINED DISK
* FILES BY THE PROGRAM
*
*   PRESSURE.....MM HG
*   SPACE VELOCITY....SCFH OF A FEED GAS/GM-CAT
*   SPACE TIME.....GM-CAT/SCFH OF A FEED GAS
*   COMPOSITION.....MOLE PERCENT
*   VOLUME.....STANDARD CUBIC FEET
*   CATALYST WEIGHT...GRAM
*
*****

```

```

DEFINE FILE 100 (13,119,U,NEXT) ,200(13,94,U,NEXT)
DIMENSION PRS(3),TEMP(2),PRESS(3),FDCOM(10),PRCOM(10)
*,
1BAL(2, 7),V(4),TC(2,3),PC(2,2),DPC(3),PCR(4,6),HC(2),
1FCR(4,6)
DATA V/22402.10,22176.10,22417.51,1901.63/
DATA TC/1.40878,18.31152,2.51827,18.21650/
DATA PC/744.61367,12.71505, 1.81379,4.05037/
DATA HC/0.31009,0.52032/
DATA DPC/0.08793,0.94999,-0.00099/

```

```

CALL GETTY(LUNR)
LUNW=LUNR
ISTR=1
IEND=0

```

```

WRITE(LUNW,121)
121 FORMAT('FILE STORAGE FLAG(1-STORE,2-NO)'/ 'FUNCTION FL'
1, 'AG(1-PROC NEW DATA OR 2-PROC FILE DATA)'/ 'PRINT FLA'
1, 'G(1-TTY,2-NONE)')
CALL FFINP(LUNR,3,0,1STOR,0,IFUNC,0,IPR,IEROR)
IF(IEROR) 998,32,999
32 GO TO(88,33),IFUNC

```

READ DATA FROM DISK FILE

```

33 WRITE(LUNW,122)
122 FORMAT('HOW MANY POINTS, AT WHAT RUN NO. IN FILE TO

```

... (CONT'D)

```

* START' )
  CALL FFINP(LUNR,2,0,NUM,0,ISTR,IEROR)
  IF(IEROR) 998,36,999
36 ISTR=ISTR-1
  IEND=ISTR+NUM
34 ISTR=ISTR+1
  NFIL=ISTR

  READ (100*NFIL) NFIL,NFDCR,NPRCR, RUN,WC,TEMP,((FCR(I,
1J),PCR(I,J),I=1,4),J=1,6),PRS,HPCT,HTMP,ATMP

  WRITE(LUNR,123) ISTR
123 FORMAT('RUN NO.'1X,A4,1X,'FINISHED')
  GO TO 35

```

C READ DATA FROM TTY

```

88 WRITE(LUNW,90)
90 FORMAT('WT OF CATALYST(GM) & NUMERIC FILE NO. ')
  CALL FFINP(LUNR,2,1,WC,0,NFIL,IEROR)
  IF(IEROR) 998,101,999
101 WRITE(LUNW,100)
100 FORMAT('RUN NO.,NO. OF FEED G.C.,NO. OF PROD. G.C. ')

  CALL FFINP(LUNR,3,3,RUN,0,NFDCR,0,NPRCR,IEROR)
  IF(IEROR) 998,103,999
103 WRITE(LUNW,105)
105 FORMAT('TEMP-REACT. INLET,OUTLET, PRESS-FEED,REACT.,D
*/P CELL')

  CALL FFINP(LUNR,5,1,TEMP(1),1,TEMP(2),1,PRS (1),1,PRS
1(2),1,PRS(3),IEROR)
  IF(IEROR) 998,104,999
104 WRITE(LUNW,106)
106 FORMAT('SPECIFY H2O FEED PUMP PCT AND TEMP')

  CALL FFINP(LUNR,2,1,HPCT,1,HTMP,IEROR)
  IF(IEROR) 998,107,999
107 WRITE(LUNW,108)
108 FORMAT ('ATMOSPHERIC PRESSURE')

  CALL FFINP(LUNR,1,1,ATMP,IEROR)
  IF(IEROR) 998,109,999
109 WRITE(LUNW,113)
113 FORMAT('FEED G.C. AREAS-N2,H2S,COS,SO2,H2O,CO2')

  DO 116 I=1,NFDCR
  CALL FFINP(LUNR,6,1,FCR(I,1),1,FCR(I,2),1,FCR(I,3),1,
1FCR(I,4),1,FCR(I,5),1,FCR(I,6),IEROR)

```

... (CONT'D)

```
IF(IEROR) 998,116,999
116 CONTINUE
```

```
WRITE(LUNW,117)
117 FORMAT('PROD. G.C. AREAS')
```

```
DO 120 I=1,NPRCR
CALL FFINP(LUNR,6,1,PCR(I,1),1,PCR(I,2),1,PCR(I,3),1
*,PCR(I,4),1,PC
IR(I,5),1,PCR(I,6),IEROR)
IF(IEROR) 998,120,999
120 CONTINUE
```

```
GO TO (40,35),ISTOR
```

```
C STORE RAW DATA IN DISK FILE
```

```
40 WRITE(100'NFIL) NFIL,NFDCR,NPRCR, RUN,WC,TEMP,((FCR(I,
1J),PCR(I,J),I=1,4),J=1,6),PRS,HPCT,HTMP,ATMP
35 CALL CHROM(FDCOM,FCR,NFDCR)
CALL CHROM(PCOM,PCR,NPRCR)
DO 444 I=1,2
TEMP(I)=TC(1,I)+TC(2,I)*TEMP(I)
TEMP(I)=TEMP(I) + 273.
444 CONTINUE
```

```
C H2O FEED RATE CALCULATION (CC/HR)
```

```
HRATE=HC(1)+HC(2)*HPCT
```

```
C H2O FEED RATE IN GRAM/HR
```

```
HRATE=HRATE / (1.00244-0.00022*HTMP )
IF(HPCT) 23,23,24
23 HRATE=0.
```

```
C REACTION TEMPERATURE
```

```
24 RTEMP=(TEMP(2)+TEMP(1))/2.
```

```
C CALCULATE ABSTRACT PRESSURE OF FEED STREAM AND
C REACTOR
```

```
PRESS(1)=0.
PRESS(2)=ATMP
DO 17 I=1,2
PRESS(1)=PRESS(1)+PC(I,1)*PRS(1)**(I-1)
17 PRESS(2)=PRESS(2)+PC(I,2)*PRS(2)**(I-1)
```

```
C FEED MIXTURE FLOW RATE
```

... (CONT'D)

```

PRS(3)=PRS(3)**0.5
PRFSS(3)=0.
DO 19 I=1,3
19 PRESS(3)=PRESS(3)+DPC(I)*PRS(3)**(I-1)

```

C FLOW RATE CORRECTION

```

ROMIX= (28.*FDCOM(1)+ 34.*FDCOM(2) +60.*FDCOM(3)+64.*
1FDCOM(4) ) / (FDCOM(1)*V(1) +FDCOM(2)*V(2) +FDCOM(3)*V
1(3) +FDCOM(4)*V(4))
PRESS(3)=PRESS(3)* (28./V(1)/ROMIX) **0.5
FH2S = PRESS(3)*FDCOM(2)
FCOS = PRESS(3)*FDCOM(3)
FSO2 = PRESS(3)*FDCOM(4)

```

C SPACE VELOCITY AND SPACE TIME

```

SV=PRESS(3)/WC
ST=1./SV
SVH2S=FH2S/WC
SVCOS=FCOS/WC
SVSO2=FSO2/WC
STH2S=1./SVH2S
STCOS=1./SVCOS
STSO2=1./SVSO2

```

C MATERIAL BALANCE

```

AVGMV=(FDCOM(1)*V(1)+FDCOM(2)*V(2) +FDCOM(3)*V(3)+FDCO
1M(4)*V(4)) /28317.016

```

C FEED COMPONENT FLOW RATE (GM-MOLE/HR)

```

DO 10 J=1,4
10 BAL(1,J) = FDCOM(J)*PRESS(3)/AVGMV
WFA = WC/BAL(1,2)
WFB=WC/BAL(1,3)

```

C H2O FEED RATE (GM-MOLE/HR)

```

BAL(1,5)=HRATE/18.0588

```

C PRODUCT COMPOSITIONS

```

L=0
BAL(2,1) = BAL(1,1)
BAL(2,2)=BAL(2,1)*PRCOM(2)/PRCOM(1)
BAL(2,3)=BAL(2,1)*PRCOM(3)/PRCOM(1)
BAL(2,4)=BAL(2,1)*PRCOM(4)/PRCOM(1)
BAL(2,5)=BAL(1,5) + BAL(1,2) - BAL(2,2)

```

... (CONT'D)

BAL(2,6) = BAL(1,3) - BAL(2,3)
 BAL(2,7) = 1.5 * (BAL(1,2) - BAL(2,2) + BAL(1,3) - BAL(2,3))

C AVERAGE MOLECULAR WEIGHT OF SULFUR
 C INITIAL ASSUMPTION XS=8.

PPS = PRESS(2)/760.*BAL(2,7)/8.
 22 CALL FREM(PPS,RTEMP,XS)
 PRS1=PRESS(2)/760.*BAL(2,7)/XS
 IF(ABS((PPS-PRS1)/PRS1) -0.005) 20,20,21
 21 PPS=PRS1
 GO TO 22
 20 BAL(2,7)=BAL(2,7)/XS

C H2S/SO2 RATIO

FHVS=BAL(1,2)/BAL(1,4)
 PHVS=BAL(2,2)/BAL(2,4)
 FCVS= BAL(1,3)/BAL(1,4)
 PCVS= BAL(2,3)/BAL(2,4)

C CONVERSION

H2SCN=(BAL(1,2)-BAL(2,2)) / BAL(1,2)
 COSCN= (BAL(1,3)-BAL(2,3)) / BAL(1,3)
 SO2CN= (BAL(1,4)-BAL(2,4)) / BAL(1,4)

C ADJUST FEED COMPOSITION WITH H2O FEED

TOT=0.
 DO 9 J=1,5
 9 TOT=TOT+BAL(1,J)
 DO 11 J=1,5
 11 FDCOM(J)=BAL(1,J)/TOT*100.

C PARTIAL PRESSURE IN THE REACTOR

TOT=0.
 DO 12 J=1,7
 12 TOT=TOT+BAL(2,J)
 DO 13 J=1,7
 13 PRCOM(J)=BAL(2,J)*PRESS(2)/TOT

C DATA OUTPUT

GO TO (43,44), IPR

C TTY OUTPUT

43 CALL OUTPT(RUN,PRESS,RTEMP,FHVS,PHVS,FCVS,PCVS,H2SCN,

... (CONT'D)

```
1 COSCN, SOZCN, FDCOM, PRCOM, BAL, LUNW, XS, WC, SV, ST, SVH2S, ST  
1H2S, SVCOS, STCOS, SVSO2, STSO2, TEMP, IPR)  
44 GO TO (41,42), ISTR
```

C

FILE OUTPUT

```
41 WRITE(200,'NFIL') WC, RTEMP, PRESS, RUN, BAL, FDCOM, PRCOM,  
1H2SCN, COSCN, SOZCN, WFA, WFB, FHVS, PHVS, FCVS, PCVS, XS, SV,  
1SVH2S, SVCOS, SVSO2  
42 IF(ISTR-IEND) 34,65,65  
  
998 WRITE(LUNW,997)  
997 FORMAT(' FFINP CALL ERROR (EXIT CALLED)')  
GO TO 65  
  
999 WRITE(LUNW,996)  
996 FORMAT(' FFINP INPUT ERROR (EXIT CALLED)')  
65 CALL EXIT  
END
```

```

C *****
C *
C *           SUBROUTINE FREM
C *
C * SUBROUTINE FREM IS USED TO CALCULATE EQUILIBRIUM
C * COMPOSITIONS FOR SULFUR MOLECULES BY FREE ENERGY
C * MINIMIZATION METHOD
C *
C *****

SUBROUTINE FREM(PRESS,T,XS)
DIMENSION FRE(3,7),X(3),GA(3,3),GB(3),C(3),F(3),A(3,3)
1,Y(3),B(3),NG1(3),GX(3)
DATA FRE/7.7838968E+00,6.0892429E+00,2.6999349E+00,
12.5099820E-02,1.8824865E-02,6.2749549E-03,-3.7148310E-
205,-2.7861233E-05,-9.2870775E-06,2.6157310E-08,1.96179
383E-08,6.5393276E-09,-7.1209128E-12,-5.3406846E-12,-1.
47802282E-12,1.0114584E+04,1.1264370E+04,1.4504935E+04,
54.7621792E+00,7.3202322E+00,1.0534222E+01 /
DATA A/8.,6.,2.,6*0.0/
DATA X/1.,1.,1./
DATA Y/1.,1.,1./
DATA B/16.,2*0.0/
M=1
N=3
DO 12 I=1,N
NG1(I)=0
FRT= FRE(I,1)*(1.-ALOG(T))-FRE(I,2)*T/2.-FRE(I,3)*T
1**2/6.-FRE(I,4)*T**3/12.-FRE(I,5)*T**4/20.+FRE(I,6)/T-
2FRE(I,7)
C(I)=FRT+ALOG(PRESS)
IF(I-N)12,12,13
13 C(I)=FRT
12 CONTINUE
DO 14 ITER=1,300
CALL FREN (Y,C,F,YBAR,N, NG1)
MG=M+ 1
CALL GSET (A,Y,GA,GB,B,F, M,MG,N)
CALL GAUSS(GA,GB,MG,GX)
DO 18 I=1,N
IF(NG1(I)) 19,19,18
19 X(I)=-Y(I)*((C(I)+ALOG(Y(I)/YBAR))-GX(I))
DO 21 J=1,M
IG= J+1
21 X(I)=X(I)+GX(IG)*A(I,J)*Y(I)
18 CONTINUE
CALL NEZE (X,Y,N ,NG1)
QUIT=1.
DO 22 I=1,N

```


...(CONT'D)

```
IF(NG1(I)) 23,23,22
23 TEST=(X(I)-Y(I))/X(I)
   IF ( ABS(TEST) -0.5E-04) 22,22,24
24 QUIT=-1.
22 CONTINUE
   IF(QUIT) 25,25,26
25 DO 27 I=1,N
27 Y(I)=X(I)
14 CONTINUE
26 DO 32 I=1,N
   NG1(I)=0
   IF(X(I)) 33,33,34
34 Y(I)=X(I)
   GO TO 32
33 Y(I)=0.000001
32 CONTINUE
   XS=(8.*Y(1)+6.*Y(2)+2.*Y(3)) / (Y(1)+Y(2)+Y(3))
   RETURN
END
```

```

C *****
C *
C *           SUBROUTINE OUTPT           *
C *
C * THIS SUBROUTINE SPECIFIES THE OUTPUT FORM OF THE *
C * MAINLINE MTBAL ON THE TELETYPE *
C *
C *****
C
SUBROUTINE OUTPT(RUN,PRESS,RTEMP, FHVS,PHVS,FCVS,PCVS,
1H2SCN,COSCN,SO2CN,FDCOM,PRCOM,BAL,LUNW,XS,WC,SV,ST,
2SVH2S,STH2S,SVCOS,STCOS,SVSO2,STS02,TEMP,IPR )
DIMENSION PRESS(3),PRCOM(7),FDCOM(7),BAL(2,7),TEMP(2)

WRITE(LUNW,1) RUN
1 FORMAT(//// 7X,'RUN NUMBER',3X,A4,///)

12 WRITE(LUNW,210) WC
210 FORMAT( 7X,'WT. OF CATALYST ',1X,F10.3)

WRITE(LUNW,219) TEMP(1),TEMP(2),PRESS(2)
219 FORMAT(/ 7X,'REACTOR INLET TEMP ',F7.2,/ 7X,
1'REACTOR OUTLET TEMP ',F7.2 / 7X,'REACTION PRESSURE',
2F11.2//)

WRITE(LUNW,778)SV,ST,SVH2S,STH2S,SVCOS,STCOS,SVSO2
*,STS02
778 FORMAT ( 32X,'SPACE VELOCITY',8X,'SPACE TIME',/ 7X,
1'BASE ON TOTAL FEED GAS',4X,F10.3,10X,F10.3,/ 7X,'BA',
2'SE ON H2S FEED RATE',5X,F10.3,10X,F10.3,/ 7X,'BASE',
3' ON COS FEED RATE',5X,F10.3,10X,F10.3,/ 7X,'BASE ON',
4' SO2 FEED RATE',5X,F10.3,10X,F10.3 )

WRITE(LUNW,218) PRESS(3)
218 FORMAT(/ 7X,'VOLUMETRIC FEED RATE',F9.3,/)

WRITE(LUNW,220) H2SCN,COSCN,SO2CN
220 FORMAT(/ 7X,'CONVERSION OF H2S ',3X,F7.2,/ 7X,'CONVER'
1,'SION OF COS ',3X,F7.2,/7X,'CONVERSION OF SO2 ',3X,
2F7.2/ )

WRITE(LUNW,250)
250 FORMAT(/ 7X,'MOLECULAR',5X,'FEED',6X,'PARTIAL PRESSUR'
1,'E',3X,'MATERIAL BALANCE ',/ 8X,'SPECIE',4X,'COMPOSI'
2,'TION',4X,'IN REACTOR',8X,'FEED',3X,'PRODUCT' )

WRITE(LUNW,789)
789 -FORMAT( 17X,'(MOLE PERCENT)',5X,'(MM HG)',8X,'(GM
*-MDL)/HR)' )

```

... (CONT'D)

```
WRITE(LUNW,211) (FDCOM(J),PRCOM(J),BAL(1,J),BAL(2,J)
*,J=1,5)
211 FORMAT (/10X,'N2 ',7X,F6.2, 9X, F6.1,8X,F7.3,2X,F7.3,/
1/10X,'H2S',7X,F6.2,9X,F6.1,8X,F7.3,2X,F7.3,//10X,
2' COS',7X,F6.2,9X,F6.1,8X,F7.3,2X,F7.3,//10X,'SO2',7X,
3F6.2,9X,F6.1,8X,F7.3,2X,F7.3,//10X,'H2O',7X,F6.2,9X,
4F6.1,8X,F7.3,2X,F7.3, )
WRITE(LUNW,911) (FDCOM(I+5),PRCOM(I+5),BAL(1,I+5),
1BAL(2,I+5),I=1,2)
911 FORMAT (/10X,'CO2',7X,F6.2,9X,F6.1,8X,F7.3,2X,F7.3,/
1/10X,'SX ',7X,F6.2,9X,F6.1,8X,F7.3,2X,F7.3 )

WRITE(LUNW,212) XS
212 FORMAT(//, 7X,'AVERAGE NO OF SULFUR ATOMS/MOLECULE = '
*,F6.2)

IF (IPR-2) 13,12,13
13 RETURN
END
```

```

C *****
C *
C *          SUBROUTINE CHROM
C * SUBROUTINE CHROM IS USED TO CALCULATE THE COMPO-
C * SITION OF FEED AND PRODUCT STREAM FROM THE GC AREA*
C * RESULTS
C *
C *****

```

```

SUBROUTINE CHROM(COMP,CR,N)
DIMENSION COMP(10),CR(4,6),HSN2(2),SON2(2),COSN2(2)
*,ATN(2)
DATA HSN2/0.00733,0.89481/,SON2/0.02466,0.77038/
DATA COSN2/-0.00149,0.65325/
DATA ATN/10.0,5.0/
XN=N

```

C CORRECTED AREA OF N2 PEAK

```

DO 20 I=1,N
20 CR(I,1)=CR(I,1)*(1.76047*ATN(2)+ 1.17312)/(0.17031
**ATN(1)+1.07781)

```

C AVERAGE AREA OF EACH PEAK

```

DO 1 J=1,6
CR(4,J)=0.
DO 1 I=1,N.
1 CR(4,J)=CR(4,J) +CR(I,J)/XN
IF(CR(4,2)) 3,3,5
3 HNRAT=0.
GO TO 7
5 HNRAT=HSN2(1) + HSN2(2)*CR(4,2)/CR(4,1)*100.
7 IF(CR(4,4)) 8,8,9
8 SNRAT=0.
GO TO 14
9 SNRAT=SON2(1) + SON2(2)*CR(4,4)/CR(4,1)*100.
14 IF(CR(4,3)) 15,15,17
15 CNRAT=0.
GO TO 16
17 CNRAT=COSN2(1) + COSN2(2)*CR(4,3)/CR(4,1)*100.
16 COMP(1)=100./ (100.+HNRAT+SNRAT+CNRAT)
COMP(2)=HNRAT*COMP(1)/100.
COMP(3)=CNRAT*COMP(1)/100.
COMP(4)=1.-COMP(1)-COMP(2)-COMP(3)
RETURN
END

```

```

C *****
C *
C *          SUBROUTINE GSET
C *
C * THIS SUBROUTINE SETS UP THE MATRIX EQUATION WHICH
C * IS SOLVED USING SUBROUTINE GAUSS.
C *
C *****

SUBROUTINE GSET (A,Y,GA,GB,B,F, M, MG, N)
DIMENSION R(3,3),A(3,3),Y(3),GA(3,3),GB(3),B(3),F(3)
DO 1 K=1,M
DO 1 J=1,K
R(J,K)=0.0
DO 2 I=1,N
2 R(J,K)=R(J,K)+A(I,J)*A(I,K)*Y(I)
1 R(K,J)=R(J,K)
DO 3 I=1, MG
DO 3 J=1, MG
3 GA(I,J)=0.0
DO 4 IG=1, M
DO 5 I=1, N
5 GA(IG,1)=GA(IG,1)+A(I,IG)*Y(I)
DO 9 J=1, M
JG= J+ 1
9 GA(IG, JG)=R(IG, J)
JG= IG+1
IGG=M+1
4 GA(IGG, JG)=GA(IG,1)
DO 10 J=1, M
GB(J)=B(J)
DO 10 I=1, N
10 GB(J)=GB(J)+A(I,J)*F(I)
JGB=M+1
GB(JGB)=0.0
DO 11 I=1, N
11 GB(JGB)=GB(JGB)+F(I)
RETURN
END

```

```

C *****
C *
C *          SUBROUTINE GAUSS          *
C *
C * THE FUNCTION OF THIS SUBROUTINE IS TO SOLVE THE *
C * SET OF EQUATIONS A*X=B USING GAUSSIAN ELIMINATION *
C * AND BACK SUBSTITUTION ROTATING ABOUT THE ELEMENT *
C * OF MAXIMUM MODULUS. *
C *
C *****

SUBROUTINE GAUSS (A,R,N,X)
DIMENSION A(3,3),R(3),X(3)
M=N-1
DO 11 J=1,M
S=0.
DO 12 I=J,N
U= ABS(A(I,J))
IF(U-S) 12,12,112
112 S=U
L=I
12 CONTINUE
IF(L-J) 119,19,119
119 DO 14 I=J,N
S=A(L,I)
A(L,I)=A(J,I)
14 A(J,I)=S
S=R(L)
R(L)=R(J)
R(J)=S
19 IF( ABS(A(J,J))-1.E-30) 115,115,15
115 WRITE(6,3)
3 FORMAT (1H , 'MATRIX SINGULAR')
RETURN
15 MM=J+1
DO 11 I=MM,N
IF( ABS(A(I,J))-1.E-30) 11,111,111
111 S=A(J,J)/A(I,J)
A(I,J)=0.0
DO 16 K=MM,N
16 A(I,K)=A(J,K)-S*A(I,K)
R(I)=R(J)-S*R(I)
11 CONTINUE
DO 17 K=1,N
I=N+1-K
S=0.0
IF(I-N) 117,17,117
117 MM=I+1
DO 18 J=MM,N

```

... (CONT'D)

```
18 S=S+A(I,J)*X(J)
17 X(I)=(R(I)-S)/A(I,I)
  RETURN
  END
```

```
C *****
C *
C *          SUBROUTINE FREN          *
C *
C * THIS SUBROUTINE CALCULATES THE FREE ENERGY *
C * CONTRIBUTION OF EACH SPECIE TO THE SYSTEM. *
C *
C *****

SUBROUTINE FREN (Y,C,F,YBAR,N, NG1)
DIMENSION Y(3),C(3),F(3),NG1(3)
YBAR=0.0
DO 1 I=1,N
1 YBAR=YBAR+Y(I)
DO 2 I=1,N
IF(NG1(I)) 3,3,4
3 F(I)=Y(I)*(C(I)+ALOG(Y(I)/YBAR))
GO TO 2
4 F(I)=0.0
2 CONTINUE
RETURN
END
```



```

C *****
C *
C *           SUBROUTINE NEZE
C *
C * THIS SUBROUTINE TESTS FOR NEGATIVE OR ZERO AMOUNTS
C * OF MOLECULAR SPECIES AND TAKES THE CORRECTIVE
C * ACTION AS INDICATED IN THE METHOD REVIEW.
C *
C *****

SUBROUTINE NEZE (X,Y,N ,NG1)
DIMENSION X(3),Y(3),NG1(3)
TEST=1.0
DO 1 I=1,N
  IF(NG1(I)) 2,2,1
2  IF(X(I)) 3,3,1
3  SLAM=-0.99*Y(I)/(X(I)-Y(I))
  IF(SLAM-TEST)4,4,1
4  TEST=SLAM
1  CONTINUE
  DO 5 I=1,N
  IF(NG1(I))7,7,5
7  X(I)=Y(I)+TEST*(X(I)-Y(I))
  IF(X(I)-0.10E-10) 6,6,5
6  X(I)=0.0
  NG1(I)=1
5  CONTINUE
RETURN
END

```

TABLE I.1

>QMTBAL
 FILE STORAGE FLAG(1-STORE,2-NO)
 FUNCTION FLAG(1-PROC NEW DATA OR 2-PROC FILE DATA)

 PRINT FLAG(1-TTY,2-NONE)
 >2 1 1
 WT OF CATALYST(GM) S NUMERIC FILE NO.
 >1.0213 1
 RUN NO.,NO. OF FEED G.C.,NO. OF PROD. G.C.
 >F-06 3 3
 TEMP-REACT. INLET,OUTLET, PRESS-FEED,REACT.,D/P CELL
 >15.4 15.4 40. 55. 91.0
 SPECIFY H2O FEED PUMP PCT AND TEMP
 >0. 0.
 ATMOSPHERIC PRESSURE
 >705.6
 FEED G.C. AREAS-N2,H2S,COS,S02,H2O,CO2
 >201267 203678 279190 117223 0 0
 >200960 200308 278458 114565 0 0
 >201201 203233 276263 122204 0 0
 PROD. G.C. AREAS
 >199037 133398 244301 62466 32932 21117
 >199785 131616 244920 63089 30115 20994
 >200025 132677 243946 62988 27860 20994

TABLE I.2

RUN NUMBER F-86

WT. OF CATALYST 1.021
 REACTOR INLET TEMP 556.40
 REACTOR OUTLET TEMP 556.05
 REACTION PRESSURE 930.18

	SPACE VELOCITY	SPACE TIME
BASE ON TOTAL FEED GAS	0.611	0.116
BASE ON H ₂ S FEED RATE	0.259	3.859
BASE ON CO ₂ FEED RATE	0.258	3.861
BASE ON SO ₂ FEED RATE	0.131	7.594

VOLUMETRIC FEED RATE 8.795

CONVERSION OF H₂S 0.33
 CONVERSION OF CO₂ 0.11
 CONVERSION OF SO₂ 0.45

MOLECULAR SPECIE	FEED COMPOSITION (MOLE PERCENT)	PARTIAL PRESSURE IN REACTOR (MM HG)	MATERIAL BALANCE (GM-MOL)/HR	
			FEED	PRODUCT
N ₂	92.45	863.5	10.285	10.285
H ₂ S	3.00	18.5	0.334	0.221
CO ₂	3.00	24.8	0.334	0.296
SO ₂	1.52	7.7	0.170	0.092
H ₂ O	0.00	9.5	0.000	0.113
CO	0.00	3.2	0.000	0.038
SX	0.00	2.6	0.000	0.031

AVERAGE NO OF SULFUR ATOMS/MOLECULE = 7.27

APPENDIX J

EXPERIMENTAL DATA FILE

Experimental data were tabulated using the following symbolic representation.

Catalyst type;

1 = γ -alumina (Kaiser S-201)

2 = 5.4% Cu - alumina

3 = 12.08% Cu - alumina

4 = 16.07% Cu - alumina

Attenuation scheme;

2 = attenuation scheme II in Appendix A

3 = attenuation scheme III in Appendix A

Experimental run;

A = $H_2S - SO_2$ reaction on catalyst type 2

B = $COS - H_2O$ reaction on catalyst type 2

C = $COS - H_2O - SO_2$ reaction on catalyst type 2

D = $COS - SO_2$ reaction on catalyst type 2

E = $COS - H_2S - SO_2$ reaction on catalyst type 2

F = $COS - H_2S - SO_2$ reaction on catalyst type 3

G = $COS - H_2S - SO_2$ reaction on catalyst type 4

H = $COS - H_2S - SO_2$ reaction on catalyst type 1

I = $COS - H_2O$ reaction on catalyst type 1

J = Test of bifunctional characteristics of catalyst type 3

K = Maximum obtainable conversion of $\text{H}_2\text{S} - \text{SO}_2$
reaction on catalyst type 1 ($\text{SV} = 100 \text{ hr}^{-1}$)

L = Maximum obtainable conversion of $\text{H}_2\text{S} - \text{SO}_2$
reaction on catalyst type 1 ($\text{SV} = 4 \text{ hr}^{-1}$)

TABLE J.1

RAW DATA

RUN	CAT TYPE	CAT WT	INLET TEMP	OUTLET TEMP	RCTOR PRESS	ATM PRESS	S.V. (/HR)	H2O PCT	ATN SCHM
A-01	2	1.0210	15.40	15.44	50.0	706.9	52.0	0.0	0.0 2

FEED GC AREA

PRODUCT GC AREA

N2	H2S	COS	S02	N2	H2S	COS	S02
216522.	6897.	0.	3814.	220930.	2181.	0.	1139.
216469.	7011.	0.	4008.	220265.	2078.	0.	1119.
219850.	6942.	0.	3722.	220874.	2161.	0.	1089.

RUN	CAT TYPE	CAT WT	INLET TEMP	OUTLET TEMP	RCTOR PRESS	ATM PRESS	S.V. (/HR)	H2O PCT	ATN SCHM
A-02	2	1.0210	15.40	15.46	50.0	706.8	41.6	0.0	0.0 2

FEED GC AREA

PRODUCT GC AREA

N2	H2S	COS	S02	N2	H2S	COS	S02
214327.	6726.	0.	3786.	220134.	1999.	0.	830.
219875.	6751.	0.	3898.	220928.	2021.	0.	853.
221286.	6864.	0.	3721.	220073.	2095.	0.	1048.

TABLE J.2
PROCESSED DATA

RUN	INLET TEMP	OUTLET TEMP	RCTOR PRESS	SPACE TIME		CONVERSION	
				H2S	COS	H2S	COS
A-01	556.05	556.78	939.14	4.702	---	0.69	0.66
A-02	556.05	557.14	939.04	5.917	---	0.69	0.70
A-03	556.05	557.44	938.94	6.395	---	0.72	0.71
A-04	556.78	557.87	939.04	9.565	---	0.73	0.72
A-05	556.05	556.78	940.14	3.622	---	0.63	0.68
A-06	556.05	556.78	941.34	3.917	---	0.68	0.74
B-01	556.78	556.78	930.34	---	5.709	---	0.13
B-02	557.14	556.78	936.94	---	5.016	---	0.11
B-03	556.78	556.05	939.99	---	4.952	---	0.12
B-04	556.05	556.05	939.64	---	3.912	---	0.04
B-05	556.78	556.78	939.94	---	7.490	---	0.26
B-06	556.78	556.78	940.24	---	11.646	---	0.39
B-07	556.78	557.87	940.24	---	16.468	---	0.61
B-08	556.05	556.05	935.54	---	8.963	---	0.27
C-01	556.41	556.05	932.94	---	5.744	---	0.08
C-02	556.05	556.05	932.44	---	4.977	---	0.01
C-03	556.05	556.05	935.44	---	4.489	---	0.03
C-04	556.05	556.05	935.94	---	6.095	---	0.07
C-05	556.05	556.05	937.54	---	7.176	---	0.09
C-06	556.41	556.41	938.14	---	10.220	---	0.15
C-07	556.05	556.05	938.14	---	17.019	---	0.29
C-08	556.41	556.05	936.64	---	9.072	---	0.13

C

TABLE J.2 (CONTINUED)

PROCESSED DATA

RUN	INLET TEMP	OUTLET TEMP	RCTOR PRESS	SPACE TIME		CONVERSION		S02
				H2S	COS	H2S	COS	
D-01	557.44	554.59	925.44	---	9.528	---	0.03	0.03
D-02	557.87	554.23	925.94	---	16.676	---	0.08	0.04
D-03	555.30	558.23	926.24	---	12.600	---	0.05	0.02
D-04	558.60	558.60	926.24	---	6.522	---	0.03	0.00
D-05	556.41	556.05	926.24	---	5.319	---	0.01	0.00
D-06	556.05	556.05	926.24	---	4.597	---	0.02	0.00
E-01	554.23	557.87	932.54	10.121	12.110	0.73	0.27	0.46
E-02	556.05	556.05	931.24	14.934	17.601	0.76	0.38	0.45
E-03	554.23	557.87	931.64	3.592	4.442	0.67	0.06	0.67
E-04	553.47	558.23	931.64	3.816	4.751	0.70	0.09	0.73
E-05	553.84	557.14	931.04	4.300	5.383	0.71	0.10	0.77
E-06	553.47	558.96	931.04	4.785	6.008	0.72	0.12	0.75
E-07	553.84	556.78	931.04	6.289	7.946	0.74	0.17	0.82
F-01	556.05	556.05	930.68	5.258	5.328	0.46	0.11	0.60
F-02	556.05	556.05	930.18	4.494	4.466	0.43	0.09	0.52
F-03	556.05	556.05	929.58	3.757	3.745	0.40	0.04	0.45
F-04	556.78	555.32	929.58	7.267	7.365	0.53	0.16	0.64
F-05	554.23	554.23	930.18	4.165	4.225	0.36	0.09	0.42
F-06	556.05	556.05	930.18	3.859	3.861	0.33	0.11	0.45
F-07	556.05	556.05	923.58	15.727	16.065	0.58	0.39	0.81

TABLE J.2 (CONTINUED)

PROCESSED DATA

RUN	INLET TEMP	OUTLET TEMP	RCTOR PRESS	SPACE TIME		CONVERSION		S02
				H2S	COS	H2S	COS	
G-01	556.05	556.05	934.08	3.863	3.843	0.06	0.07	0.17
G-02	556.05	556.05	933.88	4.211	4.229	0.09	0.07	0.18
G-03	556.05	555.32	934.08	4.687	4.696	0.11	0.09	0.17
G-04	556.05	556.05	933.88	5.816	5.861	0.11	0.09	0.21
G-05	556.05	556.05	933.98	7.985	7.885	0.11	0.12	0.23
G-06	556.78	556.78	933.58	11.876	11.772	0.12	0.14	0.28
G-07	556.05	555.68	931.78	14.618	14.726	0.13	0.18	0.33
H-01	556.05	557.87	928.43	4.321	4.394	0.27	0.44	0.37
H-02	556.05	556.41	928.43	3.874	3.903	0.25	0.42	0.36
H-03	556.41	556.41	929.93	5.784	5.780	0.35	0.49	0.47
H-04	556.41	556.41	929.93	7.993	8.028	0.38	0.59	0.56
H-05	556.05	556.05	930.23	13.474	13.388	0.52	0.74	0.70

TABLE J.2 (CONTINUED)

PROCESSED DATA

RUN	INLET TEMP	OUTLET TEMP	RCTOR PRESS	FEED COMPOSITION		SPACE-TIME (COS)	CONVERSION (COS)	
				N ₂	COS			
1-01	556.05	556.05	931.89	96.31	3.16	0.52	6.713	0.06
1-02	556.05	556.05	930.29	96.18	3.06	0.75	6.879	0.21
1-03	556.05	556.05	930.29	95.66	3.11	1.22	6.787	0.26
1-04	556.05	556.05	930.29	95.19	3.11	1.69	6.745	0.27
1-05	556.05	556.05	932.29	94.72	3.12	2.14	6.691	0.28
1-06	556.05	556.05	932.39	93.85	3.08	3.05	6.699	0.27

5

TABLE J.2 (CONTINUED)

PROCESSED DATA

RUN	INLET TEMP	OUTLET TEMP	RCTOR PRESS	SPACE TIME		CONVERSION		S02
				H2S	COS	H2S	COS	
J-01	556.78	556.05	924.24	5.585	6.361	0.49	0.11	0.51
J-02	556.78	556.05	924.24	5.585	6.361	0.53	0.11	0.54
J-03	556.78	556.05	924.24	5.585	6.361	0.50	0.10	0.55
J-04	555.68	556.78	924.04	5.518	-----	0.51	-----	0.46
J-05	555.68	556.78	924.04	5.518	-----	0.49	-----	0.43
J-06	555.68	556.78	924.04	5.518	-----	0.50	-----	0.44
J-07	555.68	556.78	924.04	5.518	-----	0.49	-----	0.43
J-08	555.68	556.78	924.04	5.518	-----	0.49	-----	0.44
J-09	557.87	556.05	924.04	-----	6.110	-----	0.09	0.07
J-10	557.87	556.05	924.04	-----	6.110	-----	0.08	0.04
J-11	557.87	556.05	924.04	-----	6.110	-----	0.08	0.01
J-12	557.87	556.05	924.04	-----	6.110	-----	0.08	0.03
J-13	557.87	556.05	924.04	-----	6.110	-----	0.09	0.01
J-14	558.23	556.05	924.44	5.552	-----	0.49	-----	0.46
J-15	558.23	556.05	924.44	5.552	-----	0.48	-----	0.46
J-16	558.23	556.05	924.44	5.552	-----	0.50	-----	0.47
J-17	558.23	556.05	924.44	5.552	-----	0.49	-----	0.47
J-18	558.23	556.05	924.44	5.552	-----	0.50	-----	0.48
J-19	558.23	556.05	924.44	-----	6.195	-----	0.07	0.03
J-20	558.23	556.05	924.44	-----	6.195	-----	0.08	0.03
J-21	558.23	556.05	924.44	-----	6.195	-----	0.08	0.04
J-22	558.23	556.05	924.44	-----	6.195	-----	0.07	0.03
J-23	558.23	556.05	924.44	-----	6.195	-----	0.07	0.04

TABLE J.2 (CONTINUED)

PROCESSED DATA

RUN	INLET TEMP	OUTLET TEMP	RCTOR PRESS	FEED COMPOSITION		SO ₂		SPACE-VEL. (PER HOUR)	CONVERSION (H ₂ S)
				N ₂	H ₂ S	H ₂ S	SO ₂		
K-01	550.18	549.85	728.06	95.44	3.03	1.52	100.0	0.95	
K-02	575.45	574.99	738.45	95.37	3.09	1.52	100.0	0.92	
K-03	604.74	604.14	739.45	95.32	3.10	1.57	100.0	0.88	
K-04	657.85	656.97	744.15	95.41	3.09	1.48	100.0	0.85	
K-05	704.54	703.42	735.65	95.35	3.09	1.54	100.0	0.77	
L-01	702.89	701.78	739.56	95.38	3.10	1.50	4.0	0.88	
L-02	555.67	555.32	734.05	95.20	3.18	1.61	4.0	0.98	
L-03	604.74	604.14	737.85	95.21	3.20	1.58	4.0	0.97	
L-04	658.95	658.06	738.75	95.17	3.18	1.63	4.0	0.89	
L-05	660.59	659.70	741.25	95.25	3.16	1.57	4.0	0.89	